VELOCITY, TEMPERATURE AND TURBULENCE MEASUREMENTS IN AIR UNDER COMBINED FREE AND FORCED CONVECTION CONDITIONS

by

MICHAEL ANTHONY CONNOR

Submitted

in fulfilment of the requirements

for the degree of

Doctor of Philosophy

University of Cape Town

October 1971

ABSTRACT

This thesis reports the results of an experimental investigation of the effect of buoyancy forces on turbulent upflow of air in a vertical pipe under conditions of constant wall heat flux at Reynolds numbers of 5000 to 14000. Preliminary velocity and axial turbulence intensity measurements in isothermal flows for Reynolds numbers of 5000 to 32000 are also reported.

Velocity and temperature distributions were measured over a range of heat fluxes at Reynolds numbers of approximately 5000 and 8000 and at a single heat flux at a Reynolds number of 14000. In addition, axial turbulence intensities, temperature intensities and $\overline{v_z t}$ values were obtained for four heat fluxes at a Reynolds number of 5000 and for a single heat flux at a Reynolds number of 14000. Marked changes in all the experimentally measured quantities were observed as the influence of free convection in the flow increased.

Forms of the continuity, momentum and energy equations applicable to the above flow situation were developed. These equations were solved, using measured velocity and temperature distributions, to give eddy diffusivities of heat and momentum and also values of $\overline{v_r t}$ and $\overline{v_r v_z}$. The changes in these calculated values, together with the changes in measured velocities, temperatures and turbulence intensities, indicate that the overall result of increasing free convection effects is to reduce the level of turbulence in the flow. This is associated, over the central 70% of the pipe, with a probable tendency towards isotropic flow conditions.

ACKNOWLEDGEMENTS

The author wishes to express his sincere appreciation and gratitude to Professor A. D. Carr and also to Dr. H. O. Buhr for their encouragement, advice and guidance throughout this study.

He is also grateful to Mr. L. C. Horton and Mr. K. E. Wheeler for their suggestions and assistance during the design and construction of the experimental apparatus. Thanks also go to Mr. P. M. M. Brown, Dr. E. A. Horsten and Mr. D. M. Fraser for their help during various stages of this project, and to Miss M. Dreyer, who typed this thesis. The financial assistance of the Council for Scientific and Industrial Research is also gratefully acknowledged.

Finally the author wishes to thank his wife, Heather, for her patience, understanding and encouragement during this study and also for her invaluable assistance during the preparation of this thesis.

TABLE OF CONTENTS

TABLE OF FIGURES

CHAPTER 1

COMBINED FREE AND FORCED CONVECTION

1.1 INTRODUCTION

In heat transfer to a moving fluid two types of convection can occur. These are forced convection, where the fluid motion is caused by some external agency, and natural, or free convection, where motion arises as a result of density differences in the fluid. It is clear from these definitions that free convection or buoyancy effects will therefore occur, superimposed on the forced convection effects, in all practical forced flow situations. Usually these buoyancy forces are very small in comparison with externally applied forces and in most industrial convective heat transfer problems they can safely be ignored. Recently, however, instances where free and forced convection effects of equal orders of magnitude occur have been investigated; examples of these include certain heat exchanger applications, problems relating to the use of liquid metals as coolants in nuclear reactors, and also several problems involving the cooling of parts of rotating equipment. In such situations the flow type is generally described as combined free and forced convection, or, more simply, as mixed convection.

The development of the literature on mixed convection was greatly stimulated by the realisation that flows where mixed convection was important did occur in practice, and in recent years the number of publications on the subject has increased steadily. (A review of those considered relevant to the present work is given in section 1.2.) A number of flow situations have been studied, among them being that dealt with in the present investigation, viz. upward flow of a fluid in a vertical pipe under uniform heat flux conditions.

Early publications on this particular problem were concerned primarily with rates of heat transfer under mixed convection conditions and attempts were made to correlate the observed variations in Nusselt numbers against free convection parameters. These met with limited success and it became obvious that a more fundamental approach to the problem was needed if expressions other than semi-empirical correlations were

to be developed. Such an approach was soon forthcoming and theoretical analyses for both laminar flow and turbulent flow were proposed. These analyses predicted that the result of increasing free convection effects is the development of velocity and temperature profiles distorted markedly from their accepted forced flow shapes. For a long time it was not possible to test these predictions against measured values, since no experimental measurements were available, but then recently, experimentally measured velocity and temperature profiles were reported for laminar flows. For turbulent flows, however, the lack of experimental measurements remained and it was in an attempt to obtain such measurements that the programme of research into turbulent mixed convection flows, of which the present work is a part, was undertaken.

For the particular flow situation studied in the present investigation, fully developed velocity and temperature profiles were measured; in addition, to obtain a better understanding of the flow structure under mixed convection conditions, measurements of axial velocity fluctuations, temperature fluctuations and the correlation $\overline{v_z t}$ were also taken. Eddy diffusivities of heat and momentum and values of the correlations $\overline{v_r t}$ and $\overline{v_r v_z}$ were then calculated using the forms of the energy and momentum equations reported in section 1.3.

The measurements were made using single hot-wire probes, held normal to the mean flow, and connected to a Transmetrics constant current anemometer. Air was chosen as the experimental fluid because it was the only fluid in which accurate turbulence measurements could be made with the equipment available.

The flow geometry was selected partly because of its practical relevance but also because flow in a vertical pipe possesses the advantages of having axial symmetry and of having the buoyancy forces acting in the mean flow direction. These considerations, together with the use of the boundary condition of uniform wall heat flux, greatly simplified the mathematical description of the system.

1.2 PREVIOUS WORK

1.2.1 Preliminary Considerations

Of the many published papers treating aspects of mixed convection a few deal specifically with the flow situation studied in the present work and these are reviewed later.

However a number of the remaining mixed convection papers also contain material relevant in some way to the present investigation, and these, too, have been included in the review, subject to the following considerations:

i) Only papers treating the flow of Newtonian fluids in vertical pipes under conditions of either
   a) upflow with heating, or
   b) downflow with cooling
   were considered. This was because these two flow situations are the only ones providing a relative orientation of buoyancy forces and mean flow direction similar to that considered in the present work.

ii) Because certain flow properties, e.g. Nusselt numbers, are similar under both sets of boundary conditions, papers dealing with both uniform heat flux and uniform wall temperature conditions were included in the review.

iii) Although the present work deals with fully developed flow, certain studies of developing flows are included in the review as they yield information on the fully developed flow condition.

iv) For profile measurements and predictions so little information was available that measurements in any Newtonian fluid were considered relevant. Because Nusselt numbers in liquid metals are very different from those in other fluids, however, papers dealing with the former were disregarded.

v) Laminar as well as turbulent flows have been considered because of the similarity in shape of the distorted profiles in both types of flow.

It must be noted that the isothermal laminar-to-turbulent transition criterion no longer holds in heated flows and for this reason the review proper is prefaced by a review of the

literature on the variation of the heated flow transition point.

Information on published papers dealing with flow situations such as downward flows, flows in horizontal pipes or ducts, etc. which are not covered here, can be found in reviews by Bhattacharyya [1], Metais [2] and Brown and Gauvin [3,4].

1.2.2 Laminar to turbulent transition.

Until the early nineteen-fifties it appears to have been generally accepted that at Reynolds numbers below 2100, all pipe flows, whether heated or unheated, would remain laminar. Within a very few years however, a considerable amount of evidence disproving this assumption became available [5,6,7,8,9] and a detailed experimental investigation of the problem by Hanratty et al [10] showed that, under strong influence of free convection, fluctuating flows could be obtained at Reynolds numbers as low as 50 for the case of opposing flow. Transition Reynolds numbers for aiding flow were higher, typically 200-300. Early attempts to define transition criteria were published by Brown [9] and Hallman [8] and further information has since been reported by Scheele and his co-workers [11,12,13] and others [3,14].

In the sections which follow, this variation in transition criteria has been allowed for and the terms laminar and turbulent refer, irrespective of Reynolds number, to flows where irregular fluctuations are respectively absent and present.

1.2.3 Velocity and temperature profiles - Laminar flow.

i) Theoretical work: The first theoretical analysis of mixed convection laminar flow was by Ostroumov [15] in 1950 (his work only became available in an English translation much later) for the case of fully developed flow under conditions of constant wall heat flux. Introducing a linear variation of density with temperature into the equations of momentum and energy, he obtained a solution, in terms of Bessel functions, for the fully developed temperature and velocity profiles. This solution predicted that the effect of heating or cooling is to distort these profiles, the magnitude of the distortion being proportional to the rate of heat transfer and inversely proportional to the mean flow velocity.

Similar analyses were later published by Hallman [16], Brown [9] and Hanratty et al [10], all of whom made the same assumptions as Ostroumov and produced predictions which, though originally expressed in terms of different free convection parameters, are identical when converted to the same basis [3]. Several of the predicted profiles for upflow with heating are shown in Fig. 1.1.

A more accurate analysis for the case of constant wall heat flux has recently been published by Lawrence and Chato [14]. They solved the equations of continuity, motion and energy using a finite-difference method, and allowing both viscosity and density to vary in a non-linear fashion with temperature. For given values of the Grashof and Reynolds numbers, velocity profiles at different distances from the pipe entrance were predicted and the predicted centre-line velocities agreed well with values estimated from multiple-exposure photographs of a dyed portion of the flow.

ii) Experimental work: The experimental verification of the above analyses proved difficult because of the problems involved in making direct measurements of velocity profiles in laminar flows. A certain amount of indirect evidence supporting the predictions for fully developed flows was, however, obtained. Thus, Hallman [8] measured Nusselt numbers and Brown [9] temperature profiles, both of which confirmed the predictions of their respective analyses. These analyses were also supported by the qualitative agreement between the shapes of predicted velocity profiles and those observed by Hanratty et al [10] in the course of their experiments using dye as a tracer.

Recently, however, directly measured velocity profiles have been reported by Greene [17,18] for the flow of water in a vertical tube under conditions of constant wall heat flux. Measured fully developed profiles showed good agreement with theoretical (constant viscosity) profiles at low values of the free convection parameter, $\frac{Gr}{Re}$, but at higher $\frac{Gr}{Re}$ values the agreement is poorer, although the general shapes are still similar. Part of the disagreement may be due to the assumption of constant viscosity since Lawrence and Chato [14] were able to obtain much closer agreement between their theoretical (varying viscosity) and measured centre-line velocities.

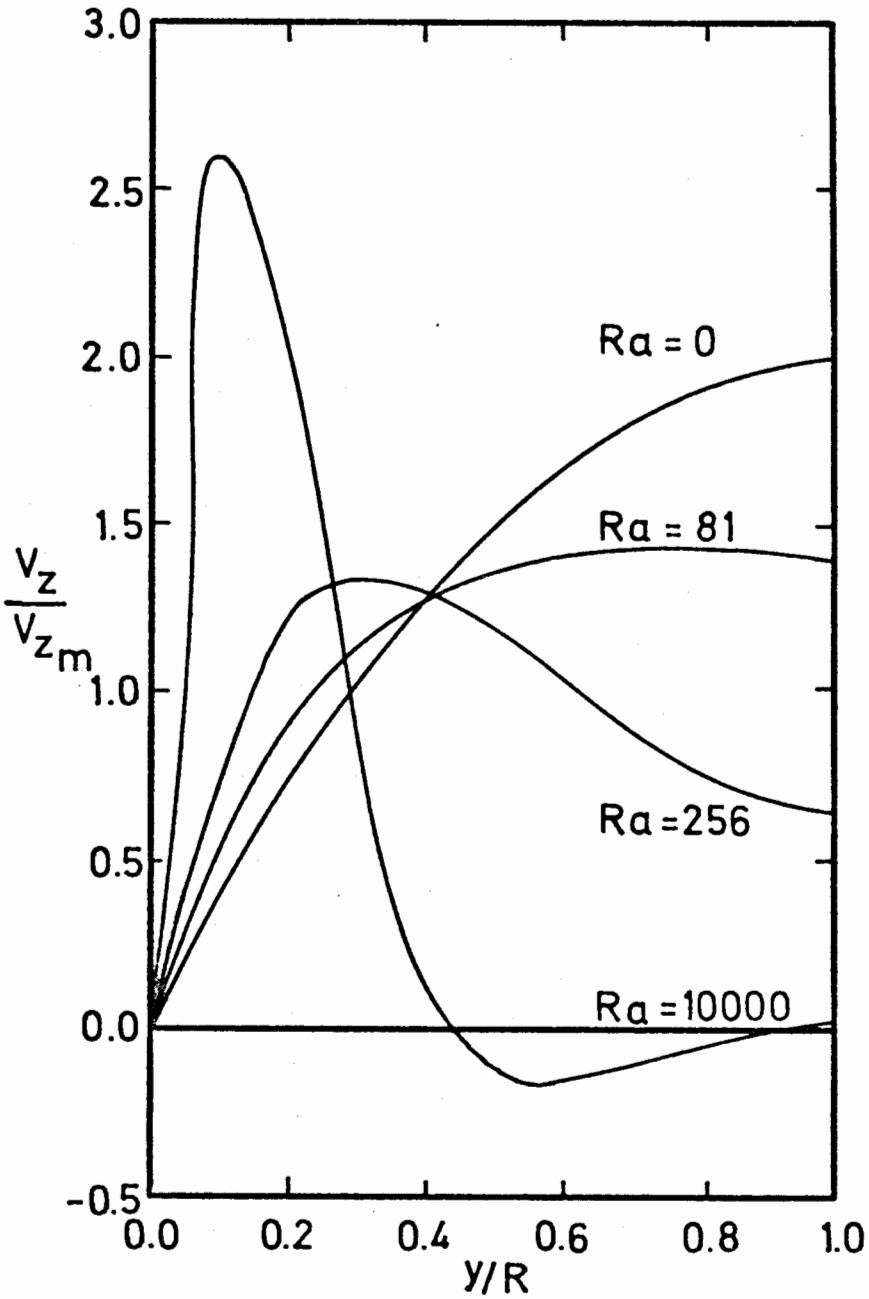

FIGURE 1.1 DISTORTED VELOCITY PROFILES FOR LAMINAR FLOW AS PREDICTED BY HALLMAN [16]

Even more recently a set of developing velocity and temperature profiles was reported by Steiner [19] for air flows under constant heat flux conditions. On the basis of auto-correlation measurements and Nusselt number trends Steiner refers to these as laminar flow profiles, despite the fact that they were measured at Reynolds numbers of between 5000 and 9000. Since the profiles measured over a similar Reynolds number range (but at considerably lower Grashof numbers than those occurring in Steiner's work) in the present investigation showed similar Nusselt number variations and velocity profile distortions, yet were undoubtedly turbulent, it is unfortunate that no comparison of his profiles with those predicted by laminar flow theory is given by Steiner.

1.2.4 Velocity and temperature profiles - Turbulent flow.

i) Theoretical work: Very few attempts to predict velocity and temperature profiles in turbulent mixed convection flows have been reported and, apart from the early, little-known work of Ber [20], the only important papers on the subject appear to be those of Ojalvo and Grosh [21] and Horsten et al [22]. For the same conditions of fully developed flow with constant wall heat flux Ojalvo and Grosh and Ber both predicted velocity and temperature distributions by substituting eddy diffusivity expressions into the equations of motion and energy and solving the resulting equations. (Ojalvo and Grosh allowed for a viscous sublayer whereas Ber did not.) The predicted distorted velocity and temperature profiles, of which examples are shown in Fig. 1.2, followed trends similar to those for laminar flow.

The major assumption made by Ojalvo and Grosh was that the flow structure, as represented by the isothermal eddy diffusivity relations, remained unchanged in heated flows. This, however, was proved to be incorrect by Horsten [22] who showed, using measured profiles taken from the present work, that predicted and measured profiles were considerably different. Horsten also investigated the differences in predicted velocity and temperature distributions which resulted when the eddy diffusivity relations were varied. He reached the conclusion that before an accurate

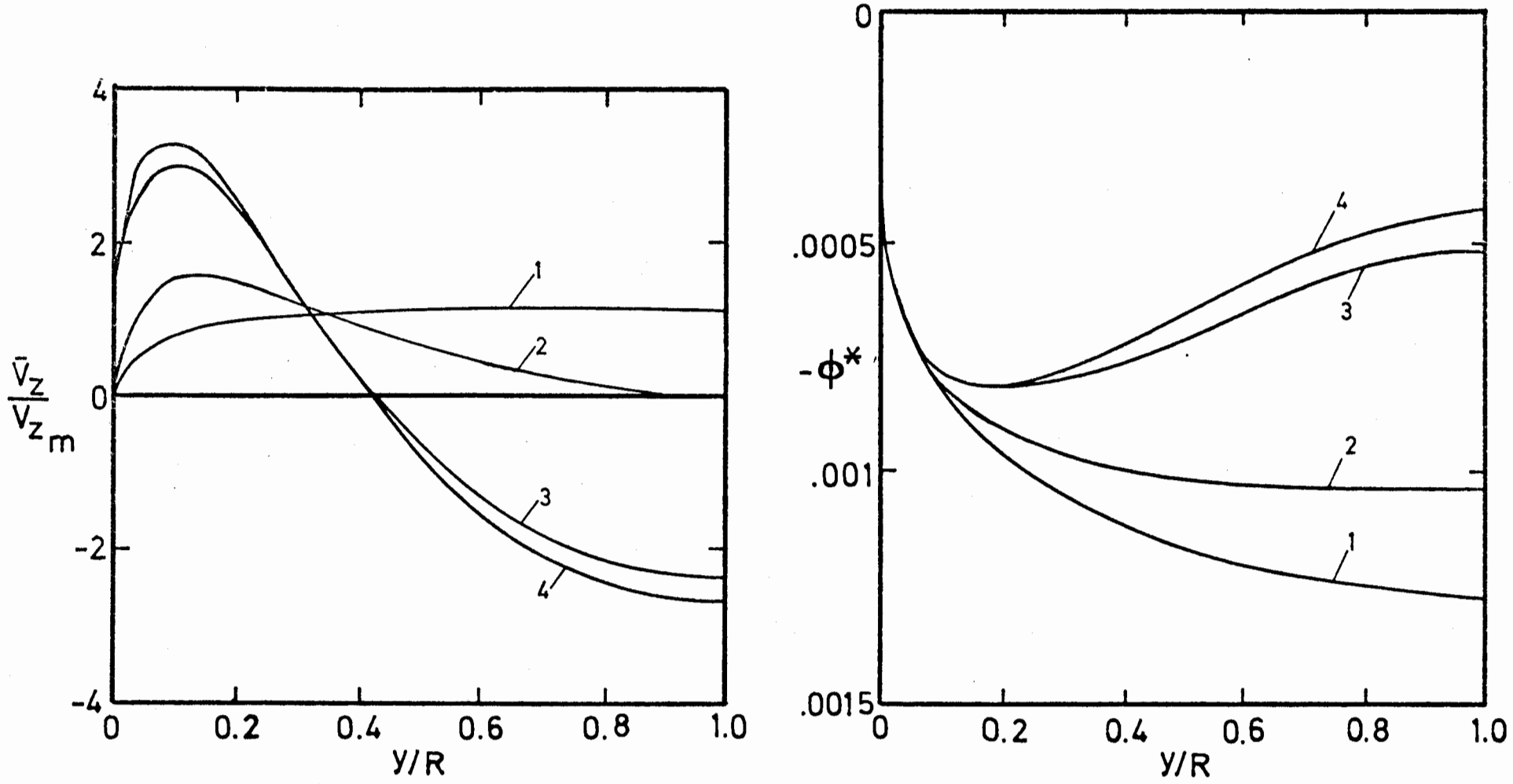

FIGURE 1.2 DISTORTED VELOCITY AND TEMPERATURE PROFILES FOR TURBULENT FLOW PREDICTED BY OJALVO AND GROSH [21]

Profiles are for Re* = 10 000 and Pr = 1.0

Ra = 0, 16, 81 and 100 for profiles 1 to 4 respectively

into account. Surprisingly, however, no attempt was made by Martinelli et al to include in their equation a factor allowing for variable viscosity effects and it was not until thirteen years later that their analysis was extended by Pigford [27] to take account of these effects. The agreement between experimental results and Pigford's predicted Nusselt number values was still not satisfactory but no better prediction has yet been proposed.

b) Uniform heat flux:

In general, predictions for the constant heat flux case have been more successful than those for the uniform wall temperature condition discussed above. Thus Hallman [8,16] and Brown [9] were both able to show good agreement between their experimental measurements and the Nusselt numbers obtained from their analyses for fully developed flow (see section 1.2.3). Recently these analyses have been investigated in more detail by other workers, two of the more interesting studies being those of Iqbal et al [28] and Mitsuishi et al [29]. Iqbal et al investigated the assumption made by Brown and Hallman that viscous dissipation terms could be neglected and showed that this was a valid approximation except, possibly, under conditions of high heat input when errors of up to 6% in predicted Nusselt numbers could result. Mitsuishi et al questioned another of Brown's and Hallman's assumptions, that of constant viscosity, and modified the analysis to allow viscosity to vary. Their final equation took the form

$$Nu = 1.411\ F\ (Gz\gamma)^{1/3} \qquad (1.1)$$

where F is a function of Gz, and γ a complicated function of Gz, Gr/Re and ε, a heat flux parameter. This prediction was tested against experimental data measured in water, where free convection effects had the greater influence on Nusselt number values, and also against data taken in sugar solutions, where viscosity effects were more important. The good agreement between measured and predicted values in both these cases suggests that Mitsuishi's analysis is the most accurate so far proposed for the uniform heat flux case, and should be used in preference to those of Brown and Hallman.

ii) Experimental work: A number of experimental measurements have already been referred to above, either directly where they were part of a combined theoretical and experimental investigation, or indirectly where they were used to produce an empirical correlation. Besides these there are a few other experimental measurements of interest and these are discussed below.

Kemeny and Somers [7] measured local Nusselt numbers in water and oil under constant heat flux conditions. No direct comparison with predicted values was attempted but the observed increase of Nusselt number values with increasing Rayleigh numbers is in agreement with the theoretically predicted trend.

Measurements in air for the constant wall temperature case have been made by Jackson et al [30] and Brown and Gauvin [3]. Little can be concluded from their reported values, however, as the results of Jackson et al are compared only with the Martinelli equation, from which they differ markedly, while Brown and Gauvin's measurements were made in a developing flow.

The only other relevant paper dealing with Nusselt numbers in laminar flows is that by Petukhov et at [31] which presents an extensive series of experimental local Nusselt number measurements. These were obtained under constant heat flux conditions in upward flows of water in a long ($^{L}/_{D}$ = 99) tube and readings were taken over a wide range of Rayleigh numbers at a number of points up the tube. Nusselt numbers were observed to vary along the tube and although no theory existed with which these developing values could be compared, the final limiting values agree well with those predicted by Hallman [8] for fully developed conditions. The results were correlated within ± 8% by the expression

$$\frac{Nu}{Nu_v} = \left(1 + \frac{Ra}{B}\right)^{0.27} \qquad (1.2)$$

where Nu_v is the value of Nu as Ra → 0

$$B = 1.35/X + 78X^{0.25} \qquad (X < 0.07)$$

$$B = 60 \qquad (X > 0.07)$$

and $X = (1/Pe)(L/D)$

which implies that the ratio Nu/Nu_v will increase steadily with increasing Rayleigh number, a trend in agreement with theoretical predictions.

One further point of importance emerges from this paper, and that is that the point of transition from laminar to turbulent flow depended on whether or not the test-section was preceded by a calming length. It is therefore clear that future analyses of developing laminar flows will have to allow in some way for varying entrance conditions.

1.2.6 Nusselt numbers - Turbulent flow.

i) Theoretical work: Theoretical and empirical Nusselt number predictions for turbulent flows are limited to those of Ojalvo and Grosh [21] and of Sherwin [32]. Ojalvo and Grosh obtained Nusselt numbers from their prediction, reviewed in section 1.2.4, for fully developed flow under constant heat flux conditions. The value of their results, however, is doubtful, since they suggest that the importance of free convection effects increases with increasing Reynolds number, a trend opposite to that occurring in practice. Sherwin also analysed the constant heat flux case but his main assumption, that buoyancy forces are concentrated in the laminar layer and tend to decrease its thickness, is not borne out by experiment. In addition, his equation predicts a steady increase of Nusselt number with increasing free convection effects, which is also not observed in practice.

It appears, therefore, that no accurate method of predicting turbulent flow Nusselt numbers is at present available and so the experimental work reported in the next section assumes additional importance.

ii) Experimental work: Experimental measurements of Nusselt numbers in turbulent flows are also limited and apart from the entrance region uniform wall temperature measurements of Brown and Gauvin [3] and Eckert et al [6,33,34], which have little bearing on the present investigation, there remain only the measurements of Petukhov and his co-workers [35,36]. Petukhov and Nolde [35] are reported by Sherwin [32] to have suggested the equation

$$Nu = 0.35\ Re^{0.3}\ Gr^{0.48} \left(\frac{D}{L}\right)^{0.48} \qquad (1.3)$$

as fitting their measured data, but this equation fails to follow the trend of later measurements by Petukhov and Strigin [36].

The latter authors carried out an investigation very similar to that by Petukhov et al [31] (discussed in section 1.2.5) except that it was performed in turbulent and not laminar flow. Distilled water was used as the test fluid, a boundary condition of constant heat flux was applied and Nusselt number measurements were made at a number of points along the tube. The results were found to be correlated within ±10% by the plot of Nu/Nu_T against Ra/Re^2 shown in Fig. 1.3. This plot was well described by the equation

$$\frac{Nu}{Nu_T} = \left(1 + B\,\frac{Ra}{Re^2}\right)^{-1} \quad \left(\frac{Ra}{Re^2} < 3 \times 10^{-4}\right) \qquad (1.4)$$

where B takes the value of 1.15×10^4 when a calming section is present and 1.5×10^3 when it is absent and Nu_T is the value of the Nusselt number at the limiting condition of no heat input. For values of Ra/Re^2 greater than 3×10^{-4} the single equation

$$\frac{Nu}{Nu_T} = 10(Ra/Re^2)^{1/3} \qquad (1.5)$$

correlates the data in both cases.

From these results two important conclusions can be drawn. The first is that the result of increasing free convection effects is initially to decrease turbulent flow Nusselt numbers to as little as 50% of their "isothermal" values, before any increase similar to that predicted by theory is observed. The second conclusion is that whereas Nusselt numbers on the decreasing portion of the curve are strongly dependent on inlet conditions, those on the rising portion of the curve are not.

iii) Conclusion: It is apparent from the papers reviewed in i) and ii) above that much remains to be learnt about turbulent flow Nusselt numbers and that many more measurements, under carefully controlled entrance conditions, may be necessary before satisfactory predictions can be developed.

1,2,7 Definition of boundaries of mixed convection.

In order to apply the results of the investigations discussed previously it is important to know when mixed convection conditions can be expected to occur. Clearly, insufficient information is presently available for the exact boundaries between free, mixed and forced convection regions to be drawn, but the attempts which have

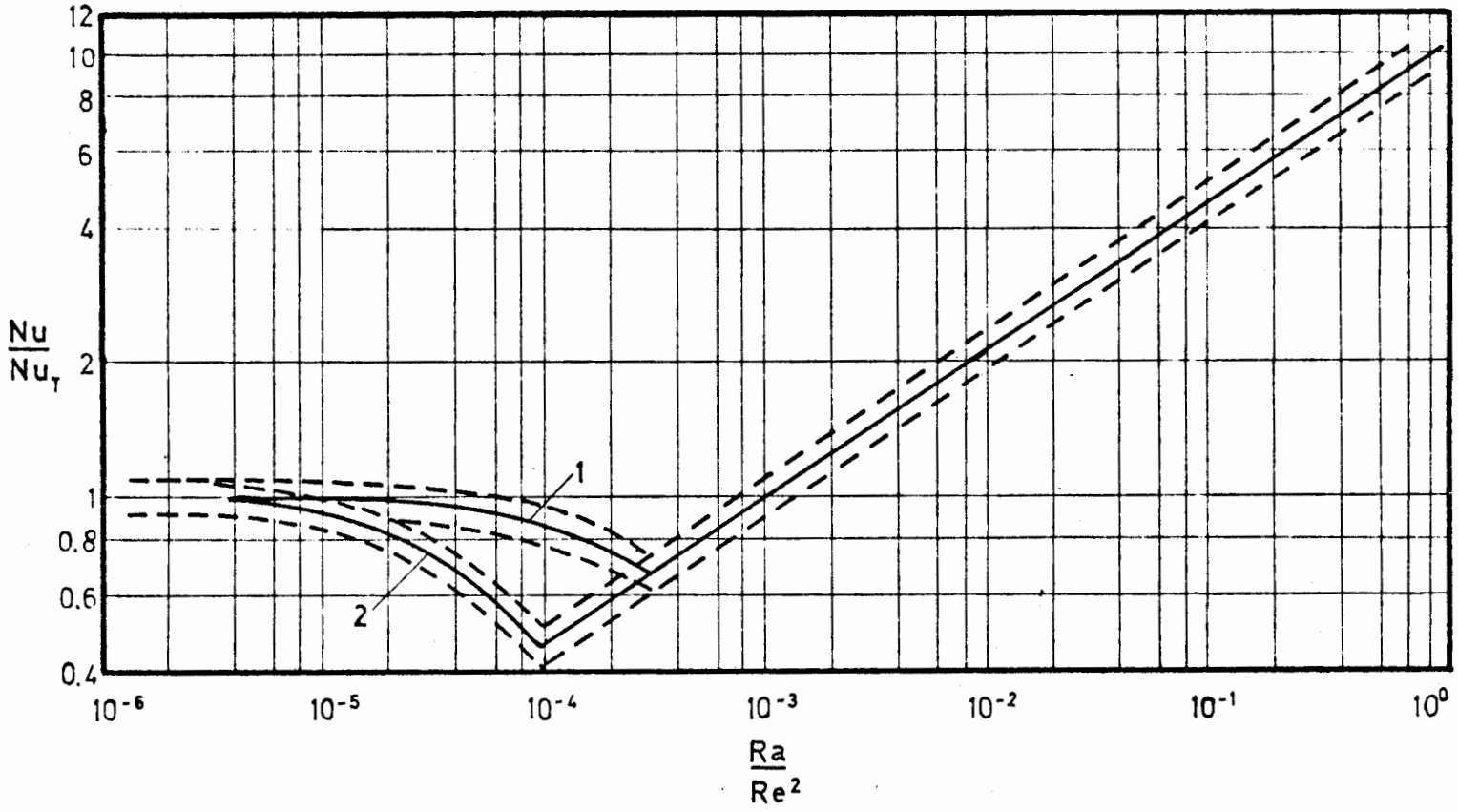

FIGURE 1.3 VARIATION OF Nu/Nu_T WITH Ra/Re^2 - FROM [36]

1 : Calming length present

2 : Calming length absent

been made to define these boundaries are nevertheless valuable. Of these attempts, the most important is that by Metais [2,37], who suggested that the limits of the mixed convection region should be given by the conditions under which a 10% variation from the pure forced or pure free convection Nusselt number occurred. These limits are shown on the plot of Reynolds number against the parameter $GrPr\,\frac{D}{L}$ given in Fig. 1.4. Although inaccurate in a number of respects - for example, it fails to allow for the Nusselt number behaviour observed by Petukhov et al [36] - this plot will probably remain in use until sufficient information is available to prepare a similar figure based on a more fundamental criterion such as velocity profile shape.

1.3 THEORY.

1.3.1 Introduction

Flows subject to both free and forced convective forces can be described by appropriate forms of the equations of continuity, motion and energy. For laminar flows the Navier-Stokes equations, derived in terms of instantaneous values, apply directly and can be used [16] to predict velocity and temperature profiles. For turbulent flows, however, the applicable equations are more involved, containing additional terms, such as $\overline{v_r t}$ and $\overline{v_r v_z}$, about which further information is needed before the equations can be solved to give velocity and temperature distributions. Since the statistical theory of turbulence has not yet been developed to the point where the values of these additional terms, $\overline{v_r t}$ and $\overline{v_r v_z}$, can be accurately predicted, the terms have either to be determined directly by experiment or else related to some other experimentally determinable quantity. In practice the latter method is used and $\overline{v_r v_z}$ and $\overline{v_r t}$ are customarily represented in terms of eddy diffusivities of momentum and heat, ε_M and ε_H respectively, defined by

$$\overline{v_r v_z} = -\varepsilon_M \frac{d\overline{V}_z}{dr} \qquad (1.6)$$

$$\overline{v_r t} = -\varepsilon_H \frac{d\overline{T}}{dr} \qquad (1.7)$$

For fully developed non-distorted turbulent pipe flows,

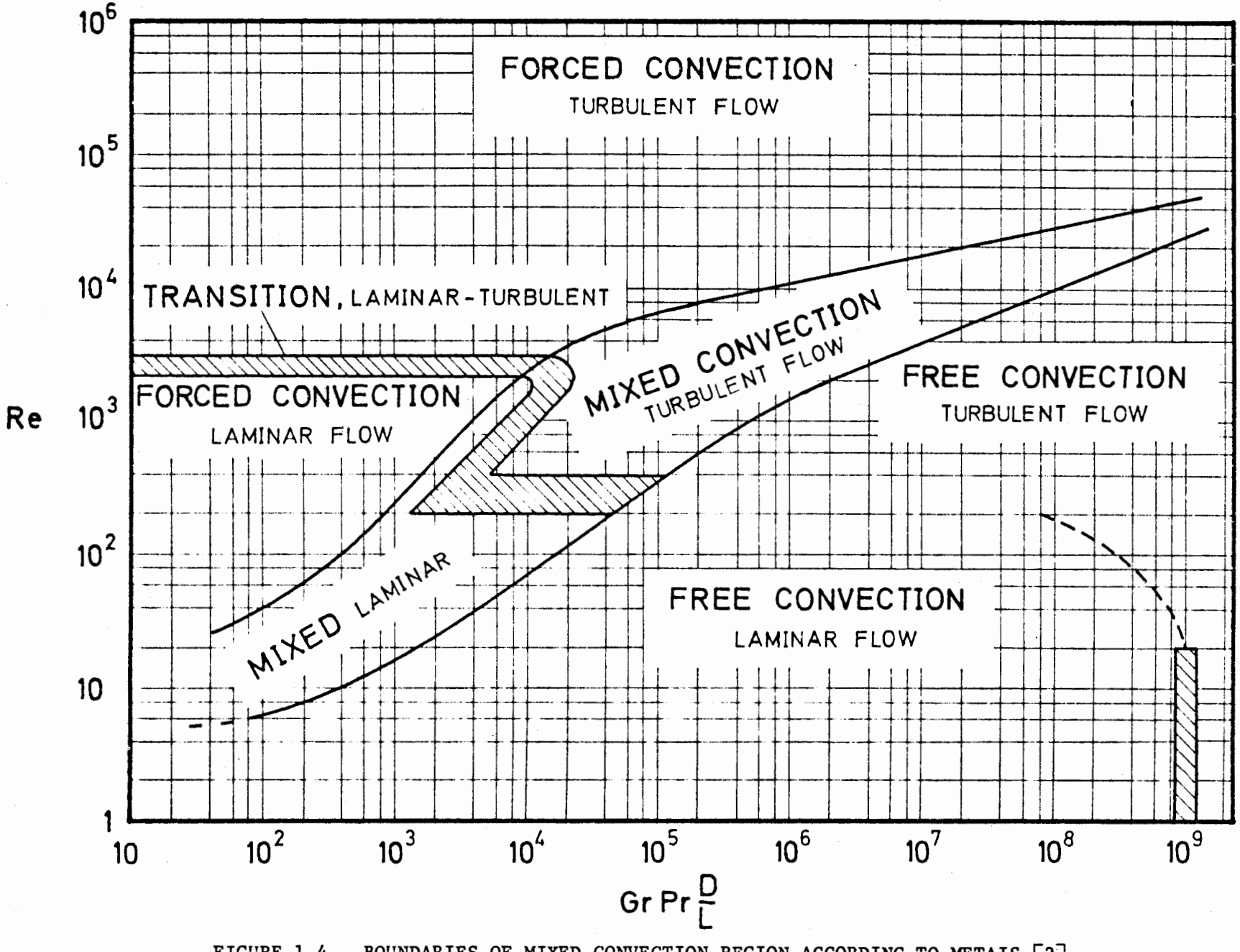

FIGURE 1.4 BOUNDARIES OF MIXED CONVECTION REGION ACCORDING TO METAIS [2]

sufficient experimental values for ε_M and ε_H are available for eddy diffusivity predictions of reasonable accuracy to be made. However, under mixed convection conditions the lack of accurate experimental velocity and temperature profiles has prevented the development of any generalised eddy diffusivity predictions.

The present investigation represents part of an attempt to obtain more information about velocity and temperature profiles, and hence about eddy diffusivities, for the particular case of turbulent upward flow of air under mixed convection conditions. Under such conditions the complete forms of the continuity, motion and energy equations are considerably more involved than the corresponding equations for turbulent incompressible flows with constant fluid properties [43]. The derivations of the applicable forms of these equations are, in consequence, rather lengthy and only the final equations are given here; the details of the derivations together with the simplifying assumptions involved can be found in Appendix A.

1.3.2 The continuity equation.

The following form of the continuity equation is derived in Appendix A :

$$\underset{\text{I}}{-\frac{1}{r}\frac{\partial}{\partial r}(-r\rho_M\beta\overline{v_r t})} \quad \underset{\text{II}}{-\frac{\partial}{\partial z}[\rho\overline{V}_z} \quad \underset{\text{III}}{-\rho_M\beta\overline{v_z t}]} \quad = \quad 0 \qquad (1.8)$$

and this equation differs from the usual form of the continuity equation for compressible flows,

$$\frac{\partial}{\partial z}(\rho V_z) \quad = \quad 0 \qquad (1.9)$$

by including terms I and III. The form of these terms results from the use of the expression

$$\rho \quad = \quad \rho_M[1-\beta(T-T_M)] \qquad (1.10)$$

as they are in fact equivalent to terms containing time-averaged products of fluctuating velocity and fluctuating density components.

1.3.3 The equation of motion

a) The equation for non-isothermal flow

The final form of the equation of motion obtained in Appendix A is:

$$\underset{I}{\left(-\overline{v_r v_z}\right)}\ \underset{II}{\left(\frac{D}{2\nu}+\frac{\partial \overline{V}_z}{\partial \eta}\right)}$$

$$= -\frac{D}{2\eta\mu}\underset{III}{\int_o^\eta \left(\rho_M \beta \overline{v_r t}\,\frac{\partial \overline{V}_z}{\partial \eta} - 2I_1\right)\eta d\eta}$$

$$+\frac{D}{2\eta\mu}\underset{IV}{\int_o^\eta \left(\frac{\overline{V}_z}{\eta}\frac{\partial}{\partial \eta}\eta\rho_M \beta \overline{v_r t} - 2I_2\right)\eta d\eta}$$

$$-\frac{D^2}{4\eta\mu}\underset{V}{\int_o^\eta \left(\overline{V}_z^2\frac{\partial \rho}{\partial z} - 2I_3\right)\eta d\eta} + \underset{VI}{\eta\frac{\mu_w}{\mu}\left(\frac{\partial \overline{V}_z}{\partial \eta}\right)_w}$$

$$-\frac{D^2}{4\eta\mu}\rho_M \beta g \underset{VII}{\int_o^\eta (\overline{T}-T_M)\,\eta d\eta} \qquad (1.11)$$

which was used to compute values of $\overline{v_r v_z}$ from measured data. Eddy diffusivity of momentum values were determined in a similar fashion by making use of the relationship

$$\left(1+\frac{\varepsilon_M}{\nu}\right)\frac{\partial \overline{V}_z}{\partial \eta} = \left(-\overline{v_r v_z}\ \frac{D}{2\nu} + \frac{\partial \overline{V}_z}{\partial \eta}\right) \qquad (1.12)$$

which follows from equation (1.6).

Because the origin and significance of some of the terms in equation (1.11) may not be immediately apparent the terms I to VII are discussed below:

I = the turbulent shear stress term, which is related to the eddy diffusivity of momentum term in equation (1.12).

II = a term representing the viscous shear stress contribution to the momentum balance.

III & IV = terms originating from the product of the fluctuating density and fluctuating radial and axial velocity components (See Appendix A). These are often small enough to be neglected except at the point of maximum velocity in distorted flows (See Chapter 5).

V = a term allowing for the effect of the flow expansion caused by the axial temperature gradient. The numerical contribution of this term is of the same order of magnitude as that of terms III and IV.

VI = the pressure drop term, expressed in terms of the wall shear stress

VII = a term describing the local effect of the buoyancy forces.

b) The equation for isothermal flow

For the special case of isothermal flow all but one of the terms on the right-hand side of equation (1.11) fall away, giving

$$\left(-\overline{v_r v_z}\,\frac{D}{2\nu}+\frac{\partial \overline{V}_z}{\partial \eta}\right) = \eta\left(\frac{\partial \overline{V}_z}{\partial \eta}\right)_w \qquad (1.13)$$

or, in terms of ε_M,

$$\left(\frac{\varepsilon_M}{\nu}+1\right)\frac{\partial \overline{V}_z}{\partial \eta} = \eta\left(\frac{\partial \overline{V}_z}{\partial \eta}\right)_w \qquad (1.14)$$

c) The isothermal equation in terms of the friction factor

In order to obtain eddy diffusivities using equation (1.14), however, it is customary to express the right-hand side of that equation in terms of the friction factor f, which is given by the relationship [131]

$$\frac{1}{\sqrt{f}} = 4.0 \log_{10}\left(\mathrm{Re}\sqrt{f}\right) - 0.4 \qquad (1.15)$$

f is related to the wall shear stress, τ_w, by [43]

$$u^* = \overline{V}_{av}\sqrt{\frac{f}{2}} = \sqrt{\frac{\tau_w}{\rho}} \qquad (1.16)$$

and τ_w, in turn is related to the slope of the velocity profile at the wall $\left(\frac{\partial \overline{V}_z}{\partial \eta}\right)_w$ by the definition

$$\tau_w = -\mu\left(\frac{\partial \overline{V}_z}{\partial r}\right)_w \qquad (1.17)$$

Hence $$\eta\left(\frac{\partial \bar{V}_z}{\partial \eta}\right)_w = -\frac{\eta \tau_w D}{2\mu}$$

$$= -\frac{D\eta}{2\mu}\rho\bar{V}_{av}^2\frac{f}{2}$$

$$= -0.25\ f\ Re\ \bar{V}_{av}\eta \qquad (1.18)$$

and equation (1.14) becomes

$$\left(\frac{\varepsilon_M}{\nu} + 1\right)\frac{\partial \bar{V}_z}{\partial \eta} = -0.25\ f\ Re\ \bar{V}_{av}\eta \qquad (1.19)$$

which is the equation used to calculate values of ε_M from measured isothermal velocity profiles.

d) The non-isothermal equation in terms of the friction factor

If the assumption is made that the relationship (1.16) is valid also for non-isothermal flow, a relationship corresponding to equation (1.18) can be written by which non-isothermal eddy diffusivities can be related to a non-isothermal friction factor. This relationship

$$\eta\frac{\mu_w}{\mu}\left(\frac{\partial \bar{V}_z}{\partial \eta}\right)_w = -0.25\ f\ Re\ \bar{V}_{av}\frac{\mu_{av}}{\mu}\eta \qquad (1.20)$$

is used in Chapter 5 to calculate non-isothermal friction factors from measured values of the slope of the velocity profile at the pipe wall.

1.3.4 The energy equation

The final form of the energy equation derived in Appendix A is:

$$\underset{\text{I}}{\left(\frac{D}{2\alpha}\overline{v_r t}\right)} - \underset{\text{II}}{\left(\frac{\partial \bar{T}}{\partial \eta}\right)} = \underset{\text{III}}{\frac{D^2}{2\eta k}C_p\frac{d\bar{T}}{dz}\int_0^\eta(\rho\bar{V}_z)\,\eta d\eta} - \underset{\text{IV}}{\frac{D^2}{2\eta k}\int_0^\eta\left(\bar{V}_z\frac{d\bar{p}}{dz}\right)\eta d\eta} - \underset{\text{V}}{\frac{D}{2\eta k}\rho_M\beta C_p\int_0^\eta\left(\overline{v_r t}\frac{\partial \bar{T}}{\partial \eta}\right)\eta d\eta} \qquad (1.21)$$

which differs from the usual form of the turbulent energy equation by terms IV and V. For the low flow rates used in this investigation the term IV is several orders of magnitude smaller than term III and can be neglected; term V, however can take values of up to 5% of term III and cannot be disregarded. Despite the presence of term V equation (1.21) can still be solved, using an iterative method, and was employed in the present work to calculate values of $\overline{v_r t}$ from measured temperature distributions. Values of the eddy diffusivity of heat were calculated in a similar way by making use of the relationship

$$\left(1 + \frac{\varepsilon_H}{\alpha}\right)\frac{\partial \overline{T}}{\partial \eta} = \left(\frac{\partial \overline{T}}{\partial \eta} - \frac{D}{2\alpha}\overline{v_r t}\right) \qquad (1.22)$$

which follows from equation (1.7).

CHAPTER 2

HOT-WIRE ANEMOMETRY THEORY

2.1 INTRODUCTION.

2.1.1 The fundamental equation and King's Law.

The principle underlying all branches of hot-wire anemometry is that the rate of loss of heat from a heated wire situated in a flowing fluid depends on the velocity of the fluid past the wire. Other factors will also affect the rate of heat loss but by choosing suitable operating conditions it is possible, as explained below, to eliminate these factors from the operating equation.

According to Bruun [46,47], under conditions where the loss of heat occurs primarily by forced convection, as in the present investigation, (natural convection is controlling only at very low fluid velocities) the relationship between the heat loss from the wire and other parameters can be expressed in its most general form as

$$Nu = f(Re, Gr, Pr, Kn, M, \ell/d, T_w/T, \alpha)_f \qquad (2.1)$$

where Kn = Knudsen number

M = Mach number

α = angle between the velocity vector and the normal to the wire

and other symbols have their usual meaning. All properties are evaluated at the film temperature T_f.

For wires in isothermal air flows of moderate to low velocity Bruun showed that equation (2.1) simplified to

$$Nu = f(Re_f, \ell/d, \alpha) \qquad (2.2)$$

For a given wire of fixed ℓ/d, positioned normal to the flow direction (as was the case for all wires employed in the present investigation), equation (2.2) simplified further to

$$Nu = f(Re)_f \qquad (2.3)$$

which is customarily written in the form

$$Nu = A' + B'(Re_f)^n \qquad (2.4)$$

In order to transform this equation to provide a useful relationship between variables of practical importance, the hot-wire

must be operated at a constant value of the overheating ratio $\frac{R_w}{R_w - R_g}$, (where R_g and R_w are the wire resistances at the flow and operating temperatures respectively). It then follows that

a) The temperature difference between the wire and the flow is constant, which means that for steady operation the heat transfer coefficient, h, and hence the Nusselt number, Nu, will be directly proportional to the power, I^2R_w, supplied to the wire.

b) Since the flow is isothermal the only varying quantity in the Reynolds number is the velocity, V.

Therefore equation (2.4) can be written

$$\frac{I^2R_w}{R_w - R_g} = A + BV^n \qquad (2.5)$$

This equation with n = 0.5 was first proposed by King [48], and, as King's Law, has been the standard hot-wire equation for many years. It was found that one or, if necessary, two or three curves of the form of King's Law provided a completely satisfactory representation of the results obtained in the present investigation and this form of equation (2.5) was therefore used in the present work.

A number of other hot-wire equations have also been proposed and these are discussed in the section which follows.

2.1.2 Previous work.

Because of the importance of hot-wire anemometry in the study of turbulent flows a number of investigations of the flow around heated wires of small diameter have been carried out. The results of these investigations, which have generally been reported as expressions in the form of equation (2.4), are shown in Table 2.1.

It can be seen that the values proposed for A', B' and n vary considerably from equation to equation and this is attributed to the difficulties involved in making accurate measurements of quantities such as the mean wire diameter and the wire surface temperature. In practice the variations in A' and B' are of little importance as differences between actual hot-wires and the ideal

TABLE 2.1

DATE	INVESTIGATOR	EQUATION	RANGE
1914	King [48]	$Nu = 0.32 + 0.8Re^{0.5}$	$Re_f > 1.0$
1933	Hilpert [49]*	$Nu = C\left\{Re_f\left(\frac{T_w}{T_\infty}\right)^{0.25}\right\}^n$	Re_f / C / n: 1-4 / 0.891 / 0.33; 4-40 / 0.821 / 0.385; 40-4000 / 0.615 / 0.466
1946	Kramers [50]	$Nu = 0.42Pr^{0.2} + 0.57Pr^{0.33}Re_f^{0.5}$	$0.01 < Re_f < 10^4$
1954	McAdams [51]	$Nu = 0.32 + 0.43\ Re_{Mc}^{0.52}$	$Re_{Mc} = (\rho_\infty \bar{V} D)/\mu_f$
1956	van der Hegge Zijnen [52]	$Nu = 0.35 + 0.5Re_f^{0.5} + 0.001Re_f$	$10^{-1} < Re_f < 10^5$
1959	Collis and Williams [53]	$Nu = (A+BRe_f^n)\left(\frac{T_f}{T_\infty}\right)^{0.17}$	Re_f / A / B / n: .02-44 / 0.24 / 0.56 / 0.45; 44-140 / 0 / 0.48 / 0.51
1966	Tsubouchi and Masuda [54]*	$Nu = 0.36 + 0.48Re_f^{0.5}$	$0.5 < Re_f < 10^3$
1970	Hatton, James and Swire [55]	$Nu\left(\frac{T_f}{T_\infty}\right)^{-0.154} = 0.384 + 0.581Re_f^{0.439}$	$10^{-2} < Re_f < 40$

* Taken from Hatton et al [55].

wires used in the above investigations are large enough to make it necessary to determine A' and B' experimentally for each hot-wire. Variations in n, on the other hand, are important as the accuracy of the experimentally determined values of A' and B' depends on the correctness of the assumed value of n. Most of the workers quoted in Table 2.1 follow King [48] and use a value of n = 0.5; however, recently, Collis and Williams [53] have suggested that a value of 0.45 is more accurate and equation (2.5) with n = 0.45 (Collis' Law) has

been preferred to King's Law in a number of recent experimental fluid flow investigations. Though Collis' value of n = 0.45 is supported by the work of Hatton et al (n = 0.44), measurements by van Thinh [56], Kjellstrom [57] and Bruun [46] show that no single value for n is accurate since n is a function of fluid velocity which changes at an increasing rate as the fluid velocity is reduced. This was confirmed by the present work where a slight decrease of n with decreasing velocity was noted.

Equations to predict the way in which calibration curves deviate from a straight line as a result of this variation of n have been proposed by, among others, Kielbasa and Rysz [58] and Wasan et al [59]. These equations, however, have considerable disadvantages. The Kielbasa and Rysz expression is a relatively simple but inexact empirical relation which provides an approximate description of observed low velocity variations in terms of the calibration parameters A and B. The Wasan equation, on the other hand, is extremely complex, and though reported to be in good agreement with experimental measurements, is most cumbersome to use.

The conclusion drawn from a detailed study of the papers discussed above is that although ideally the variation of n with velocity should be determined for each individual hot-wire, in practice this makes the use of hot-wires extremely complicated. It also appears, however, that provided the range of velocities of interest is small, as in the present work, no significant errors are introduced by representing the power vs velocity curve (equation (2.5)) by one, or possibly a series of two or three equations in which n is kept constant.

To check on the effect of using different values of n in these equations, turbulence intensities were evaluated from one set of the present measurements by using first, a calibration equation involving $V^{0.5}$ and second, a calibration equation involving $V^{0.4}$. The difference in calculated results was not significant, a fact attributed to the small range of velocities involved, and it was decided that the advantages of using a fixed value of n = 0.5 - for which derivations of most of the turbulence intensity and other equations introduced later in this chapter were already available - far outweighed any slight increases in accuracy which the use of

another value for n might introduce. Accordingly the equation

$$\frac{I^2 R_w}{R_w - R_g} = A + BV^{0.5} \qquad (2.6)$$

was made the starting point for the development of the different relationships employed in the calculation of various turbulence quantities under both isothermal and non-isothermal conditions. These relationships are presented in later sections of this chapter.

2.1.3 Practical considerations in hot-wire anemometry.

Because a number of factors such as the finite length of the hot-wire, the presence of wire supports and the failure of actual hot-wires to meet the requirements for an ideal turbulence sensing element affect the operation of hot-wire equipment, a detailed review of these and other practical considerations is included in Appendix C of the present work.

2.2 THE AXIAL TURBULENCE INTENSITY EQUATION FOR ISOTHERMAL FLOW.

2.2.1 Derivation of the equation.

When a hot-wire is inserted into a fluctuating air flow the rate of loss of heat from the wire will vary as the air velocity, V, varies. If the constant-current mode of hot-wire operation is employed this means that the wire temperature, and hence the wire resistance, R_w, will vary correspondingly. Provided, therefore, that a relationship between velocity and wire resistance (or a related quantity such as e, the voltage drop across the wire) can be developed, the fluctuating signal from the hot-wire can be used to supply information on velocity fluctuations. Such a relationship is derived below, following Hinze [40], for the particular case of axial velocity fluctuations measured with a hot-wire normal to the flow.

The instantaneous values of V_z, the axial velocity and of R_w, the operating resistance, can be expressed in terms of mean and fluctuating quantities by

$$V_z = \bar{V}_z + v_z \qquad R_w = \bar{R}_w + r_w$$

These expanded forms are substituted into equation (2.5) to give

$$\frac{I^2(\bar{R}_w + r_w)}{(\bar{R}_w + r_w) - R_g} = A + B(\bar{V}_z + v_z)^{\frac{1}{2}} \qquad (2.7)$$

which can be written

$$\frac{I^2\bar{R}_w}{(\bar{R}_w - R_g)}\left(1 + \frac{r_w}{\bar{R}_w}\right)\left(1 + \frac{r_w}{\bar{R}_w - R_g}\right)^{-1} = A + B\bar{V}_z^{\frac{1}{2}}\left(1 + \frac{v_z}{\bar{V}_z}\right)^{\frac{1}{2}} \qquad (2.8)$$

Expanding both sides in a Taylor expansion gives

$$\frac{I^2\bar{R}_w}{(\bar{R}_w - R_g)}\left(1 + \frac{r_w}{\bar{R}_w}\right)\left(1 - \frac{r_w}{(\bar{R}_w - R_g)} + \frac{r_w^2}{(\bar{R}_w - R_g)^2} + \cdots\cdots\cdots\right)$$

$$= A + B(\bar{V}_z)^{\frac{1}{2}}\left(1 + \frac{v_z}{2\bar{V}_z} + \frac{1}{8}\left(\frac{v_z}{\bar{V}_z}\right)^2 + \cdots\cdots\right) \qquad (2.9)$$

Assuming low relative intensities of turbulence, i.e.

$$\frac{v_z}{\bar{V}_z} << 1$$

it follows that

$$\frac{r_w}{(\bar{R}_w - R_g)} << 1$$

(and hence $\dfrac{r_w^2}{\bar{R}_w(\bar{R}_w - R_g)} << 1$)

and the second-order and higher terms in equation (2.9) can be neglected. Multiplying out the terms on the left hand side, equation (2.9) then becomes

$$\frac{I^2\bar{R}_w}{(\bar{R}_w - R_g)}\left(1 - \frac{r_w}{(\bar{R}_w - R_g)} + \frac{r_w}{\bar{R}_w} - \frac{r_w^2}{\bar{R}_w(\bar{R}_w - R_g)}\right)$$

$$= A + B(\bar{V}_z)^{\frac{1}{2}}\left(1 + \frac{v_z}{2\bar{V}_z}\right) \qquad (2.10)$$

The term $\frac{r_w^2}{\bar{R}_w(\bar{R}_w-R_g)}$ is small and can be neglected (see above) and equation (2.10) then rearranges to

$$\frac{I^2\bar{R}_w}{(\bar{R}_w-R_g)}\left(1-\frac{\bar{R}_w r_w-\bar{R}_w r_w+R_g r_w}{(\bar{R}_w-R_g)\bar{R}_w}\right) = A + B(\bar{V}_z)^{\frac{1}{2}}\left(1+\frac{v_z}{2\bar{V}_z}\right) \qquad (2.11)$$

which simplifies to

$$\frac{I^2\bar{R}_w}{(\bar{R}_w-R_g)}\left(1-\frac{R_g r_w}{(\bar{R}_w-R_g)\bar{R}_w}\right) = A + B(\bar{V}_z)^{\frac{1}{2}}\left(1+\frac{v_z}{2\bar{V}_z}\right) \qquad (2.12)$$

Subtracting from equation (2.12) the steady state equation

$$\frac{I^2\bar{R}_w}{(\bar{R}_w-R_g)} = A + B(\bar{V}_z)^{\frac{1}{2}}$$

gives

$$-\frac{I^2 R_g r_w}{(\bar{R}_w-R_g)^2} = B(\bar{V}_z)^{\frac{1}{2}}\frac{v_z}{2\bar{V}_z} \qquad (2.13)$$

The change e in voltage across the hot-wire is therefore given by

$$e = Ir_w = -\frac{(\bar{R}_w-R_g)^2}{2IR_g}B(\bar{V}_z)^{\frac{1}{2}}\frac{v_z}{\bar{V}_z} \qquad (2.14)$$

Defining the sensitivity, s*, of the hot-wire to velocity fluctuations by

$$\sqrt{\overline{e^2}} = s^*\sqrt{\overline{v_z^2}} \qquad (2.15)$$

gives

$$s^* = \frac{(\bar{R}_w-R_g)^2}{2IR_g}\frac{B\sqrt{\bar{V}_z}}{\bar{V}_z} \qquad (2.16)$$

and

$$e = -s^* v_z \qquad (2.17)$$

and these equations provide the desired expression relating the fluctuations in wire resistance (the value of the fluctuating voltage is directly related to the wire resistance for constant current operation) to velocity fluctuations.

In practice, however, this relationship is affected by various factors, of which the four most important are

i) the finite thermal inertia of the wire
ii) the heat conduction to the supports
iii) the non-uniform velocity distribution along the wire
iv) the effect of large turbulent fluctuations.

These are discussed in the following sections.

2.2.2 Thermal inertia

It has been shown [40] that for the case of a hot-wire with finite thermal inertia the sensitivity, s*, of the hot-wire, for a velocity fluctuation of frequency, ω, is reduced to

$$s^* = \frac{1}{\sqrt{1+\omega^2 M^2}} \cdot \frac{(\bar{R}_w - R_g)^2 \, B\bar{V}_z^{\frac{1}{2}}}{2IR_g\bar{V}_z} \qquad (2.18)$$

where M is the "time constant" of the wire. From equation (2.18) it can be seen that the hot-wire will respond accurately to low frequency fluctuations but as the frequency is increased the frequency response of the wire decreases.

In practice this effect can be compensated for by first measuring the time constant of the hot-wire, and then using this information to adjust the gain of a compensation amplifier so as to exactly offset the effect of the decreasing frequency response. Such a method was employed in the present investigation.

2.2.3 Heat conduction to the probe supports.

This effect is most important for low values of the hot-wire length to diameter ratio, as discussed in Appendix C. The wires used in the present work were relatively long ($\ell/d \approx 500$ to 600), however, and according to Champagne et al [60] heat conduction effects for wires as large as this are negligible.

2.2.4 Velocity distribution along the wire.

Hinze [40] states that to obtain a uniform velocity distribution along the wire, the length of the hot-wire should be less than the microscale of turbulence. This conflicts with the requirements of section 2.2.3 and the whole question of choosing the optimum value for the ℓ/d ratio is discussed in detail in Appendix C.

A correction for the effect of wire length on hot-wire measurements has been proposed by Frenkiel [61] but before it can be evaluated for the flows investigated here, the length of the microscale for these flows needs to be established.

2.2.5 The effect of large turbulent fluctuations.

Because the heat loss from a hot-wire is proportional to the square root of the velocity and not to the velocity itself, it follows that the hot-wire response to a negative velocity fluctuation differs from the response to a positive velocity fluctuation of equal magnitude. This difference increases with increasing relative intensity and an estimate by Schubauer and Klebanoff [62] of the errors in measured $v'_z/\overline{V}_z$ values introduced in this way is given below

$\frac{v'_z}{\overline{V}_z}$	Percentage error
0.1	0.2
0.15	1.5
0.2	7
0.25	12.5
0.3	19

It can be seen that the error is negligible for intensities less than 0.1 and well within the limits of experimental error (see Chapter 4) for intensities less than 0.2. Since the intensities are less than 0.2 over the inner 90% of the pipe for isothermal flow (and over an even greater percentage of the pipe cross-section for most non-isothermal flows) this error is likely to be significant only in the region near the wall where uncertainties in measured values are in any case generally greatest.

2.3 MEAN VELOCITY CORRECTIONS AT HIGH TURBULENCE INTENSITIES.

Provided the intensity of turbulence is less than a certain

value, usually taken as 0.1† [40], the effective cooling velocity over the wire and the mean velocity $\bar{V}_z$ can be assumed equal without introducing significant inaccuracies. Where intensities exceed 0.1, however, the contributions of the radial and axial turbulent velocity fluctuations to the effective velocity, V_{eff}, can no longer be ignored. (It has been shown [60] that for wires normal to the mean flow direction the contribution of velocity fluctuations parallel to the wire axis, in this case $\overline{v_\theta^2}$, to the effective cooling velocity is negligible.) Equation (2.6) must therefore be rewritten as

$$\frac{I^2 R_w}{R_w - R_g} = A + B V_{eff}^{0.5} \tag{2.19}$$

where

$$V_{eff} = \left[(\bar{V}_z + v_z)^2 + v_r^2\right]^{0.5} \tag{2.20}$$

Expanding this latter equation as shown in Appendix C, section C.3.1, leads to the relationship

$$V_{meas} \simeq \bar{V}_z \left\{ 1 - \frac{1}{4} \frac{\overline{v_z^2}}{\bar{V}_z^2} + \frac{1}{2} \frac{\overline{v_r^2}}{\bar{V}_z^2} \right\} \tag{2.21}$$

which was used in this work, as explained in Appendix G, to correct the isothermal velocity measurements reported in Chapter 4.

An alternative expression

$$\bar{V}_{meas} = \bar{V}_z \left(1 - \frac{3}{16} \frac{\overline{v_z^2}}{\bar{V}_z^2} \right) \tag{2.22}$$

was used by Laufer [63] but since this equation fails to take variations of $v_r^2/\bar{V}_r^2$ into account, equation (2.21) was preferred.

---

† The correction to the mean velocity applied when relative intensities of turbulence exceed 0.1 should not be confused with the correction in the same range of relative turbulence intensities which is applied to turbulence intensity measurements in section 2.2.5.

2.4 MEASUREMENTS WITH A HOT-WIRE IN HEATED FLOWS.

2.4.1 Introduction.

In making measurements of mean velocity with a hot-wire under non-isothermal conditions the same basic equation (equation (2.6)) as was used in isothermal flows, still applies. In the non-isothermal case, however, the temperature dependency of the calibration parameters A and B has to be allowed for, and this introduces a number of problems, discussed in more detail in the section which follows.

The measurement of turbulence quantities in heated flows involves procedures more complicated than those employed in isothermal flow measurements and methods employed to separate the individual contributions of velocity fluctuations and temperature fluctuations to the measured hot-wire signal are considered in section 2.5.

2.4.2 The temperature dependence of the calibration parameters A and B.

Because the exact mechanism of heat transfer from a hot-wire is not known the temperature dependence of the constants A and B in equation (2.6) was for a long time uncertain. This uncertainty was not helped by the fact that equations, such as those of Betchov [64] and Hinze [40], which attempted to predict the variation of A and B with temperature were contradicted by the only experimental evidence available. Lawn [65] made this clear, stating that whereas a rise of 0.1% in A per ^{o}C increase in temperature is predicted by theory, the experimental results of Cooper and Collis indicate a decrease of 0.15% per ^{o}C in the value of A.

It is therefore obvious that either the theoretical predictions or the experimental measurements are in error and the investigation described in Appendix E was carried out in an attempt to determine where the errors lay. The results of this investigation were not entirely satisfactory but they did show conclusively that the theoretically predicted trend in the variation of A was correct and that previous experimental results were in error. Furthermore, they showed that the observed variations of A - approximately 0.05% per ^{o}C - could be represented within the limits of experimental error by the equation of Hinze, derived in Appendix C and given

below:

$$\frac{I^2R_w}{R_w-R_g} + A_g\left[1 + \frac{a_1}{2(a+a_1T_g)\beta R_0}(R_w-R_g)\right] + BV_z^{0.5} \qquad (2.23)$$

The value of B in this equation is taken to be independent of temperature, an assumption which is confirmed by the observation, made during the course of this investigation, that calibration curves measured at different overheating ratios had slopes which were identical.

Since the variation of A (which in any case was relatively small) was reasonably well represented by equation (2.23), this equation was used to calculate the non-isothermal velocity profiles given in Chapter 5. A detailed calculation showing how it was applied can be found in Appendix I.

2.5 MEASUREMENT OF NON-ISOTHERMAL TURBULENCE QUANTITIES.

2.5.1 The fundamental equation.

In order to obtain values for the longitudinal velocity intensities and for the temperature intensities it is necessary to develop an equation relating the fluctuations of the voltage across the wire to the fluctuations of temperature and velocity. The derivation of such an equation can be found in Appendix C, section C.3.3, and leads to the equation

$$\overline{e^2} = s^2\overline{v_z^2} + s_t^2\overline{t^2} - 2ss_t\overline{v_z t} \qquad (2.24)$$

where s and s_t, the sensitivities of the hot-wire to velocity and temperature fluctuations respectively, are given by

$$s = \frac{1}{(1+PK)} \frac{(\bar{R}_w - \bar{R}_g)^2 B\bar{V}_z^{0.5}}{2I\bar{R}_g\bar{V}_z} \qquad (2.25)$$

$$s_t = \frac{(1-P)}{(1+PK)} \frac{\beta I\bar{R}_w R_0}{\bar{R}_g} \qquad (2.26)$$

and P and K are given by the expressions

$$P = \left(\frac{A_0 a_1}{2(a+a_1 T_0)\beta R_0} \right) \Big/ \left(\frac{\bar{A}_f + B\bar{V}_z^{0.5}}{\bar{R}_w - \bar{R}_g} \right) \qquad (2.27)$$

$$K = \frac{\bar{R}_w}{\bar{R}_g} \qquad (2.28)$$

If equations (2.25) and (2.26) are compared with the corresponding equations given by Hinze [40], it will be seen that the present equations differ from Hinze's equations by the factors in P and K. The importance of these differences is considerable and in Appendix C, section C.4, it is shown that the two sets of equations can give rise to sensitivities differing by up to 30%.

Equation (2.24) provides the desired relationship between observed fluctuations of the voltage, e, across the hot-wire and the values of $\overline{t^2}$ and $\overline{v_z^2}$ and also of $\overline{v_z t}$. In theory by determining $\overline{e^2}$, s and s_t at three different overheating ratios, three equations can be set up and solved for $\overline{t^2}$, $\overline{v_z^2}$ and $\overline{v_z t}$. In practice this technique is very sensitive to even slight experimental inaccuracies [66] and the method outlined in section 2.5.2 gives very much more accurate results.

Should only the value of $\overline{t^2}$ be of interest, it can be determined by operating the hot-wire at a very low overheating ratio. Under such conditions $(\bar{R}_w - \bar{R}_g)$ becomes very small and the value of s tends to zero. Hence equation (2.24) becomes

$$\overline{e^2} = s_t^2 \overline{t^2} \qquad (2.29)$$

from which $\overline{t^2}$ can be easily and accurately obtained.

2.5.2 Determination of $\overline{t^2}$, $\overline{v_z^2}$ and $\overline{v_z t}$ in practice.

The method followed was that recommended by Arya and Plate [67], based on work by Morkovin [68] and Kovasznay [69]. This method is described below.

If equation (2.24) is divided by s_t^2 it becomes

$$\frac{\overline{e^2}}{s_t^2} = \overline{v_z^2}\left(\frac{s}{s_t}\right)^2 - 2\overline{v_z t}\,\frac{s}{s_t} + \overline{t^2} \qquad (2.30)$$

which, by defining

$$X = \frac{s}{s_t} \qquad \text{and} \qquad Y = \frac{\overline{e^2}}{s_t^2}$$

can be rewritten in the form

$$Y = \overline{v_z^2}\, X^2 - 2\overline{v_z t}\; X + \overline{t^2} \tag{2.31}$$

Equation (2.31) is a parabola with abscissa X and ordinate Y whose shape can be determined by measuring as many X and Y values as possible and fitting the best parabola through them. It was shown [67], however, that experimental points become increasingly inaccurate as $X \to 0$ (i.e. as the overheating ratio $\to 0$) and since $\overline{t^2}$ and $\overline{v_z t}$ are defined principally by conditions near $X = 0$, they could still not be determined with sufficient accuracy.

To overcome this problem an independent measurement of $\overline{t^2}$ was made using the hot-wire as described in section 2.5.1 (Arya and Plate [67] employed a platinum resistance thermometer in their measurements). Equation (2.31) was then rearranged to

$$Z = \overline{v_z^2}\, X^2 - 2\overline{v_z t}\; X \tag{2.32}$$

where $Z = Y - \overline{t^2}$

Using this equation Arya and Plate found that consistent values of $\overline{v_z^2}$ and $\overline{v_z t}$ could be obtained from four to six (X, Z) points together with a value for $\overline{t^2}$. Following their recommendation, the value of $\overline{t^2}$ and values of Z and X at five different overheating ratios were used in the present work to determine $\overline{v_z^2}$ and $\overline{v_z t}$, the measured values of which are presented in Chapter 5.

CHAPTER 3

EXPERIMENTAL EQUIPMENT

3.1 INTRODUCTION

Measurements were taken in two different test loops, the second of which, Loop II, was an improved version of the earlier one, Loop I. The isothermal runs I-1 to I-17 and the non-isothermal runs N-1 to N-9 were obtained in Loop I while the later isothermal runs, IT-1 to IT-5, and the two sets of non-isothermal runs, N-10 to N-14, and NT-1 to NT-5, were measured in Loop II. The description which follows deals only with Loop II and its associated equipment since a full description of Loop I has been previously given by Brown [91]. All important differences between the two systems are, however, summarised later in this chapter.

Minor pieces of equipment, marked with an asterisk * in the text, are not described in this chapter, but full details are given in Appendix D.

3.2 TEST LOOP.

3.2.1 Preliminary considerations.

In selecting a suitable tube to use as a test-section two conditions had to be satisfied:-

i) The diameter of the tube had to be large in order that accurate measurements could be made in the flow regions close to the wall.

ii) The distance from the tube entrance to the measuring station had to be long enough for the flow to have attained a fully developed condition before reaching the measuring station. As is shown in Chapter 4, entrance length values of 40 to 60 diameters would be expected to apply in the present situation - however, Sleicher [92] had noted slight changes in his measured velocity profiles 81 diameters from the inlet of his test section, and so, to be on the safe side, a minimum value of 100 for the pipe length to diameter ratio was designed for.

Taking into account these requirements, as well as the height of the laboratory (50 feet) and the different sizes of tube available commercially, a 40 foot length of 4" aluminium tubing with a total $\frac{L}{D} \simeq 120$ was chosen for the test section.

To achieve a boundary condition of uniform heat flux the test section was wrapped with a closely wound helix of electrical heating ribbon which was covered with thermal insulation to minimise heat losses to the surrounding air. Other forms of heating were also considered but, despite having advantages from a constructional point of view, these invariably failed to provide as uniform a heat input at the wall as the selected method.

As can be seen from Fig. 3.1 a closed loop system was used in the present experiment. The reasons for this were:

i) It eliminated the effects of the sometimes considerable pressure fluctuations in the laboratory.

ii) Since the air was being recirculated through several filters the dust concentration in the air could be reduced to very low levels, a great advantage when using hot-wire probes.

Since air was the experimental fluid it was not necessary for the system to be completely sealed and this simplified problems in construction of the equipment. Leaks were, however, kept to a minimum.

3.2.2 General description.

The test loop is shown schematically in Fig. 3.1. Air was circulated by a centrifugal blower*, flow to the test section being controlled by a butterfly valve at the blower exit. Air passed from the valve to the test-section through a flexible polythene sleeve, which minimised transmission of vibrations from the blower. At the base of the test-section a flow-straightener* was inserted to cut down circumferential components of the mean velocity. No turbulence promoter was used, previous experience in Loop I having shown that the presence or absence of wire gauze or other turbulence promoters at the inlet of the tube made no detectable difference to measured profiles.

From the test section. described in detail in section 3.2.3, the air passed through the mixing cup shown in Fig. 3.2 and

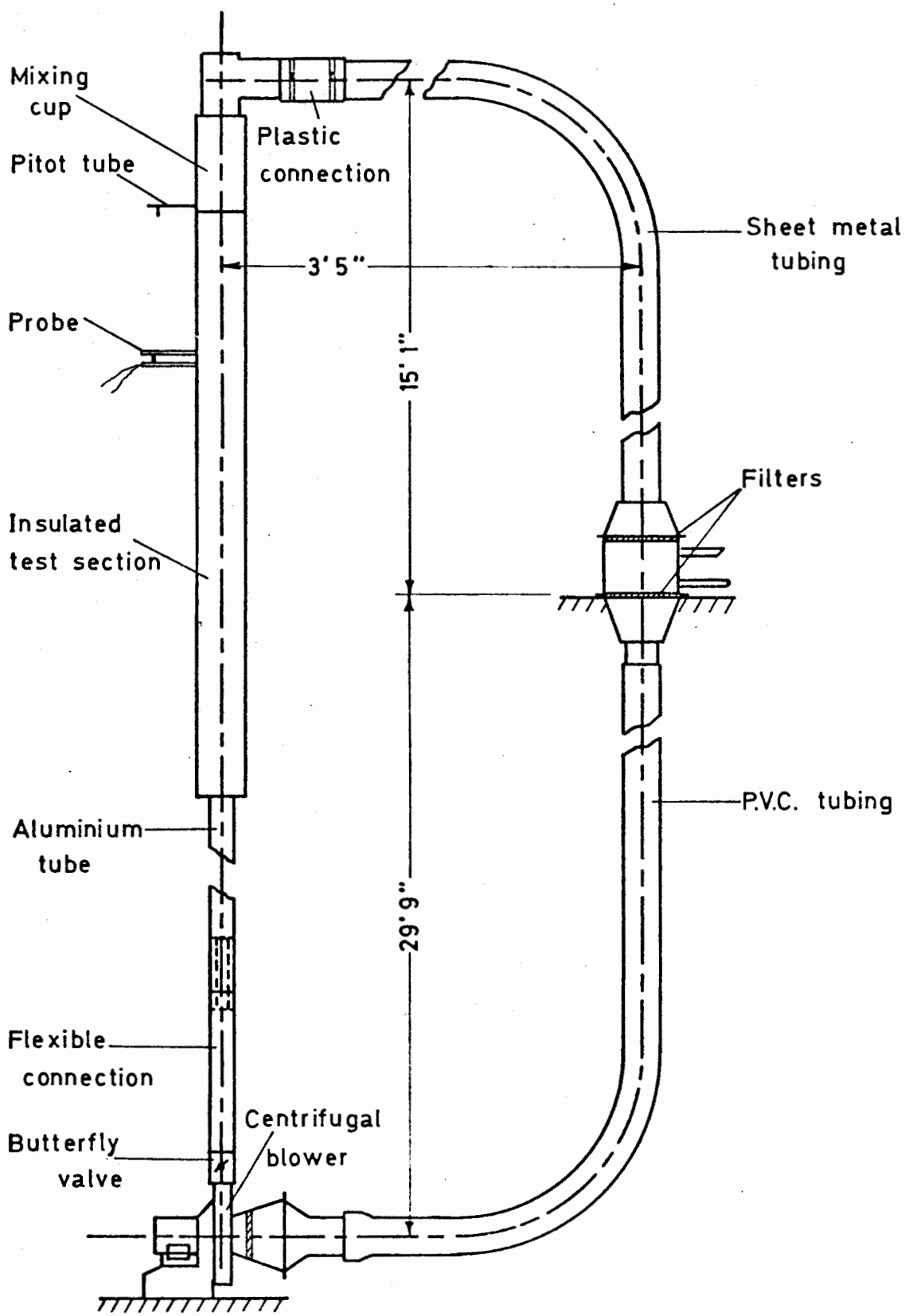

FIGURE 3.1 SCHEMATIC DIAGRAM OF TEST LOOP

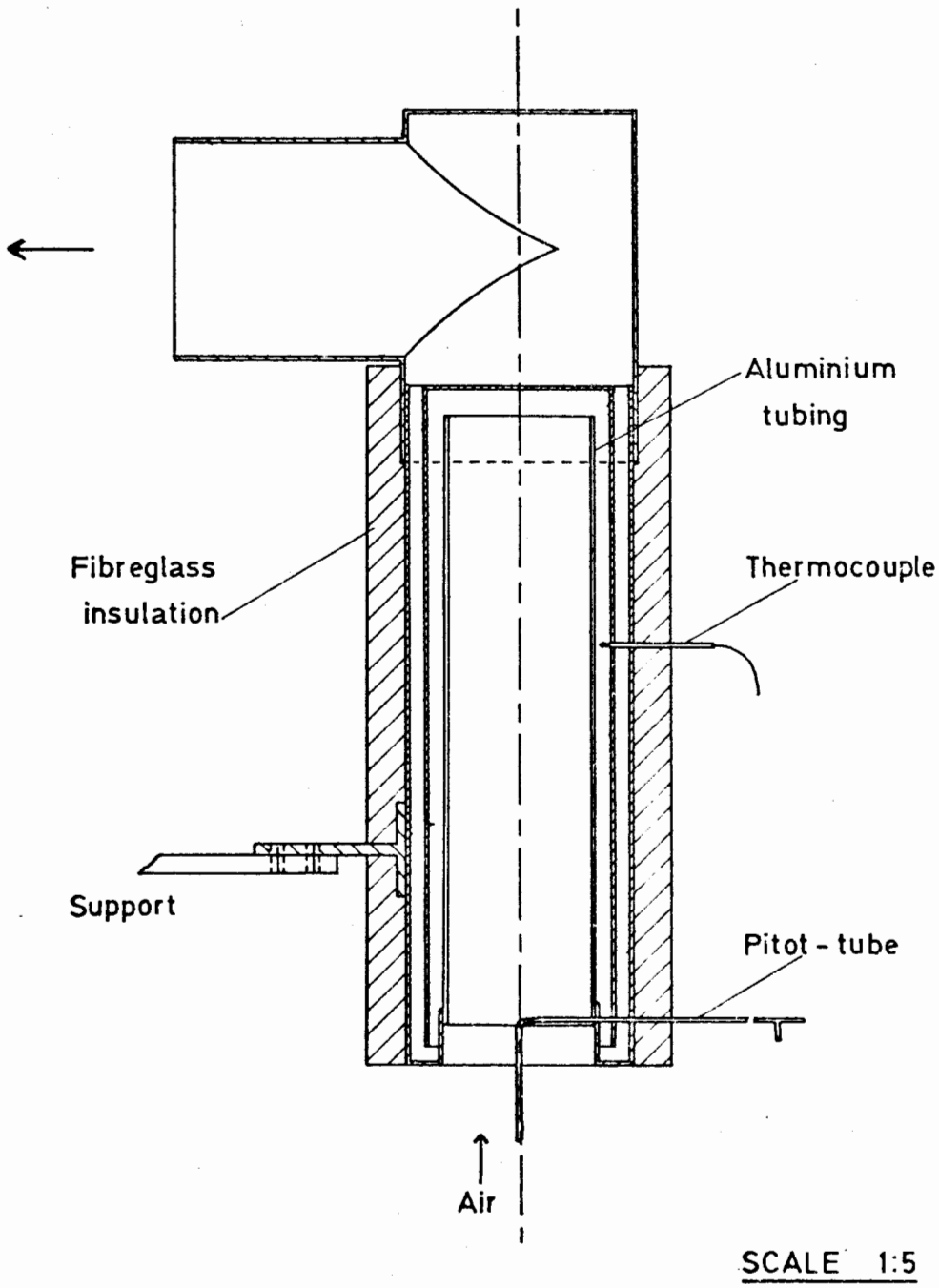

FIGURE 3.2 THE MIXING CUP

from there through a 6" diameter sheet metal duct to an air/water heat exchanger*. The cooled air was then returned through a length of 160 mm nominal diameter PVC tubing to the inlet of the blower. Filters* were installed immediately before and after the heat exchanger and also at the blower inlet.

Since it was necessary to be able to look into the test-section from above when inserting probes, the mixing-cup was designed to be easily removable. To minimise disturbance of the flow at the joint between the mixing cup and the test-section, the innermost section of the mixing cup was made of a $16\frac{1}{2}$" length of tubing similar to that used for the test-section. The end of this was filed so as to be flush with the end of the test-section when the mixing-cup was in place, thus effectively constituting a 4-5 diameter extension of the test-section. It was held in place by a wooden guide which fitted tightly over the top 1" of the test-section. A 12" wide strip of vinyl plastic, held to the ducting and the mixing-cup by jubilee clips, was used to connect the mixing-cup to the sheet metal duct. It also served to reduce transmission of vibrations from the blower to the test-section via the return leg.

The flow rate through the test-section could be determined from the velocity in the centre of the tube measured using a pitot-static tube* mounted on the base of the mixing-cup. The tip of this pitot tube extended 3" into the test-section and was therefore 5 diameters from the upper end of the aluminium section of the mixing-cup. This satisfied the downstream length requirement laid down in British Standards [93]. The pitot tube was held in a specially constructed traversing mechanism which enabled it to be positioned accurately along the axis of the test-section. The pressure difference between the impact and static taps was measured by a micromanometer* accurate to ± 0.0002" butyl alcohol (specific gravity ≈ 0.82).

3.2.3 The test section.

The 40-foot test section was formed by joining two 20-foot lengths of 4" outside diameter thin-walled aluminium tubing with a steel sleeve 7" long and $\frac{1}{8}$" thick. This sleeve, designed to hold the aluminium tubes tightly in a press fit, was machined in such a

way as to ensure that there was no discontinuity at the joint between the tubes. The exact dimensions of the test-section were

Length	40.04'
Wall thickness	0.056"
Mean inside diameter	3.886"

Sixteen iron-constantan thermocouples* were embedded in the wall of the tube at the following distances from the tube outlet: 6", 1', 2', 4' (4), 7', 10', 13', 16', 19', 21', 25', 29', 33'. The bead of each thermocouple, prepared by welding in an inert atmosphere, was placed in a hole only slightly larger than the bead diameter, drilled into but not through the tube wall. The thermocouple bead was held in place by forcing the surrounding aluminium into intimate contact with it. The insulated leads were held in a shallow groove, one to two inches long, aligned perpendicular to the tube axis to keep the lead temperature constant and minimise conduction errors. Before being led along the tube wall to outlet points at the top or middle of the test-section the leads were wrapped a further two or three inches around the tube to further reduce the chance of any significant conduction errors occurring. From the outlets the thermocouple leads were taken to a thermocouple selector switch*.

To electrically insulate the tube from the heating ribbon, the tube and the thermocouples were covered by a 0.007" thick layer of asbestos paper, over which was wrapped a helix of 2" wide, 0.015" thick, woven fibre-glass tape. The asbestos paper was glued down with sodium silicate which stood up well to the highest temperatures developed but had the disadvantage of being hygroscopic. Because of this, after a period of disuse the electrical resistance of the insulation was low and to prevent excessive current leakage to earth during operation the tube had first to be warmed up slowly to dry it out.

The heating ribbon was wound from a point 4'3" from the test section inlet to 2" from the outlet. Adjacent coils of ribbon were separated by asbestos string, giving an even pattern over the entire heated section - see Fig. 3.3. The coils of heating ribbon were held in place by wraplock clamps, also shown in Fig. 3.3, which were insulated from the heating ribbon by a double layer of asbestos paper.

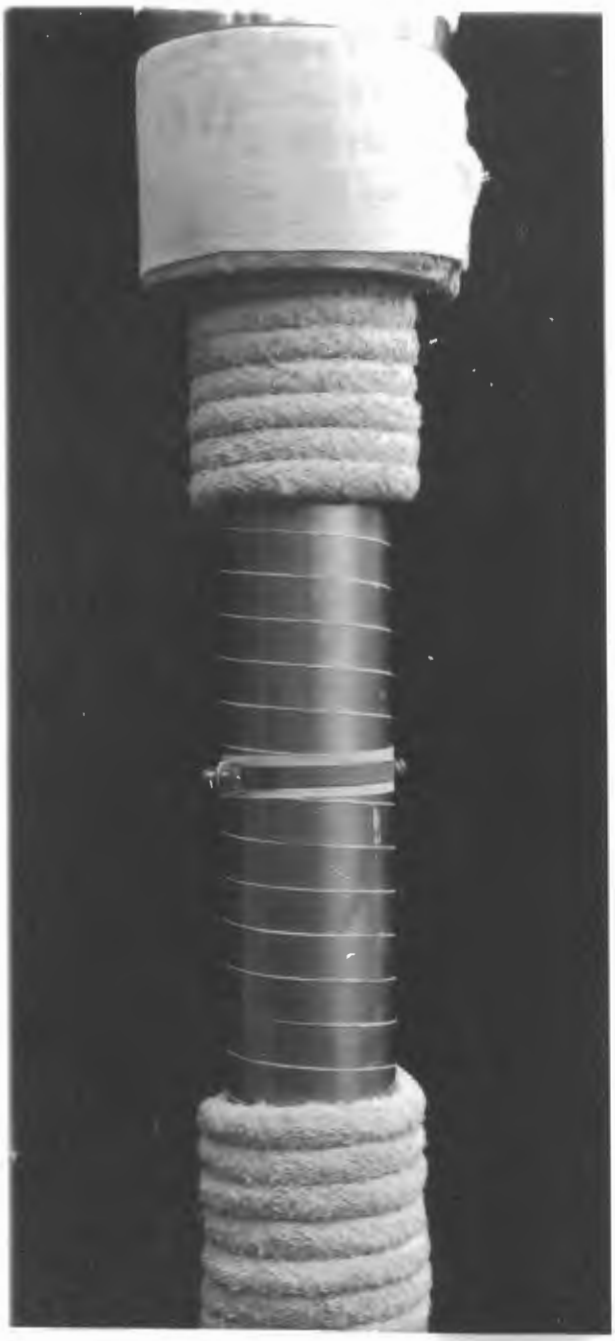

FIGURE 3.3 VIEW OF THE TEST SECTION SHOWING HEATING RIBBON AND INSULATION

An opening for the probe was made 2'2-3/8" from the test-section outlet at a point between two adjacent coils of heating ribbon. Allowing for the fact that the probe tip was 2" below this point, this gave an unheated length to diameter ratio of 113 and a heated length to diameter ratio of 100. A slot just over $\frac{1}{4}$" in width and just less than $\frac{1}{2}$" in height was cut in the tube wall and just sufficient heating ribbon cut away to prevent the probe inadvertently forming an electrical connection between the tube and the heating ribbon.

The probe and the traversing mechanism were supported by a steel clamp 3/16" thick and 3" long. This clamp had two sections, bolted together around the heating tape and insulated from it by fibre-glass tape. The inside surface of the clamp was machined to fit exactly over the tube and provide a firm mount for the traversing mechanism. This mechanism, shown in Fig. 3.4, was constructed from a pair of vernier calipers.

The pipe was lagged with a layer of 1" nominal diameter asbestos rope over which were placed sections of 1" thick preformed fibre glass pipe lagging as shown in Fig. 3.3. To estimate the heat losses through the insulation iron-constantan thermocouples were inserted inside and outside the fibre glass lagging at points 3', 15' and 26' from the tube outlet.

To obtain mixed mean temperatures at inlet and outlet to the test-section iron-constantan thermocouples were also placed at the entrance to the tube, where the air was considered to be sufficiently mixed for the measured temperature to be the same as the mean value, and in the mixing-cup, as shown in Fig. 3.2. The bead of this latter thermocouple was inserted into the inner annulus of the mixing-cup where previous experience in Loop I had shown that accurate mean outlet temperatures could be measured. Heat losses at this point are minimal as the air is insulated from the outside air by the hot air in the outer annulus as well as by a 1" layer of preformed fibre glass pipe lagging covering the mixing-cup.

The test-section was mounted in a vertical position, its weight being supported by a steel clamp 8-3/8" from the inlet.

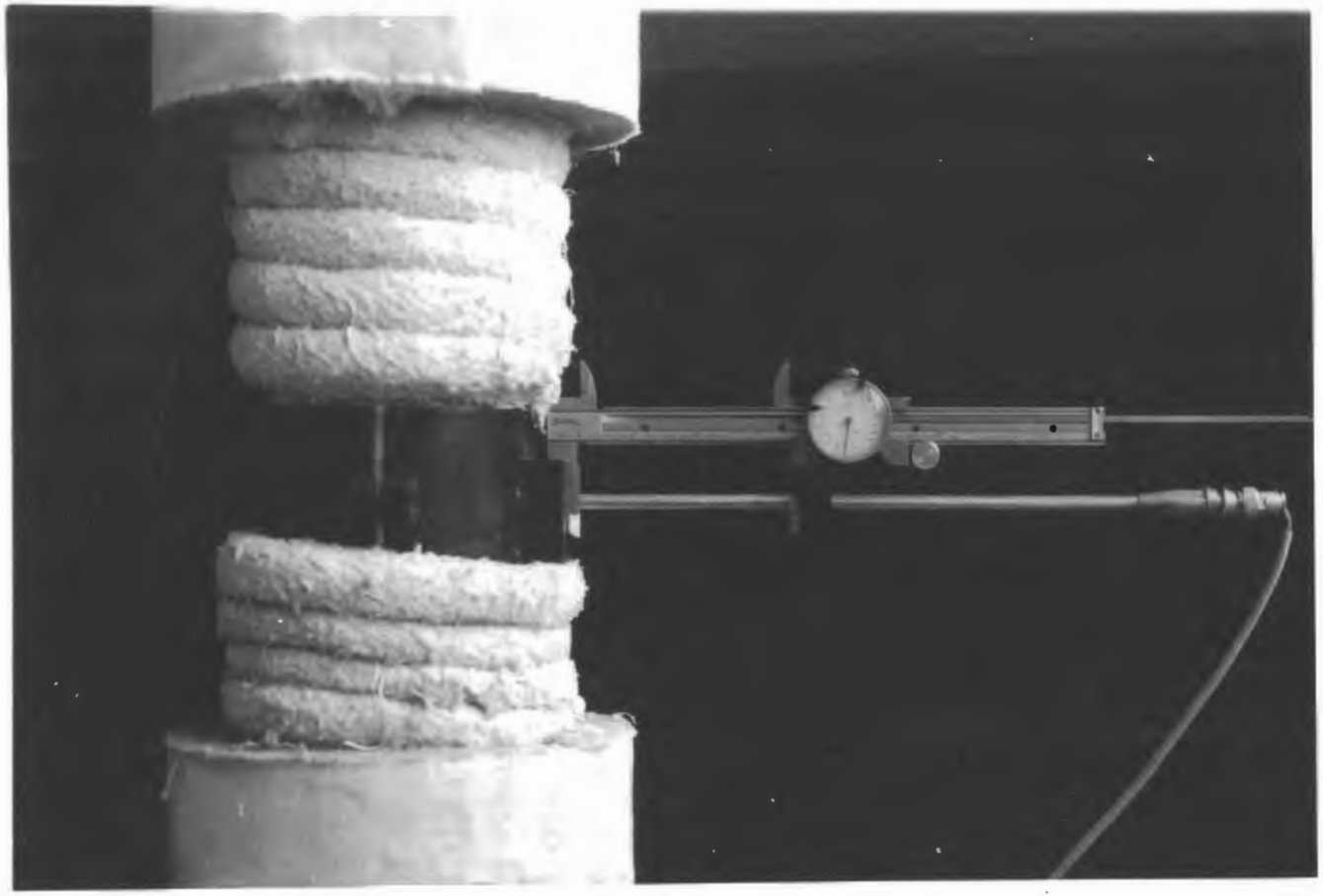

FIGURE 3.4 THE TRAVERSING MECHANISM

This clamp was electrically insulated from the tube by thin strips of tough plastic. Two wooden clamps, designed to fit around the heating ribbon, were placed 18'6" and 36'7" from the test-section inlet, and were used to align and hold the test-section accurately in a vertical position.

Before being erected the test section was cleaned, degreased and polished on the inside with a mildly abrasive nylon mat. Afterwards, before use, it was again cleaned thoroughly.

3.3 THE HEATING CIRCUIT.

The electrical circuit used to control the power supplied to the heating ribbon is shown in Fig. 3.5. The power input was regulated by a variac and could be measured by timing a known number of revolutions of the rotating disc of the kilowatt-hour meter*. This gave results which agreed closely with the power input obtained by multiplying together the volt meter* and ammeter* readings, and so, during runs, the power input was regulated according to the readings of these two meters.

3.4 PROBES AND PROBE POSITIONING.

3.4.1 Probe construction.

The hot-wire probes used in the present experiments were prepared as described below. A typical probe is shown in Fig. 3.6.

To make the hot-wire supports narrow grooves were cut into the fine ends of size 12 Sharps beading needles. Two of these needles were then glued about 0.1" apart in a $\frac{1}{2}$" long piece of 0.15" diameter four-hole ceramic tubing, care being taken to make sure that the grooves were aligned parallel to a line joining the two needles. To ensure that the sensing element would be perpendicular to the probe axis it was made certain that the fine ends of the two needles protruded equal distances from the piece of ceramic tubing. The probe body was then mounted in a holder made from $\frac{1}{4}$" diameter stainless steel tubing (nominal inside diameter = 0.180"). Leads were soldered to the eyes of the needles and led out through the stainless steel tubing.

The sensing element employed was tungsten wire, 0.00015"

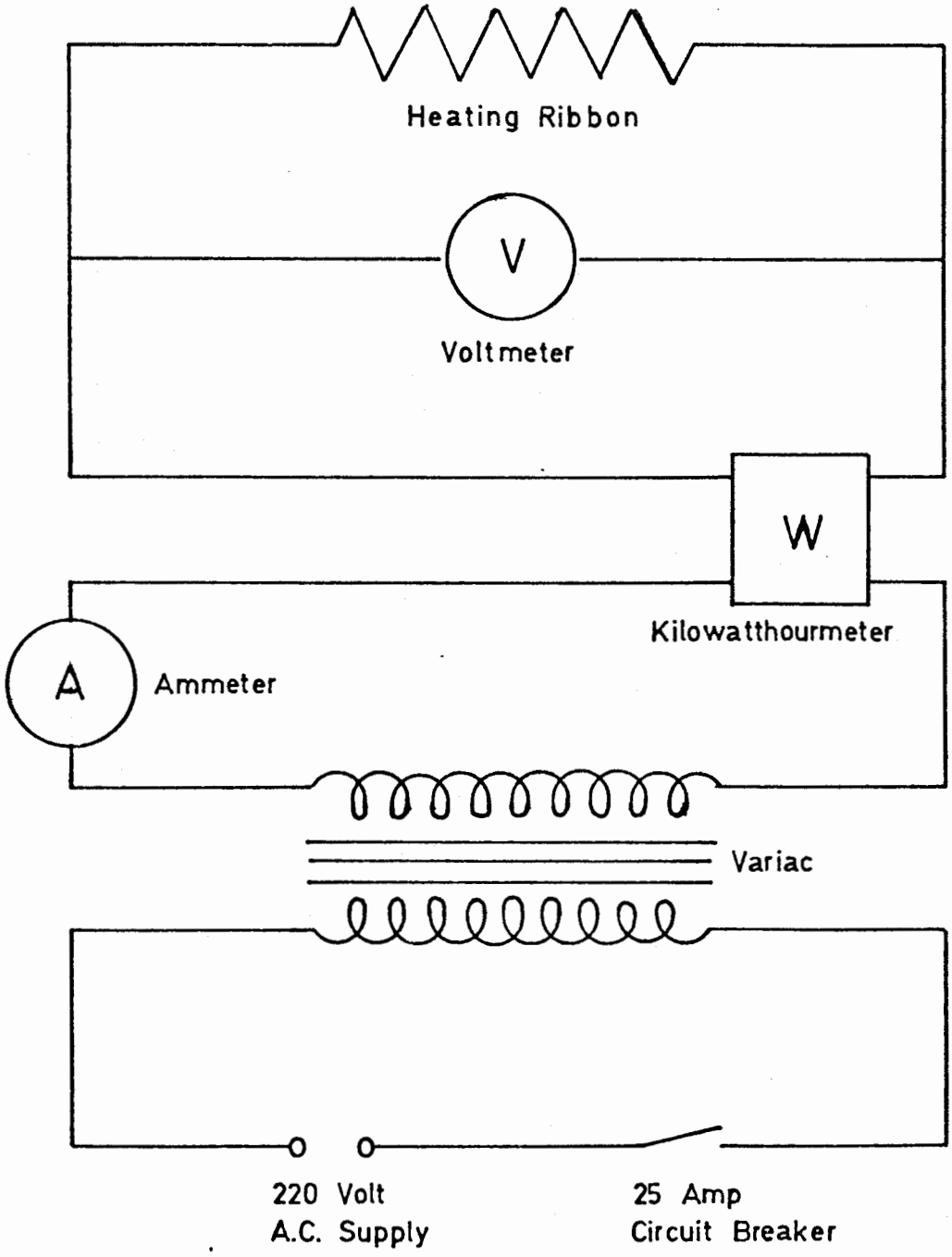

FIGURE 3.5 THE HEATING CIRCUIT

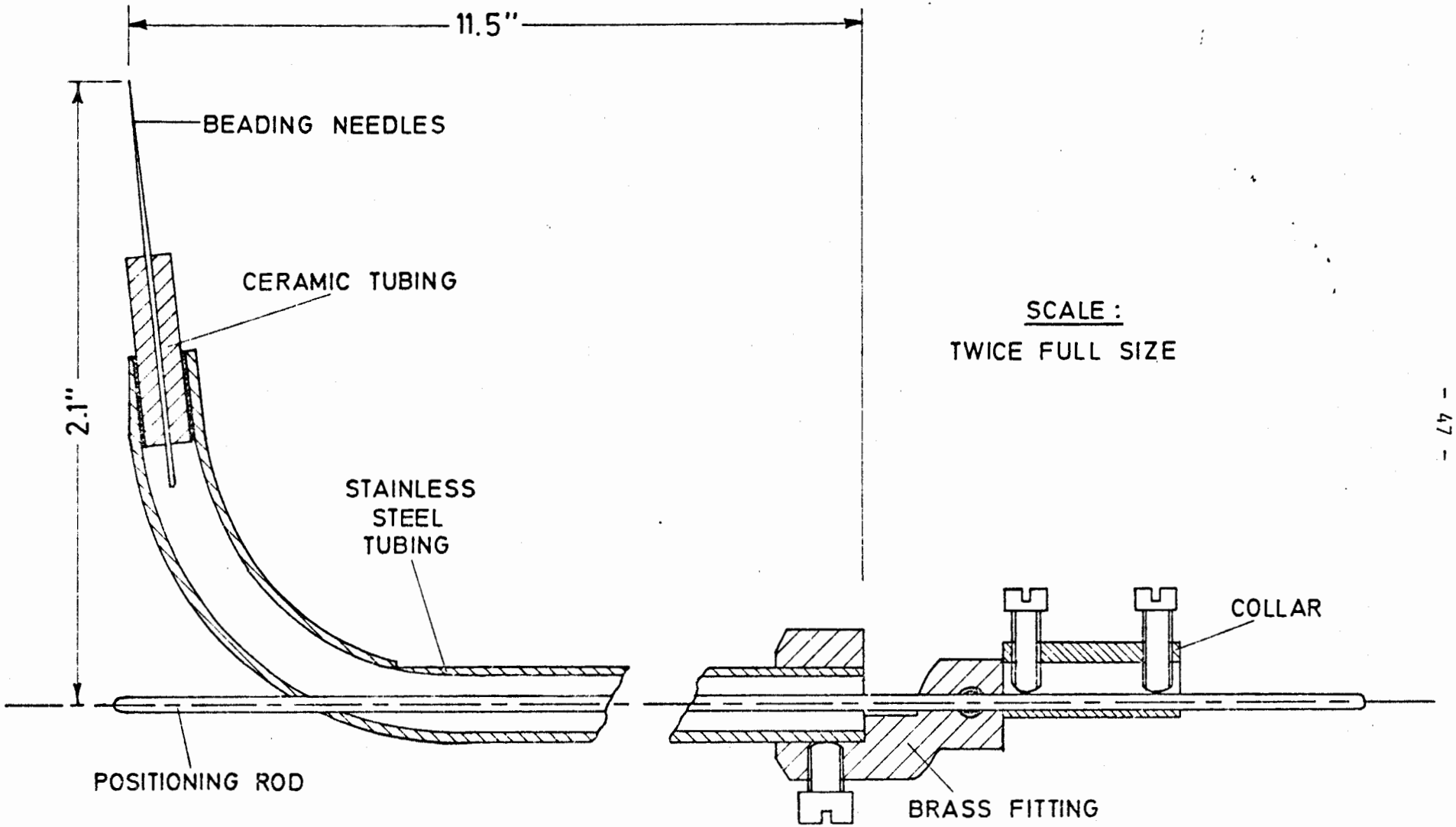

FIGURE 3.6 DIAGRAM OF A TYPICAL HOT-WIRE PROBE

in diameter, supplied by Sigmund Cohn Corp., Mt. Vernon, New York. Lengths of this wire were copperplated at the ends, leaving a 0.08" - 0.09" unplated active section between, and then soldered to the needle tips as described in section 3.4.3.

The results of early experiments in Loop I, supported by the work of van Thinh [56,74], showed that the hot-wire supports should be parallel to the mean flow direction in order to minimise interference effects. To approach this condition as closely as possible, while still being able to move the hot-wire itself right up to the tube wall to take measurements in the viscous sublayer, the stainless steel probe holder was bent through 80° and the leading edge filed down as shown in Fig. 3.6.

3.4.2 Probe positioning.

Probes were inserted into the test-section at the measuring station and measurements could be made in a horizontal plane 2.1" below the point of entry of the probe holder. The horizontal range of these hot-wire probes extended from a point located about 1/3 of the way across the pipe through to the opposite wall.

The traversing mechanism, carefully mounted horizontally on the steel clamp described previously, permitted the probe to be positioned to an accuracy of ± 0.001" once the position of the hot-wire relative to the tube wall had been established. Positioning the hot-wire in the plane perpendicular to the probe axis was done by eye and, surprisingly, this proved to be as accurate as the other method tried, namely, fastening a pointer to the outer end of the probe holder and aligning it parallel to the hot-wire before inserting the probe into the test-section.

To position the hot-wire relative to the tube wall the following method was employed. A straight rod with a rounded tip was inserted into the outer end of the probe holder through a small brass fitting attached to the holder. The rod was then passed along inside the probe holder and out through a small hole at the front - see Fig. 3.6. To this rod was attached a brass collar, one face of which could be brought up flush with the outer face of the brass fitting on the probe holder. Both the brass fitting and the collar could be clamped to the rod by grub screws. The

probe, together with the additional pieces described above, was set up on the jig shown in Fig. 3.7. On this jig the probe could be moved horizontally towards a vertical polished brass plate with two faces, the lower of which was 0.010" further from the probe than the upper. The probe was moved slowly towards the polished plate until the probe supports and their reflections in the plate coincided, a method which gave the position of the needle edge relative to the upper face to an accuracy of ± 0.001". This was checked by advancing the probe 0.001" at a time, controlling the movement with the blades of a feeler gauge inserted between the rod described above and the lower face of the jig. As soon as the needles touched the polished upper face turning the probe about its axis produced a faint but audible scratching noise as the needles moved across the plate. The position of the probe at this point agreed with the position obtained using the visual method.

With the probe held firmly in this position the straight rod was advanced to the lower face and clamped in position by the fitting attached to the probe holder. The tip of the rod was now 0.010" in front of the needle (and hence 0.0135" in front of the hot-wire axis, since the needle points were .007" in diameter). The collar was then moved along the rod until its inner face was flush against the outer face of the fitting and in this position, was again secured to the rod. This arrangement permitted the rod to be withdrawn as the probe was inserted into the test-section and then, once inside, it could be returned to its previously set position a known distance in front of the hot-wire. The location of the hot-wire relative to the tube wall was then established by noting the reading of the dial gauge on the traversing mechanism when the rod touched the wall.

3.5 HOT-WIRE MANUFACTURE.

A number of different methods of preparing hot-wires have been used and references to many of these can be found in Brown [91]. Generally they can be divided into two classes, those using a method involving welding to attach the sensing wire to the probe supports and those using a soldering method. In the present investigation a method of the latter type was used but, because solder does not

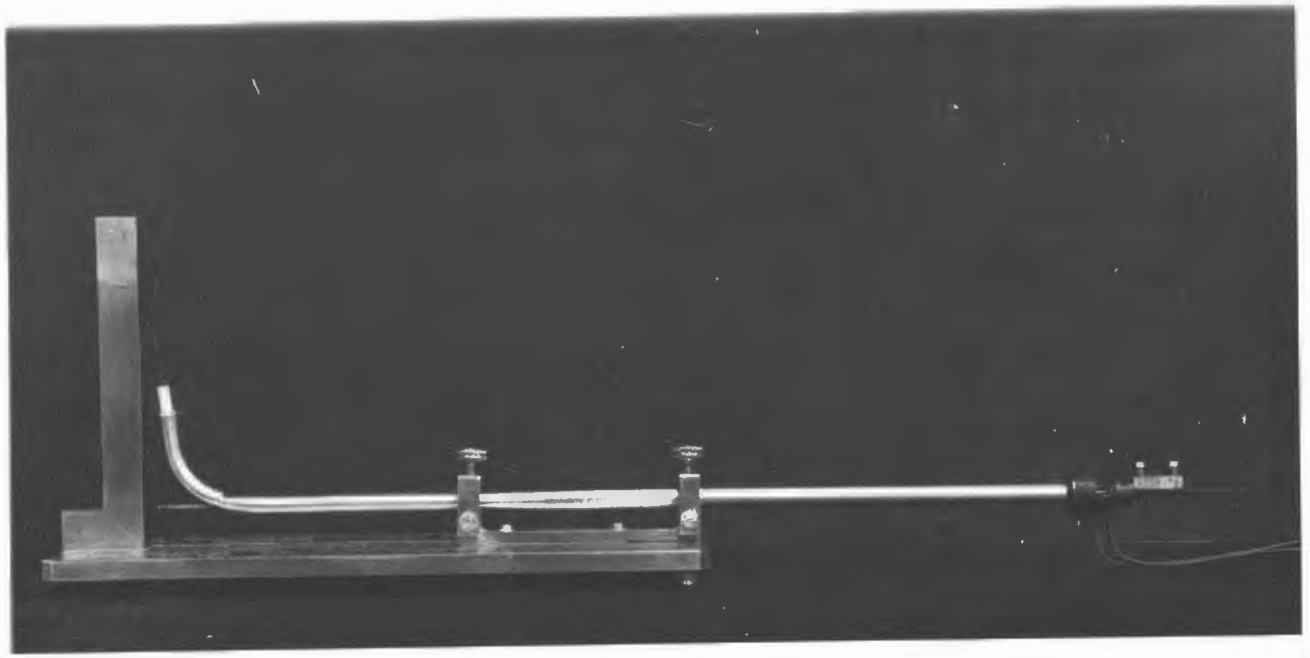

FIGURE 3.7 JIG USED TO ESTABLISH THE POSITION OF THE HOT-WIRE RELATIVE TO THE POSITIONING ROD

"wet" tungsten, it was first necessary to copperplate sections of the tungsten wire before attaching it to the supports. Some hot-wires used in early measurements were prepared by a method due to Wichner [94] which used unplated wires and relied on the surface tension of the solder forcing the wire into the groove in the needle to form a strong mechanical joint. Acceptable results were obtained with some hot-wires prepared in this way but the method described below, based partly on the work of Schubauer and Klebanoff [62], was found to be more reliable.

To copper plate the tungsten wires the special plating bath shown in Fig. 3.8 was employed. Acidified copper sulphate solution was placed in chambers A and B (see Fig. 3.8) and by screwing down the plungers inserted through the tops of A and B a bubble of electrolyte was established on top of cups C and D. A short length of tungsten wire, weighted at its ends, was laid across the cups and then across the copper rods E and F. Then, by establishing a potential difference between rods E and F and the electrolyte in A and B two electrolytic cells in which the tungsten wire acted as cathode were formed. In this way the wire was plated for a short distance on either side of an active unplated section, the length of which could be varied by varying the distance between cups C and D. By ensuring that the tungsten wire was clean and by using a relatively low current a smooth uniform plating was obtained.

The plated wire was taped to a cork support and mounted on the jig, shown in Fig. 3.9, which enabled the wire to be accurately positioned in a horizontal plane. Also mounted on the jig was the probe holder, which could be moved in a vertical direction. The relative positions of the probe and the wire were adjusted until the plated wire lay in the grooves of the wire supports with the unplated section of the wire symmetrically between the supports. The wire was then soldered to the supports and excess wire carefully removed.

Before use a hot-wire prepared in this way was heated for several hours to a temperature higher than normal operating temperatures. Measurement of its resistance before and after this period established whether its characteristics would remain constant during operation.

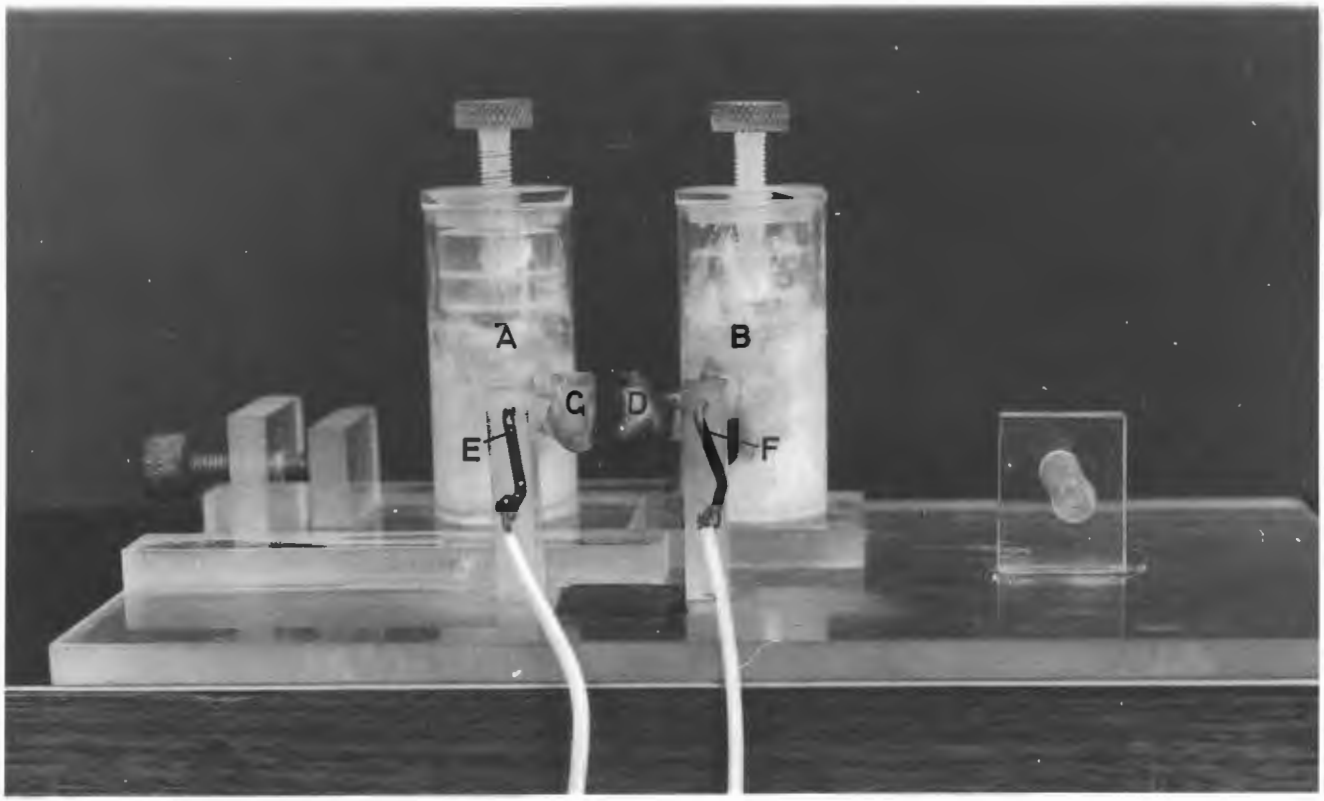

FIGURE 3.8 THE PLATING BATH

A and B : Chambers containing electrolyte
C and D : Cups on which bubble of electrolyte is formed
E and F : Copper rods providing contact with wire

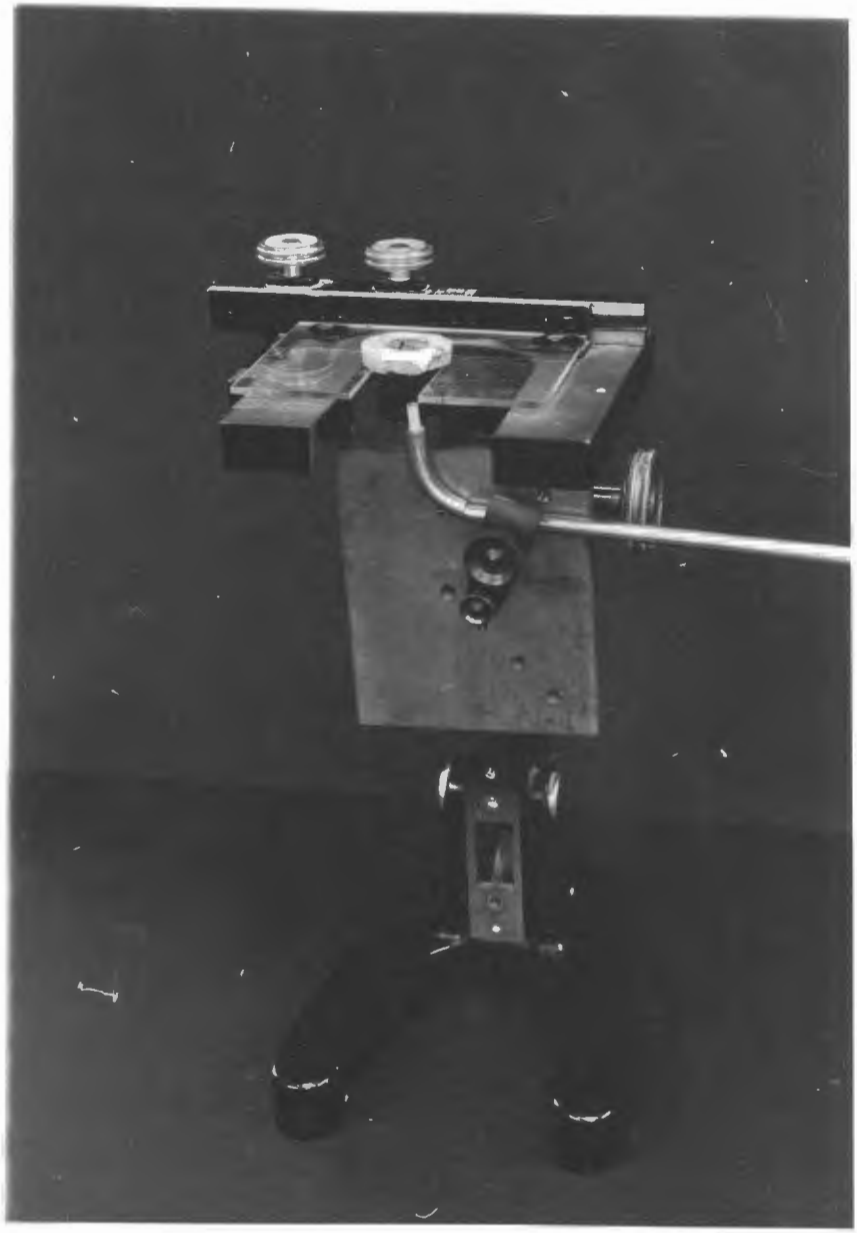

FIGURE 3.9 JIG FOR MAKING HOT-WIRE PROBES

3.6 THE HOT-WIRE ANEMOMETER.

The anemometer used to measure mean velocities, temperatures and various turbulence quantities was a Transmetrics Model 6401 Constant Current Hot-wire Anemometer. A photograph of the instrument, together with a description of methods of operation and other details may be found in Appendix D.

The units comprising the instrument are

i) Current control panel.

ii) Bridge unit:- accuracy ± 0.01 ohms; resolution better than 0.005 ohms.

iii) Potentiometer :- accuracy ± 0.01% full scale; resolution ± 0.005% full scale.

iv) Mean square output meter.

v) Amplifier:- gain 50 000; specified frequency response: flat ± 1% for 1 Hz < ν < 30 kHz, < 10% for 0.2 Hz < ν < 150 kHz, < 30% for 0.1 Hz < ν < 300 kHz compensation circuit included.

vi) Square wave generator.

vii) Power supply.

3.7 TEMPERATURE MEASUREMENT

3.7.1 Thermocouple measurements.

Temperatures along the wall of the test-section, in the insulation, and at the inlet and outlet of the test-section, were obtained from thermocouple measurements. Individual thermocouple e.m.f.s were measured with a differential voltmeter*, or with a portable potentiometer*, connected to the thermocouple selector switch. The reference junction was formed by an iron-constantan thermocouple kept in melting ice in a double-walled container. Temperatures along the wall of the test-section were also displayed on a multipoint recorder*, making it easy to decide when steady state conditions had been reached. The recorder was also used to ensure that the test-section was not overheated in the event of a blower breakdown. An arm bearing a grounded metal contact was attached to the recorder chassis in such a way that it could be moved by the temperature indicator on the recorder towards a second

metal contact. This contact was connected to the heating circuit and positioned so that if the temperature exceeded a preset maximum value the two contacts touched and the heating circuit was earthed through a resistor, tripping an earth leakage switch and thus cutting the power to the heating ribbon.

The thermocouple wire used was guaranteed to give readings accurate to within ± 2°F. Checks against a standard thermometer showed no significant difference between the observed calibration line and the standard values given in British Standards [95] and more precisely in [96].

3.7.2 Hot-wire measurements.

Temperature profiles were measured using the hot-wire anemometer as a resistance thermometer. The practical problems involved in applying this technique to measurements in pipe flows are well treated by Maye [82], whose work is discussed more fully in Appendix C. Experiment showed that for hot-wire currents less than 1 mA no detectable increase in wire resistance occurred and so the 0.4 mA current used in the present investigation would not have affected the measured resistances in any way. These resistances could be measured with a precision better than ± 0.005 ohms using the Bridge circuit on the hot-wire anemometer.

3.8 DIFFERENCES BETWEEN TEST LOOPS I AND II.

The major differences in design and methods of operation of the two loops, I and II, are summarised below:

i) Loop I had a 29' long test-section and Loop II a 40' test-section. This gave heated and unheated $^{L}/_{D}$ ratios of 70 and 83 and of 100 and 113 for Loops I and II respectively.

ii) No flow straightener was used in Loop I.

iii) For Loop I the pressure difference developed across the taps of the pitot tube was measured on a Hook Gauge* accurate to ± 0.001" water. For Loop II a micromanometer* accurate to ± 0.0002" butyl alcohol was used.

iv) The test-section wall thermocouples for Loop I were made from copper-constantan wire and were held against the tube

surface by strips of asbestos paper glued to the tube wall with sodium silicate; those for Loop II were of iron-constantan wire and were attached to the test-section wall as described previously. The method used in Loop I was not effective at high temperatures and the erratic behaviour of certain thermocouples in Loop I was one of the main reasons for the construction of Loop II, where an improved method of attaching thermocouples to the tube wall was used.

v) In Loop I hot-wire probes were positioned relative to the wall by eye; in Loop II the much more accurate procedure described in section 3.4 was used.

vi) For measurements taken in Loop I low velocity calibration points were relatively inaccurate, being obtained from pressure differences measured on the Hook Gauge (accuracy ± 0.001" w.g.). For measurements taken in Loop II the calibration device described in section 3.9 and used as explained in 3.10, permitted far more accurate calibration points to be established.

3.9 CALIBRATION EQUIPMENT - TEMPERATURE.

Hot-wires to be calibrated were placed in an air-stream at the mouth of a horizontal plastic tube 1" in diameter. The probe was held so that the probe supports were horizontal and extended as far as the bent probe holder allowed into the mouth of the tube. A standardised thermometer was clamped so that it was aligned parallel to the axis of the plastic tube and then moved until its bulb was close to the hot-wire. When held in this way the stem of the thermometer remained in the air-stream throughout its length, minimising emergent stem errors. The air supplied to the tube passed over an electric heater whose output could be varied, enabling steady air flows at several different temperatures to be obtained. At each temperature a number of measurements of hot-wire resistance and of temperature were made and the full set of readings was used to prepare a calibration curve of temperature against resistance. Except for occasional points at the highest temperature these readings could be accurately represented by a straight line. The slight deviation of the high temperature points

was attributed to errors in the thermometer reading rather than to a second order dependence of the wire resistance on temperature. This was because at the higher temperatures it was difficult to ensure that the air-stream remained at a uniform temperature throughout. Under such conditions, despite careful positioning of both hot-wire and thermometer, slightly different sets of readings could be obtained by altering their relative positions. Under the present conditions, radiation losses were taken as negligible [92,98].

3.10 VELOCITY CALIBRATION EQUIPMENT - DESIGN AND USE.

3.10.1 Calibration against the pitot tube.

For measurements taken at Reynolds numbers above about 10 000 the hot-wire could be accurately calibrated against a pitot tube over the whole range of velocities measured. To do this the hot-wire was placed at the centre of the test-section and the total flowrate varied to give centre velocities covering the entire range of expected values. At each flow rate the reading of the hot-wire and of the pitot tube mounted on the mixing-cup was noted and the full set of readings was used to prepare a calibration curve of $\frac{I^2\overline{R}_w}{\overline{R}_w-\overline{R}_g}$ against $\frac{1}{\overline{V}_z^2}$. Details of the equation used to obtain $\frac{1}{\overline{V}_z^2}$ from the pitot tube reading are given in Appendix G.

To check that the hot-wire anemometer did not interfere with the pitot tube reading a series of pitot tube readings was taken as the hot-wire was moved across the tube. The first sign of an interference effect came only at the 0.8 y/R position (measured from the wall opposite the point of entry), confirming that there was no interference effect during calibration.

3.10.2 Low velocity measurements.

It was shown in Chapter 2 that, to make accurate measurements in non-isothermal low velocity flows, equipment enabling hot-wires to be calibrated over a range of temperatures was needed.

Hot-wires used in moderate velocity air flows are generally calibrated against pitot tubes as described above,

provided neither the turbulence intensity of the flow nor the velocity gradient is very large. At low flow rates, however, the pressure difference across the pitot tube becomes too small to be measured accurately and other methods of calibration must be employed. Several methods of measuring low velocities have been investigated, e.g. by Kung and Binder [99] who discuss the hot-spot and drag anemometers and by Tanney [100] who developed a low velocity anemometer based on fluid amplification. A new type of anemometer announced by D.I.S.A. [101] may also be useful for very low velocities. Most workers lacking accessibility to accurate low velocity wind tunnels have, however, calibrated hot-wires in fully developed laminar air flows at known total flow rate [58,87]. None of these methods is entirely suitable for the measurement of low velocities over a range of temperatures and so the apparatus described in section 3.10.3 was developed for this purpose.

3.10.3 Low velocity calibration device - description.

The apparatus used for this purpose was originally designed to provide an air stream of known temperature and velocity into which the hot-wire probe could be inserted. As described in Appendix E, subsequent experiments with this device involved establishing a calibration method for low velocity isothermal flows and this method was later employed for calibrating hot-wires before they were used in the test-section described previously.

The apparatus is shown schematically in Fig. 3.10. Air was forced by a centrifugal blower* through a flexible polythene connection into a heater consisting of a 1 kilowatt electrical heating bar mounted axially in a 2" I.D. asbestos pipe and controlled by a variac. The air leaving the heater was passed through a short 2" copper pipe, lagged with a layer of asbestos rope and a layer of 1" preformed fibreglass insulation, into the calibration "box" shown in Fig. 3.11. Since the cross-sectional area of the box near the air inlet (10" x 10") was about 30 times larger than that of the central 2" copper tube the air moved relatively slowly to the expanded (18" x 18") end of the box where its velocity was decreased still further. The air was then drawn into the central 2" copper pipe through a contracting cone designed according to the recommendations of Smith and Wang [102] to give

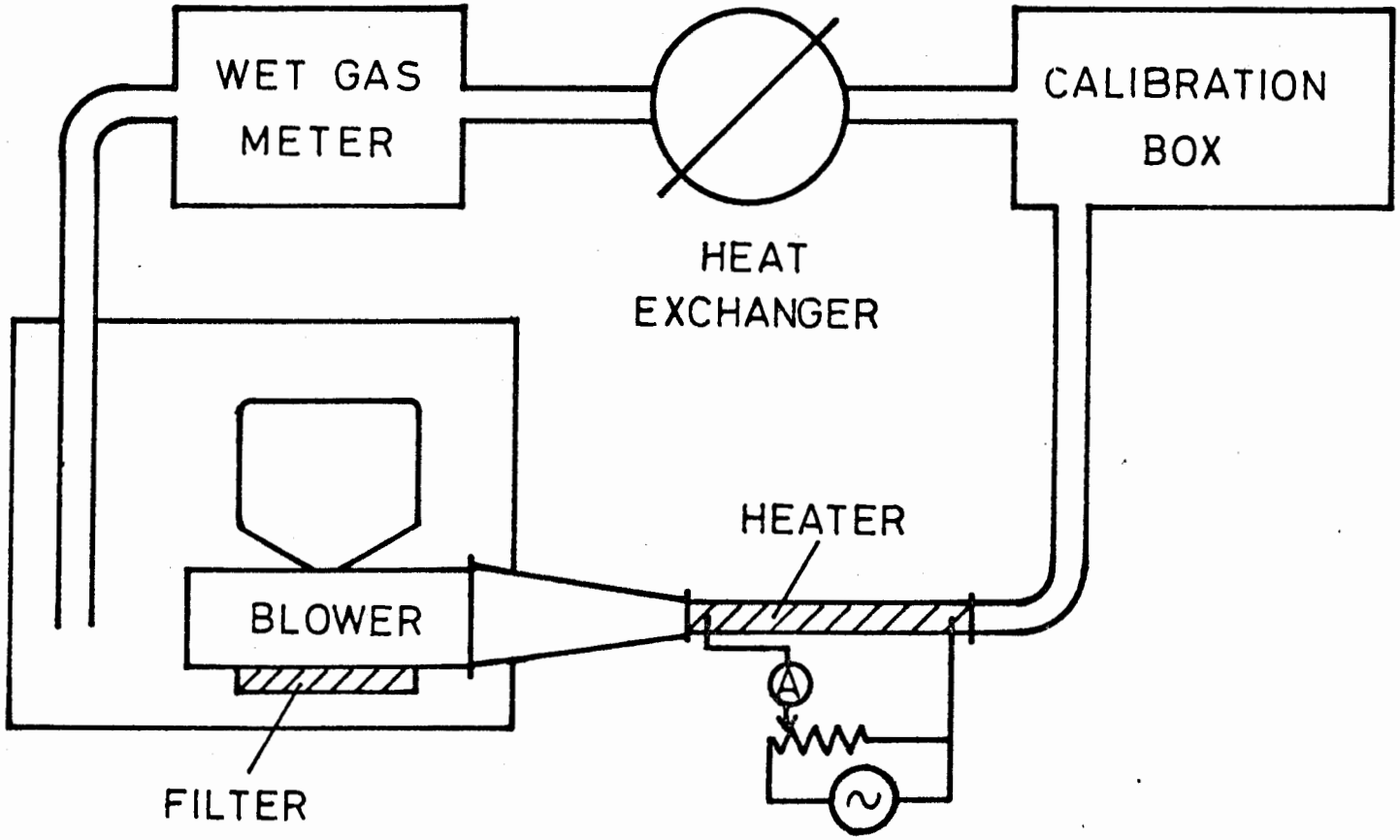

FIGURE 3.10 DIAGRAM OF CALIBRATION SYSTEM

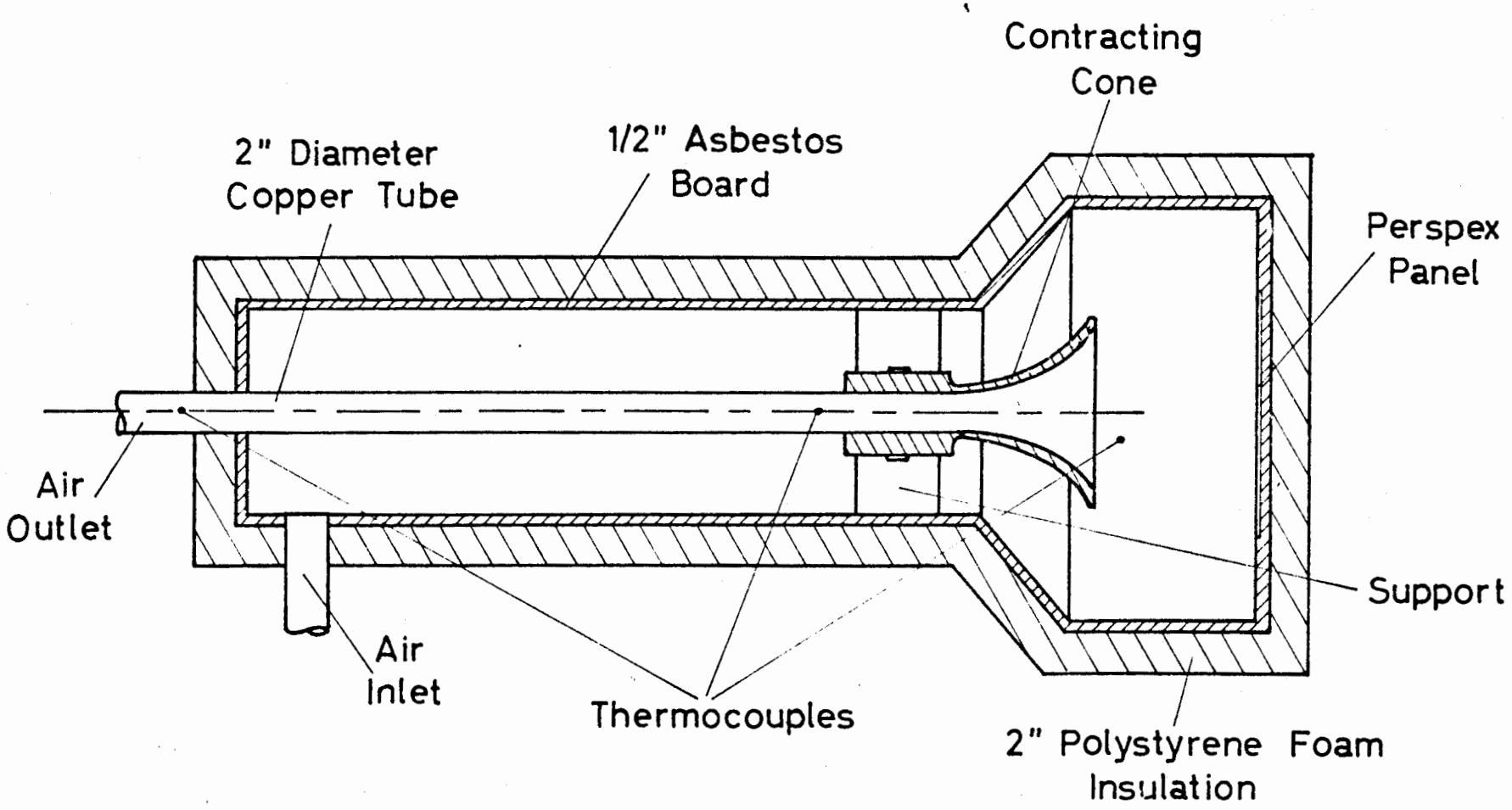

FIGURE 3.11 HORIZONTAL SECTION THROUGH CALIBRATION BOX

as flat a velocity profile as possible in the throat.

The air passed from the outlet of the copper tube through a flexible rubber connection to a water-cooled double-pipe heat exchanger. This exchanger was designed to handle efficiently widely varying quantities of air and could operate, depending on total air flow rate, with one, two, three or four double-pipe hairpin sections in parallel. From the exchanger the air passed into a large capacity wet-gas meter*. The rate of flow through the system was controlled by a valve situated immediately before the wet-gas meter. Air was exhausted from the wet-gas meter into an enclosure around the blower so that the air recycled, being more humid than the outside air because of its passage through the wet-gas meter, would evaporate less water from the wet-gas meter and increase the meter's accuracy of operation. A filter made of the same material as the filters in the test-section was fitted over the inlet to the blower.

Three copper-constantan thermocouples, shown in Fib. 3.11, were used to establish when constant temperature conditions had been achieved in the cone and copper tube. The box was heavily insulated to cut down heat losses and minimise the effect of fluctuations in ambient temperature. In all, the insulating layers consisted of the 0.1" thick hardboard of which the box was made, a layer of 0.5" thick asbestos board and a layer of 2" thick polystyrene foam. The hot-wire probe was inserted into the throat of the cone as shown in Fig. 3.12. It was held in a traversing mechanism, made from a pair of vernier calipers, which permitted measurements to be taken in a vertical plane across one half of the throat. As before, the hot-wire was connected to the constant current hot-wire anemometer described in section 3.6. Positioning the hot-wire in the throat was carried out in the same way as for the test-section - see section 3.4. A transparent panel on the front of the calibration box enabled the positioning of the probe to be checked visually.

3.10.4 Low velocity calibration device - isothermal calibration.

In the experiment described in Appendix E it was shown that the velocity in the throat of the cone was constant over much of the cross-section, decreasing only near the walls. Also a

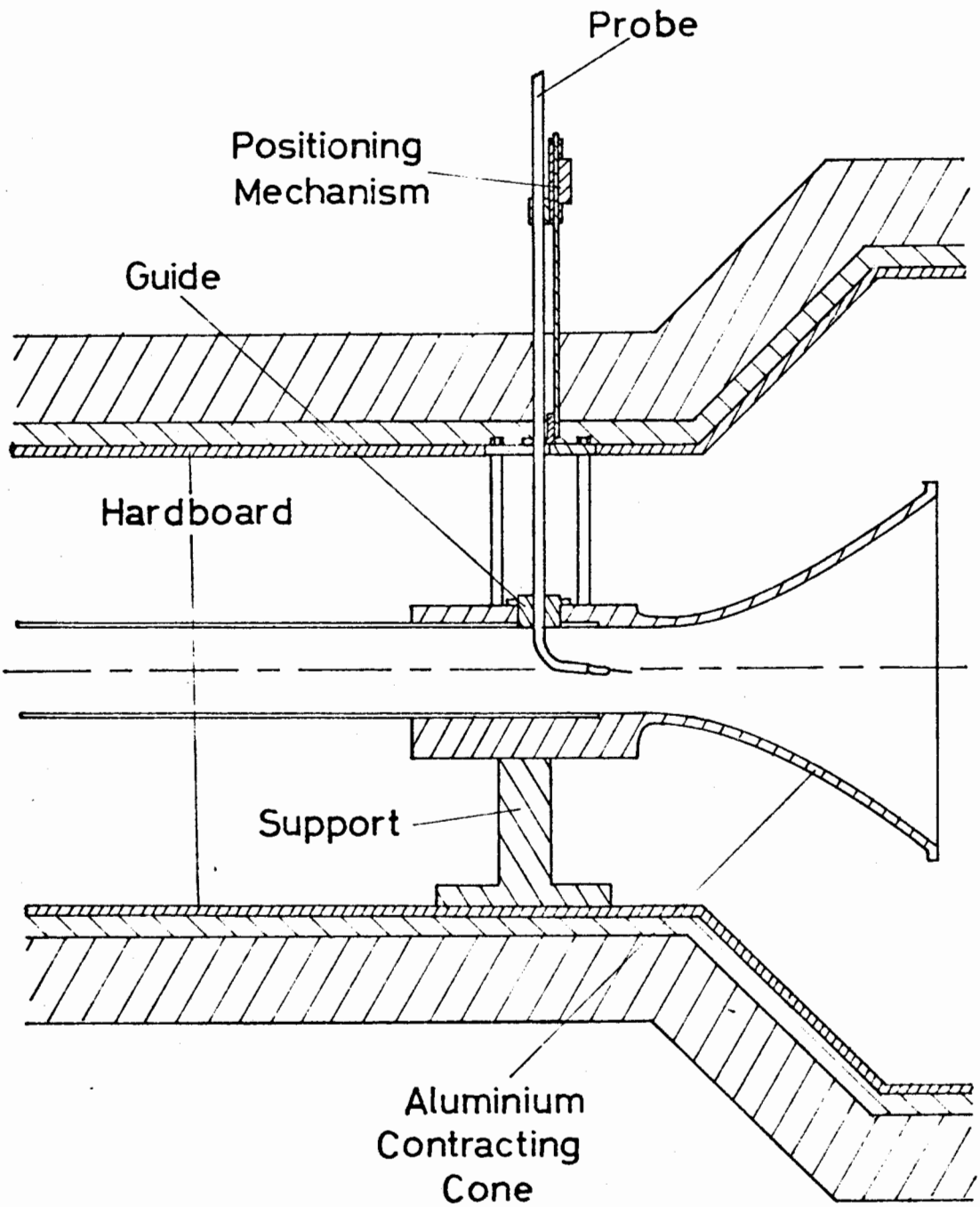

FIGURE 3.12 VERTICAL SECTION THROUGH CALIBRATION BOX SHOWING TRAVERSING ARRANGEMENT

curve in the form of a plot of $\frac{\bar{U}_{ave}}{\bar{U}_{max}}$ against $\bar{U}_{ave}$ was derived, where $\bar{U}_{ave}$ represented the mean velocity through the throat and $\bar{U}_{max}$ the maximum velocity in the throat. Use of this curve made probe calibration a relatively simple procedure.

The probe to be calibrated was inserted into the calibration apparatus and positioned in the region of constant velocity towards the centre of the throat. Readings on the wet-gas meter and on the hot-wire anemometer were then taken at a number of different flowrates, four or five usually being sufficient. The wet-gas meter reading gave values of $\bar{U}_{ave}$ and from the curve described above the corresponding value of $\bar{U}_{max}$, the velocity of the air passing over the hot-wire, could be obtained. A calibration curve for the hot-wire was then prepared by plotting $\frac{I^2R_w}{R_w-R_g}$ against $(\bar{U}_{max})^{\frac{1}{2}}$. To check the accuracy of the calibration curve obtained in this way, readings taken at low flowrates were compared with those obtained at higher flowrates using the pitot tube in the test-section. The results, plotted on Fig. 3.13, show that very good agreement was obtained in the region of overlap.

3.11 OPERATING PROCEDURES

The operating procedures followed in obtaining the different sets of measurements reported in this work are outlined below, details being given only where points of particular practical importance are discussed. Further details of calibration procedures and methods of operation can be found in section 3.10 and Appendix D respectively.

Practical points relevant to all runs include

i) During both heated and unheated runs it was desirable that changes in ambient temperature should be as small as possible and for this reason most measurements were taken at night between 9 p.m. and 4 a.m. when temperatures varied least.

ii) It was noted that, during unheated runs, an alteration in air flow rate caused the air temperature to change

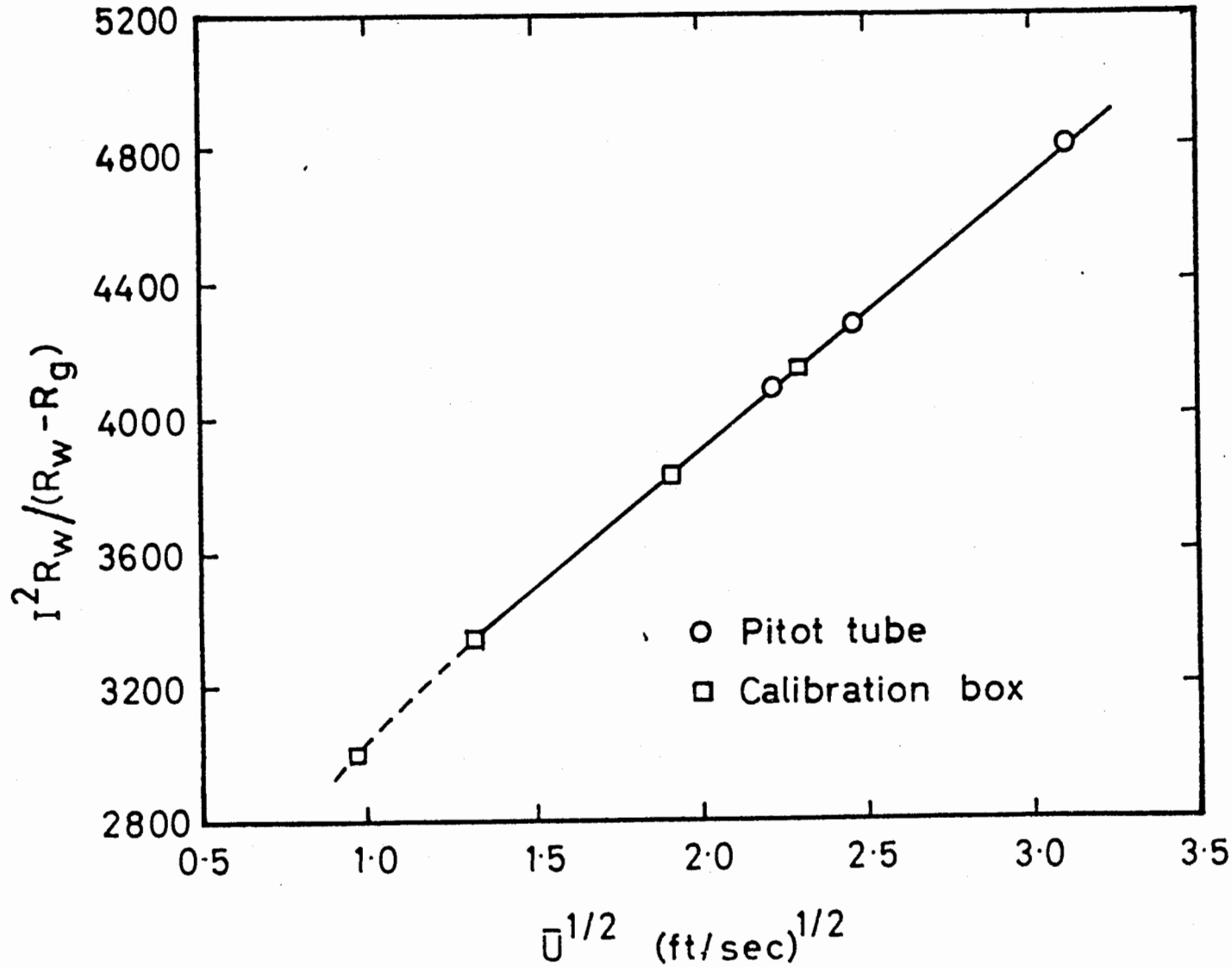

FIGURE 3.13 COMPARISON OF CALIBRATION POINTS OBTAINED IN THE CALIBRATION SYSTEM AND WITH THE PITOT TUBE

slightly for up to an hour afterwards. This change resulted from an alteration in the rate of heat loss from the blower which generated a small but significant amount of heat. During calibration runs, where great accuracy was essential, it was therefore necessary to wait for up to an hour after each flowrate change before taking further measurements.

3.11.1 Isothermal velocity and turbulence measurements.

The general procedure followed to obtain the isothermal mean velocity and turbulence intensity measurements reported for runs IT-1 to IT-5 is given below:

a) The hot-wire was calibrated either in the calibration system described in section 3.10.3 (Re ≈ 5000) or against the pitot tube in the test-section as explained in section 3.10.1 (Re ≈ 14000).

b) The hot-wire was positioned in the pipe as described in section 3.4.2.

c) The flow rate was adjusted to the desired value and the equipment left for up to an hour to attain equilibrium.

d) The time constant of the hot-wire was determined.

e) Velocity and turbulence intensity measurements were made at a number of y/R positions, following the procedures laid down in Appendix D. Changes during operation were taken into account by checking the centre-line values every four or five readings.

f) The hot-wire was recalibrated to determine whether significant changes in calibration parameters had occurred during the run.

The procedure for runs I-1 to I-17 differed from that given above in that:

i) No turbulence measurements were taken.

ii) The calibration of the hot-wire was always carried out using the pitot-tube.

iii) The probe was initially positioned relative to the pipe wall by a visual method. The accuracy of this setting

was then checked by measuring velocities at the 0.04, 0.03, 0.025, 0.02, 0.015, 0.01 and 0.005 y/R positions and extrapolating the resulting velocity profile to zero to find the intercept on the y/R axis.

iv) The abbreviated method of measuring a mean velocity profile, described in Appendix D, was followed.

3.11.2 Non-isothermal velocity, temperature and turbulence measurements.

The operating procedures for the three sets of runs, N-1 to N-9, N-10 to N-14 and NT-1 to NT-5 differed in a number of respects. The most complicated procedure was that for the runs NT-1 to NT-5 and this is described below; the ways in which the procedures for the other two sets of runs differed from that described are given at the end of this section.

a) The variation with temperature of the "cold" resistance, R_g, of the hot-wire was determined.

b) Calibration curves of velocity against current were determined, either in the calibration system (Re ≃ 5000) or against the pitot tube in the pipe (Re ≃ 14000), for up to 6 overheating ratios between 0.01 and 0.7.

c) The hot-wire was positioned in the pipe as described in section 3.4.2.

d) The flowrate through the pipe and the power input to the heating ribbon were set to the desired levels and the equipment left for a minimum of 8 hours to reach a steady condition.

e) The variations of the time constant of the hot-wire with overheating ratio and with position in the tube were determined.

f) Velocity and turbulence intensity readings were made, as described in Appendix D, at a number of positions over the pipe cross-section. At each position readings were taken at up to six values of the overheating ratio, and, in addition, measurements of the intensity of the temperature fluctuations were made. Since the readings at a single y/R position took as long as four or five hours to complete, measurements were spread over four days, with

the result that the final velocity profiles were less accurate than those for runs N-1 to N-14.

g) When the above readings were completed a temperature profile was measured.

h) Thermocouple readings were noted.

i) The temperature and velocity calibration curves were checked.

The procedure for runs N-10 to N-14 was similar to that given above except as stated below:

i) No turbulence measurements were obtained.

ii) Measurements were taken at one overheating ratio (0.5) only.

iii) The run lasted only about 8 hours and temperatures were determined from R_g measurements made during velocity measurements. Readings were taken at a much larger number of y/R positions.

The procedure for runs N-1 to N-9 differed from that for runs N-10 to N-14 only in so far as positioning and calibration procedures were concerned. Details of the procedures used are the same as those given for runs I-1 to I-17 in section 3.11.1.

CHAPTER 4

ISOTHERMAL RESULTS.

4.1 PRELIMINARY CONSIDERATIONS

4.1.1 Introduction

Although the main emphasis in the present investigation was on measurements in heated flows a number of preliminary measurements were made in isothermal flows. These measurements served the following purposes:

i) They enabled familiarity with the method of operation of the hot-wire to be obtained.

ii) They could be compared with existing results, thus providing a check on the accuracy of the measuring techniques employed.

iii) They permitted a body of results to be established with which later measurements in heated flows could be compared. This was important as it ensured that both isothermal and non-isothermal measurements were obtained by similar methods and using the same equipment and any differences between the two sets of results could therefore not be attributed to differences in experimental apparatus or technique.

Altogether 22 isothermal velocity profiles were obtained and these are reported as runs I-1 to I-17 and IT-1 to IT-5. Four isothermal axial intensity profiles, runs IT-1 and IT-3 to IT-5, were also measured. A description of the apparatus, together with an outline of the operating procedures, is given in Chapter 3, while the experimental results are tabulated in Appendix F. Sample calculation procedures can be found in Appendix G.

4.1.2 Entrance lengths.

In order to ensure that the velocity profile in the vicinity of the measuring station is fully developed, the distance from the pipe entrance to the point of measurement must exceed a certain minimum number of pipe diameters known as the entrance length. Opinions on what value this minimum should take differ considerably and Brown [91] and Christiansen [103] show in reviews of published information on entrance lengths that values ranging

from 40 to 100 have been proposed. Most of the recommended values lie between 40 and 60, however, and higher values are in general only required when the initial turbulence level in the pipe is low. Since the turbulence levels in the entrances to the present test sections were high it was therefore concluded that the lower entrance length values of 50 to 60 would apply in the present work and hence the actual L/D values used - 83 for Loop I and 113 for Loop II - would be more than sufficient to ensure that fully developed conditions were established well upstream of the measuring stations. This conclusion is confirmed by the measured results which indicate that no further profile change takes place after 83 diameters from the pipe entrance.

4.2 VELOCITY PROFILES.

4.2.1 Previous work-Theory.

The subject of isothermal velocity profiles has been extensively investigated and because several detailed reviews of published information are already available [105,106], only a brief summary of previous work is given below.

It is possible to describe any steady isothermal turbulent flow using the time-averaged momentum equation but a solution of this equation can be obtained only if a complete knowledge of the statistical functions describing the turbulent motion is available. For the particular flow situation studied here this means that there must be precise information on the correlation $\overline{v_r v_z}$ before an exact solution for the velocity distribution in the pipe can be obtained. Since information of the desired accuracy is not yet available other methods of predicting velocity profiles have therefore had to be developed. These methods have all been based on semi-empirical or empirical hypotheses, most of which have involved ε_M, the eddy viscosity or eddy diffusivity of momentum, which is related to $\overline{v_r v_z}$ by

$$\varepsilon_M \frac{\partial \overline{V}_z}{\partial r} = - \overline{v_r v_z} \qquad (4.1)$$

The earliest theories of importance developed in connection with velocity profile predictions were the mixing-length hypotheses of Taylor [108], Prandtl [107] and von Karman [109]. Though each of these workers defined the mixing length in a different

way, all these hypotheses gave rise to an equation of the form

$$u^+ = \frac{1}{K} \ln y^+ + B \qquad (4.2)$$

the so-called log law, on which many subsequent velocity profile predictions have been based. Equations of the form of equation (4.2), for which a variety of values of K and B have been proposed [106], have been shown to provide a good fit to measured velocity data, though significant differences between measured and predicted values are observed both near the pipe centre and also near the pipe wall where viscous effects predominate over turbulent effects. Of these differences that near the wall is more important and the "laminar" relation

$$u^+ = y^+ \qquad (4.3)$$

which provides a good fit to experimental results, is generally employed to describe velocity profiles in the wall region.

Probably the best known theoretical velocity distribution based on the above equations is that due to von Karman, with the constants evaluated from the experimental results of Nikuradse [115]. This distribution

$$\begin{aligned} u^+ &= y^+ && y^+ < 5 \\ u^+ &= 5 \ln y^+ - 3.05 && 5 \leq y^+ < 30 \\ u^+ &= 2.5 \ln y^+ + 5.5 && y^+ > 30 \end{aligned} \qquad (4.4)$$

is known as the universal velocity profile.

In the same way that equation (4.3) was introduced to allow for deviations from the log law near the pipe wall, equations have also been developed to take account of deviations from the log law in the centre of the pipe. These equations have taken two main forms, the first of which involved a velocity defect law of the form

$$u_c^+ - u^+ = f(y/R) \qquad (4.5)$$

which has been employed by several workers with fair success. A full review of proposed equations taking the form of (4.5) can be found in [106] and only the equations of von Karman [110],

$$u_c^+ - u^+ = -\frac{1}{0.3} \left(\ln\left[1 - \sqrt{1 - y/R}\right] + \sqrt{1 - y/R} \right) \qquad (4.6)$$

of Ruth and Yang [111],

$$u_c^+ - u^+ = 3.08 - 5.695 \log [e^{1.5(1-n^{3/2})} - 1] \quad (4.7)$$

and of Hinze [40]

$$u_c^+ - u^+ = -\frac{1}{0.41} \ln y/R + 0.8 + h_2(y/R) \quad (4.8)$$

(where $h_2(y/R)$ is a correction term introduced to make the equation agree with the results of Laufer [112])

are compared with present measurements (see Fig. 4.5).

The second method of accounting for deviations from the log law in the pipe centre involved the introduction of a correction function into the log law equation. Typical equations of this form are those of Millikan [113],

$$u^+ - h_1(y/R) = 5.75 \log y^+ + 5.0 \quad (4.9)$$

and of Bogue and Metzner [114],

$$u^+ - C(y/R,f) = 5.57 \log y^+ + 5.57 \quad (4.10)$$

where

$$C(y/R,f) = 0.05(2/f)^{\frac{1}{2}} \exp\left\{\frac{-(y/R - 0.8)^2}{0.15}\right\}$$

These two equations are compared with present measurements in Figs. 4.6 and 4.7 respectively.

Several other hypotheses, such as that of Reichardt [128], have also been proposed in attempts to find a basis on which more accurate velocity distributions can be predicted. These have not been significantly more successful than the mixing length hypothesis already considered and in consequence are not discussed here.

Apart from predictions which have been developed from theories such as the mixing-length hypothesis a number of empirical attempts to correlate mean velocity distributions have been proposed. Of these the most important are the predicted distributions of Reynolds et al [129] and Travis et al [130] which not only allow for deviations from the log law in the centre of the pipe and near the pipe wall, but also take account of variations in velocity profile shape with Reynolds number. These predictions are compared with measured results in the following sections.

4.2.2 Previous work - Experimental measurements.

Experimental velocity measurements in isothermal turbulent flows of air, water and other fluids have been made by a large number of workers and important papers dealing with the low to moderate Reynolds number range ($\leq$ 40 000) are listed in Table 4.1.

4.2.3 Experimental results.

Tabulated values of the isothermal velocity profiles obtained in the present work are given in Table F.1. Measurements were made at six nominal† Reynolds numbers - 5000, 7000, 11000, 16000, 22000, 32000 - at least two profiles being measured at each Reynolds number to make sure results were reproducible. In general very good agreement was obtained, particularly between runs IT-1, IT-2 and IT-3 (Re $\simeq$ 5000) and between runs IT-4 and IT-5 (Re $\simeq$ 16000). Certain profiles were also checked for symmetry by taking measurements at y/R values up to 1.3. Agreement between measurements at equal distances from the axis was very good (see, for example, run I-1) confirming that the profiles were symmetrical.

4.2.4 Discussion of results

The change of velocity profile shape with Reynolds number is shown clearly in Fig. 4.1 where, for Reynolds numbers of 5000, 16000 and 32000, velocities as $\overline{V}_z/\overline{V}_{z_c}$ are plotted against radial position. As expected, the greatest changes occur at the lower Reynolds numbers.

In Fig. 4.2 five measured profiles covering the Reynolds number range of 5000 - 32000 are compared on a u^+ vs y^+ plot with the universal velocity distribution defined by equation (4.4). The agreement is seen to be good except at high y/R values where the experimental values lie above the predicted line by amounts which increase as the Reynolds number decreases, a trend similar to

---

† The term nominal is introduced here to indicate that measurements were not obtained at Reynolds numbers of exactly 5000, 7000 etc. but at different Reynolds numbers close to these values.

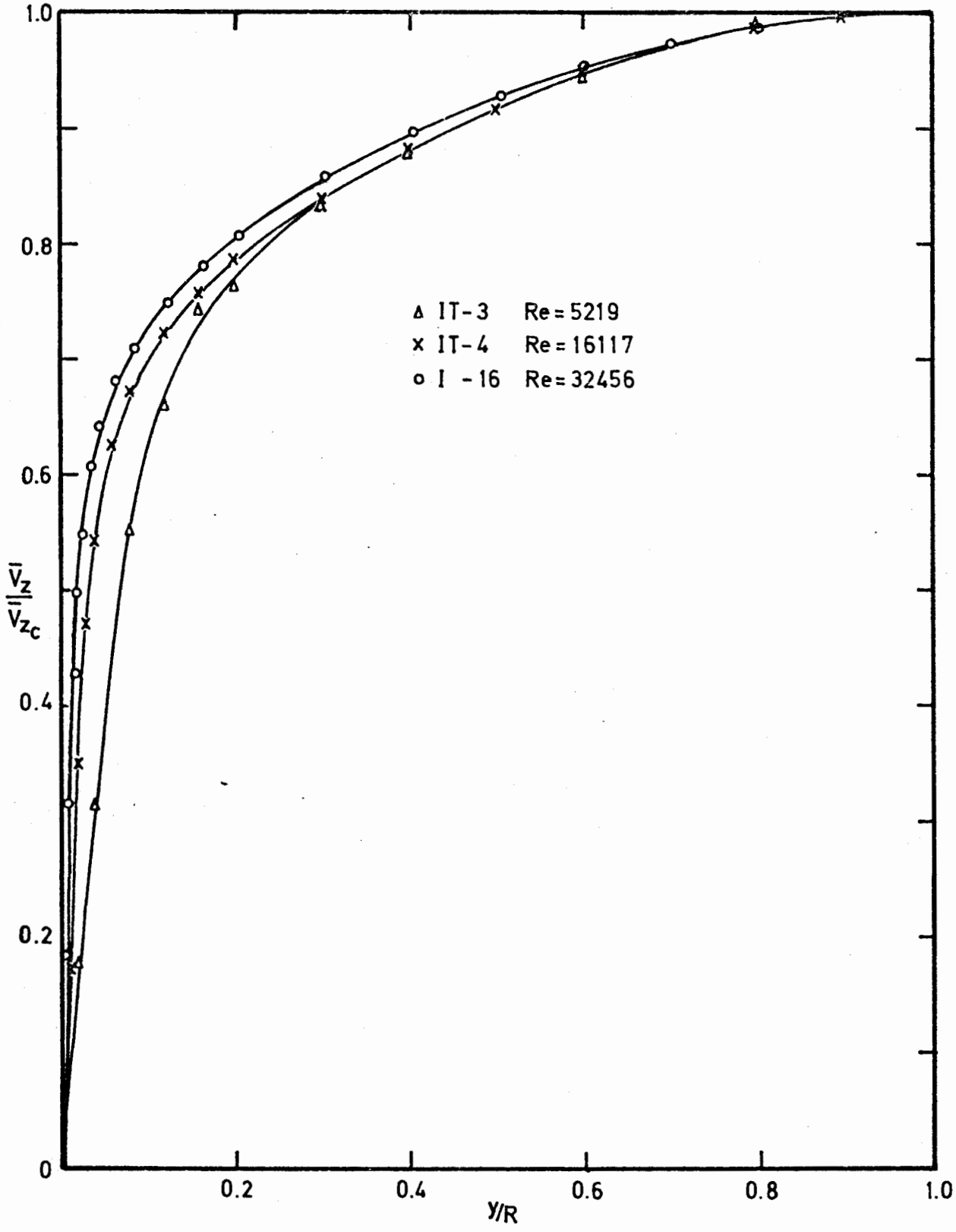

FIGURE 4.1 EFFECT OF REYNOLDS NUMBER ON VELOCITY PROFILE SHAPE

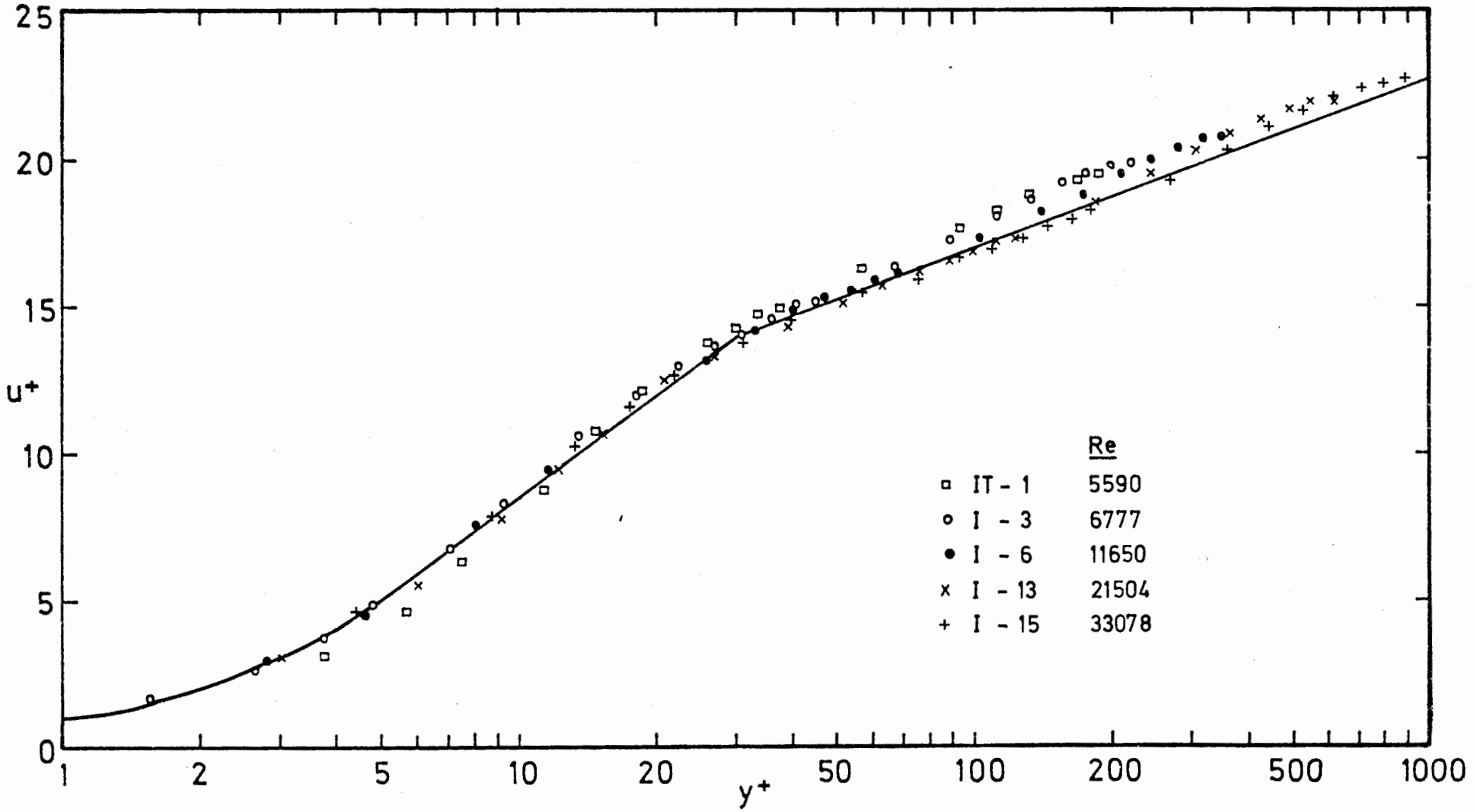

FIGURE 4.2 MEASURED VELOCITY PROFILES COMPARED WITH THE UNIVERSAL VELOCITY DISTRIBUTION

TABLE 4.1

EXPERIMENTAL ISOTHERMAL VELOCITY PROFILE MEASUREMENTS.

INVESTIGATOR	YEAR	FLUID	REYNOLDS NUMBER RANGE $Re \times 10^{-3}$	ENTRANCE LENGTH L/D
Nikuradse [115]	1932	Water	3.0-3240	200 and 125
Deissler [116]	1950	Air at 40 p.s.i.	8.0-220	100
Senecal [117]	1951	Air	3.0-4.1	360 and 240
Laufer [112]	1954	Air	40.3-403	49
Sandborn [38]	1955	Air	40.2-241	55
Sleicher [92]	1956	Air	11.3-60.0	81
Abbrecht and Churchill [104]	1960	Air	15.0-65.0	< 44
Brookshire [134]	1961	Air	4.8-201	96
Johnk [132]	1961	Air	18.0-71.0	121
Beckwith and Fahien [118]	1963	Water	10.7-18.9	84
Bogue and Metzner [114]	1963	Sugar solution	0.8-26.0	150
Christiansen [103]	1965	Air	8.9-56.0	41
Lindgren [119]	1965	Water	6.1-49.0	186
Bakewell [120]	1966	Glycerine	8.7	≈ 25
Rein [106]	1967	Air	10.1-39.7	97
Coantic [89]	1967	Air	40.0-360	49
Koo [135]	1967	Air	7.3-58.3	52
Genin et al [121]	1967	Mercury	20.0-42.5	88
Sherwood et al [136]	1968	Water	8.6-59.2	≈ 81
Reynolds et al [129]	1968	Air	3.0-15.0	255
Gardner [122]	1969	Mercury	16.0-157	53
Kudva [123]	1970	Ethylene glycol	5.9-6.0	132
Horsten [24]	1971	Mercury	18.3-84.4	95

that observed by other workers, e.g. Senecal [117], Reynolds et al [129] and Corcoran et al [137]. A tendency for the results to be slightly greater than predicted values in the buffer layer region is also apparent.

Fig. 4.3 shows representative profiles at Re ≈ 5000 and Re ≈ 7000 in comparison with those of other workers. Particularly good agreement between the profiles from the present work and those of Senecal [117] and Reynolds [129] is observed. Patel and Head's [138] measurements fall only slightly below these but Lindgren's [119] results fall much further below, lower even than results at much higher Reynolds numbers, and their accuracy must in consequence be suspect.

A representative profile at Re ≈ 32000 is shown in comparison with other measured results in Fig. 4.4; all the profiles are observed to be very similar and no particular trends are observed, confirming (as does Fig. 4.3, also) that the measuring techniques evolved in the present investigation give accurate results.

In section 4.2.1 details were given of three velocity defect equations (4.6 to 4.8) and these are shown in Fig. 4.5 in comparison with experimental results at Reynolds numbers of 5000, 16000 and 32000. It is apparent that, in general, the measured data lie below the predicted values and none of the proposed expressions agrees well with the experimental measurements over the whole y/R range.

Section 4.2.1 also deals with the equations of Millikan (4.9) and of Bogue (4.10) which contain correction functions introduced to take account of differences between theoretical and measured velocities in the pipe centre. The values proposed for these correction functions are compared in Figs. 4.6 and 4.7 with those evaluated from measured velocity profiles at Reynolds numbers of 5000, 16000 and 32000, and it is clear that considerable differences between proposed and measured values exist. In particular it can be seen that Millikan's equation fails to allow for any variation with Reynolds number while Bogue's equation predicts a dependence of correction function on Reynolds number

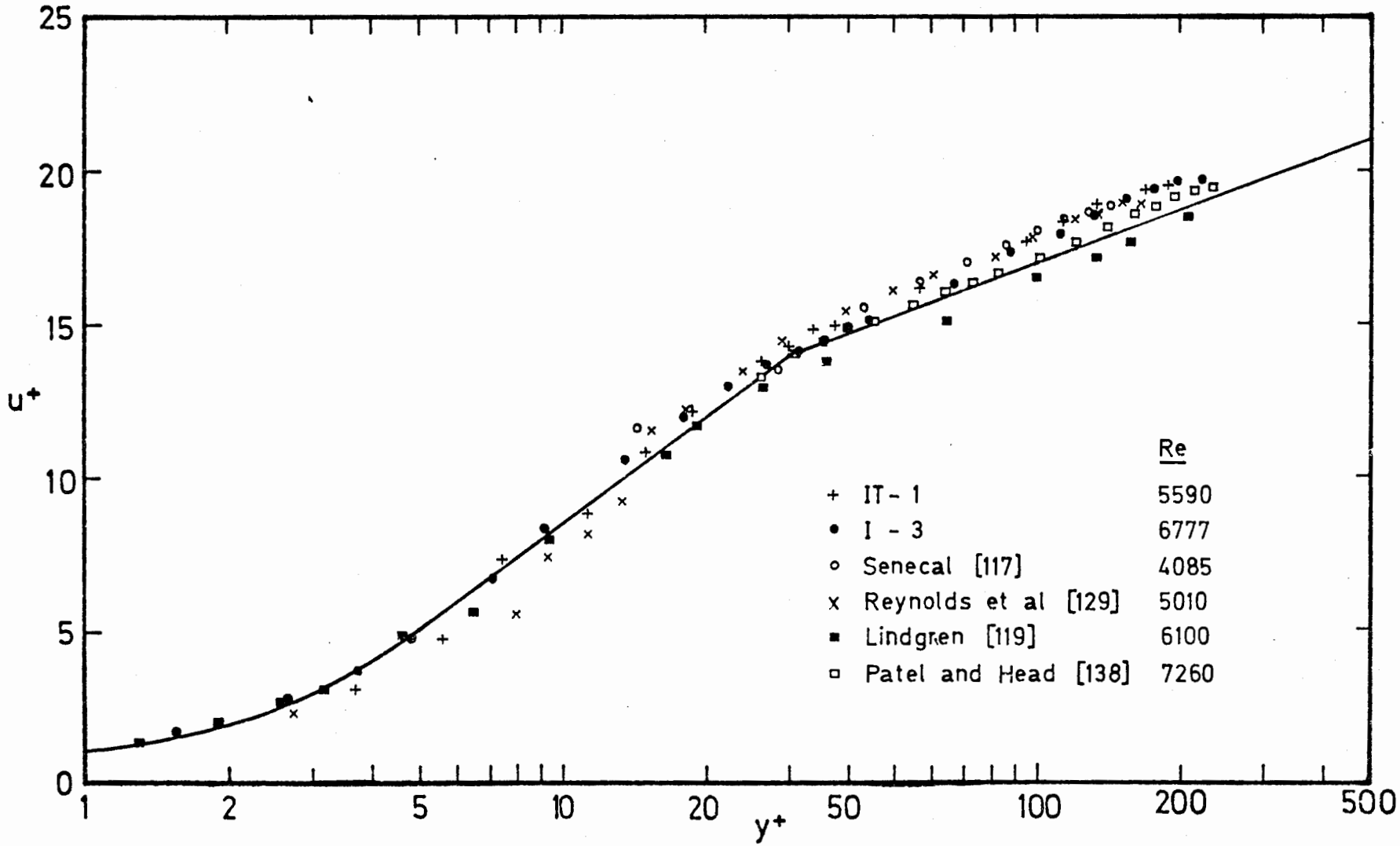

FIGURE 4.3 VELOCITY DATA AT LOW REYNOLDS NUMBERS IN COMPARISON WITH THE RESULTS OF OTHER WORKERS

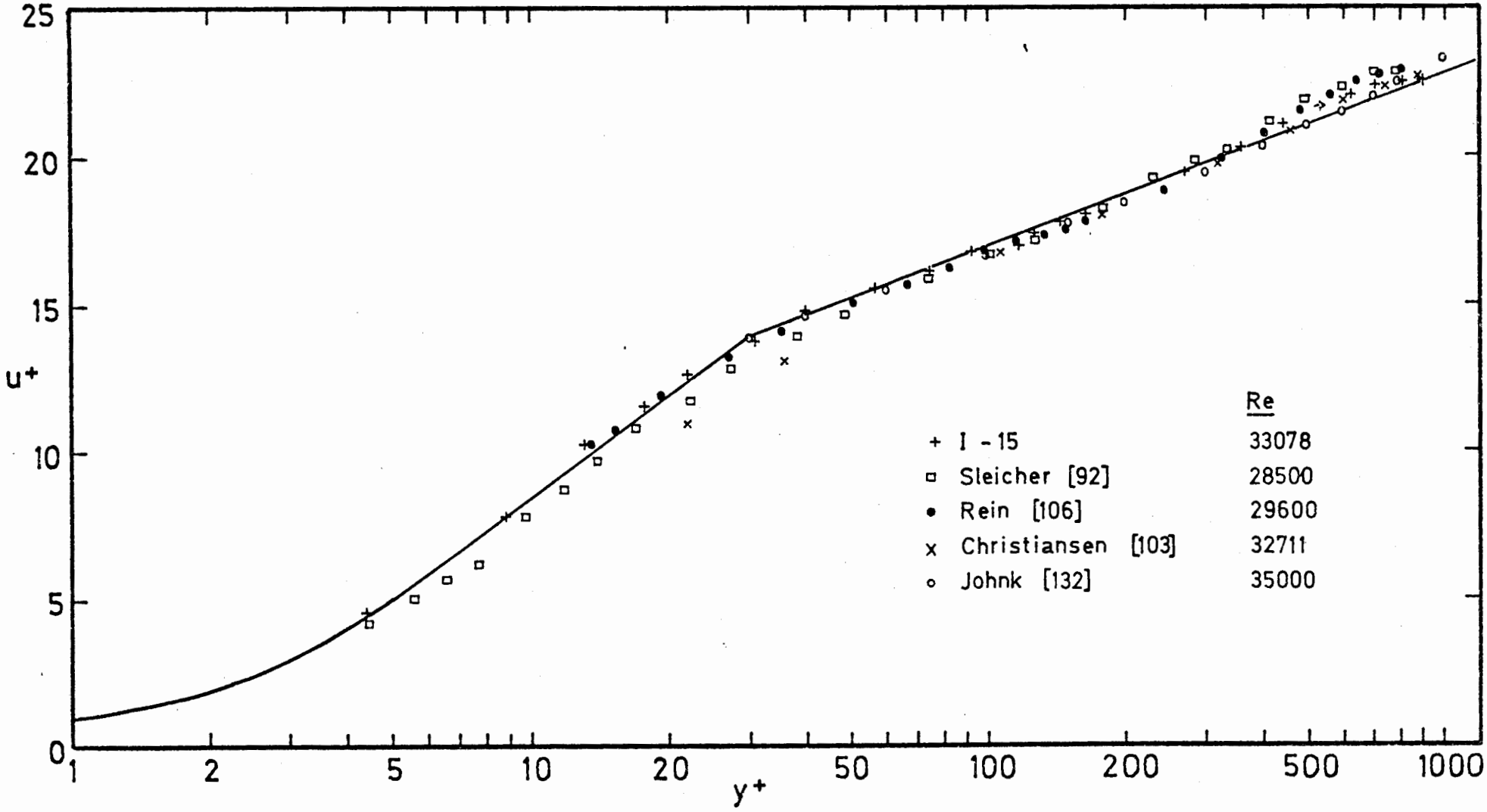

FIGURE 4.4 VELOCITY DATA AT Re ≃ 32000 IN COMPARISON WITH THE RESULTS OF OTHER WORKERS

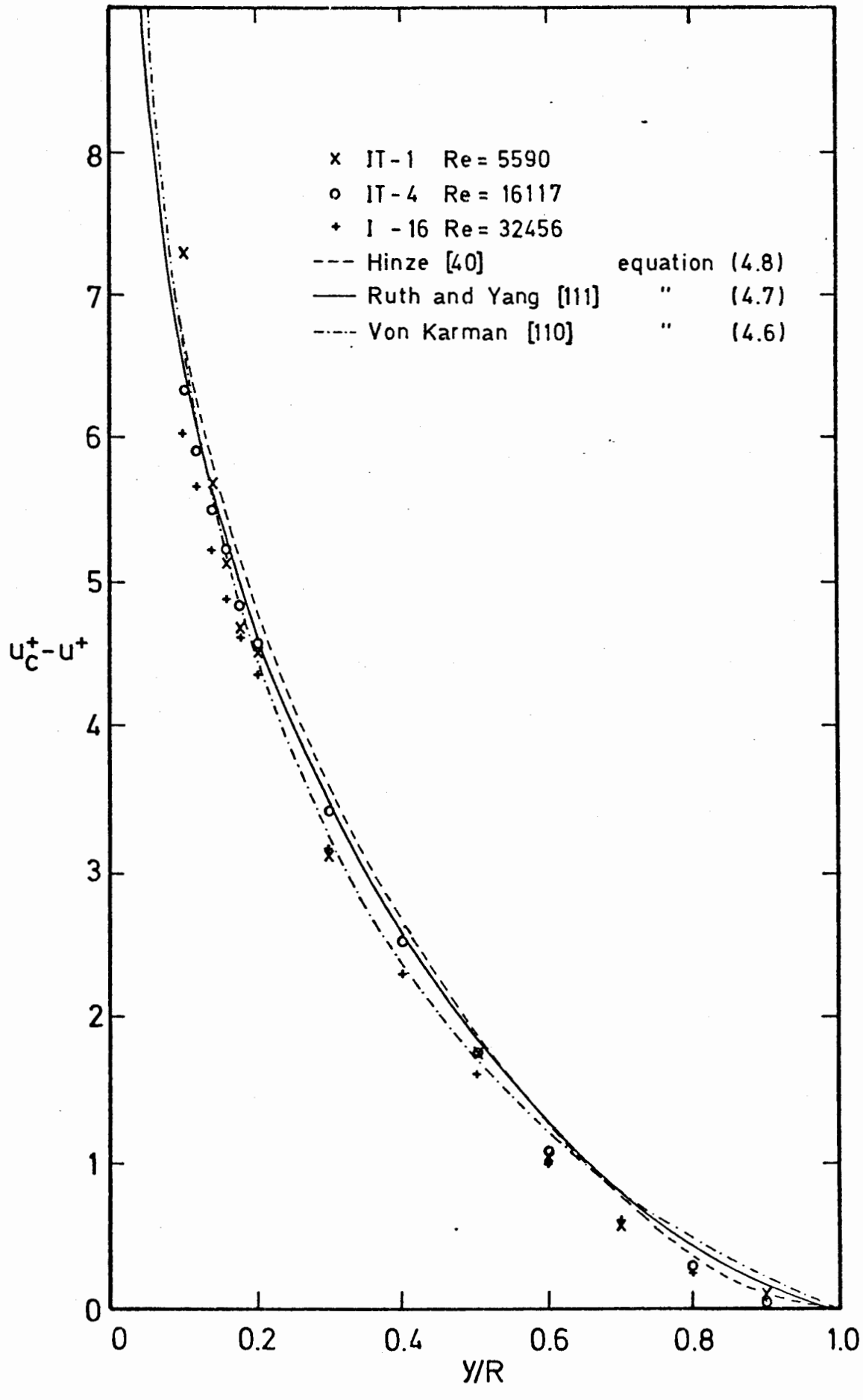

FIGURE 4.5 COMPARISON OF TYPICAL DATA WITH VELOCITY DEFECT EQUATIONS

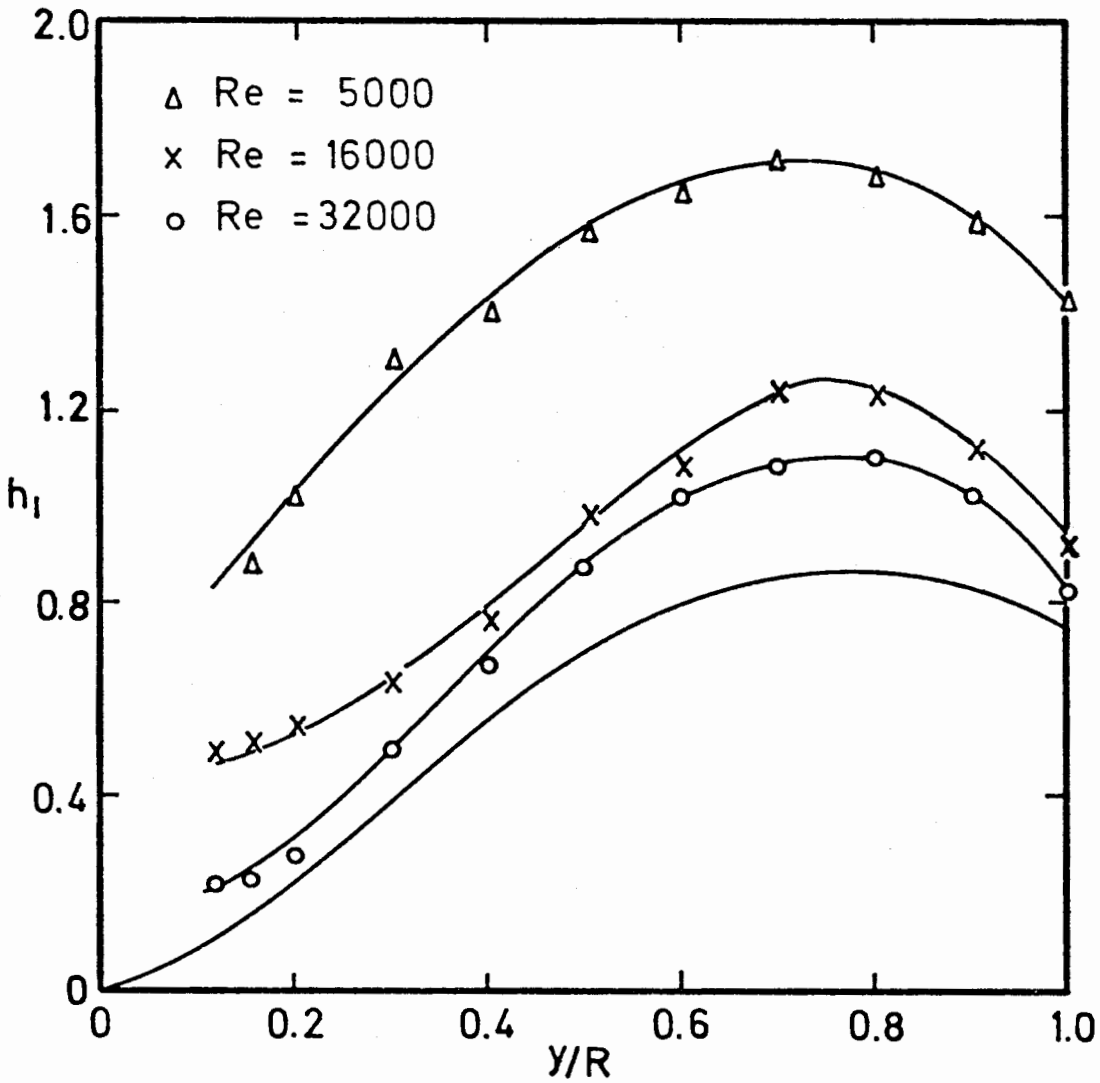

FIGURE 4.6 MILLIKAN'S VALUES FOR h_1 COMPARED WITH VALUES CALCULATED FROM THE PRESENT RESULTS AT Re ≃ 5000, 16000 AND 32000

—— Millikan's h_1 curve

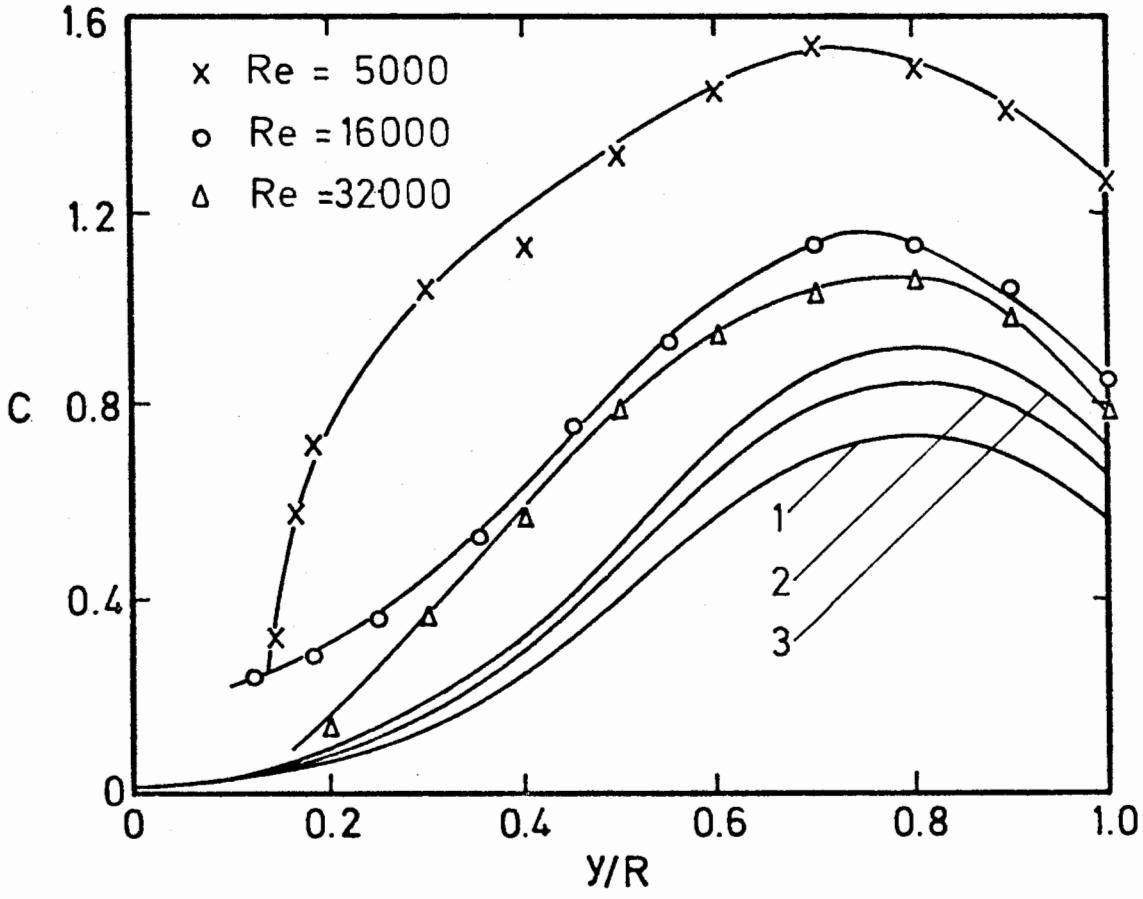

FIGURE 4.7 COMPARISON OF VALUES OF C CALCULATED FROM EQUATION (4.10) WITH VALUES FROM PRESENT RESULTS

1 : Calculated value for Re = 5000
2 : Calculated value for Re = 16000
3 : Calculated value for Re = 32000

which is opposite to that observed in practice.

A comparison was also made between the present data and the predictions of other workers, particular attention being paid to the low Reynolds number region where errors in predictions are usually most apparent. Excellent agreement with the predictions of Travis et al [130] was observed at all Reynolds numbers, Travis' profile at Re ≈ 5000, for example, being practically identical to that shown in Fig. 4.1, and it is concluded that Travis' prediction is the best presently available.

In Fig. 4.8 values of $\overline{V}_{z_m} / \overline{V}_{z_c}$, the ratio of mean to centre velocity, for the present results are compared with curves proposed by Robertson [139] and Ross [97]. Although the results show a certain amount of scatter it is clear that at the lowest Reynolds numbers (Re ≈ 5000, 7000) agreement with Robertson's proposed curve is good, whereas at higher Reynolds numbers (Re > 16000) Ross' curve is closer to the data.

4.3 EDDY DIFFUSIVITIES.

4.3.1 Introduction.

As explained in Chapter 1, it is customary to represent variations of the Reynolds stress component $\overline{v_r v_z}$ in terms of variations of the eddy diffusivity of momentum, ε_M. This latter quantity is related to the velocity distribution and the friction factor by equation (1.19) which was used in the present work to calculate eddy diffusivities from measured velocity data.

4.3.2 Previous work.

Because of the importance of being able to predict isothermal velocity profiles, a large number of papers on eddy diffusivities in isothermal pipe flows have been published. Most of these papers have dealt with semi-empirical and empirical correlations for predicting eddy diffusivity values, and an extensive and up-to-date review of these correlations has been presented by Horsten [24]. In a number of these papers, however, measured eddy diffusivity values have also been reported, and a selection of these measurements, plotted as ε_M/Ru^*, is shown in Fig. 4.9, in which two early eddy diffusivity predictions, those of

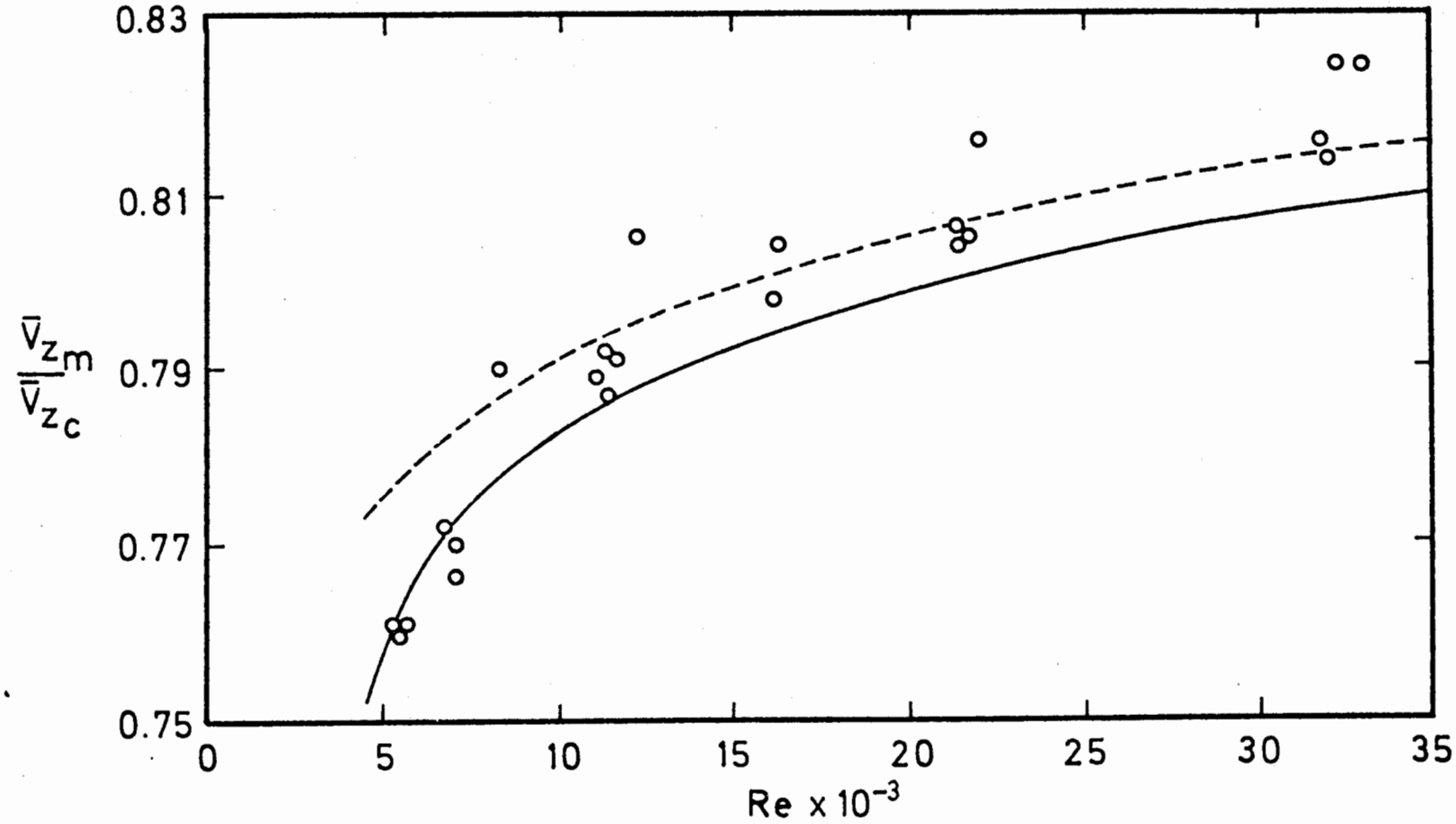

FIGURE 4.8 VARIATION OF $\bar{V}_{z_m}/\bar{V}_{z_c}$ WITH REYNOLDS NUMBER

o Present results

— Robertson [139] (--- Nikuradse as in Ross [97])

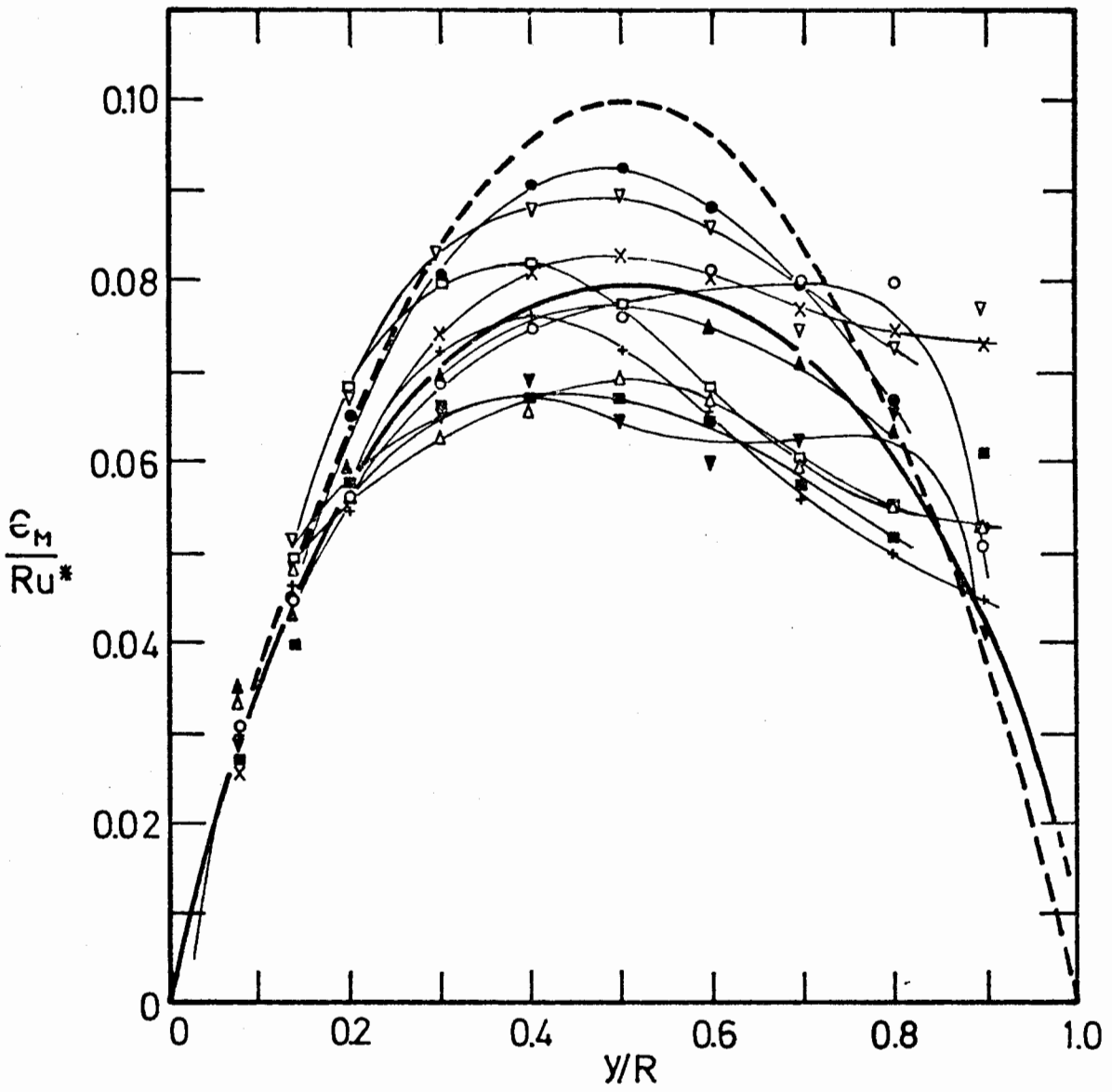

FIGURE 4.9 VALUES OF ε_M/Ru* FROM VARIOUS SOURCES - FROM [24]

—o— Laufer [112], Re=428000 Air
—▼— Laufer [112], Re=40300 Air
—+— Rein [106], Re=36700 Air
—■— Sleicher [92], Re=40000 Air
—▲— Stanton [150], Re=40900 Air
——— Nikuradse [115], Re > 10^5 Water
—×— Page et al [146], Re=53200 Air
—●— Sesonske et al [147], Re=99000 Hg
—▲— Sesonske et al [147], Re=62000 Hg
—□— Buhr [23], Re=89200 Hg
—▽— Buhr [23], Re=89700 Hg
– – – von Karman [109], eqn (4.4)

von Karman [109] and Nikuradse [115] are included for comparison. The more recent correlations of Reynolds et al [129] and Travis et al [130], which allow for variations of eddy diffusivity with Reynolds number, are shown in Figs. 4.12 and 4.13 in comparison with experimental data at Reynolds numbers of 5000 and 32000 respectively. In general these and other theoretical predictions agree fairly well with one another in the intermediate y/R range but differ widely in the regions near the pipe wall and near the pipe centre. Near the pipe wall the extent of the differences is shown by Fig. 4.10 where the ε_M/ν values predicted at low y^+ values for a Reynolds number of 11500 are shown, together with experimental values from the present work. Nearer the pipe centre equally large variations in predicted and measured eddy diffusivities occur, these differences being due to the difficulties involved firstly, in obtaining velocity data accurate enough to define clearly the exact shape of the velocity profile in the central region, and secondly in establishing a differentiation procedure which will yield correct values for the very small velocity profile slopes occurring in this region.

4.3.3 Experimental results.

Eddy diffusivity values obtained from the velocity profiles reported in section 4.2 are tabulated in Table F.2, Appendix F, together with the smoothed velocity values from which they were computed as explained in Appendix C.

The mean of the calculated eddy diffusivity values at each of the 6 nominal Reynolds numbers - 5000, 7000, 11000, 16000, 22000 and 32000 - are shown as ε_M/Ru^* values in Fig. 4.11; individual values for the runs at Re ≈ 5000 and Re ≈ 32000 are shown in Figs. 4.12 and 4.13 where they are compared with several predicted ε_M/Ru^* distributions. A comparison of results in the wall region with a selection of theoretical eddy diffusivity predictions is given in Fig. 4.10.

4.3.4 Discussion of results.

The comparison of present eddy diffusivity results with previous measurements given in Fig. 4.9 shows that the present results lie close to values reported by other workers. For $y/R > 0.3$ Fig. 4.11 shows that the present results are closely grouped about

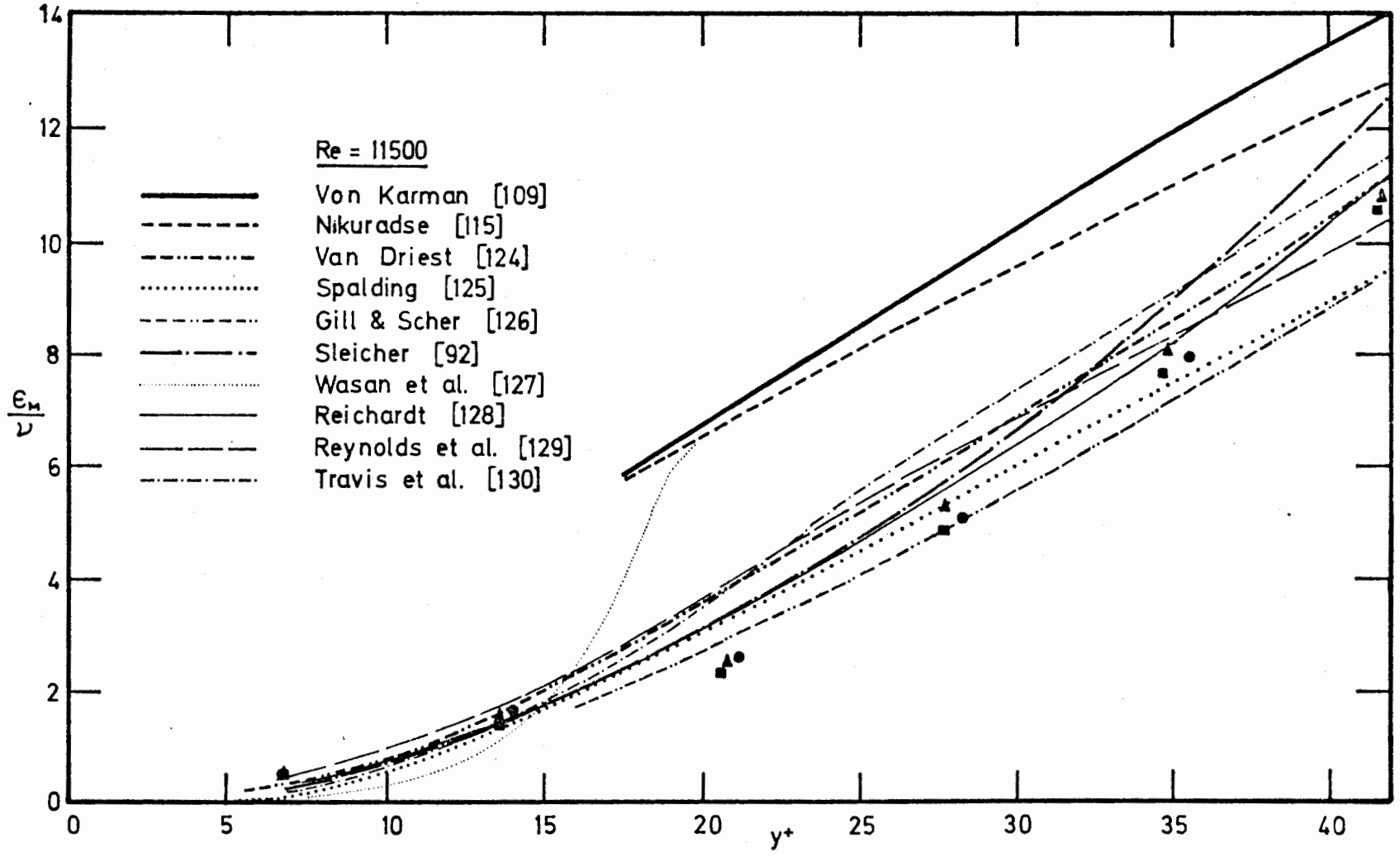

FIGURE 4.10 PREDICTED ε_M/ν VALUES FOR THE WALL REGION COMPARED WITH ε_M/ν VALUES FROM THE PRESENT WORK

■ I-5 Re = 11334 ● I-6 Re = 11650 ▲ I-7 Re = 11412

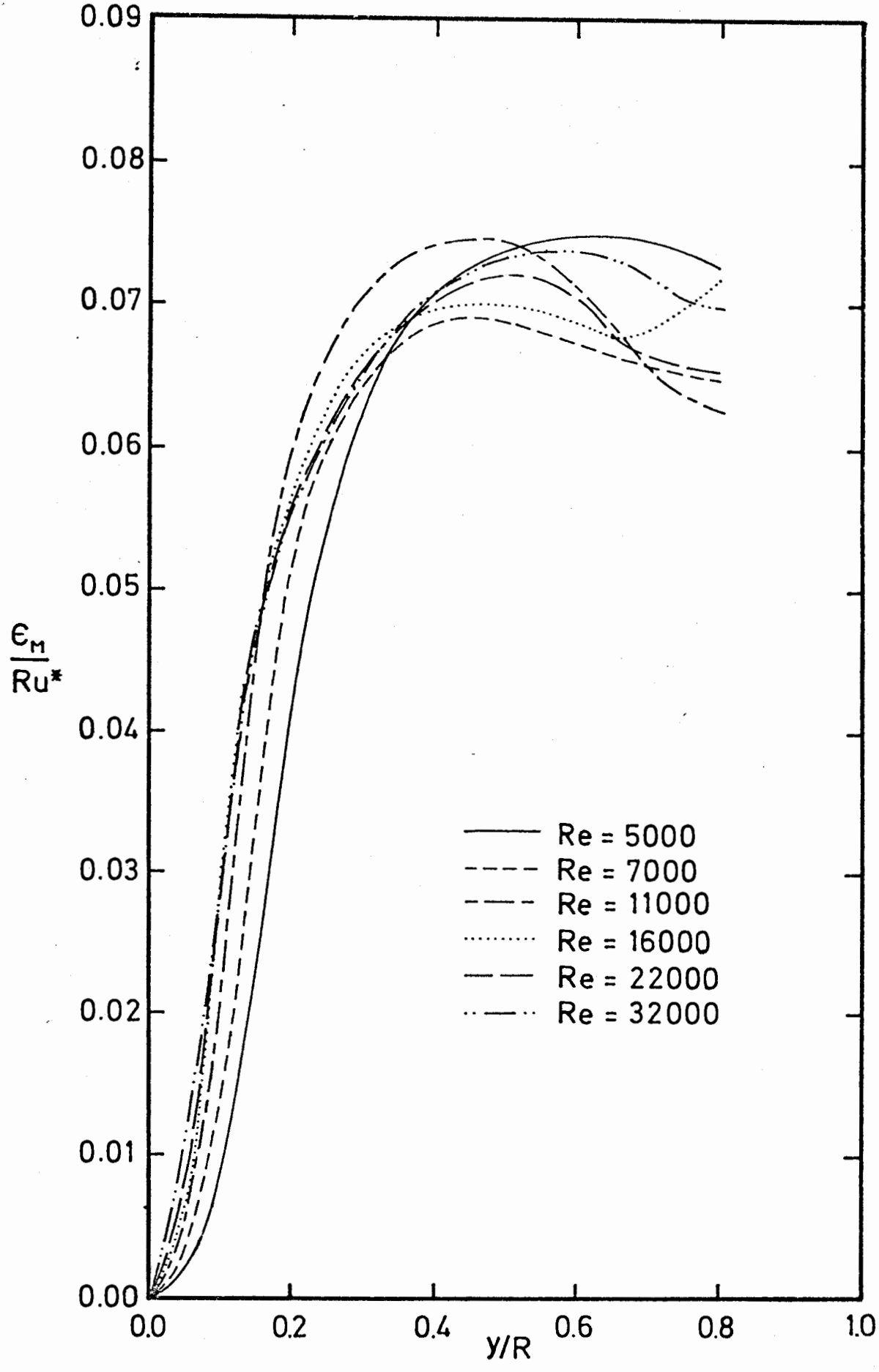

FIGURE 4.11 MEAN ϵ_M/Ru^* VALUES AT DIFFERENT REYNOLDS NUMBERS

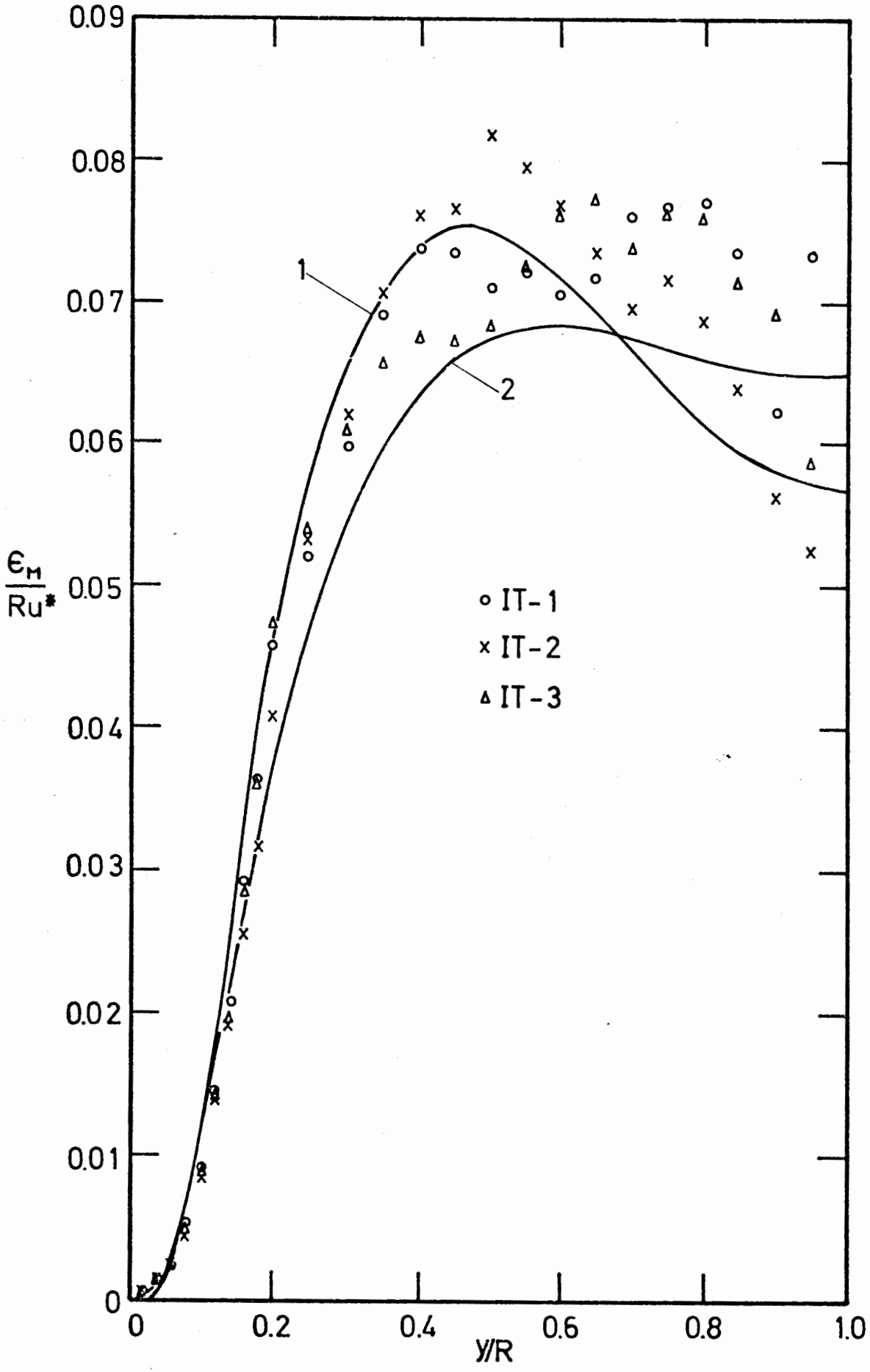

FIGURE 4.12 ε_M/Ru^* VALUES AT Re ≃ 5000 COMPARED WITH PREDICTIONS OF TRAVIS ET AL [130] AND REYNOLDS ET AL [129]

1 : Travis et al [130] 2 : Reynolds et al [129]

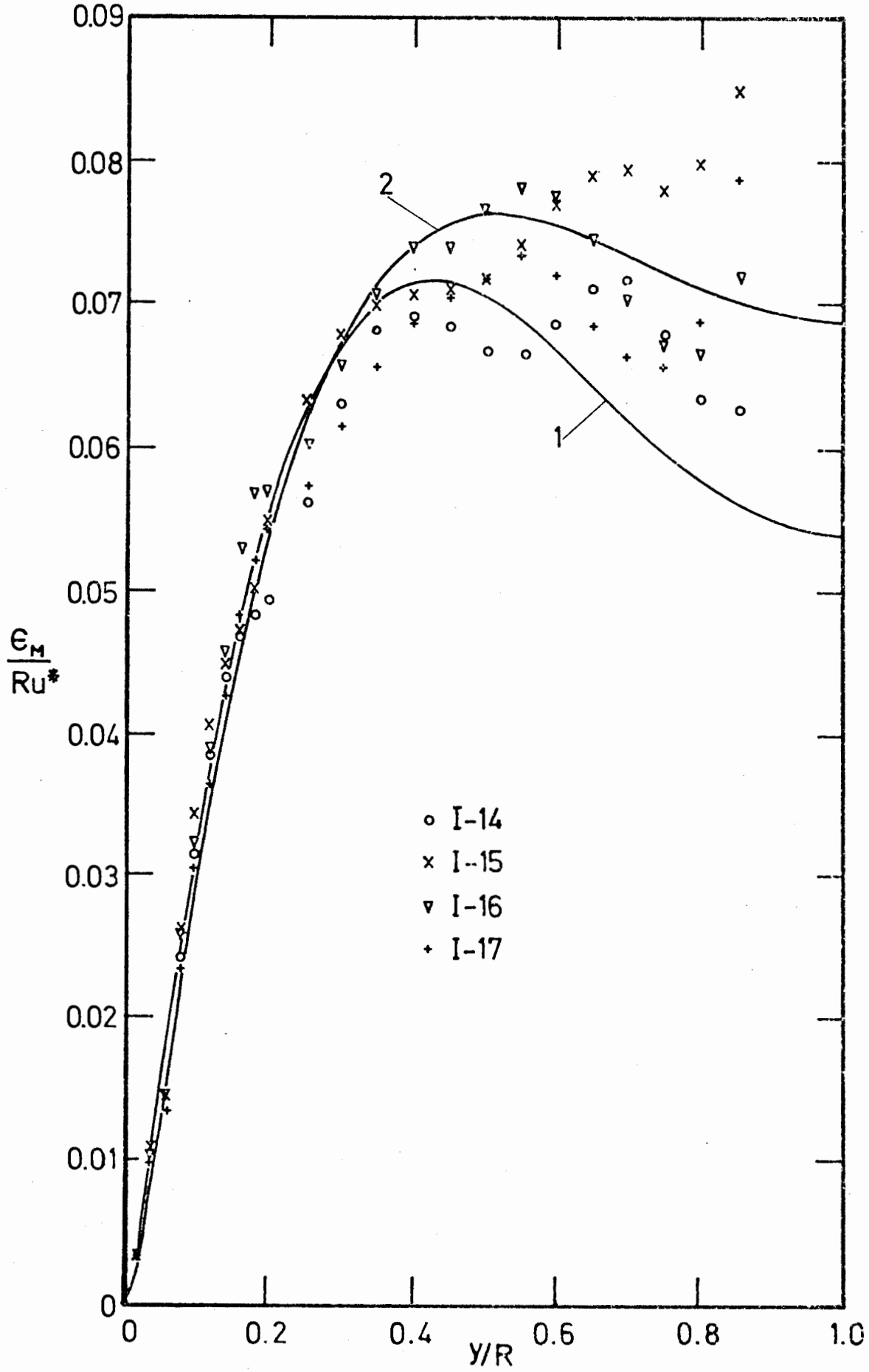

FIGURE 4.13 ε_M/Ru^* VALUES AT Re ≃ 32000 COMPARED WITH PREDICTIONS OF TRAVIS ET AL [130] AND REYNOLDS ET AL [129]

1 : Travis et al [130] 2 : Reynolds et al [129]

an ϵ_M/Ru^* value of 0.07 and follow no particular trend with Reynolds number. For $y/R < 0.3$, however, a definite trend with Reynolds number is apparent, corresponding to the increase in thickness of the viscous sublayer as the Reynolds number decreases. It is clear from this observation that eddy diffusivity predictions, such as those of von Karman [109] and of Nikuradse [115], which make no allowance for such a dependence on Reynolds number, are therefore of little use at the low Reynolds numbers of interest in the present work.

More recent eddy diffusivity correlations, such as those of Reynolds et al [129] and Travis et al [130] do take the Reynolds number variation into account and eddy diffusivity curves predicted by these two sets of authors are shown in comparison with measured values at $Re \simeq 5000$ and $Re \simeq 32000$ in Figs. 4.12 and 4.13 respectively. In the important range of $y/R < 0.6$ there appears to be little to choose between the curves in Fig. 4.13 but Fig. 4.12 suggests that the Travis correlation is better at low Reynolds numbers. At very low y/R values on the other hand, the situation is reversed and according to Fig. 4.10 the prediction of Reynolds et al lies closer to the measured data. In the $y/R > 0.6$ region, although the trend of the present results suggests that Reynolds' prediction is more nearly correct than that of Travis, the uncertainty in the measured results is too large for firm conclusions on this point to be reached.

It is apparent from the above discussion that the predictions of Reynolds and Travis agree equally well with the present results. However, because it has been shown [24] that Travis' prediction agrees better with results in mercury, the Travis correlation is recommended in preference to that of Reynolds et al.

4.4 AXIAL TURBULENCE INTENSITIES.

4.4.1 Introduction.

Axial turbulence intensities are usually the turbulence quantities most easily measured in a given flow situation and besides giving an excellent indication of the flow structure they

are useful in calculating corrections to be applied to measured velocities. (Details of these corrections are given in Chapter 2.) For the particular situation studied in this work measurements were taken using a single hot-wire probe held normal to the mean flow direction, and intensities were calculated using the relationships developed in Chapter 2.

Values for the axial intensity $v'_z = \sqrt{\overline{v_z^2}}$ have been measured in pipe flows by a number of workers and results for the low Reynolds number (< 20 000) range are listed in Table 4.2. These values, with the exception of the present results, are plotted as v'_z/u^* in Fig. 4.14. From Fig. 4.14 it can be seen that although the shapes of these turbulence intensity profiles

TABLE 4.2

INVESTIGATOR	YEAR	REYNOLDS NUMBER	L/D
Hall [140]	1938	5100 11700	80
Brookshire [134]	1961	4800 9780 20000	96
Gessner [141]	1965	16000	130
Koo [135]	1967	7300	52
Brown [91]	1968	20200	93
Present work	1971	5000 16000	113

are similar, values at any given radial position differ by as much as 40% in the worst cases. Several possible reasons for these differences have been advanced:

i) Coantic [89] has shown that the failure of many workers to allow for very low frequency fluctuations when measuring turbulence intensities can introduct significant errors. For the case investigated by Coantic these errors increased from 3% at Re ≈ 150 000 to 8% at Re ≈ 41 000 and, since the percentage of the total turbulence energy contained in the low frequency fluctuations increases with decreasing Reynolds number, even larger errors will occur in the

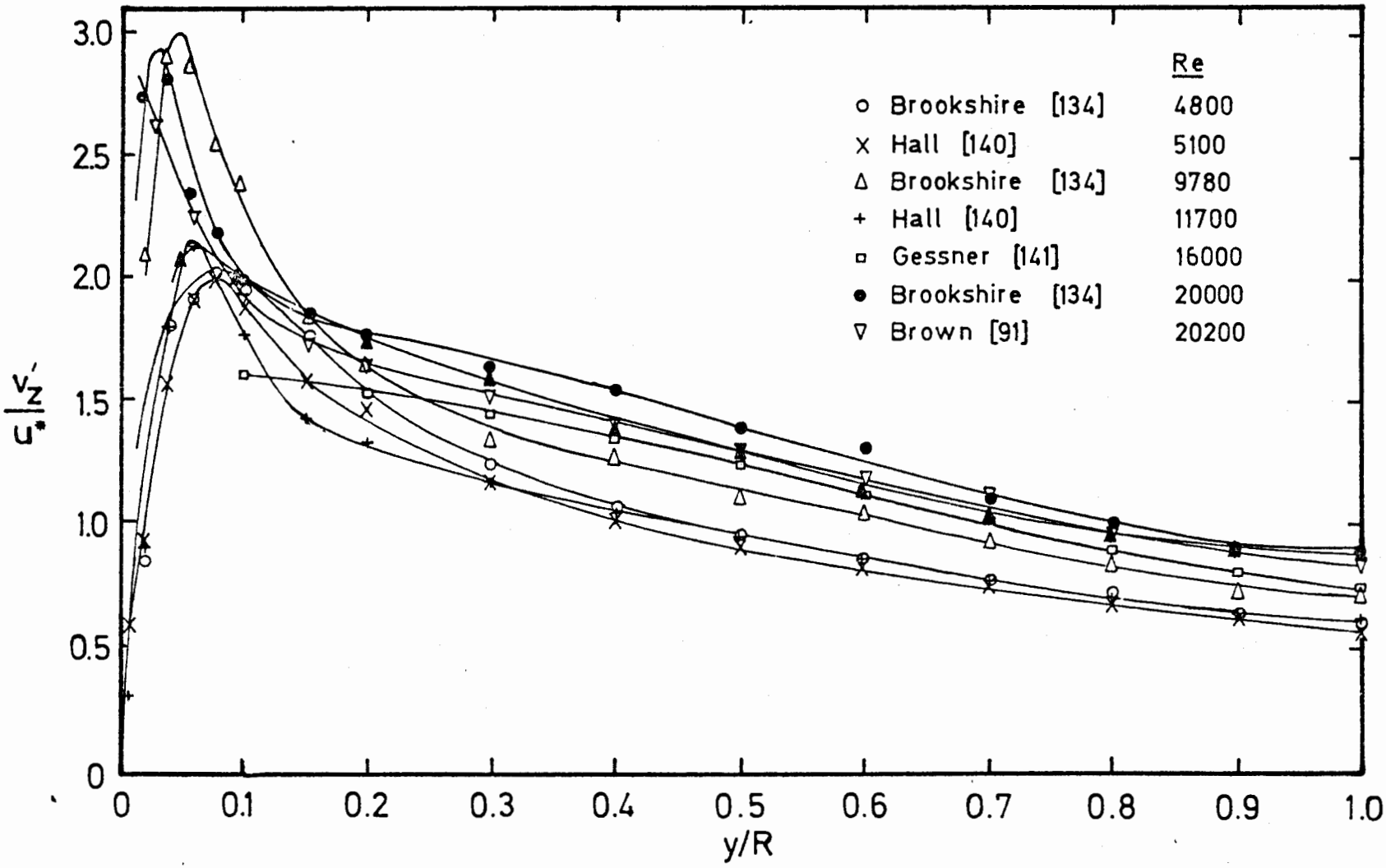

FIGURE 4.14 LOW REYNOLDS NUMBER AXIAL TURBULENCE INTENSITIES REPORTED BY OTHER WORKERS

Reynolds number range considered here. The importance of the low frequencies is emphasised by some approximate energy spectra obtained in the present study. These showed that at Re ≈ 5000 the turbulence energy is concentrated in the frequencies below 100 Hz, with a relatively high percentage of the energy being contained in the very low frequencies (below 5 Hz) where the frequency response of many amplifiers begins to decrease rapidly.

ii) Operation of hot-wires by the different methods of constant current and constant temperature operation also affects measurements, particularly at higher relative intensities [40].

iii) The non-linear dependence of wire voltage on velocity also introduces errors in turbulence intensity readings, particularly at high relative intensities - see Chapter 2. These errors can be reduced, though not completely eliminated, by using a linearised hot-wire system.

4.4.2 Experimental results.

During runs IT-1 and IT-3 to IT-5 axial turbulence intensity profiles at Reynolds numbers of 5000 and 16000 were measured. The experimental results are reported in Appendix F, Table F.3 and sample calculation procedures are given in Appendix G.

These results are plotted as v'_z/u^* in Fig. 4.15 with the measurements of Gessner [141] at Re ≈ 16000 and of Brookshire [134] at Re ≈ 9800 for comparison. Unlike the results plotted in Fig. 4.14 the present measurements are seen to increase slightly with decreasing Reynolds number, a difference attributable to the very low cut off frequency in the present amplifier which enabled a far greater proportion of the energy contained in the low frequency fluctuations to be taken into account. A secondary trend noted in the present results is that of the movement of the peak intensity nearer the wall as the Reynolds number increases. It has been pointed out by Rein [106], however, that this trend disappears when results are plotted against y^+ instead of y/R.

Fig. 4.15 also shows that the present results at each individual Reynolds number agree well, confirming that the measured

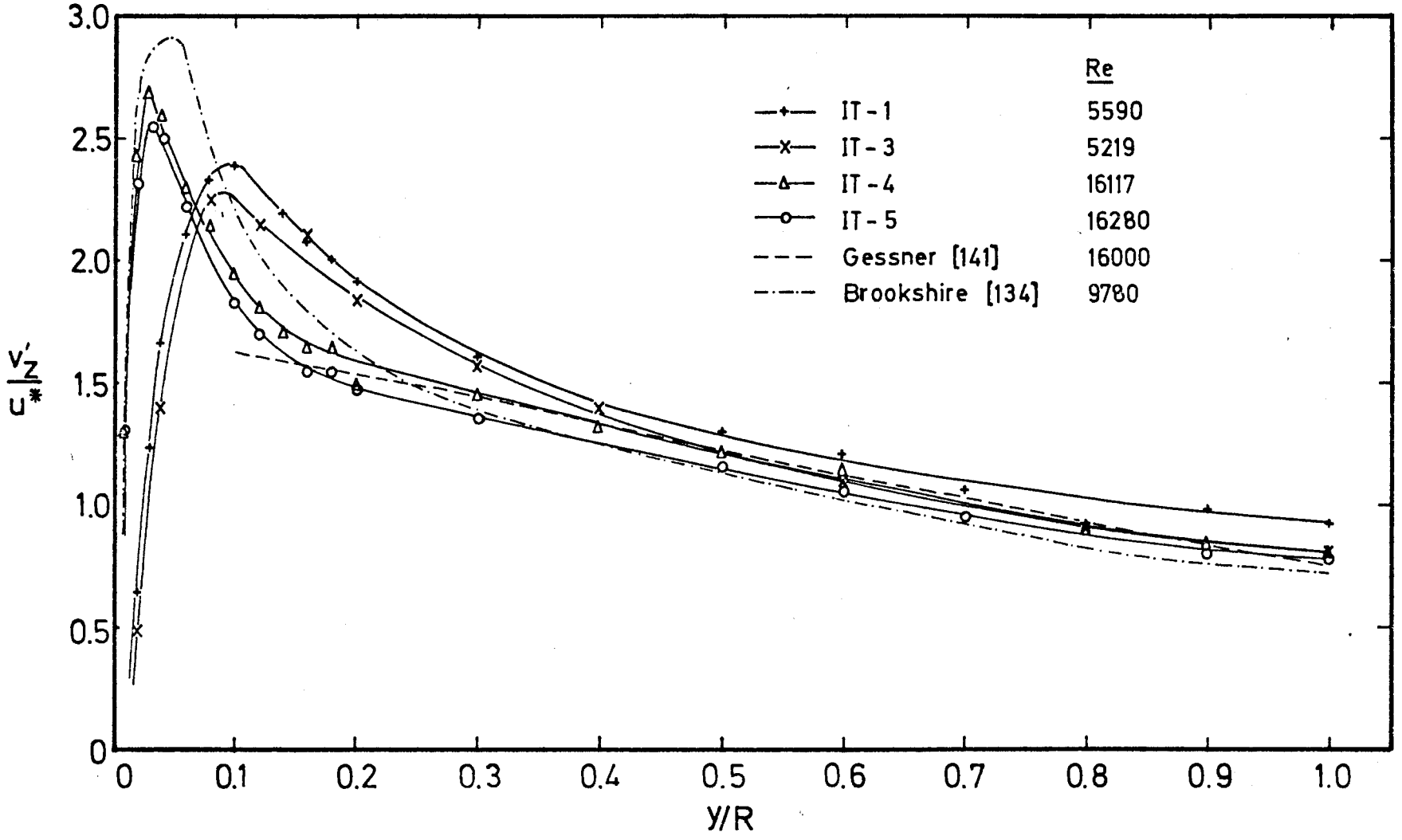

FIGURE 4.15 PRESENT AXIAL TURBULENCE INTENSITY MEASUREMENTS COMPARED WITH RESULTS OF OTHER WORKERS

profiles are reproducible. Since these profiles also lie close to the bulk of other experimentally measured values it was concluded that the turbulence measuring section of the hot-wire anemometer was performing well and could be used with confidence for later measurements in heated flows.

CHAPTER 5

NON-ISOTHERMAL RESULTS

5.1 INTRODUCTION

5.1.1 Preliminary considerations

The aim of the present experiments was to measure fully-developed velocity and temperature distributions in low Reynolds number heated flows and hence to determine the values of the eddy diffusivities of heat and momentum under mixed convection conditions. At the same time measurements of axial turbulent velocity intensities and temperature intensities were also to be made, in order to gain a greater understanding of the effect of buoyancy forces on the flow structure.

It was expected that these buoyancy forces would be significant only at relatively high heat inputs and low Reynolds numbers and this wa confirmed by later measurements. An initial run (N-1) at Re ≈ 25000 and a relatively high heat input showed that no significant changes in the velocity profile occurred at this Reynolds number and subsequent measurements showed that considerably distorted velocity profiles could only be obtained in the present equipment at Reynolds numbers below about 10000 In order to measure as wide a range of distorted profiles as possible most of the experimental readings were therefore taken at Reynolds numbers of 8000 and 5000, though a few measurements of relatively undistorted profiles at a Reynolds number of 14000 were made for comparative purposes. The detailed conditions for these runs are given in Table 5.1 below. (In this table N is used t describe runs where the emphasis was on velocity and temperature profile measurements while NT refers to runs where the emphasis was on turbulence measurements and temperature profile measurements.)

TABLE 5.1

Run No.	Re	Heat flux Btu/hr ft^2	Ra	Gr x 10^{-6}	Gr/Re_2 x 10^{-2}	Y
N-2	8031	64.9	1463	4.14	5.15	15.3
N-3	8016	57.3	1268	4.25	5.30	15.7
N-4	8638	31.9	948	3.49	4.04	11.3
N-5	8474	28.3	878	3.22	3.80	10.8
N-6	8507	28.1	776	3.24	3.81	10.8
N-7	8783	11.6	406	1.13	1.28	3.5
N-8	8659	19.5	660	2.76	3.19	8.9
N-9	6794	41.6	1203	4.07	5.98	20.0
N-10	5354	8.4	490	0.92	1.71	8.0
N-11	5258	13.3	725	1.99	3.78	17.3
N-12	5278	20.7	960	2.47	4.67	18.2
N-13	5032	26.9	1110	2.66	5.29	19.5
N-14	13978	89.4	1264	2.38	1.71	3.4
NT-1	5405	5.0	345	0.58	1.06	4.2
NT-2	5525	10.7	700	1.27	2.29	8.9
NT-3	5419	13.4	774	2.20	4.05	16.0
NT-4	5154	21.1	1055	2.80	5.41	22.2
NT-5	14701	103.9	1346	2.64	1.80	3.4

The experimental results are tabulated in Appendix H and presented in sections 5.2 to 5.5; section 5.6 and later sections are concerned with eddy diffusivities and other calculated parameters, which were evaluated by substituting measured velocity and temperature distributions into the continuity, motion and energy equations derived in Appendix A. Since the derivation of these equations involved the assumptions that profiles were fully developed and that uniform heat flux conditions existed at the pipe wall, the accuracy of the above substitution depended on the extent to which these conditions were realised in practice, and this is discussed in sections 5.1.2 and 5.1.3 below.

5.1.2 The fully developed flow condition.

The question of fully developed flow is discussed in Appendix A where it is pointed out that in flows where there exists

an axial temperature gradient the resulting variation of viscosity in the axial direction will prevent the formation of a fully developed normalised velocity profile. It is also pointed out, however, that far from the pipe entrance a condition is reached where the rate of change of normalised profiles is very slight and the profiles can for all practical purposes be assumed to have reached a fully developed condition.

Several observations from the present results indicate that such a condition had been attained by most, if not all, of the flows investigated in the present study and this conclusion is supported by the experimental velocity profiles shown in Fig. 5.1. These profiles were obtained under comparable†, if not exactly similar, conditions of Reynolds number and heat flux; one profile, however, was obtained in Loop I (heated L/D = 70) and the other in Loop II (heated L/D = 100). As can be seen from Fig. 5.1, despite this L/D difference the shapes of the profiles are similar (the slight difference in degree of distortion in the region of y/R = 0.3 is to be expected, since the Reynolds numbers of the two profiles are not quite the same) and differ by a maximum of just over 1%. As this figure lies within the limits of experimental error it was concluded that after an L/D of 70 further changes in velocity profile shape are small and an effectively fully developed condition exists.

Additional evidence in support of this conclusion is provided by the measurements in mercury of Louw [151], who showed that velocity profiles obtained under mixed convection conditions were fully developed after 60 diameters.

5.1.3 Uniform heat flux

Because the heat transfer coefficient from a heated surface to a gas is relatively low a significant percentage, typically 15%, of

---

† It was very difficult to reproduce the conditions of one test-section in another test-section as Reynolds numbers and wall heat fluxes could only be evaluated with accuracy once a velocity profile had been measured and various temperature measurements obtained.

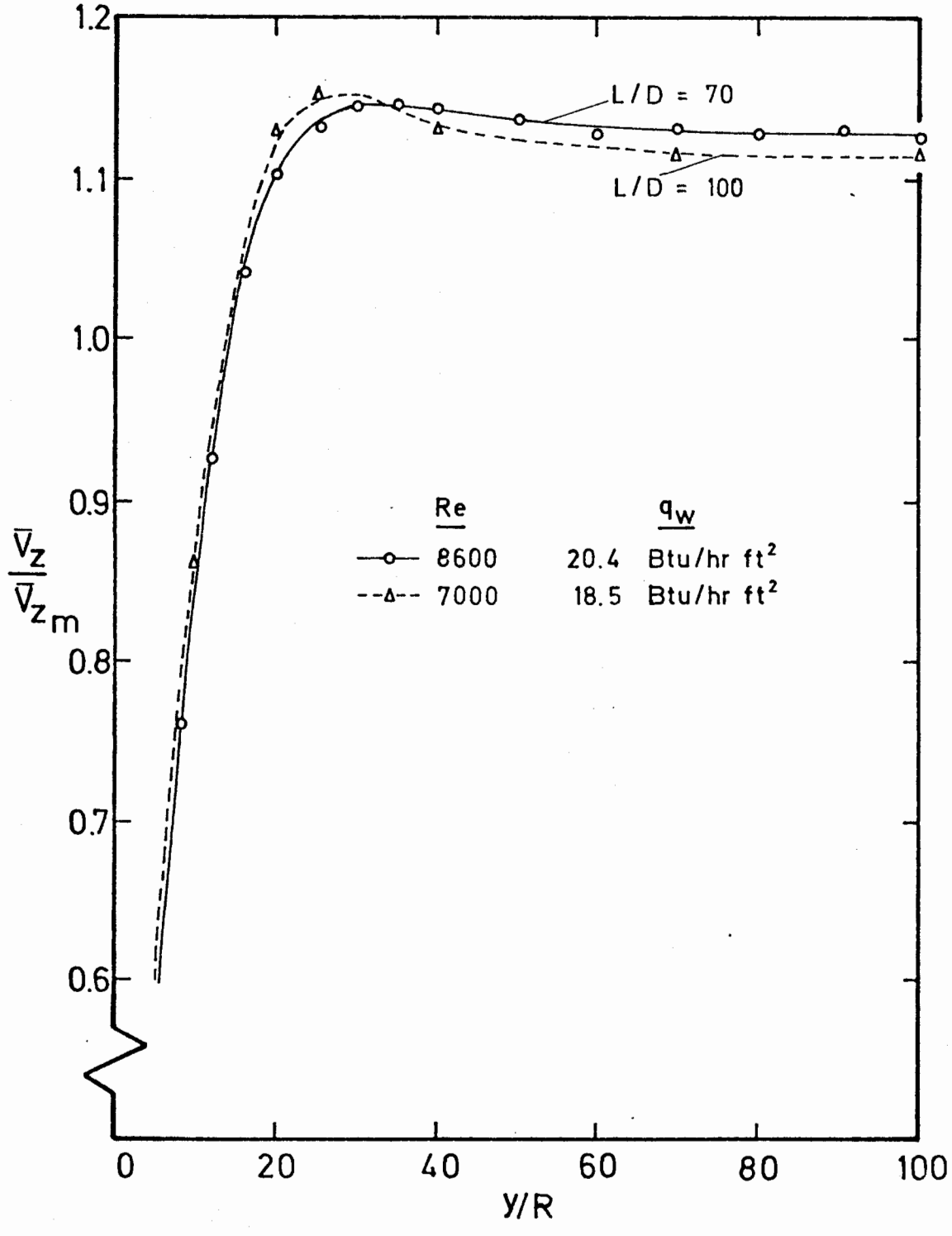

FIGURE 5.1 DISTORTED VELOCITY PROFILES AT DIFFERENT L/D VALUES

the heat generated in a heating coil is lost to the surroundings, despite the presence of insulation. It is consequently less easy to obtain a uniform wall heat flux condition with air than it is with other liquids. However, a typical plot of wall temperatures along the present pipe, such as that shown in Fig. 5.2, shows that a uniform wall temperature gradient exists and it can therefore be inferred that a uniform heat flux condition was achieved.

5.2 VELOCITY MEASUREMENTS

5.2.1 Introduction

A summary of the present velocity measurements (with the exception of run N-1) made under non-isothermal conditions is provided in Table 5.1 on page 97. Of these runs, N-1 to N-9 were measured in Loop I (L/D = 70) while the remainder were obtained in Loop II (L/D = 100). The operating procedures followed in taking these measurements are summarised in Chapter 3 and the experimental results tabulated in Appendix H, Table H.1. Sample calculation procedures are given in Appendix I.

5.2.2 Previous work

As discussed in Chapter 1, Ojalvo and Grosh [21] attempted to predict velocity profiles under mixed convection conditions but their assumption that isothermal values of the eddy diffusivities could be used under such conditions rendered their predictions invalid.

Measured velocity profiles under mixed convection conditions have recently (1971) been reported by Horsten [24] for mercury flows and by Steiner [19] for air flows. As mentioned in Chapter 1, Steiner considered that his profiles had re-laminarised but because they were measured at Reynolds numbers similar to those investigated in the present work, they are included in this discussion.

5.2.3 Experimental results

A selection of velocity profiles measured during the present work is reported in Figs 5.3, 5.4 and 5.5, which show measured values at nominal Reynolds numbers of 5000, 8000 and 14000 respectively. Isothermal results at the same Reynolds numbers are included for comparison. Several profiles at Re ≈ 8000 are omitted from Fig. 5.4 as only one representative profile from each

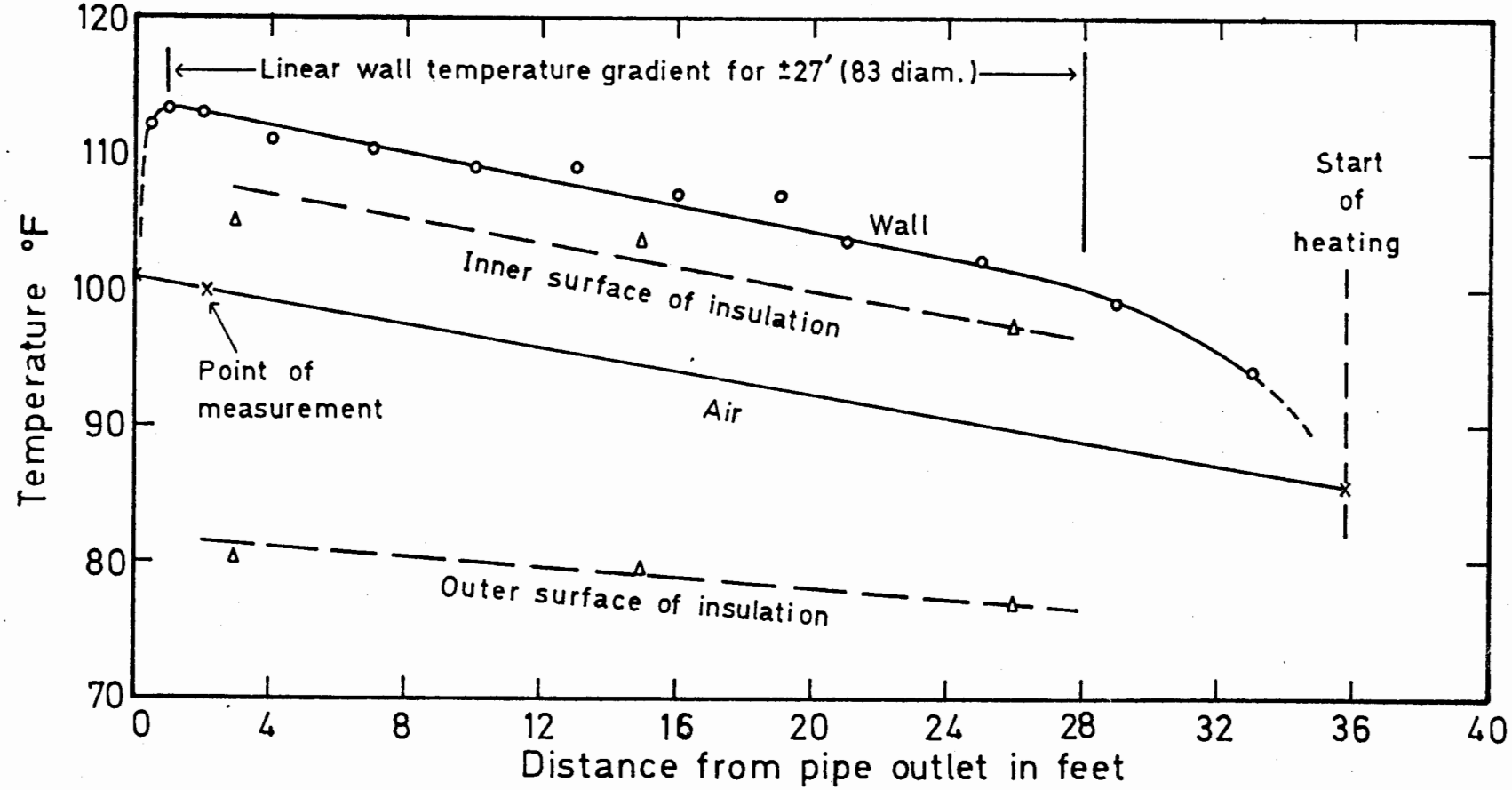

FIGURE 5.2 THE TEMPERATURE DISTRIBUTION IN THE TEST SECTION

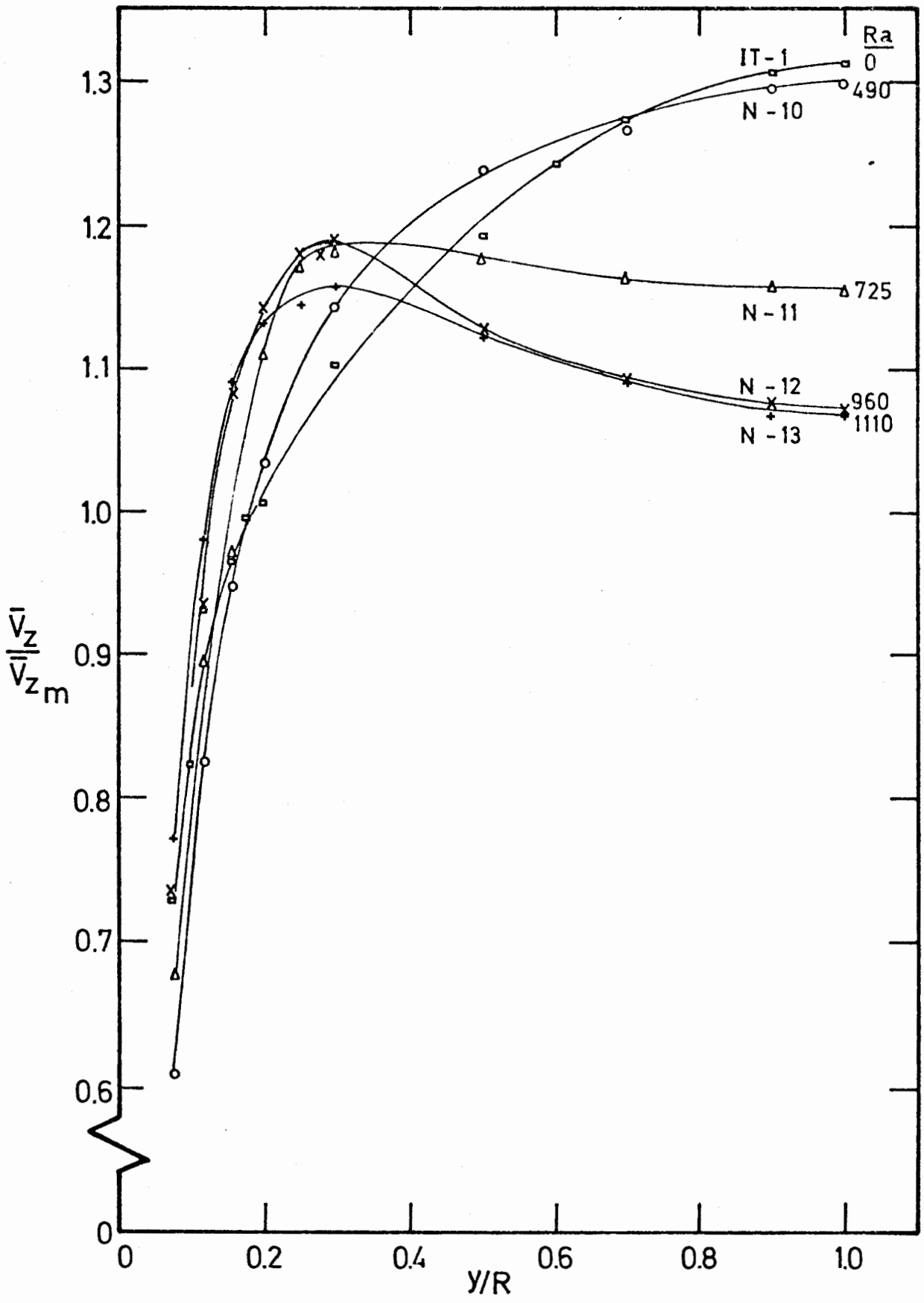

FIGURE 5.3 NON-ISOTHERMAL VELOCITY PROFILES AT Re ≃ 5000

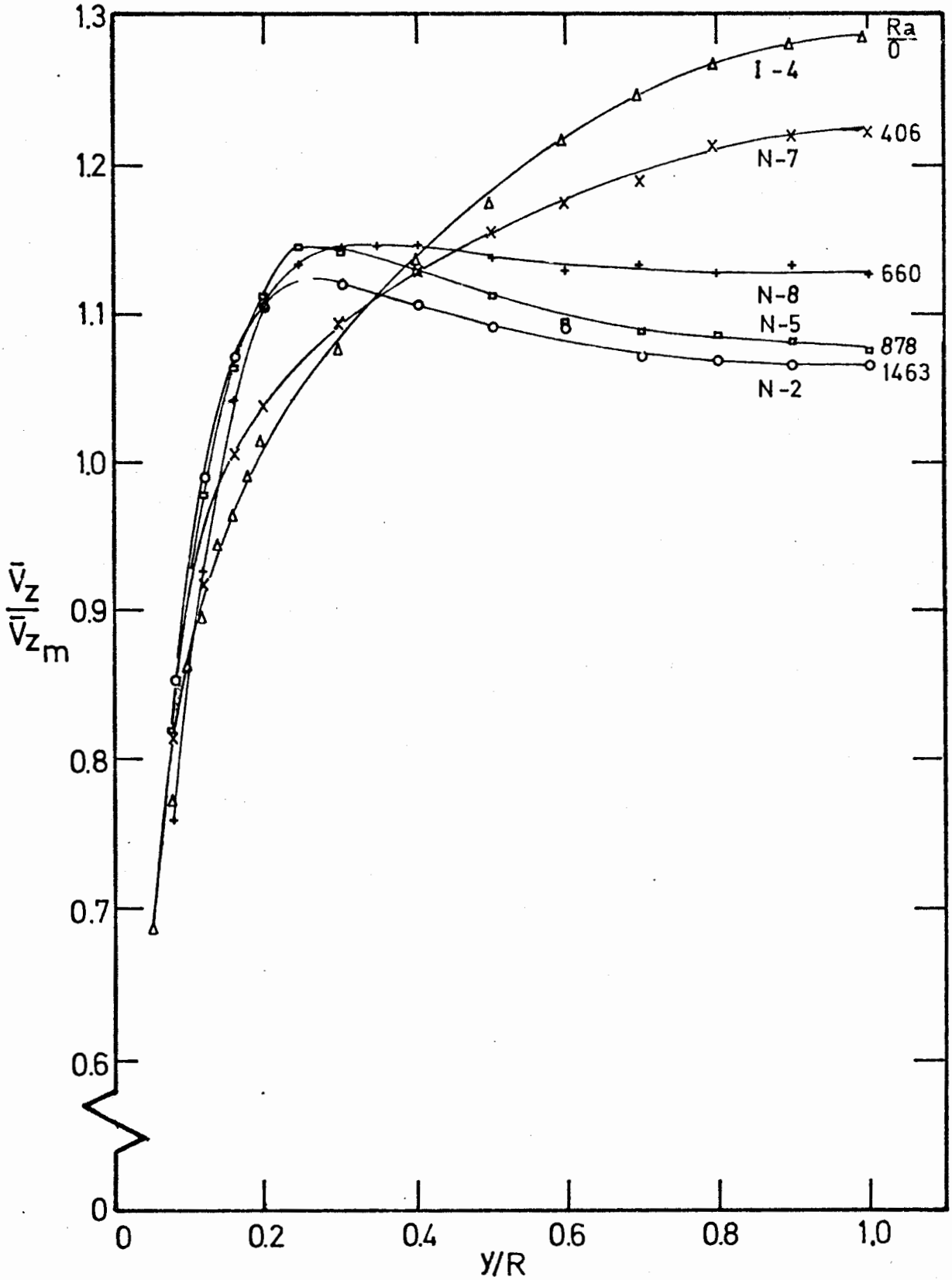

FIGURE 5.4 NON-ISOTHERMAL VELOCITY PROFILES AT Re ≃ 8000

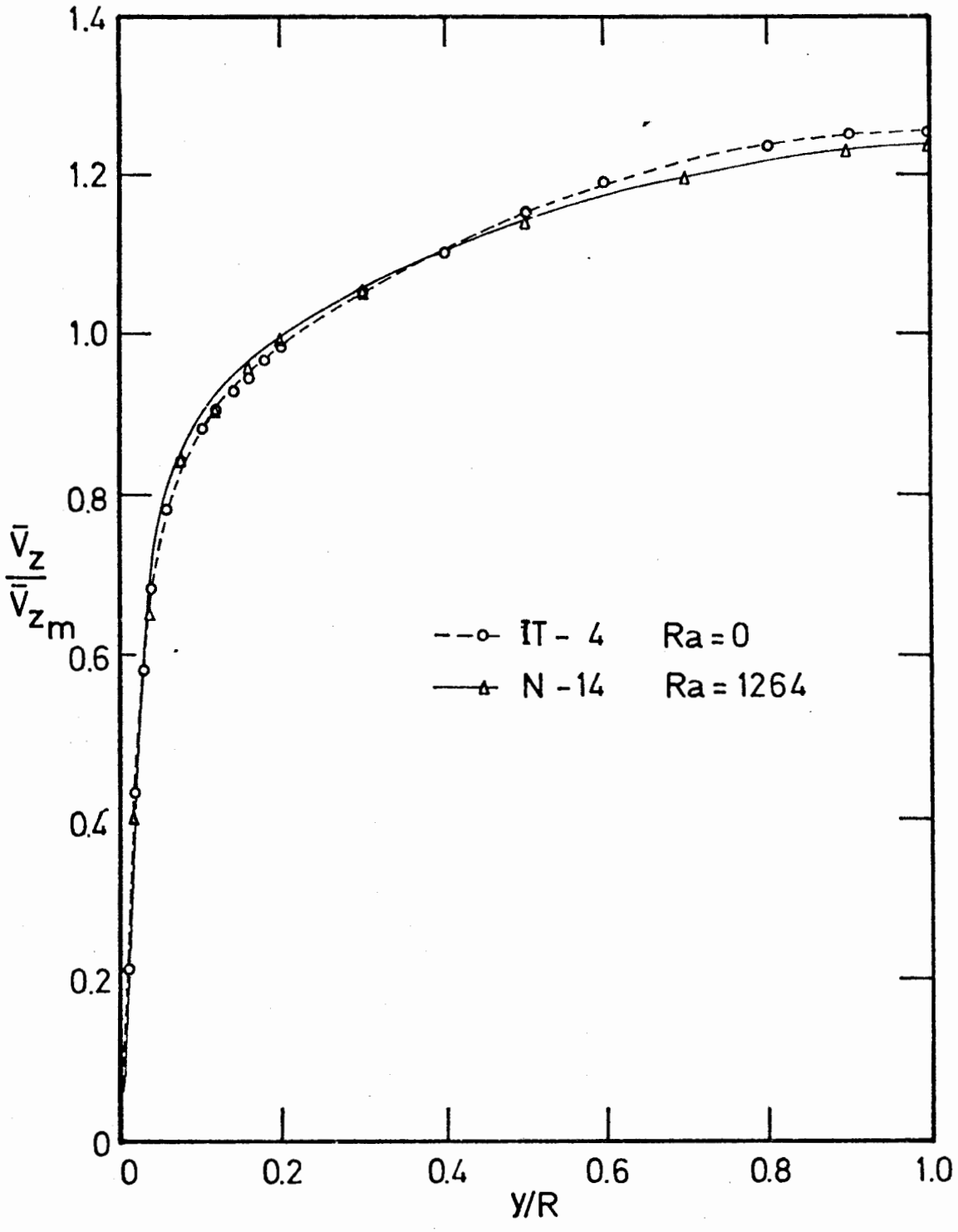

FIGURE 5.5 NON-ISOTHERMAL VELOCITY PROFILE AT Re ≃ 14000

of the two groups N-2 and N-3, and N-4, N-5 and N-6, is shown. (The runs in each of these groups were measured under similar conditions and in each case a series of very similar velocity profiles was obtained.)

The figures mentioned above show that even at a relatively high Rayleigh number the velocity profile at Re ≈ 14000 is only very slightly distorted. At lower Reynolds numbers, however, considerable distortion occurs and at the higher Rayleigh numbers velocity profiles with the point of maximum velocity displaced from the pipe centre are obtained. The variation of profile shape with increasing Rayleigh number is observed to follow a similar pattern at each Reynolds number:

> As the Rayleigh number increases the centre velocity is observed to decrease steadily while the velocity nearer the wall increases due to buoyancy effects. The profile thus assumes a relatively flat shape over much of the pipe. With a small further increase in Rayleigh number a pronounced change in profile shape (and, as will be seen later, in flow structure) takes place and the point of maximum velocity moves from the pipe centre to a position much closer to the wall. The rapidity with which this transition occurs was very noticeable during certain runs when small changes in heat input were observed to cause large variations in profile shape. Further increases in Rayleigh number result in the centre velocity continuing to decrease and the maximum velocity moving higher and nearer the wall, though a point is arrived at where a "saturation" condition, such as that shown by profiles N-12 and N-13 in Fig. 5.3, is reached. In the present results for both Re ≈ 5000 and Re ≈ 8000 this point of saturation occurs when $\bar{V}_z/\bar{V}_{z_m}$ at the pipe centre attains a value of 1.07.

The above observations indicate that the central zone of reverse flow predicted for turbulent flow by Ojalvo and Grosh [21] does not in fact occur. Instead it appears from the work of Bankston [152] that the tendency of the flow is to become progressively more laminar in character until, at heat inputs an order of magnitude greater than those employed in the present experiments, complete

relaminarisation takes place. Support for this conclusion is provided by the results of Steiner [19], which were obtained in the same Reynolds number range but at higher heat fluxes than the present work, and which showed trends in Nusselt number and auto-correlation measurements similar to those expected in laminar flows.

In Fig. 5.6 measured velocity profiles are shown on a u^+ vs y^+ basis and it is clear that such a plot is unsuitable for correlating velocity profiles in "distorted" flows. An attempt was therefore made to correlate the results against various free and mixed convection parameters. It was found that, of the parameters tested, only Gr/Re, introduced by Scheele et al [12] and others to characterise the degree of distortion of laminar mixed convection profiles, and the Yantovskii [153] number, Gr/Re^{*2}, could be used as correlating factors for the present data. The free convection criterion Z, introduced by Buhr [23] and employed by Horsten [24] to correlate his velocity profile measurements in mixed convection mercury flows, proved unsuccessful as a correlating factor for the present results.

The particular correlation prepared using Gr/Re as a parameter is shown in Fig. 5.7, where, for four different radial positions, values of $(\overline{V}_z/\overline{V}_{z_m})/(\overline{V}_z/\overline{V}_{z_m})_{\text{isothermal}}$ are plotted against Gr/Re. Originally a plot showing the variation of $\overline{V}_z/\overline{V}_{z_m}$ at a particular radial position against Gr/Re was prepared but at very low Grashof numbers separate curves for each Reynolds number were obtained. To make this plot universal, at each radial position the $\overline{V}_z/\overline{V}_{z_m}$ values for the different heated flows at a given Reynolds number were divided by the value of $\overline{V}_z/\overline{V}_{z_m}$ at that same Reynolds number under isothermal conditions.

It can be seen from Fig. 5.7 that this plot correlates the present results for $5000 \lesssim Re \lesssim 14000$ with a maximum error of ± 5%. In addition, the results show a clear break between Gr/Re values of 2.3×10^2 and 3.2×10^2 and this corresponds to the sudden increase of $T_w - T_c$ and hence of Grashof number, which occurs as the flow velocity maximum moves from the pipe centre to a position nearer

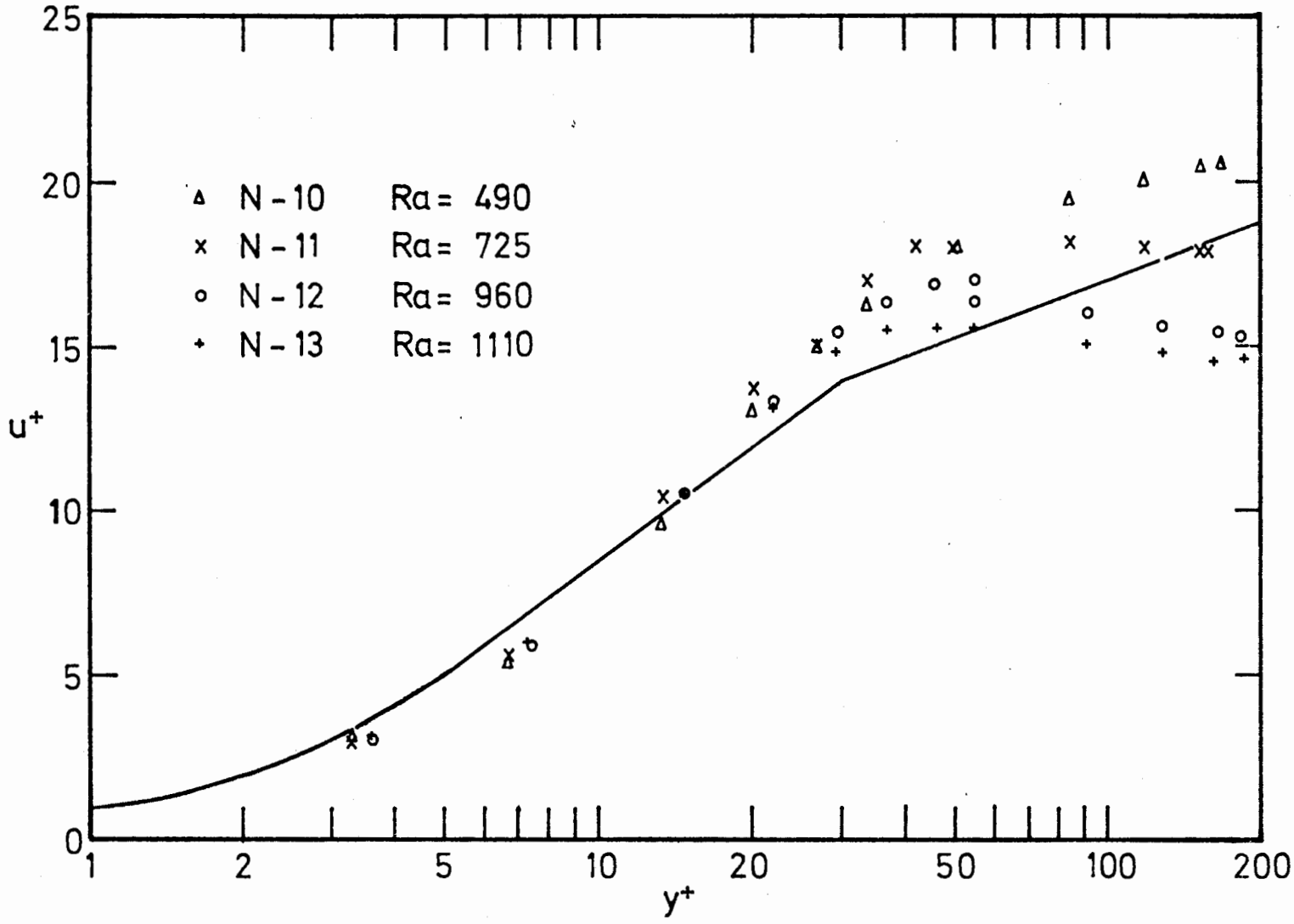

FIGURE 5.6 $u^+ - y^+$ VALUES FOR NON-ISOTHERMAL VELOCITY PROFILES AT Re ≃ 5000 COMPARED WITH THE UNIVERSAL VELOCITY DISTRIBUTION

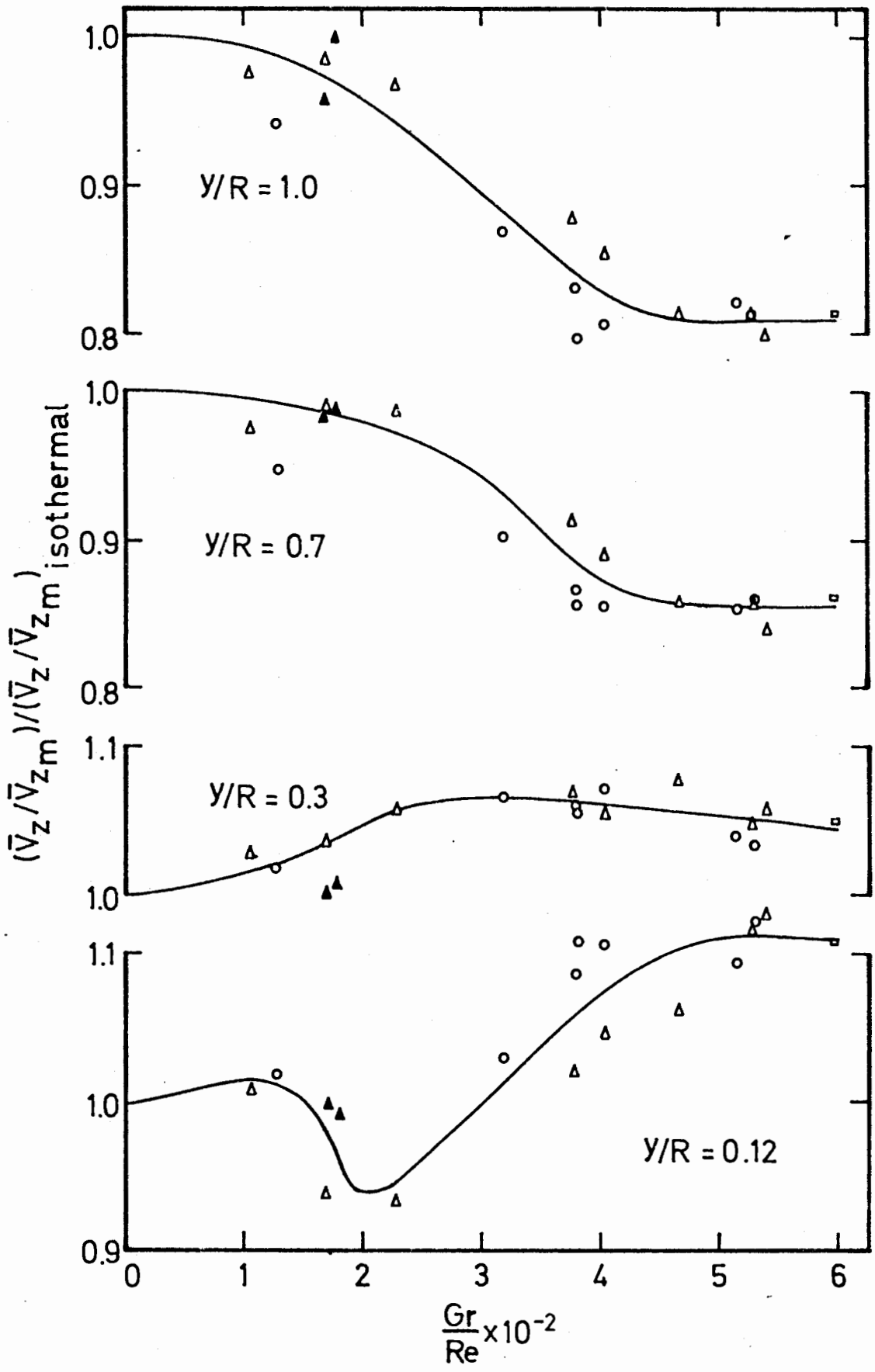

FIGURE 5.7 CORRELATION OF NON-ISOTHERMAL VELOCITY DATA AGAINST Gr/Re AT FOUR RADIAL POSITIONS

the pipe wall. It is also apparent from Fig. 5.7 that at high Gr/Re values the plots at each radial position show a tendency to flatten out, thus providing a very good illustration of the "saturation" effect mentioned earlier in this section.

Besides the Gr/Re parameter, the only other useful correlating parameter is the Yantovskii number Gr/Re^{*2}. Though less successful than Gr/Re as a correlating factor for the present results (plots of $\bar{V}_z/\bar{V}_{z_m}$ vs Gr/Re^{*2} are in general not independent of Reynolds number), the Yantovskii number remains the only other parameter for which the transition from flows with a velocity maximum at the pipe centre to flows with a displaced velocity maximum occurs at a constant value independent of Reynolds number. Furthermore this value of 8-10 is found to apply not only to the present results but also to the mercury data obtained by Horsten [24], indicating that the parameter Gr/Re^{*2} may provide a basis on which future measurements in different fluids can be compared.

5.3 TEMPERATURE MEASUREMENTS

5.3.1 Introduction

Temperatures were obtained from values of the hot-wire cold resistance R_g as explained in Appendix D. Generally the R_g values from which temperatures were determined were those obtained during velocity measurements but for runs NT-1 to NT-5 a separate series of R_g values was measured at the end of each run. Particular care was taken during these latter readings to obtain enough measurements to define the profile very clearly, especially in the region close to the pipe wall. These measurements are therefore regarded as providing the most accurate temperature profiles obtained during this study.

The measured temperature profiles were assumed to be fully developed. The reasons for this assumption are:

i) Johnk [132], in the only important study to date of developing temperature profiles in air under uniform heat flux conditions, concluded that after 24 diameters from the pipe entrance temperature profiles remained essentially unchanged: since the hydrodynamic entrance

length under similar conditions is of the order of 40, this indicates that, in general, temperature profiles become established earlier than velocity profiles. Since it was concluded in section 5.1.2 that present velocity profiles were effectively fully developed, it follows that the temperature profiles were also fully developed.

ii) Under conditions of constant wall flux heating it is necessary, if velocity profiles are to be effectively fully developed, for temperature profiles to have already reached a fully developed condition.

Experimental temperature measurements are presented in Appendix H.

5.3.2 Previous work

As discussed in Chapter 1 temperature profile measurements in mixed convection air flows are scarce, being limited to a single observation by Brown [91] and several profiles reported by Steiner [19] for conditions outside the range of the present results. Extensive measurements in mixed convection mercury flows have, however, been made by Buhr [23], Horsten [24] and Louw [151]. These measurements in mercury, though not directly comparable with the present results because of the dependence of temperature profile shape on Prandtl number, do show trends with which the variations in the present results can be compared.

Apart from the work of Ojalvo and Grosh [21] there are no important temperature profile predictions for turbulent mixed convection flows.

Temperature profiles in relatively undistorted flows, such as occur in runs N-14 and NT-5, have, on the other hand, received much attention and a number of predictions of undistorted or pure forced convection temperature profiles have been proposed. Several sets of experimental measurements of undistorted temperature profiles in air at low Reynolds numbers (< 20 000) have also been reported - details of these are given in Table 5.2 below:

TABLE 5.2

YEAR	INVESTIGATOR	Re x 10^{-3}	Boundary condition
1952	Deissler and Eian [149]	8.1 - 77	UHF
1955	Sleicher [92]	14.5 - 80.3	UWT
1961	Nunner [154]	10 - 60	UWT
1961	Johnk [132]	17.6 - 71	UHF
1968	Brown [91]	10.9 - 42.4	UHF
1971	Present work	5 - 14	UHF

UHF = Uniform heat flux

UWT = Uniform wall temperature

5.3.3 Experimental results

Measured temperature distributions are shown, as $\frac{T_w - T}{T_w - T_c}$, in Figs. 5.8 and 5.9.

Fig. 5.8 presents results at Re ≃ 5000 in comparison with a relatively undistorted profile at Re ≃ 14000 while Fig. 5.9 shows several profiles at Re ≃ 8000.

By comparing the results from both figures it is clear that, as in the case of the velocity profiles, a consistent trend of profile distortion is observed as the Rayleigh number increases. For y/R < .25 to .3 values are observed to decrease with increasing Rayleigh number until a certain point is reached after which there is again an increase. For y/R > .25 to .3 a steady increase in temperature values with Rayleigh number is evident, though at high Rayleigh numbers a "saturation" effect similar to that observed for the velocity profiles is noted. These trends are similar to those observed by Horsten [24] for profiles measured in mercury.

In Fig. 5.10 the profile at Re ≃ 14000 is shown in comparison with experimental measurements of Johnk [132] and Sleicher [92] and also with the profile predicted by Boelter et al [133] for a Reynolds number of 14000. Although the shapes of the profiles are in general similar, the agreement between the different profiles is not, however, very good and more temperature measurements

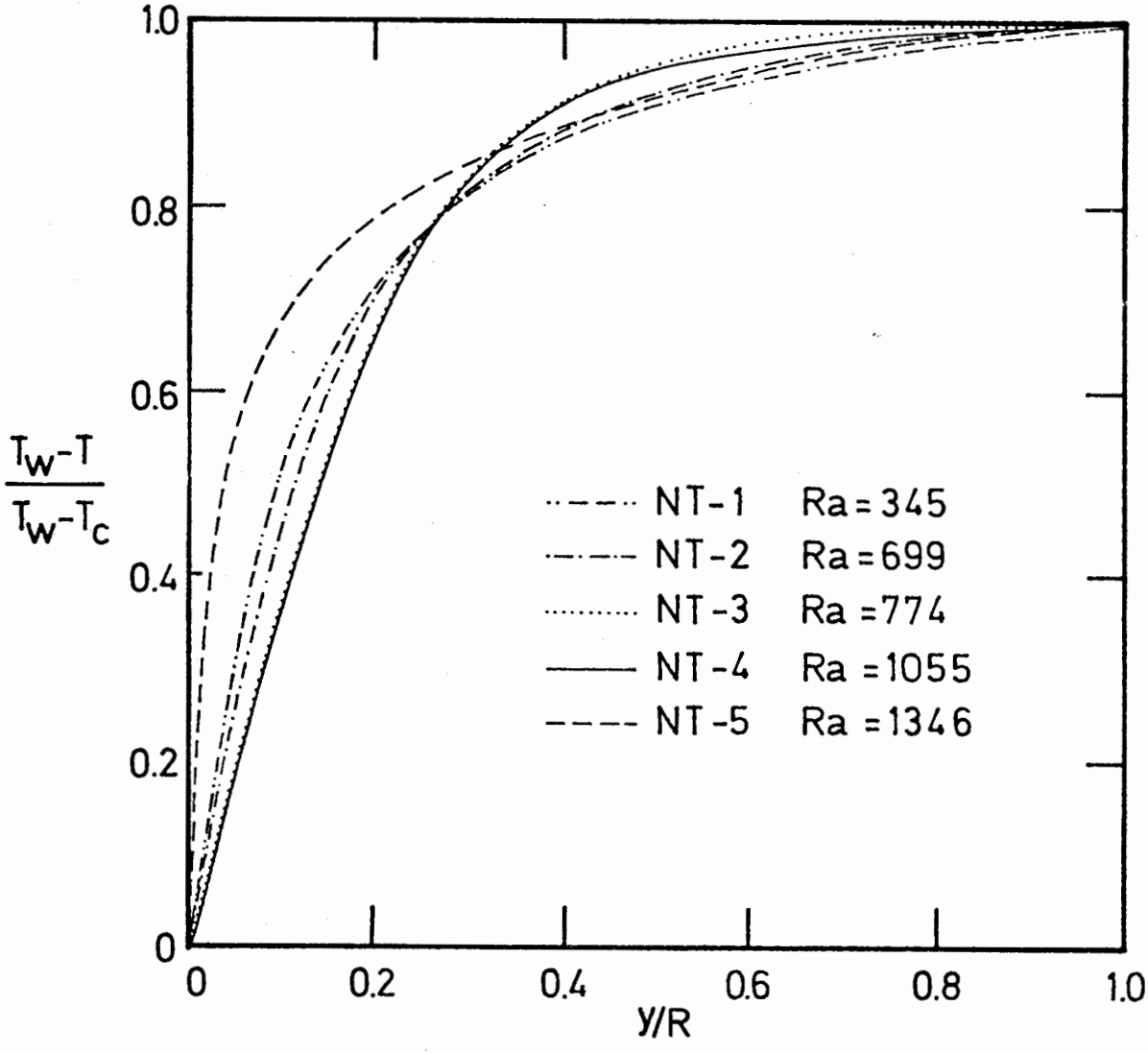

FIGURE 5.8 TEMPERATURE PROFILES AT Re ≃ 5000 (RUNS NT-1 TO NT-4) AND AT Re ≃ 14000 (RUN NT-5)

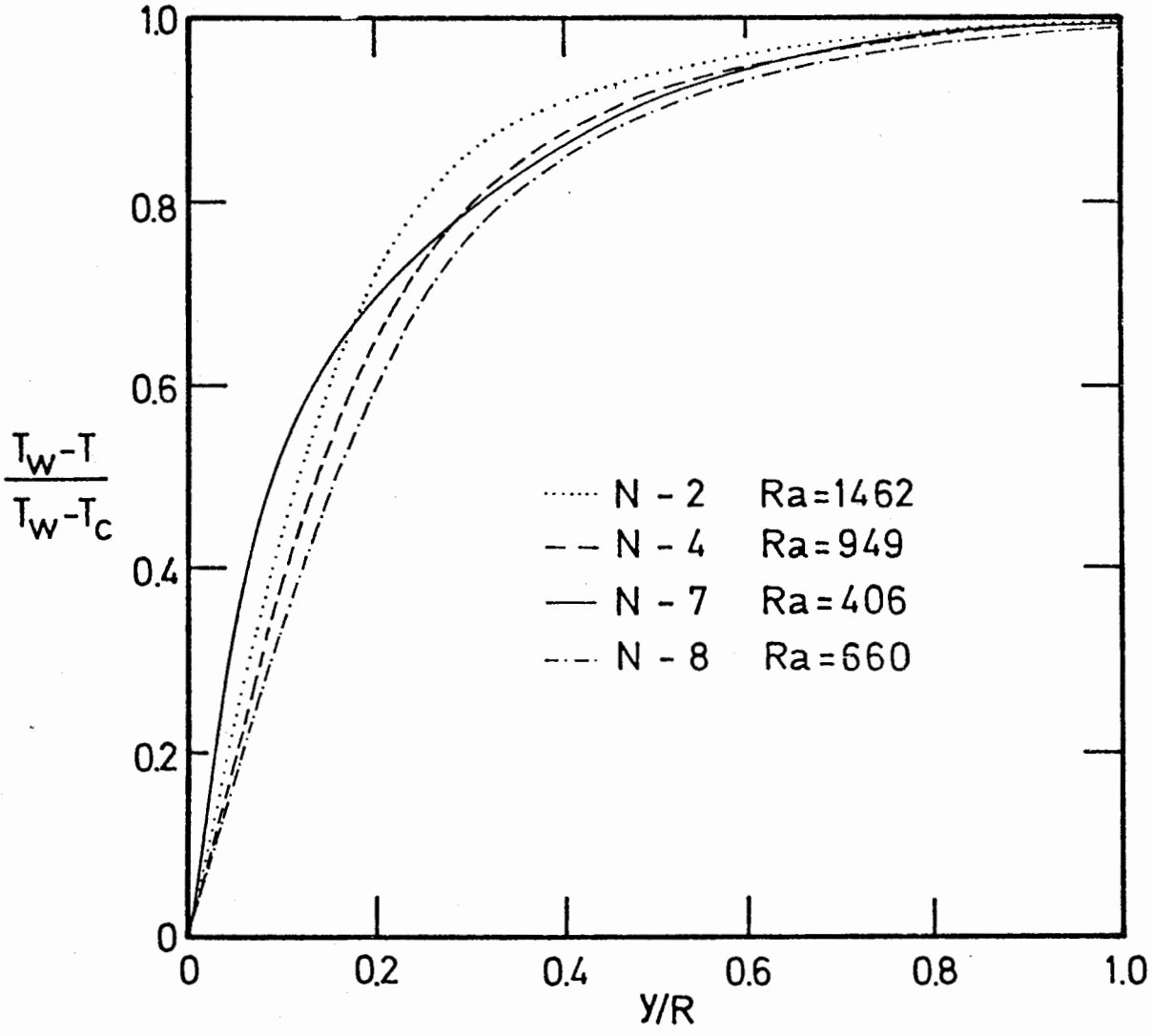

FIGURE 5.9 TEMPERATURE PROFILES AT Re ≃ 8000

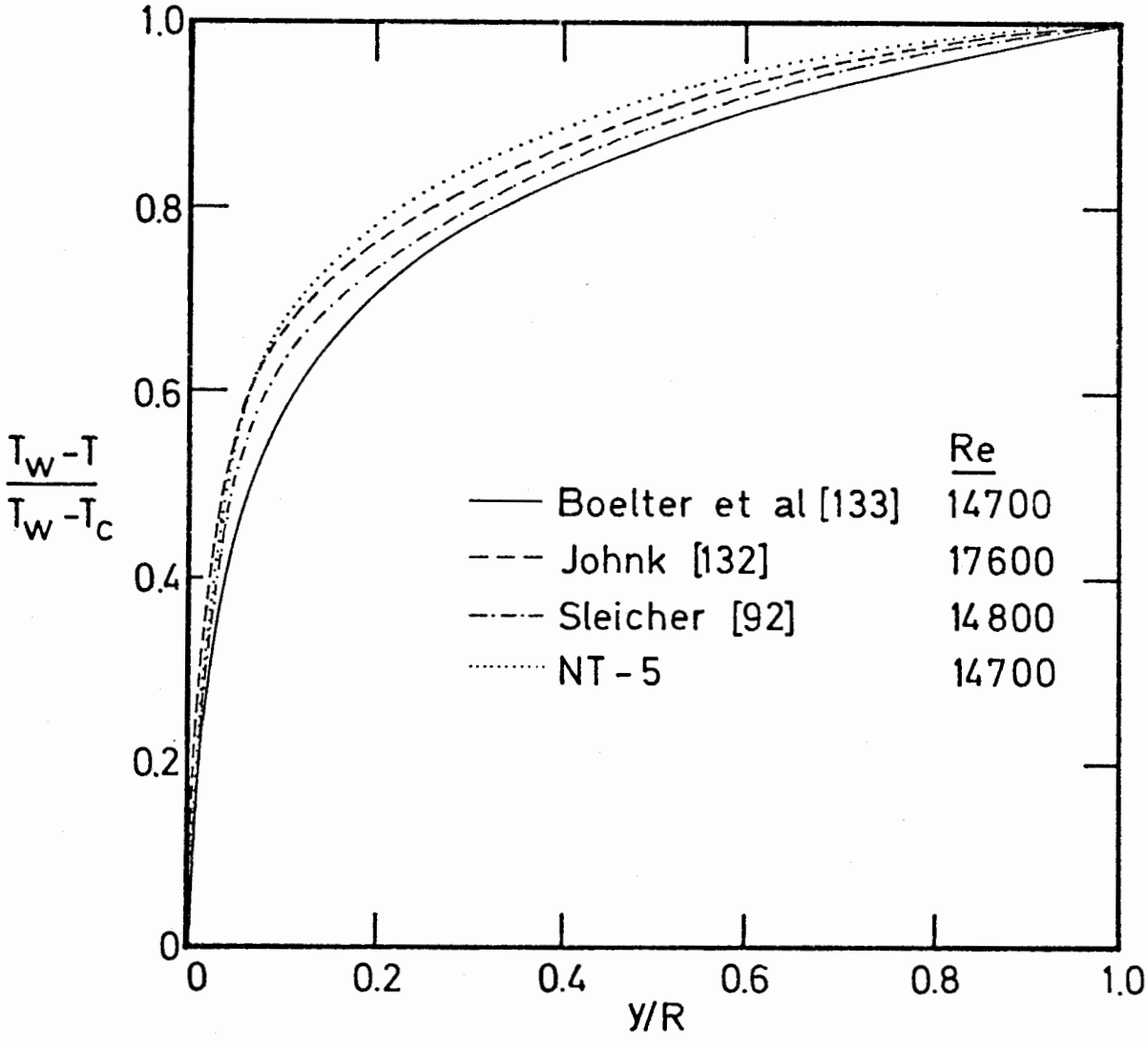

FIGURE 5.10 COMPARISON OF MEASURED TEMPERATURE PROFILE AT Re ≃ 14000 WITH OTHER MEASURED AND PREDICTED TEMPERATURE PROFILES

need to be taken at low Reynolds numbers under relatively undistorted conditions before the reasons for these differences can be found.

Fig. 5.11 shows a plot of $\frac{T_w-T}{T_w-T_c}$ values at several radial positions against the parameter Gr/Re. The points are relatively widely scattered, especially at y/R = 0.12, and a definite trend with Reynolds number is apparent. This observation is in agreement with the conclusion reached by other workers, for example Brown [91], that, particularly at low Reynolds numbers, temperature profiles plotted on a $\frac{T_w-T}{T_w-T_c}$ basis show a definite Reynolds number dependence.

An alternative method proposed for representing temperature profiles on a universal basis is to plot values of t^+ against y^+, a representation analogous to the u^+ vs y^+ plot successfully used for correlating isothermal velocity distributions. Such a plot for runs N-10 to N-14 is given in Fig. 5.12 which also includes the results of Johnk [132] and Deissler and Eian [149]. It is apparent that the temperature distributions corresponding to relatively undistorted velocity profiles agree reasonably well with the measurements of other workers. However, the data for runs N-11 to N-13, for which the velocity profile has undergone a basic change of shape, all lie very close together at positions well above those for data obtained in less distorted flows. This trend with heat flux is opposite in direction from that predicted by Deissler and Eian [149] for t^+ values in undistorted flows with increasing wall to bulk temperature ratios.

5.3.4 Discussion of results

The observed initial decrease and subsequent increase of the slope of the temperature profile as the heat flux is increased is related to the behaviour of the eddy diffusivity of momentum (see section 5.7). Initially as the velocity profile flattens out the eddy diffusivity of momentum drops, until as the velocity profile passes through a state of being practically uniform over the inner 70% of the pipe, ε_M values near the wall decrease almost to zero. Under these conditions heat transfer near the wall occurs

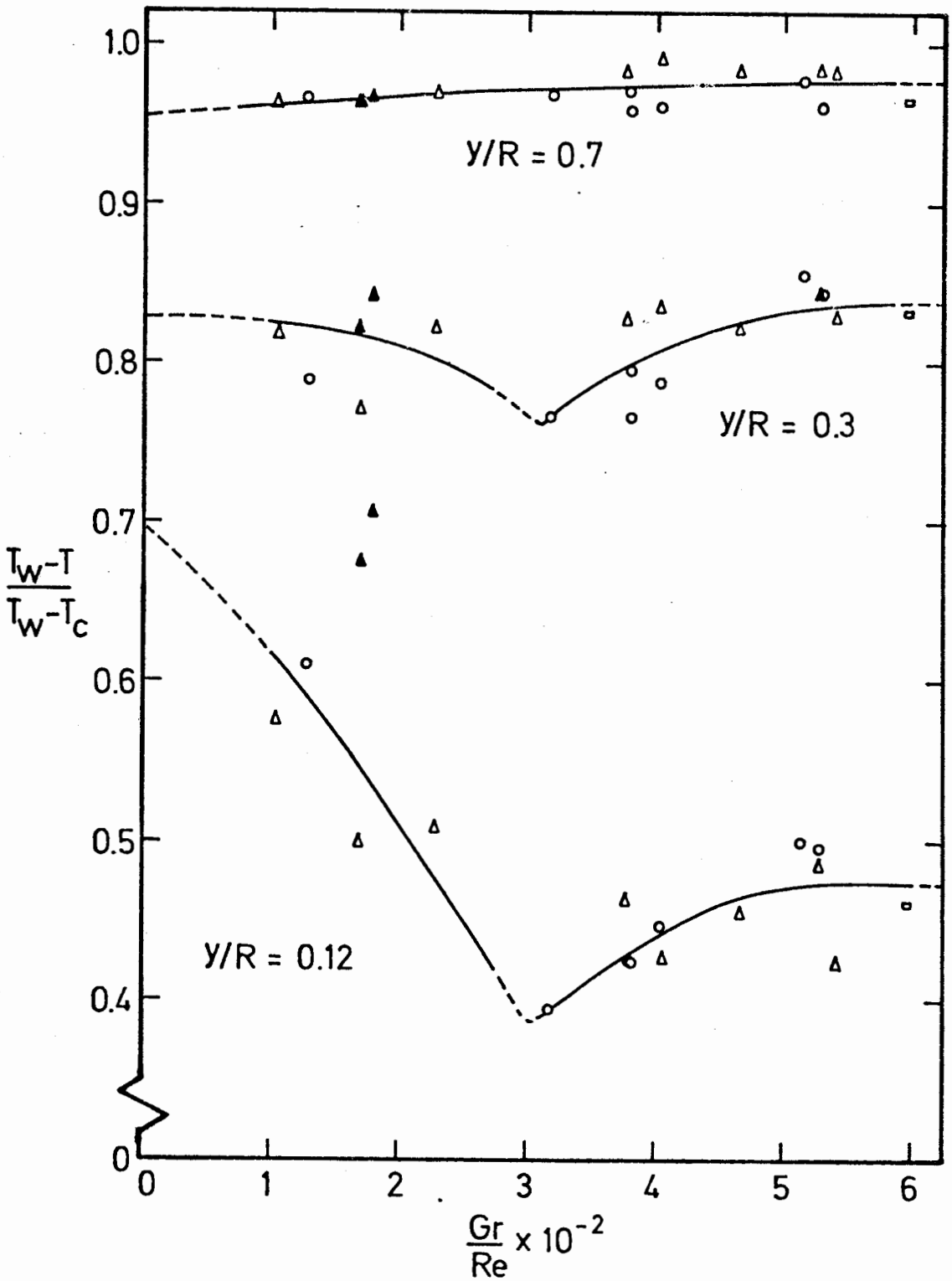

FIGURE 5.11 TEMPERATURE PROFILE VARIATIONS WITH Gr/Re AT THREE RADIAL POSITIONS

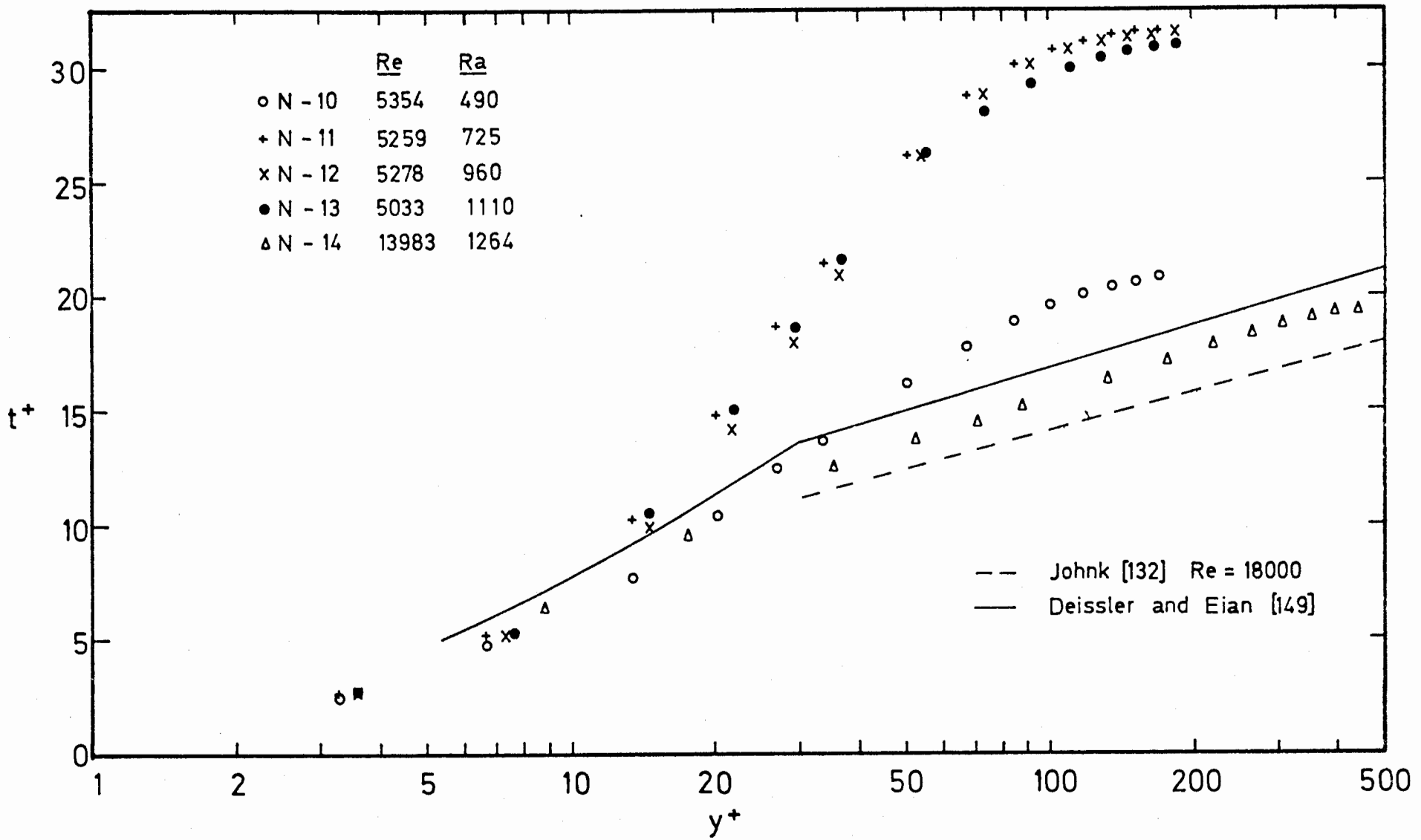

FIGURE 5.12 MEASURED TEMPERATURE PROFILES COMPARED ON A $t^+ - y^+$ BASIS WITH THE PREDICTIONS AND RESULTS OF OTHER WORKERS

predominantly by molecular effects, the rate of heat transfer decreases and the slope of the temperature profile decreases. Further increases in heat flux produce a more distorted velocity profile, eddy diffusivity values increase and the temperature profile slope increases again.

5.4 TURBULENCE MEASUREMENTS

5.4.1 Introduction

Axial turbulence intensities, temperature intensities and values of $\overline{v_z t}$ were measured at Re ≈ 5000 at four different heat inputs (Runs NT-1 to NT-4) and at Re ≈ 14000 at one heat input (Run NT-5). The theory underlying the method of measurement employed is given in Chapter 2 and the operating procedure is summarised in Chapter 3. Sample calculation procedures are reported in Appendix I while the actual experimental values are tabulated in Appendix H.

5.4.2 Axial turbulence intensities

The results obtained in the present experiments are shown as v_z'/u^* in Fig. 5.13. It is seen that although the axial turbulence intensity profiles for the relatively undistorted flows of runs NT-1 and NT-5 are of a similar shape to isothermal axial intensity profiles, increasing free convection effects cause the axial intensities to change considerably. At Re ≈ 5000 the effect of increasing Rayleigh number is to reduce the intensities to as little as one-third of their isothermal values. Near the wall the values are observed to fall steadily until a "saturation" condition is observed; nearer the pipe centre, however, values fall initially but then rise again, giving, for the two highest Rayleigh numbers, an intensity profile which is practically uniform over 90% of the radius.

No published results exist with which the intensities measured in strongly distorted flows can be compared. However a few axial intensity measurements in undistorted heated flows have been reported by, for example, Bremhorst and Bullock [142] at Re ≈ 34 700 and Ibragimov et al [143] at Re ≈ 32 500, and these are shown, in comparison with the results from runs NT-1 and NT-5,

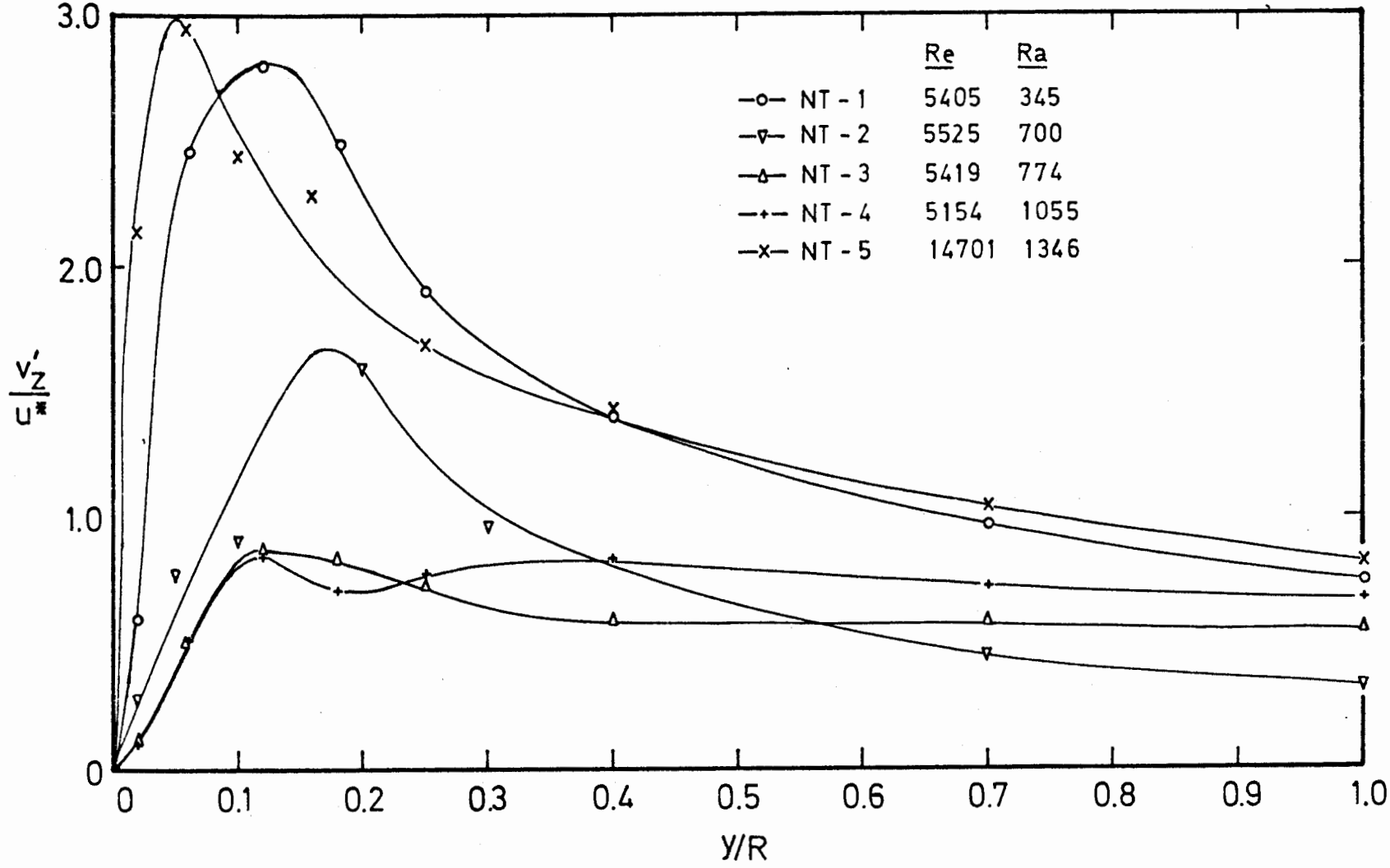

FIGURE 5.13 MEASURED v_z'/u^* VALUES

in Fig. 5.14. The mean of the isothermal axial intensities measured at Re ≈ 5000 and Re ≈ 16000 and discussed in the previous chapter are also shown in this Figure. All the curves are seen to be extremely similar for y/R > 0.5; however for y/R < 0.5 the curves differ considerably. Considering the results from the present experiments, it is apparent that in heated flows the intensities at lower y/R values are up to 20% greater than the isothermal values while the position of peak intensity has moved further from the pipe wall. It is also apparent that in the low y/R region differences exist between the results of the present work and those of other workers. These differences arise, in the case of Ibragimov's results, from differences in Reynolds number, while in the case of Bremhorst and Bullock's results the main differences arise from what Bremhorst and Bullock refer to as a wire length effect. In so far as comparison is possible, however, the agreement between the present results and those of other workers is very good.

5.4.3 Temperature intensities

The present results are shown on a t'/T* basis in Fig. 5.15. For the results at Re ≈ 5000 it is clear that although the change with increasing heat input is slight for y/R > 0.5, at lesser y/R values a considerable change occurs with increasing Rayleigh number. It is observed that in this region of low y/R the intensity at first drops and then increases as the heat flux increases. At the same time the peak in the intensity moves from y/R ≈ 0.12 to y/R ≈ 0.25. These changes can be explained as follows:

The temperature intensity $t' = \sqrt{t^2}$ is determined principally by the values of the velocity intensity v' and the temperature gradient $\frac{dT}{dr}$. With the initial increase in heat flux $\frac{dT}{dr}$ increases, but this increase is offset by the large simultaneous decrease in v' which causes t' to decrease slightly. At higher heat fluxes, however, v' reaches a more or less constant value and hence increases in heat flux result in corresponding increases in t'. The change in the position of the peak intensity is linked to the decrease in importance of eddy diffusion near the wall which occurs at higher heat fluxes (see section 5.7).

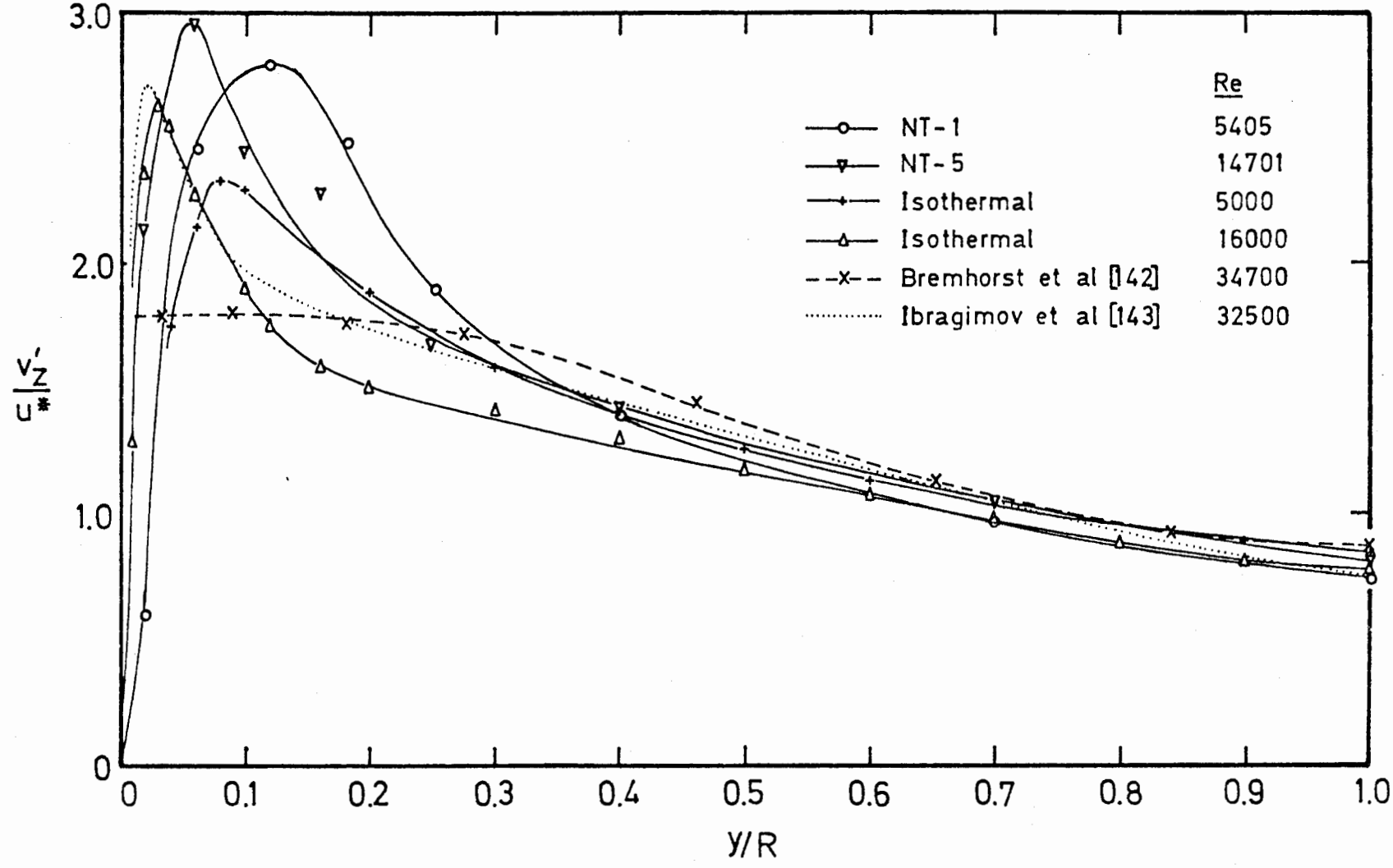

FIGURE 5.14 v'_z/u^* VALUES COMPARED WITH RESULTS OF OTHER WORKERS

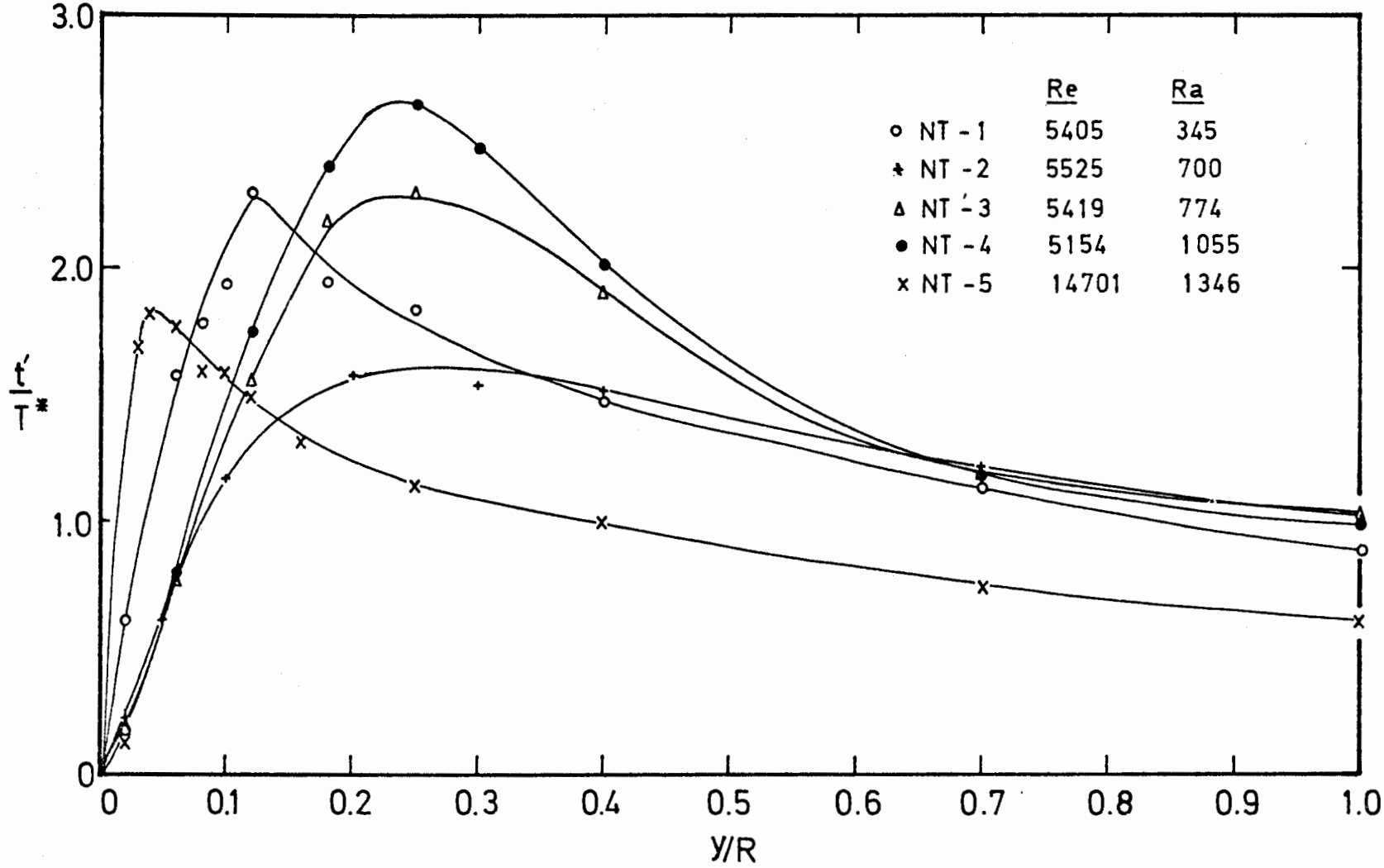

FIGURE 5.15 MEASURED t'/T* VALUES

As was the case also for the turbulent velocity intensities, no measurements of temperature intensities in distorted flows are available. A number of measurements in undistorted flows have, however, been reported and a selection of these is shown in Fig. 5.16 in comparison with the results from runs NT-1 and NT-5. It is apparent from this figure that the intensities for run NT-5, the least distorted of the present results, are in close agreement with the data for air reported by other workers, and also, over the range $y/R > 0.3$, with the results for mercury reported by Hochreiter [145]. Nearer the wall considerable differences between the air and mercury data are evident; these are due, as has been shown by Hochreiter, to the large difference in Prandtl number between the two fluids. Variations between the air data of different workers are the result either of differences in Reynolds number, or in the case of Bremhorst and Bullock's results, of the probe effect mentioned in the previous section.

Several workers have compared axial velocity intensity data with temperature intensity data and two different comparisons have been made. Bremhorst and Bullock [142] compared $\frac{v'_z}{u^*}$ values with $\frac{t'}{T^*}$ values while Tanimoto and Hanratty [144] and Ibragimov et al [143] compared $\frac{v'_z}{u^*}$ values with $\frac{t'}{T^*Pr}$ values. Since very close to the wall [144]

$$\frac{(T_w - T)}{T^*Pr} = \frac{\overline{V}_z}{u^*}$$

the latter comparison seems the more logical; however both $\frac{t'}{T^*}$ and $\frac{t'}{T^*Pr}$ values have been included in Figures 5.17 and 5.18, which show $\frac{v'_z}{u^*}$, $\frac{t'}{T^*}$ and $\frac{t'}{T^*Pr}$ values for $Re \simeq 5000$ and $Re \simeq 14000$ respectively. At $Re \simeq 14000$ (run NT-5) very good agreement between $\frac{v'_z}{u^*}$ and $\frac{t'}{T^*Pr}$ values is noted - similar agreement was observed also by Ibragimov et al [143] and Tanimoto and Hanratty [144]. At $Re \simeq 5000$ (run NT-1) the $\frac{v'_z}{u^*}$ results do not agree well with either $\frac{t'}{T^*}$ or the $\frac{t'}{T^*Pr}$ results, though the former are closer to the $\frac{v'_z}{u^*}$ values over most of the tube. This difference between the $Re \simeq 5000$ case and the $Re \simeq 14000$ case is attributed to the fact

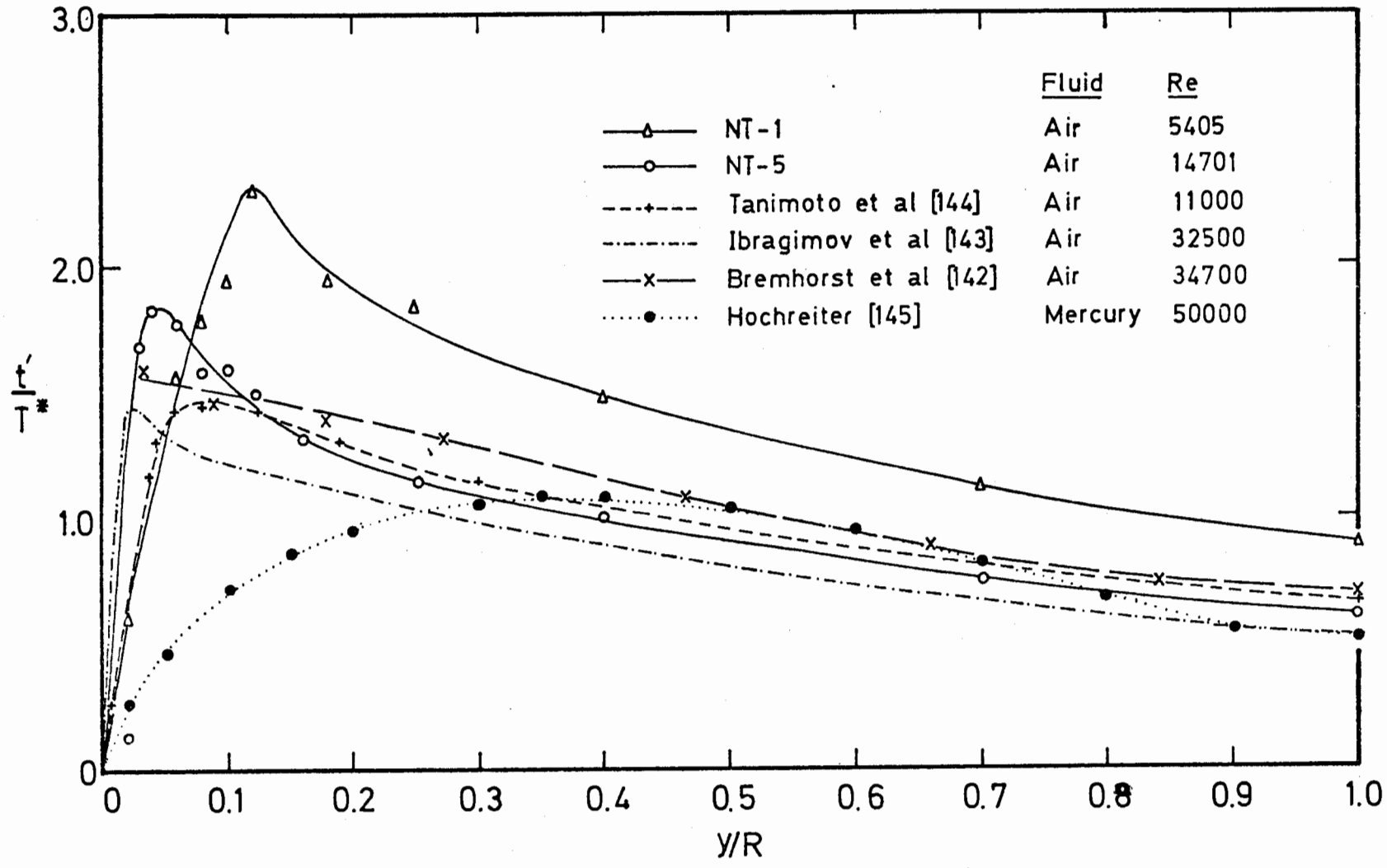

FIGURE 5.16 t'/T* VALUES COMPARED WITH RESULTS OF OTHER WORKERS

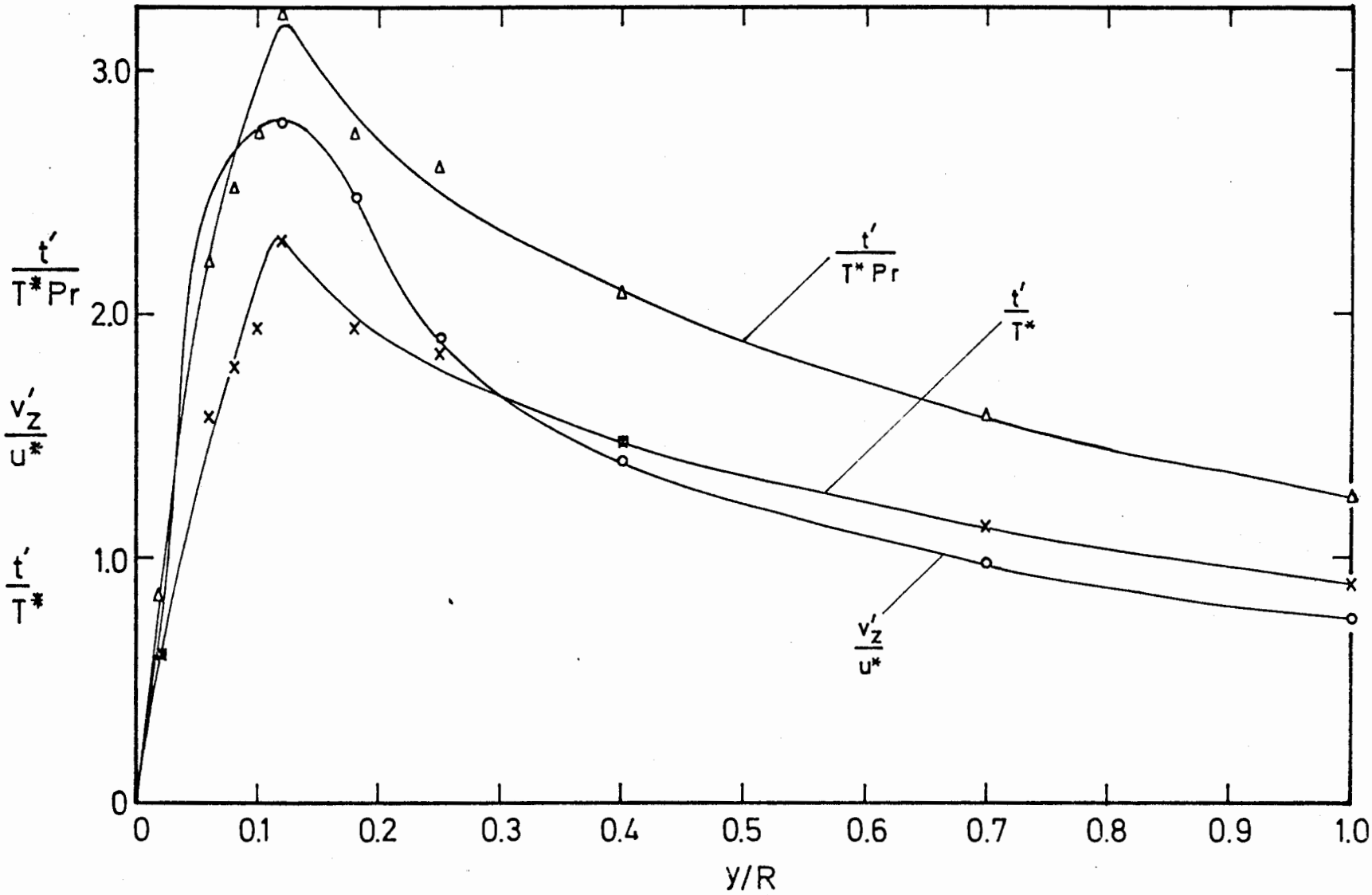

FIGURE 5.17 COMPARISON OF v_z'/u^*, t'/T^* and t'/T^*Pr VALUES AT Re ≈ 5000

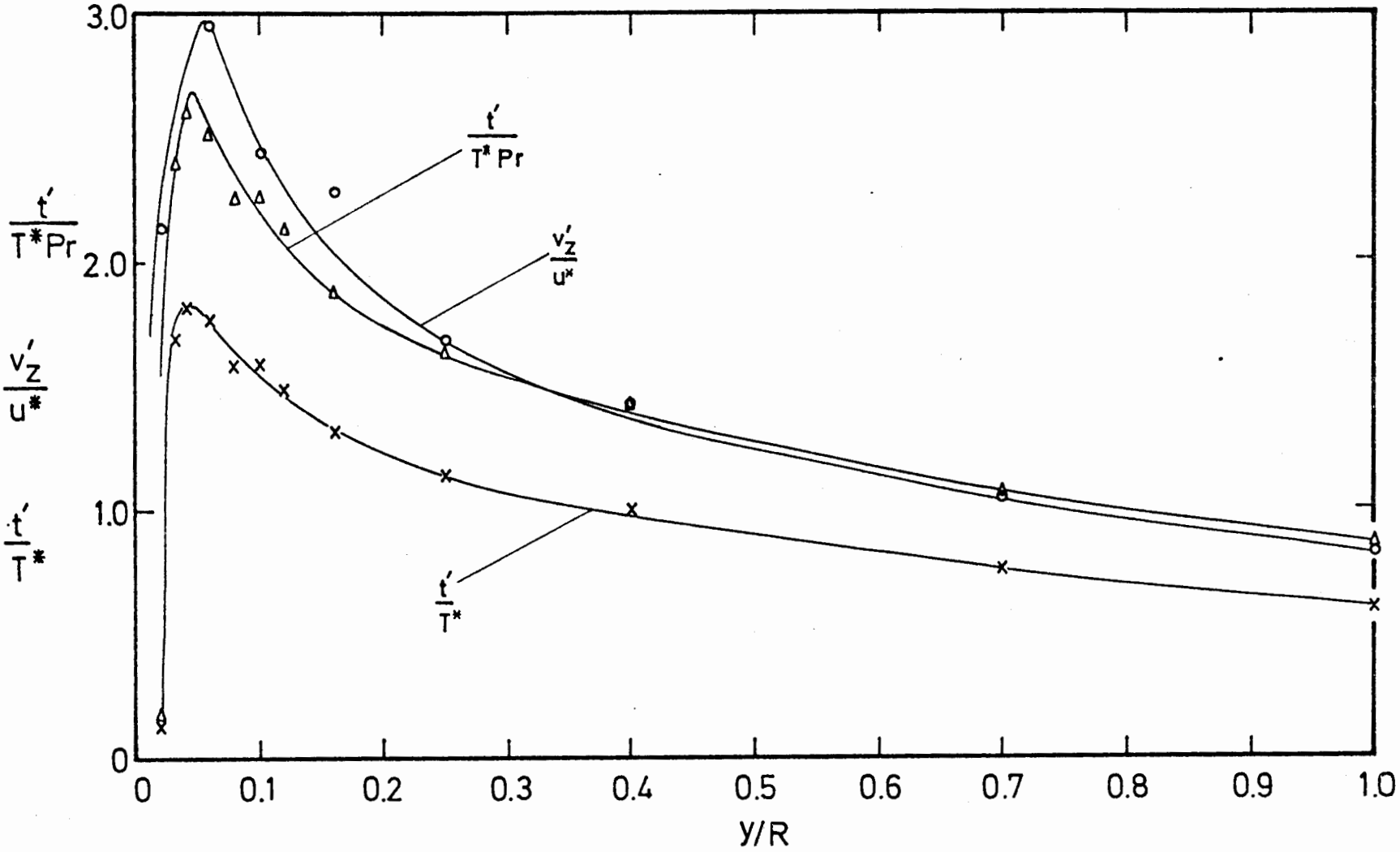

FIGURE 5.18 COMPARISON OF v_z'/u^*, t'/T^*Pr AND t'/T^* VALUES AT Re ≃ 14000

that while the latter flow was practically undistorted, free convection effects were already significant in the former flow.

5.4.4 The correlation $\overline{v_z t}$

The results of the present experiments are shown in Fig. 5.19 as $-\frac{\overline{v_z t}}{u^* T^*}$, a form which is equivalent to $-\frac{\rho C_p \overline{v_z t}}{q_w}$, the ratio of the axial heat flux to the wall heat flux. Despite the problems involved in obtaining $\overline{v_z t}$ values by the present method (Verollet [66] showed that of the values v_z', t' and $\overline{v_z t}$, the latter were most affected by experimental inaccuracies) clear trends with increasing Rayleigh number are apparent.

For $y/R > 0.3$ the axial heat flux is observed to change from a positive value at low Rayleigh numbers to a negative value at high Rayleigh numbers, a change which occurs first at the pipe centre and then at lower y/R values as the Rayleigh number increases. It has been postulated that this change is linked to the change in slope of the velocity profile from negative to positive - however the axial heat flux for run NT-2 has already changed sign in comparison with that for run NT-1, whereas the slopes of the velocity profiles for both runs have the same sign. Also, it has been shown [145] that for mercury large negative values of the axial heat flux occur while the velocity profile is relatively undistorted.

In the region $y/R < 0.3$ the behaviour of the axial heat flux is less explicable since in some cases it is observed to change rapidly from a positive to a negative value and then, very close to the wall, to again take a positive value. The only conclusion that can be drawn from the results in this region is that very close to the wall the axial heat flux is always positive. A partial explanation for this observation can be obtained by considering the structure of the fluid layers close to the wall. According to recent workers such as Corino and Brodkey [155] the main radial movements in the viscous sub-layer occur as sections of the sub-layer break away into the main flow. Under these conditions negative axial velocity fluctuations and positive temperature fluctuations would be associated, producing a negative $\overline{v_z t}$ value and hence a positive axial heat flux.

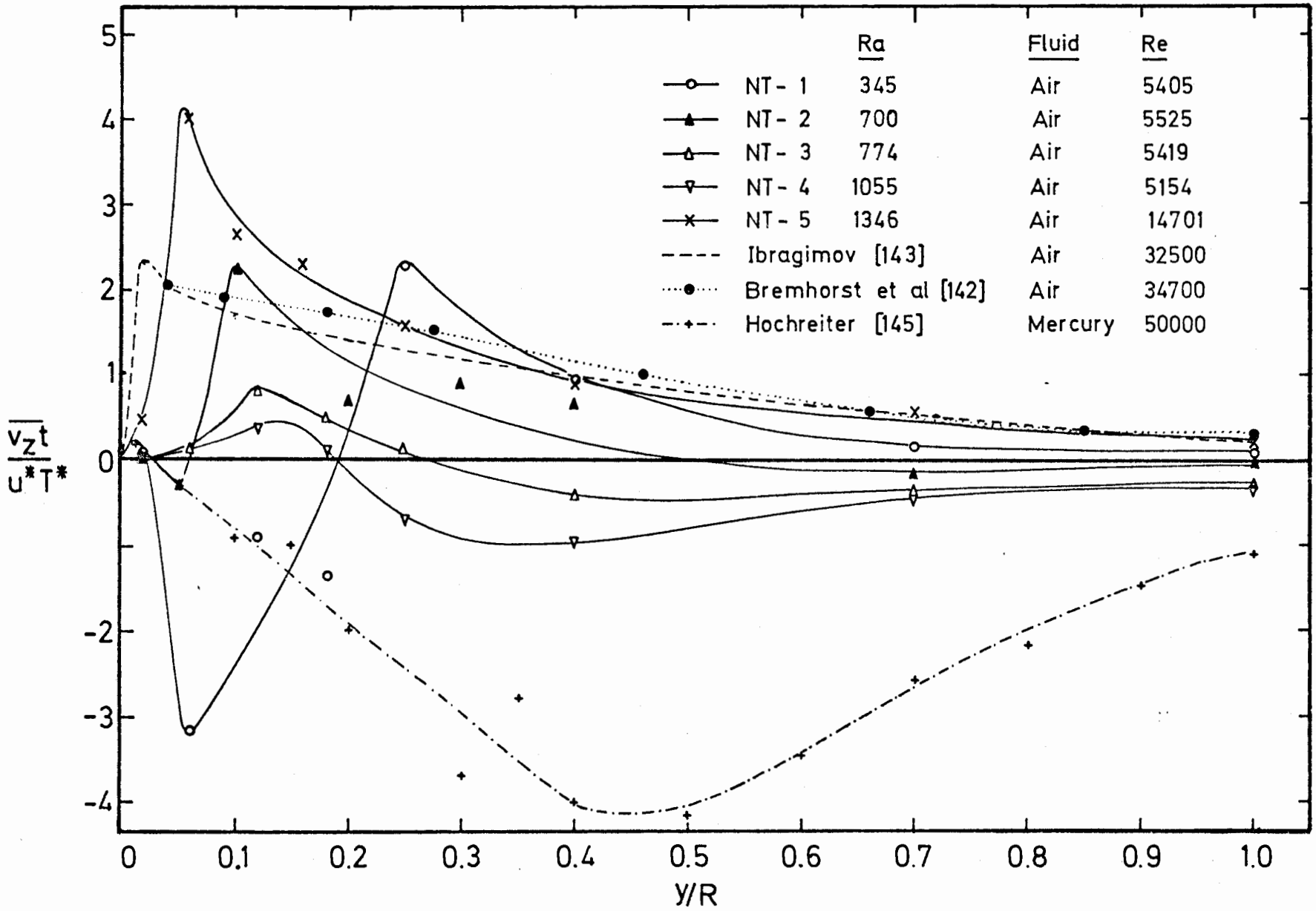

FIGURE 5.19 MEASURED $\overline{v_z t}/u^*T^*$ VALUES COMPARED WITH RESULTS OF OTHER WORKERS

Measured axial heat flux values have been reported by several workers, though no measurements in mixed convection flows have been published. Among the reported values are those of Kudva [123] in ethylene glycol (these values lie considerably above the present results) and those of Ibragimov et al [143] and of Bremhorst and Bullock [142] in air, and those of Hochreiter [145] in mercury. The results for air and mercury are shown in comparison with the present results in Fig. 5.19.

Over the $y/R > 0.3$ range extremely good agreement is observed between the air measurements of Bremhorst and Bullock [142], Ibragimov et al [143] and the present run NT-5 which was measured in a flow where free convection effects were only of slight importance. At lower y/R values agreement is not as good but this is expected because of the differences in Reynolds number. In contrast to the results of Bremhorst and Bullock [142] and Ibragimov et al [143] those of Hochreiter [145] fall considerably below all of the other results and this difference led Hochreiter to question the accuracy of his measurements. However, it is clear that his results are similar in form to those for run NT-4, the differences being attributable to the very much lower value of the Prandtl number in mercury (0.02) than in air (0.7). (The existence of this Prandtl number effect is clearly demonstrated by a comparison of results in ethylene glycol, water, air and mercury presented by Hochreiter.)

It is apparent from the present and other $\overline{v_z t}$ measurements discussed above that the changes in axial heat flux under combined free and forced convection conditions are complex and before the variation of $\overline{v_z t}$ values can be predicted further measurements of $\overline{v_z t}$ over a range of Reynolds numbers in fluids of different Prandtl number are needed.

5.5 NUSSELT NUMBERS

5.5.1 Previous work

It was shown in Chapter 1, section 1.2.6, that no acceptable generalised Nusselt number predictions exist at present for turbulent mixed convection flows. It was also shown that the only useful set of measurements in such flows was that of Petukhov and Strigin [36] who showed that their measurements in water could be

correlated on a plot of Nu/Nu_T vs Ra/Re^2 (where Nu_T is the Nusselt number at the limiting condition of zero heat flux, i.e. the pure forced convection Nusselt number).

For flows where the effects of free convection can be neglected, however, a number of Nusselt number correlations have been proposed and several sets of Nusselt number measurements have been reported. Of these correlations and measurements those relevant for the range of Reynolds numbers investigated in the present work are reviewed below.

i) Measurements

Relevant measurements of Nusselt numbers in air under uniform heat flux conditions are summarised in Table 5.3. Nusselt number values at Re ≈ 5200, 8200 and 14000 were obtained from the results of each of these investigations by interpolating between measured data points and these values are also shown in Table 5.3.

Of the sets of measurements reported in Table 5.3 the most important is that of McEligot et al [159] which reports a large

TABLE 5.3

DATE	INVESTIGATOR	$Re \times 10^{-3}$	Nu (Re=5200)	Nu (Re=8200)	Nu (Re=14000)
1952	Deissler and Eian [149]	8.1 - 500	-	(20)	36
1960	Barnes [156]	4.2 - 130	17	26	41
1962	Depew [157]	11.4 - 41.4	-	-	38
1962	Mills [158]	10 - 110	-	-	37.6
1966	McEligot et al [159]	1.45 - 15	18	24	38

number of measurements covering the whole Reynolds number range of interest. Since these results were purposely obtained at very low heat fluxes they should be the closest of all the results to the pure forced convection Nu_T values.

ii) Correlations

Apart from the usually recommended correlations such as the Dittus-Boelter and the Friend and Metzner [160] equations, others

have been suggested by Mills [158] and Sparrow et al [161]. (This latter equation was originally derived for Reynolds numbers greater than 50000 but Depew [157] showed that it applied well down to Reynolds numbers of 10000.) In addition Haberstroh and Baldwin [162] have developed a method for predicting Nusselt numbers which yields values comparable with those reported in section i) above. However all these equations, though providing a good fit to results for Re > 10000 generally predict results which are too high at lower Reynolds numbers and so the correlation (a modified Dittus-Boelter equation) found by McEligot et al [159] to give the best fit to their data is adopted here. This equation is

$$Nu = 0.021\ Re^{0.8}\ Pr^{0.4} \qquad (5.1)$$

and from it were calculated the Nu_T values given in section 5.5.2.

5.5.2 Experimental results

The measured Nusselt number results obtained for runs N-2 to N-14 and NT-1 to NT-5 are shown in Table 5.4 below. The results for Re ≈ 5000 and Re ≈ 8000 are also shown in Fig. 5.20, plotted against Gr/Re; in each case a single curve correlates all the data fairly well. The points on the Nu axis were calculated from equation (5.1). The results at Re ≈ 14000 are not plotted but

TABLE 5.4

Run	Re	Nu	Nu_T	Nu/Nu_T	Gr/Re^2 x 10^2	Ra/Re^2 x 10^6
N-2	8031	14.4	24.3	0.59	5.15	22.7
N-3	8016	12.3	24.25	0.51	5.30	19.7
N-4	8638	12.6	26.1	0.48	4.04	12.7
N-5	8474	12.2	25.3	0.48	3.80	12.2
N-6	8507	11.2	25.5	0.44	3.81	10.7
N-7	8783	16.2	26.3	0.62	1.28	5.3
N-8	8659	11.3	26.0	0.43	3.19	8.8
N-9	6794	10.5	21.2	0.49	5.98	26.0
N-10	5354	14.8	17.6	0.84	1.71	17.1
N-11	5258	9.6	17.4	0.55	3.78	26.2
N-12	5278	10.6	17.4	0.61	4.67	34.4
N-13	5032	10.7	17.2	0.62	5.29	43.8
N-14	13978	36.4	38.6	0.94	1.71	6.5
NT-1	5405	16.1	17.7	0.91	1.06	11.8
NT-2	5525	14.8	18.1	0.82	2.29	22.9
NT-3	5419	9.8	17.7	0.55	4.05	26.3
NT-4	5154	10.1	17.1	0.59	5.41	39.7
NT-5	14701	38.2	39.4	0.97	1.80	6.2

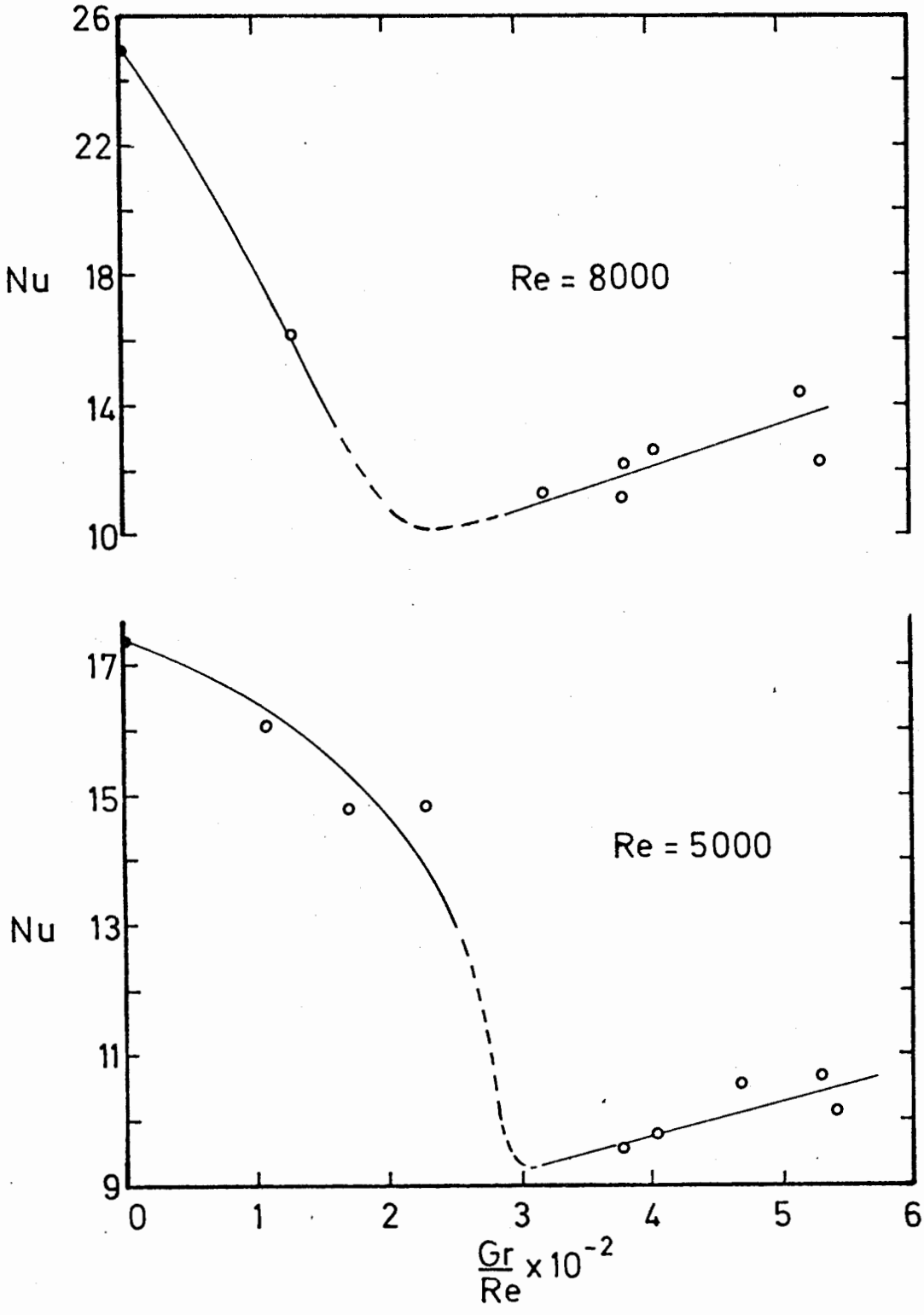

FIGURE 5.20 VARIATION OF NUSSELT NUMBERS WITH Gr/Re AT Re ≃ 5000 AND Pe ≃ 8000

o Experimental points

● Calculated from equation (5.1)

can be seen to agree well with the values from other investigations reported in Table 5.3.

It can be seen from Fig. 5.20 that as the value of the Gr/Re parameter increases Nusselt number values decrease rapidly, reaching a minimum at a Gr/Re value corresponding to that at which the point of maximum velocity moves from the pipe centre to a position nearer the wall. Thereafter, with increasing Gr/Re values a slow linear increase in Nusselt number values is observed. It is noteworthy that even at very low Grashof numbers significant departures from the pure forced convection Nusselt number occur, making it very difficult to measure pure forced convection Nusselt numbers at low to moderate Reynolds numbers.

The experimental results were also plotted (see Fig. 5.21) as Nu/Nu_T vs Ra/Re^2 in order to compare the trends of the present air measurements with those observed for water by Petukhov and Strigin [36] (see Fig. 1.3). It can be seen that in the same way as Petukhov and Strigin's results initially follow one of two different curves, depending on whether the pipe was preceded by a calming length or not, so the present results for measurements in the two different test loops also fall initially along two different curves. Thereafter, for both sets of results a stage is reached where the Nu/Nu_T values become independent of inlet conditions. For the present results the start of this latter stage occurs as the point of maximum velocity in the flow moves from the pipe centre nearer to the pipe wall; once such a flow has been attained Nu/Nu_T values all fall along a single line which rises gradually with increasing Gr/Re. The conclusion suggested by these observations is that although the profiles with the point of maximum velocity displaced from the pipe centre are stable and independent of inlet conditions the profiles with the velocity maximum at the pipe centre are not, as concluded before, fully developed, but will continue to change until a stable profile shape is reached. However, the present evidence is too slight for definite conclusions on the stability of the different types of profiles to be drawn and further investigations of this aspect of mixed convection flows would be profitable.

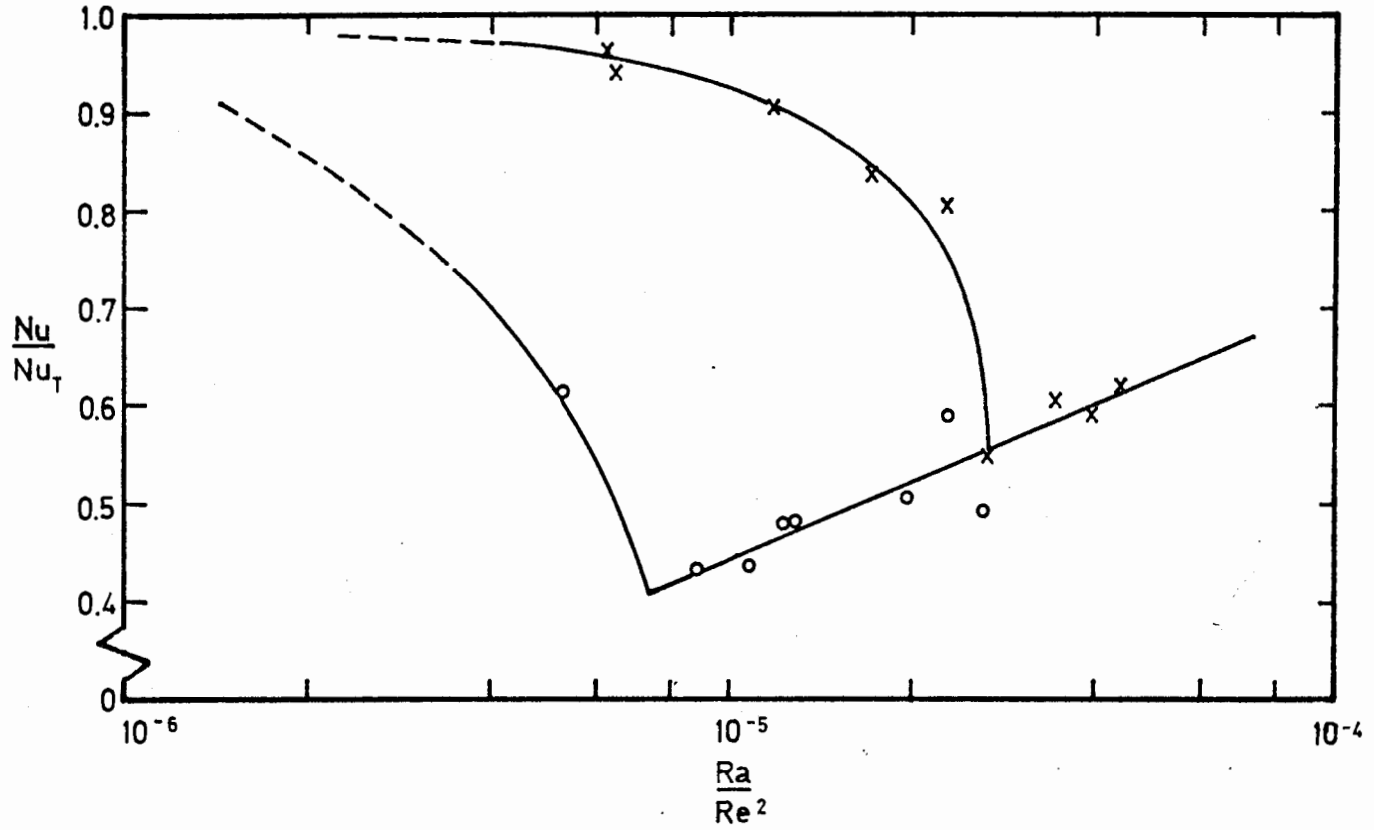

FIGURE 5.21 VARIATION OF Nu/Nu_T WITH Ra/Re^2

o Test loop I (L/D=70)

x Test loop II (L/D=100)

5.5.3 Discussion of results

The behaviour of the Nusselt number with increasing Gr/Re values is linked to the changes in the slope of the temperature profile (see section 5.3) which are in turn associated with the changes in eddy diffusivity (see section 5.7). It is shown that the minimum values of the eddy diffusivities in the region $y/R < 0.2$ occur as the velocity profile changes from a profile with a maximum at the pipe centre to one with a maximum nearer the pipe wall. Under these conditions, therefore, the rate of heat transfer and hence the Nusselt number will pass through a minimum value.

5.6 THE CALCULATION OF DIFFUSIVITIES AND CORRELATIONS FROM THE ENERGY AND MOMENTUM EQUATIONS

In order to calculate values of the eddy diffusivities, and of $\overline{v_r t}$ and $\overline{v_r v_z}$, measured temperature and velocity distributions have to be substituted into the forms of the equations of motion and energy given in Chapter 1. It is clear that enough measured information exists to solve equations (1.21) and (1.22) for $\overline{v_r t}$ and ε_H/α but before equations (1.11) and (1.12) can be solved to give $\overline{v_r v_z}$ and ε_M/ν values further information either about the slope of the velocity profile at the wall, or about some related quantity, such as the friction factor, is needed. Except in the case of runs N-10 to N-14 this introduces considerable difficulties, as explained later.

5.6.1 Non-isothermal friction factors and $\left(\frac{d\bar{V}_z}{dr}\right)_w$

Since in general it is not possible to measure the slope of the velocity profile at the wall with any accuracy it is customary, for non-isothermal as well as isothermal flows, to represent this slope in terms of a friction factor. For isothermal flows the friction factor is a function only of Reynolds number but in heated flows friction factors are affected both by Reynolds number and the wall to bulk temperature ratio T_w/T_b, and a number of different expressions relating friction factors to these two parameters have been proposed. (Reviews of the different types of relationships proposed have been given by Lafay [163] and Costa [164].)

For the present work it was originally decided to use a recent correlation due to Taylor [148]:

$$\frac{f}{2} = \left(0.0007 + \frac{0.0625}{Re_w^{0.32}}\right)\left(\frac{T_b}{T_w}\right)^{0.5} \qquad (5.2)$$

Although this expression was employed successfully by Horsten [24] in mixed convection mercury flows it soon became apparent that for the present air data it yielded most improbable results, except in the case of the practically undistorted flows of runs N-14 and NT-5, measured at Re ≈ 14000. Because directly measured pressure drop data were not available from the present experiments (the accurate measurement of local $\frac{dp}{dz}$ values in heated flows is extremely difficult) the only remaining sources of information on the slope of the velocity profiles at the wall were the measured velocity distributions. For runs N-2 to N-9 and NT-1 to NT-5 either the velocity profile data near the wall were not extensive enough (NT-1 to NT-5) or the velocities near the wall were too great (N-2 to N-9) for the slope at the wall to be determined accurately; however for runs N-10 to N-13 accurate velocity data were available and because of the low Reynolds number the magnitude of the slope was small enough to be determined with reasonable precision. For these four runs and run N-14 the equation of motion could therefore be solved - the values, at a number of radial positions, of the individual terms in the equation of motion (1.11) are given for these five runs in Appendix H, Table H.4, and are discussed in more detail in section 5.6.2.

The values of the friction factor obtained from the measured slopes at the wall for runs N-10 to N-13 are shown in Fig. 5.23 in comparison with the variation of friction factor predicted by Taylor's [148] correlation (equation 5.2). The isothermal friction factor values were obtained from the slopes at the wall of profiles IT-3 and IT-5. It is evident from Fig. 5.23 that Taylor's prediction does not hold in flows where the effect of free convection is significant.

Since runs NT-1 to NT-4 were measured at Reynolds numbers similar to those for runs N-10 to N-13, friction factors for the former set of runs could be obtained with reasonable accuracy

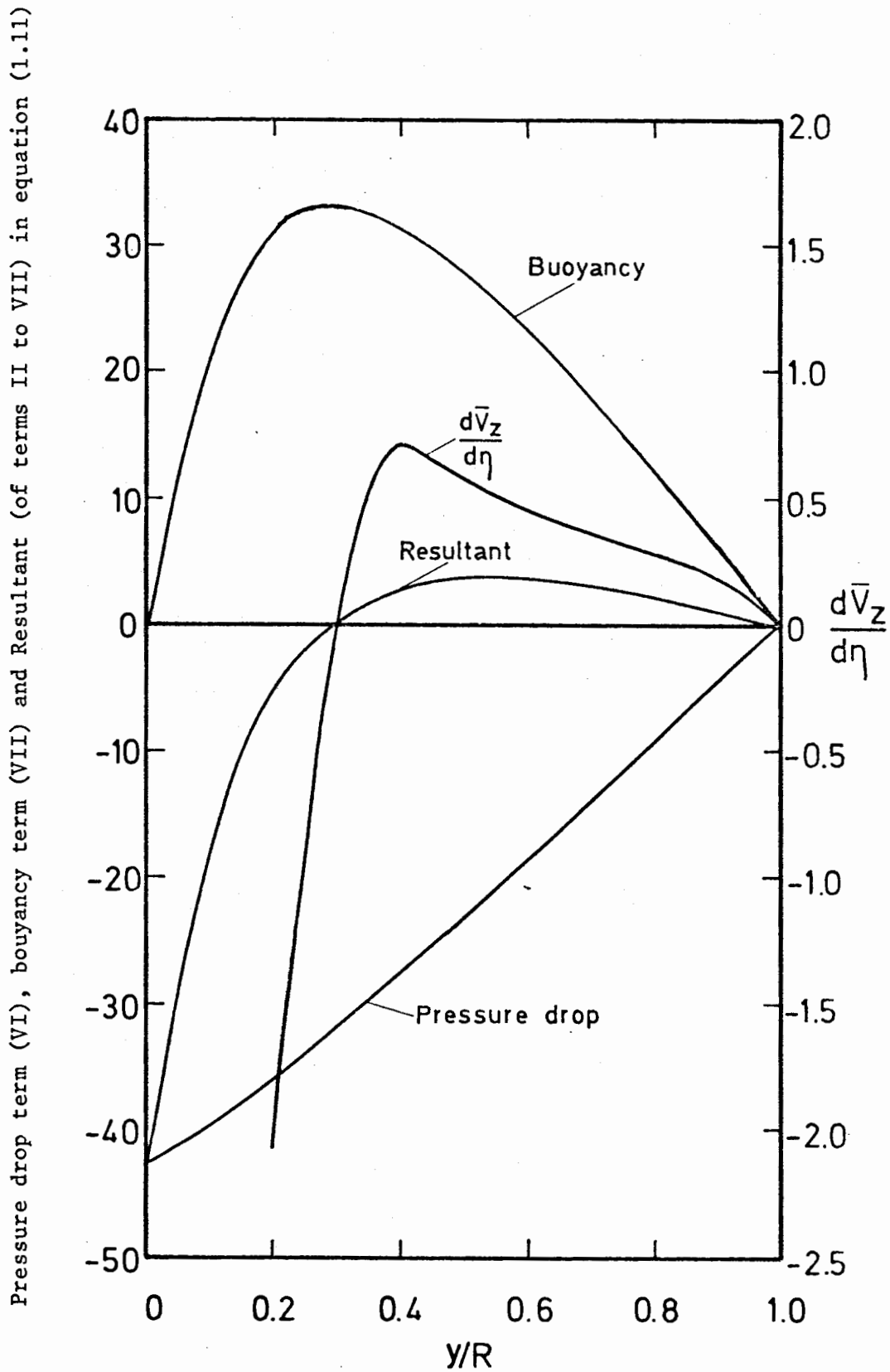

FIGURE 5.22 EVALUATION OF TERMS IN EQUATION OF MOTION FOR RUN N-13

(For clarity the small terms III, IV and V from equation (1.11) have been omitted from the figure)

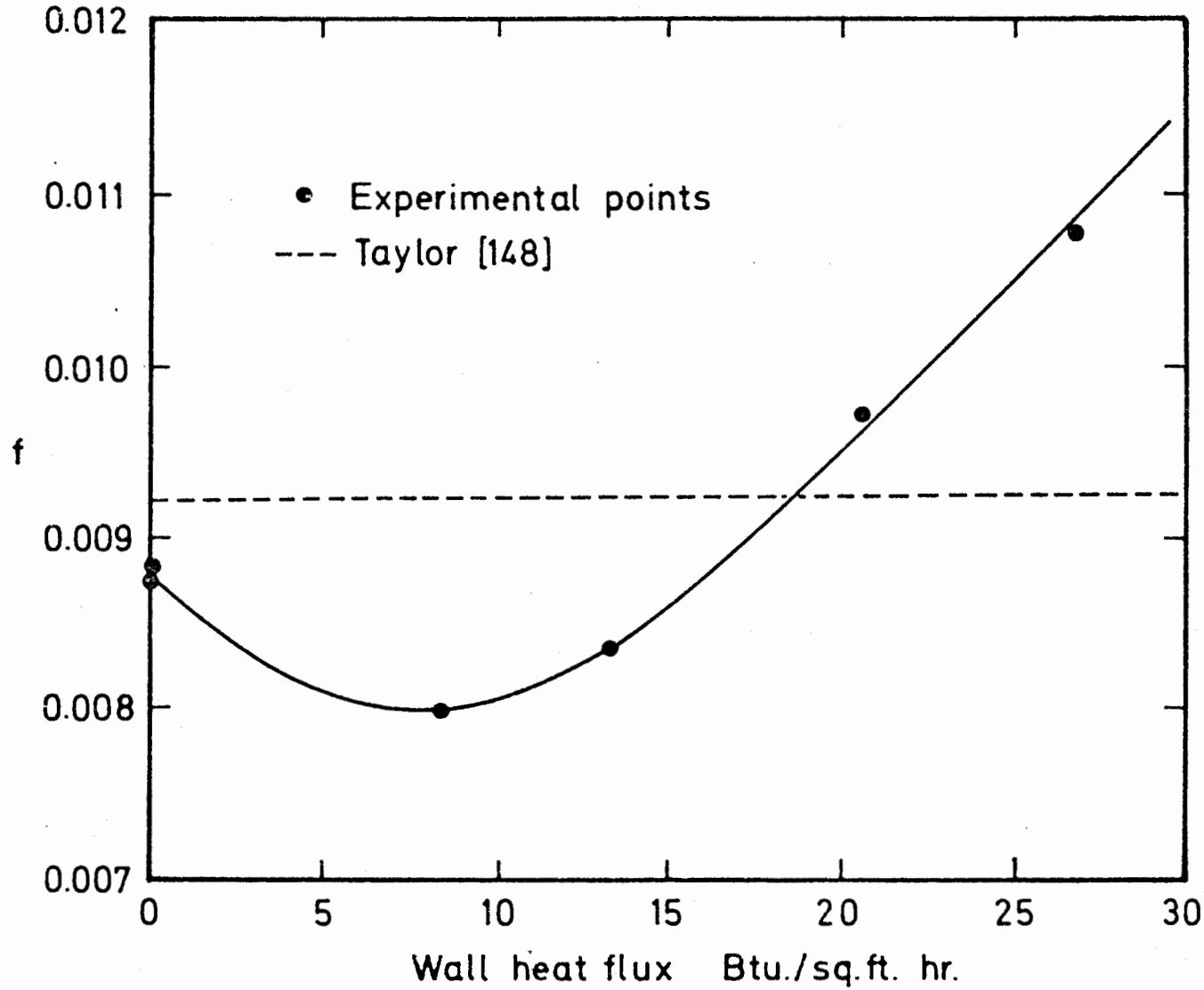

FIGURE 5.23 MEASURED FRICTION FACTORS COMPARED WITH RESULTS FROM TAYLOR'S [148] CORRELATION

from Fig. 5.23. Values obtained in this way were used in the calculation of u* ($\bar{V}_{z_m}\sqrt{\frac{f}{2}}$) and T*, employed as normalising parameters when reporting the turbulence measurements discussed in section 5.4.

At a given Reynolds number u* and T* vary considerably with heat flux, making their use less satisfactory in non-isothermal than in isothermal flows. However no more suitable method of comparing isothermal and non-isothermal turbulence results has been proposed and u* and T* are therefore retained as normalising parameters for the turbulence measurements in the present work.

5.6.2 The resultant of the principal terms of the equation of motion.

For the strongly distorted profiles N-11 to N-13 a check on the accuracy of the measured data is available, since it would be expected, at the point of maximum velocity where $\frac{d\bar{V}_z}{d\eta}$ is zero, that the value of $\overline{v_r v_z}$ and hence also the resultant of terms III to VII in equation (1.11) would be zero. It can be seen from the values for the individual terms in equation (1.11), tabulated for runs N-10 to N-14 in Appendix H, Table H.4, that for the very distorted runs N-11 to N-13 the slope of the velocity profile and the resultant of the terms III to VII in equation (1.11) do in fact pass through zero at radial positions that are relatively close. Fig. 5.22, which shows the results for run N-13, makes this clear. (In Fig. 5.22 only the buoyancy and pressure drop terms together with the total resultant of all terms III to VII are shown - the terms III to V lie very close to the zero line on the figure and, for clarity, are omitted. Despite their small values these terms make a significant contribution to the value of the resultant in the region where the resultant passes through zero, and are retained in the equation for that reason.)

For runs N-11 to N-13 the closeness of the agreement between the radial positions at which $\frac{d\bar{V}_z}{d\eta}$ and the resultant pass through zero confirms the correctness of the value of f shown in Fig. 5.23; use of the values of f predicted by, for example, Taylor's [148] correlation, gives values of the resultant which pass through zero

at radial positions very different from that at which the velocity profile maximum occurs. (In certain runs where the velocity maximum occurs away from the pipe centre, use of values of f calculated from Taylor's equation gave values of the resultant which did not pass through zero at all.)

The determination of the slope of the velocity profile at the wall and hence of f and of the position where the "resultant" passes through zero are all dependent on the accuracy of the velocity profile measurements near the wall in runs N-11 to N-13. The uncertainty in these measurements is difficult to assess but is probably within ± 2-3%. Variations of this order of magnitude in f would then allow the zero positions of the velocity profile slope and the resultant to be taken as identical within the limits of experimental error and this assumption was made in calculating ε_M and $\overline{v_r v_z}$ values for runs N-11 to N-13. ε_m and $\overline{v_r v_z}$ values were also calculated for runs N-10 and N-14 and the results are discussed in sections 5.7 and 5.8.

It has been shown by Hinze [165] and Eskinazi and Erian [166] that for jets and other flows where velocity maxima occur away from the flow axis, the shear stress and velocity profile slope pass through zero at slightly different radial positions. No information on non-isothermal flows is presented, however, and since the differences in the present results appear to show an effect opposite to that indicated by Hinze it was concluded that the particular effect described by Hinze and Eskinazi and Erian is not applicable here.

5.7 EDDY DIFFUSIVITIES

5.7.1 Introduction

As indicated in section 5.6 accurate ε_H/α values could be obtained for all heated runs except run N-1 but accurate ε_M/ν values could be determined directly only for runs N-10 to N-14. Values of ε_M/ν could be obtained for the remaining runs but their accuracy is less certain than those from runs for which the slope of the velocity profile at the wall could be measured directly.

5.7.2 Eddy diffusivity of momentum ε_M

Eddy diffusivity of momentum values for runs N-10 to N-14 are tabulated in Appendix H, Table H.5 and are plotted, as $\frac{\varepsilon_M}{Ru^*}$, in Figs. 5.24 and 5.25. Fig. 5.24 shows the results for Re ≈ 5000 in comparison with the mean isothermal eddy diffusivity curve at Re ≈ 5000 (reported in Chapter 4). It is apparent from this figure that the general trend with increasing free convection effect, as evidenced by the Rayleigh number, is for eddy diffusivity values to decrease, suggesting a definite decrease in the turbulence level of the flow. This decrease is particularly marked in the region near the wall ($y/R < 0.2$) where the eddy diffusivity values drop practically to zero at a Rayleigh number corresponding to that at which the maximum velocity moves from the pipe centre to a position nearer the wall. At higher Rayleigh numbers the eddy diffusivity values increase again, though they still remain relatively small.

Fig. 5.25 shows the results for run N-14 in comparison with the average isothermal eddy diffusivity curve for Re ≈ 16000 (given in Chapter 4). As would be expected, since the velocity

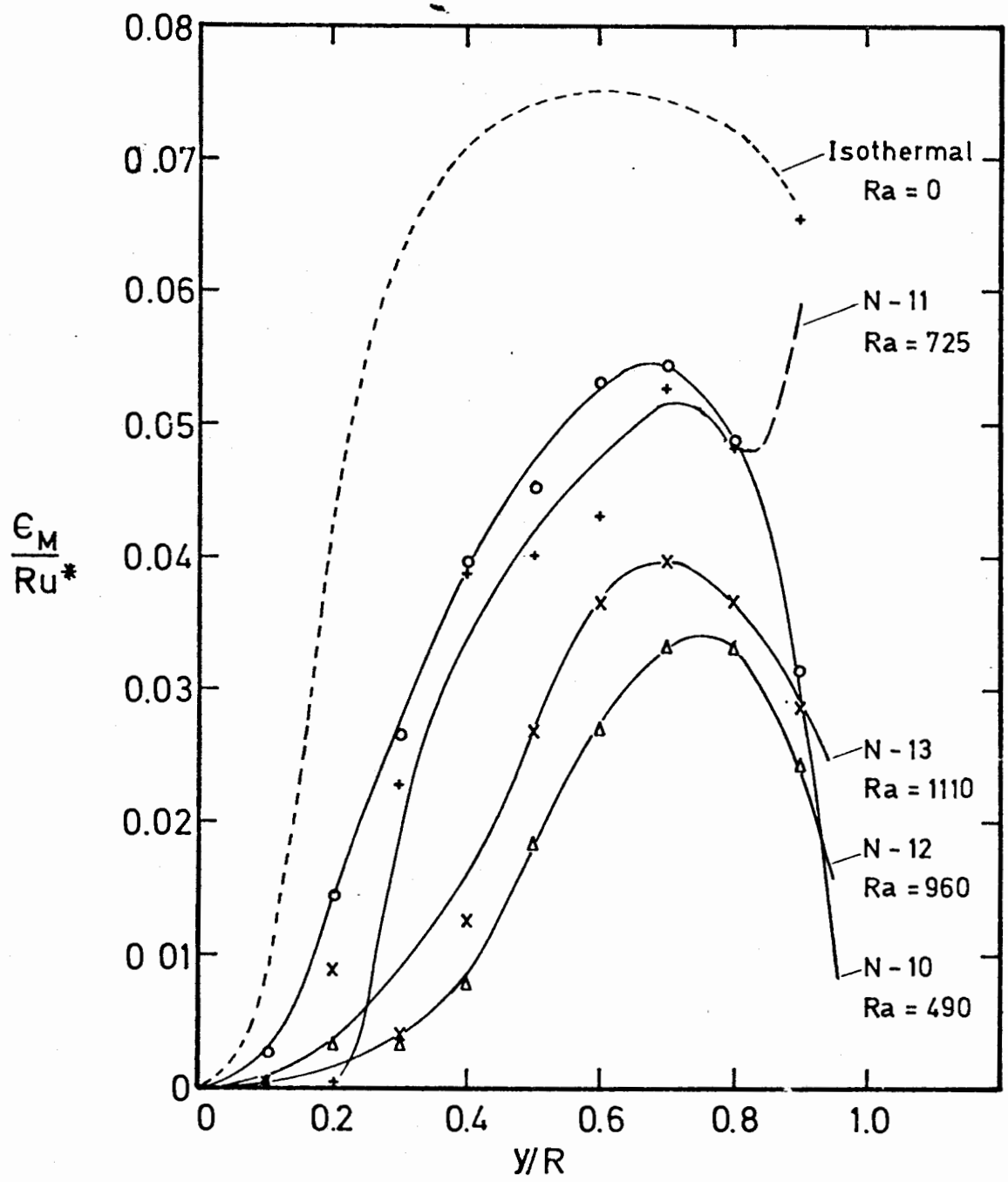

FIGURE 5.24 NON-ISOTHERMAL ϵ_M/Ru^* VALUES AT Re ≃ 5000

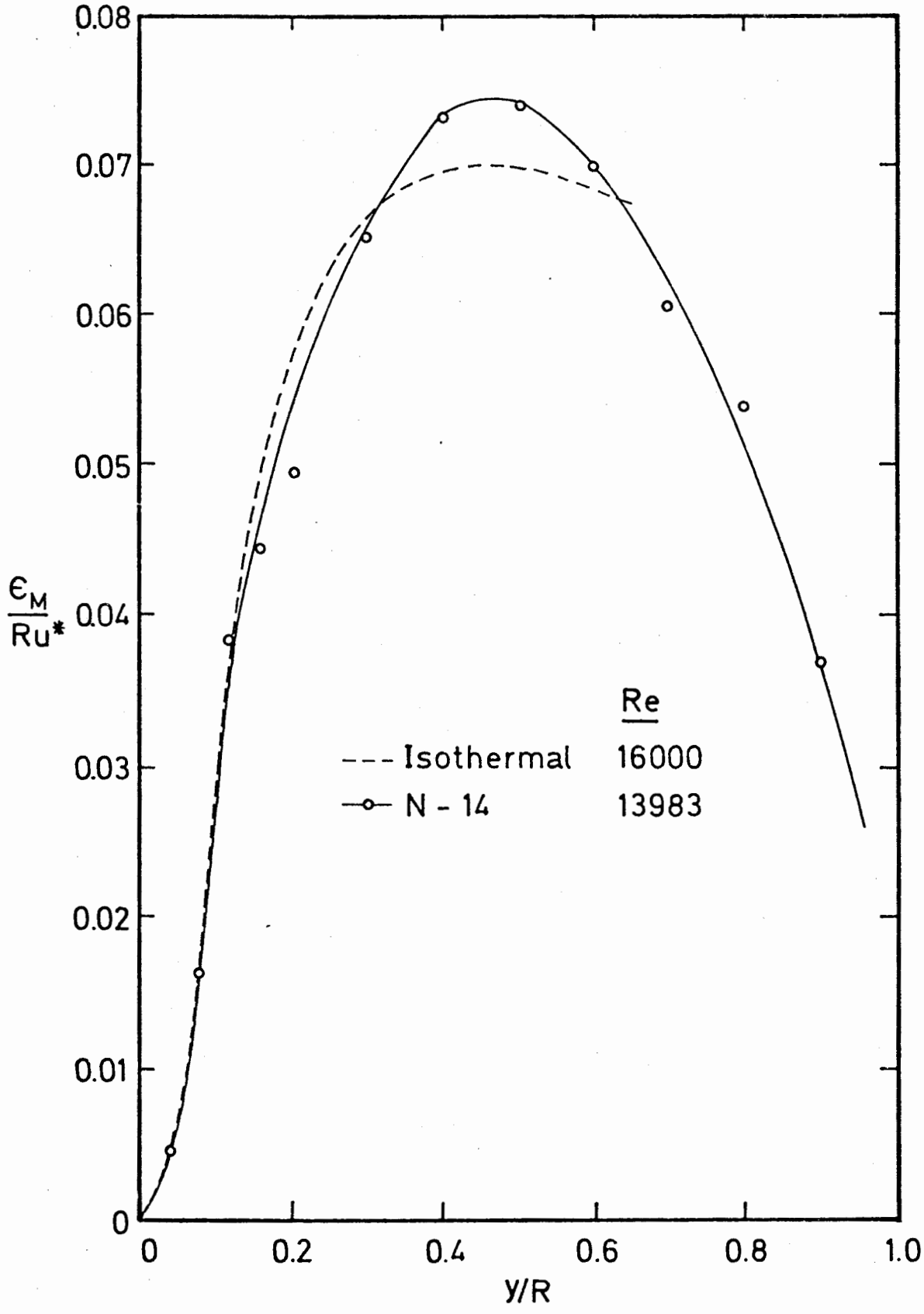

FIGURE 5.25 NON-ISOTHERMAL ε_M/Ru* VALUES AT Re ≃ 14000

profile for run N-14 is barely distorted there is a close similarity between the two eddy diffusivity curves.

Eddy diffusivity of momentum values for mixed convection flows have been reported previously only by Horsten [24] (for mercury). The trends in his results are fairly similar to those described above but, as with the present values, no general correlation is apparent.

5.7.3 Eddy diffusivity of heat

Eddy diffusivity of heat values, as ε_H/α are reported in Appendix H. Values for runs N-10 to N-14 are given in Table H.5 and values for the remaining runs in Table H.6.

Apart from the results reported for mercury flows by Horsten [24] there is no other published information on mixed convection ε_H/α values with which the present results can be compared. For the results obtained in the relatively undistorted flows at Re ≈ 14000 (runs N-14 and NT-5), however, a number of comparable measurements are available [92, 132].

To illustrate the trend of the present results under mixed convection conditions the calculated ε_H/α values for runs N-10 to N-13 are shown in Fig. 5.26. It is apparent from this figure that as the Rayleigh number increases there is a tendency for ε_H/α values in the region $y/R < 0.5$ to decrease, though the change is not as large as that observed for the correxponding ε_M/Ru^* values (see Fig. 5.24). This decrease in ε_H/α values supports the conclusion drawn from Fig. 5.24 that with increasing Rayleigh number the turbulence level in the flow near the wall decreases.

Nearer the pipe centre there is a tendency for the peak in the eddy diffusivity curve to increase and move closer to the wall as the Rayleigh number increases, although a comparison of results at Re ≈ 5000 and Re ≈ 8000 shows that no general correlation for this region can be determined.

The results for Re ≈ 14000 are shown in Fig. 5.27 in comparison with the profiles obtained by Johnk [132] and Sleicher [92] at similar Reynolds numbers. It can be seen that the general shape of all four profiles is fairly similar and that the

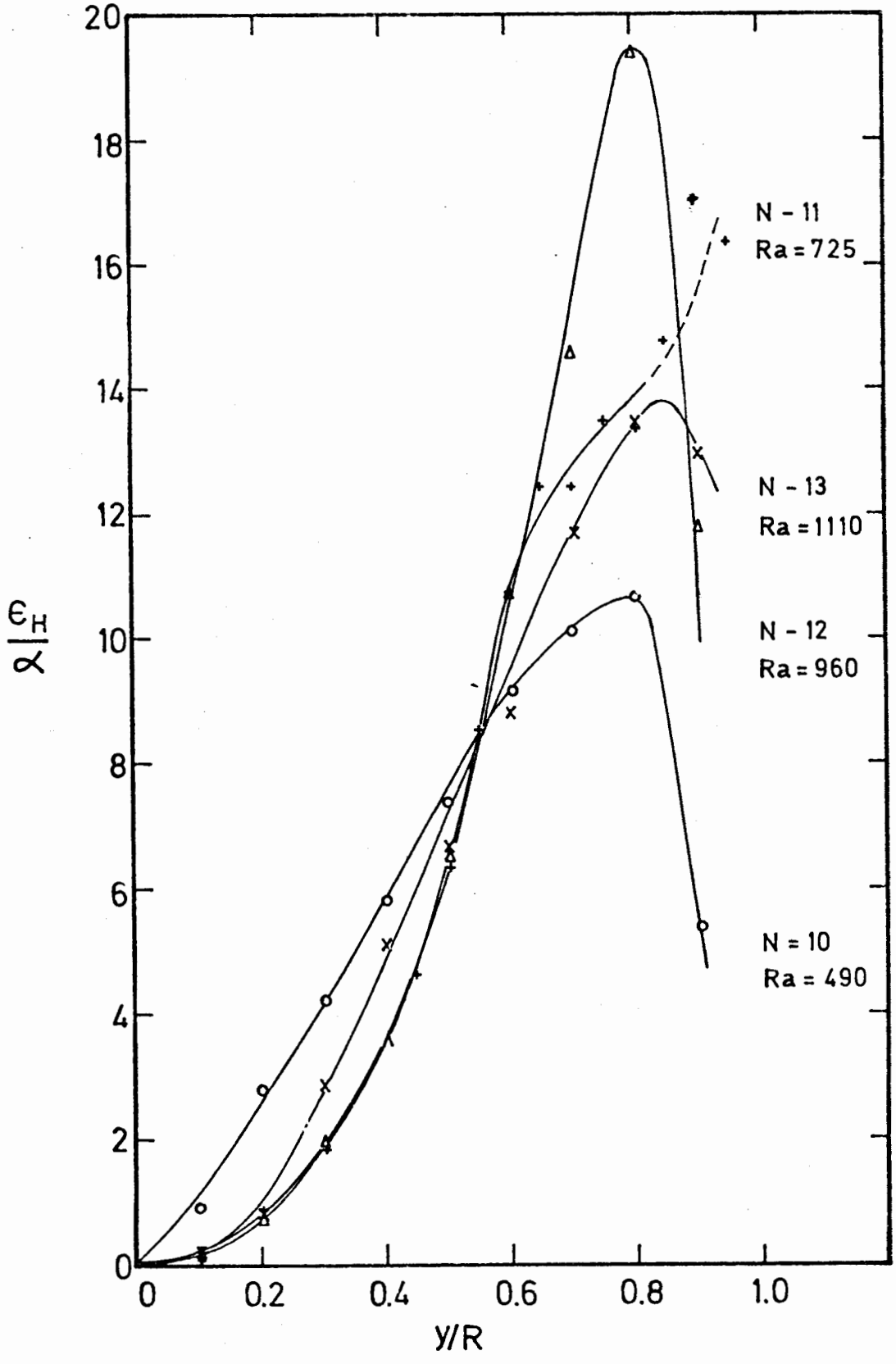

FIGURE 5.26 ε_H/α VALUES AT Re ≃ 5000

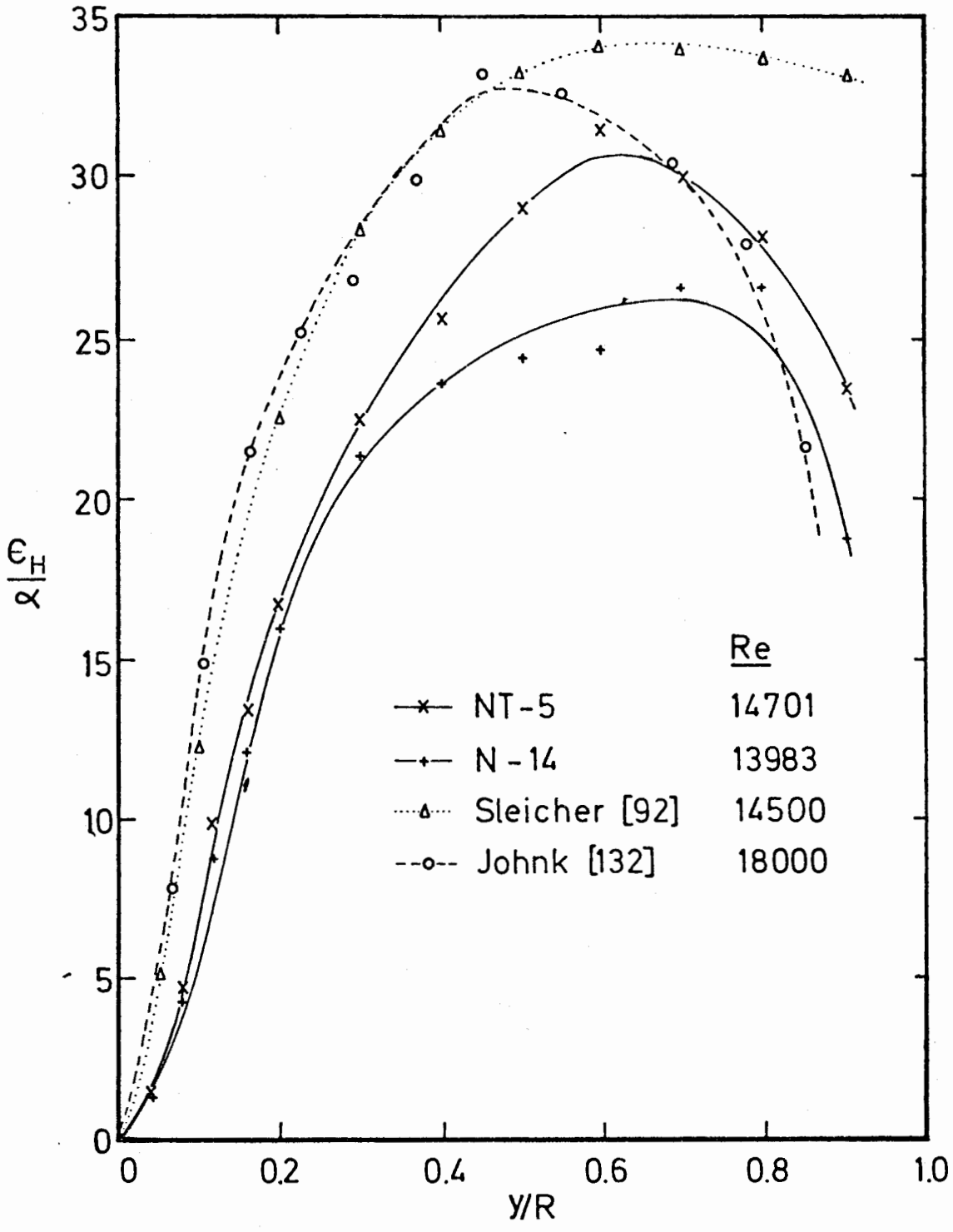

FIGURE 5.27 ε_H/α VALUES AT Re ≃ 14000 COMPARED WITH RESULTS OF OTHER WORKERS

values for run NT-5, believed to be more accurate than those for run N-14, are in fair agreement with the results of the other workers.

5.7.4 The eddy diffusivity ratio

Since accurate values of ε_M were available only for runs N-10 to N-14 $\varepsilon_H/\varepsilon_M$ values were calculated only for these runs. These calculated values are given in Appendix H, Table H.7.

The results are plotted in Fig. 5.28 and it can be seen that at low Rayleigh numbers, i.e. under conditions where velocity profiles are relatively undistorted, the calculated $\varepsilon_H/\varepsilon_M$ values lie for the most part between 1.2 and 1.8, fairly close to, if slightly higher than, the values given by, for example, Sleicher [92] and Page et al [146]. At higher Rayleigh numbers, however, there is a tendency for the $\varepsilon_H/\varepsilon_M$ values to increase, though again no particular correlation is apparent.

5.7.5 Discussion of results

It is clear from the experimental results that the measured eddy diffusivities at a given Reynolds number diverge rapidly from the pure forced convection values as the Rayleigh number increases. This shows that at low Reynolds numbers the effect of free convection on the flow structure is important even at low heat fluxes. The change in flow structure which is suggested by the present results is that the turbulence level in the flow is reduced. However the fact that eddy diffusivity values pass through a minimum and thereafter increase steadily indicates that the changes in structure are not simple and more measurements, particularly at high heat fluxes, will be necessary before the changes can be fully explained.

5.8 THE CORRELATIONS $\overline{v_r v_z}$ AND $\overline{v_r t}$

5.8.1 Introduction

As well as giving eddy diffusivities the solution of the equations of motion and energy (equations (1.11) and (1.22) respectively) also gives values of the correlations $\overline{v_r v_z}$ and $\overline{v_r t}$, which are often discussed in the forms $\rho\overline{v_r v_z}$, the turbulent shear stress and $-\rho C_p \overline{v_r t}$, the radial turbulent heat flux, respectively. Because of the problems encountered during the solution

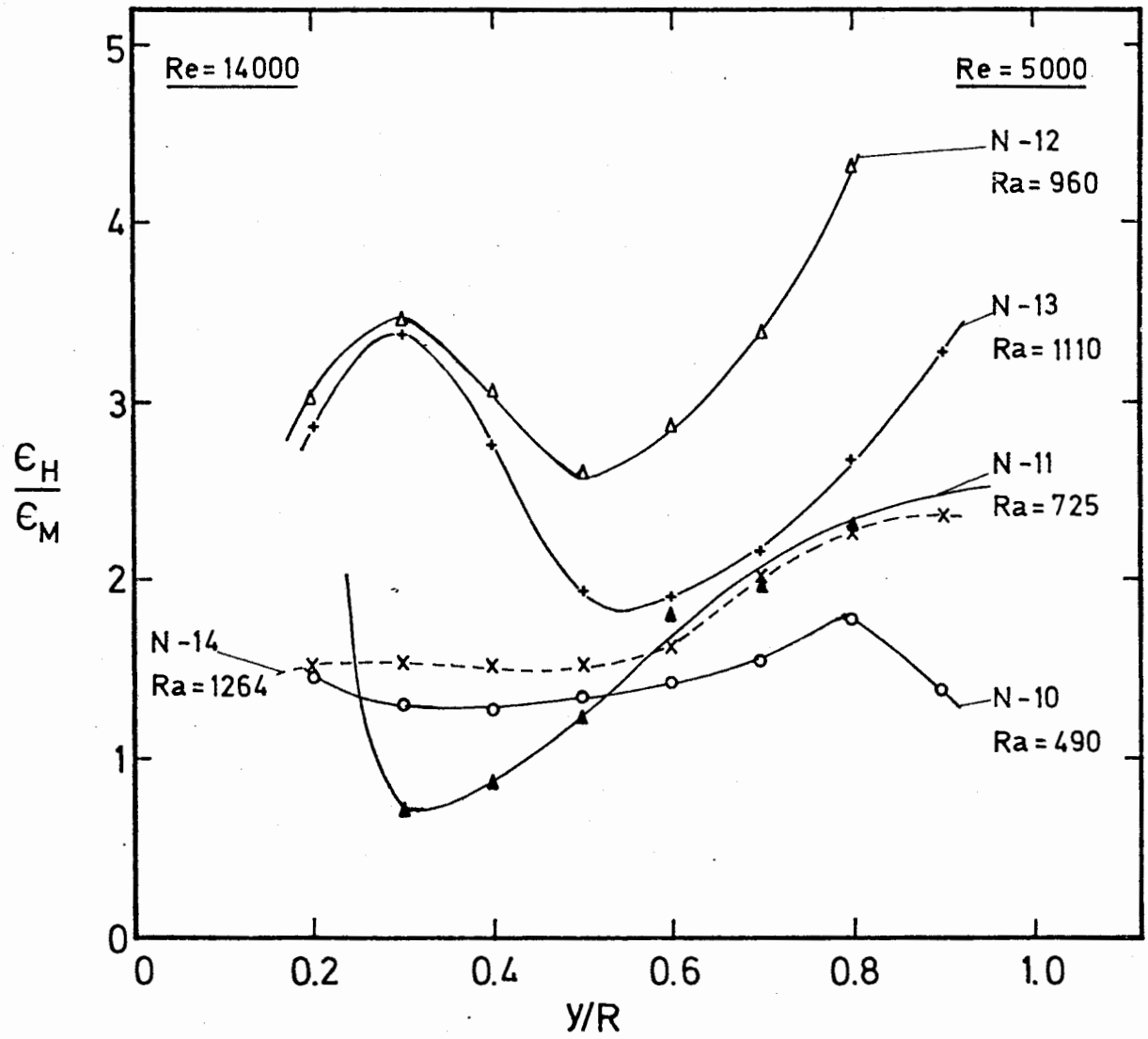

FIGURE 5.28 CALCULATED $\varepsilon_H/\varepsilon_M$ VALUES

of the non-isothermal equation of motion (see section 5.6) accurate $\overline{v_r v_z}$ values could be obtained only for runs N-10 to N-14; however, accurate $\overline{v_r t}$ values could be obtained for all heated runs except run N-1. The calculated values of both $\overline{v_r v_z}$ and $\overline{v_r t}$ are reported in Appendix H, Tables H.5 and H.6, and are discussed in detail in sections 5.8.2 and 5.8.3 below. Sample calculation procedures are given in Appendix I.

5.8.2 The correlation $\overline{v_r v_z}$

Values of $\overline{v_r v_z}$ for runs N-10 to N-13 (Re ≈ 5000) and N-14 (Re ≈ 14000) are shown in Fig. 5.29 in comparison with the theoretical isothermal total shear stress curve. Also included in this figure are $\overline{v_r v_z}$ values for isothermal runs I-3 (Re ≈ 5000) and I-4 (Re ≈ 16000) which were calculated, using equation (1.13), from the measured velocity profiles reported in Chapter 4.

It is apparent that the effect of increasing heat flux at a given Reynolds number is to decrease the $\overline{v_r v_z}$ values and even the barely distorted flow (N-14) at Re ≈ 14000 gives results lying significantly below the isothermal values. For Re ≈ 5000 there is seen to be an initially rapid drop in $\overline{v_r v_z}$ values with increasing heat flux until, as the maximum in the velocity profile moves from the pipe centre to a position nearer the wall, $\overline{v_r v_z}$ values become negative in the region $y/R > 0.3$. Thereafter, with increasing heat flux the values remain small and fairly constant, although a slight increase is observed in the neighbourhood of $y/R = 0.2$.

5.8.3 The correlation $\overline{v_r t}$

Typical $\overline{v_r t}$ values at Re ≈ 14000 (run NT-5) and Re ≈ 5000 (runs NT-1 to NT-4) are shown in Fig. 5.30, plotted as $-\rho C_p \overline{v_r t}/q_w$, i.e. the ratio of the radial turbulent heat flux to the wall heat flux. Also shown on this figure are values of the total heat flux, as q/q_w, which were calculated from the relationship [167]:

$$\frac{q}{q_w} = \frac{\frac{1}{r}\frac{d\bar{T}}{dz}\int_o^r (\rho C_p \bar{V}_z) r \, dr}{\frac{1}{r}\frac{d\bar{T}}{dz}\int_o^R (\rho C_p \bar{V}_z) r \, dr} \qquad (5.3)$$

It is apparent that with increasing heat flux the turbulent contribution to the total heat flux decreases,

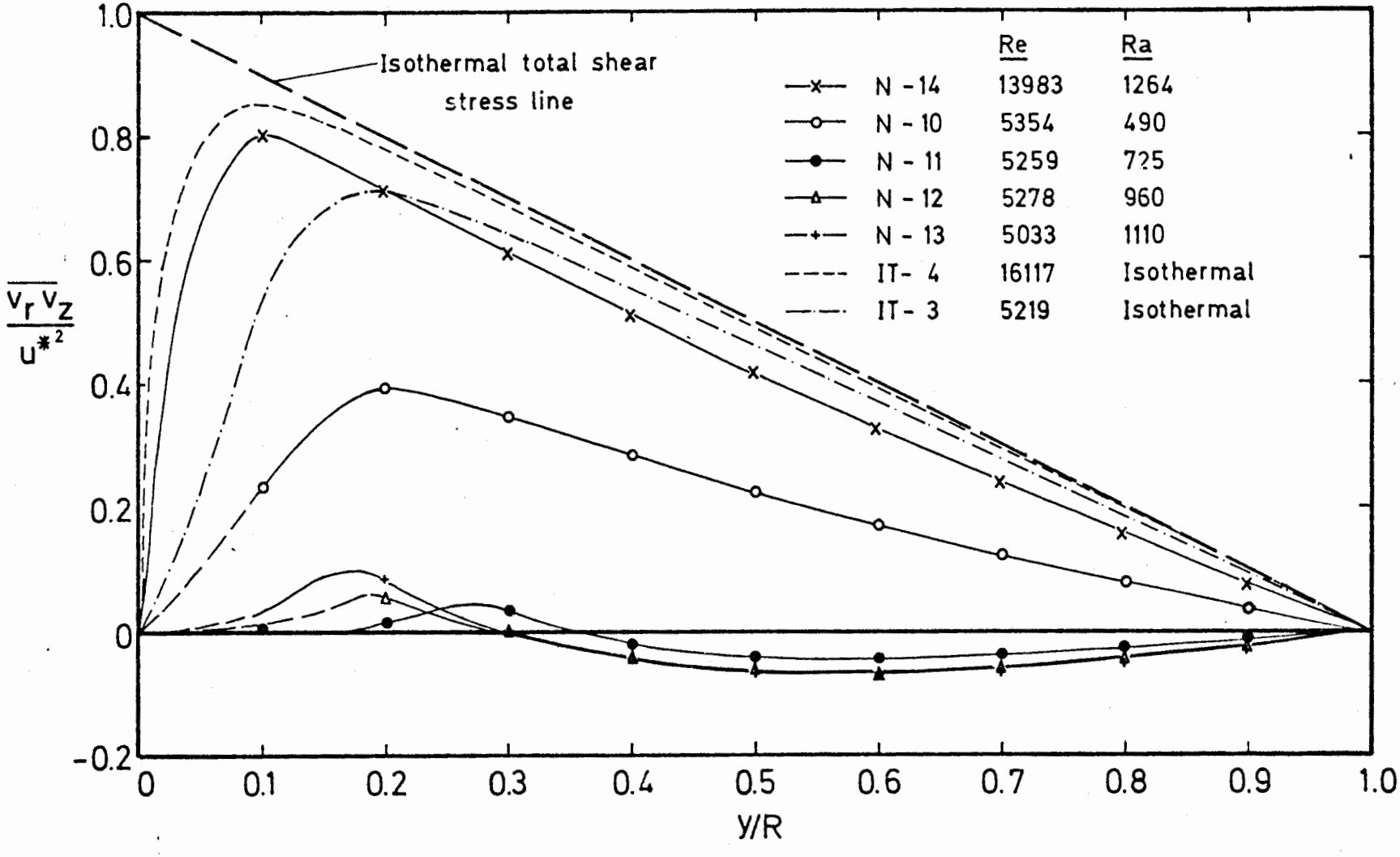

FIGURE 5.29 CALCULATED $\overline{v_r v_z}/u^{*2}$ VALUES

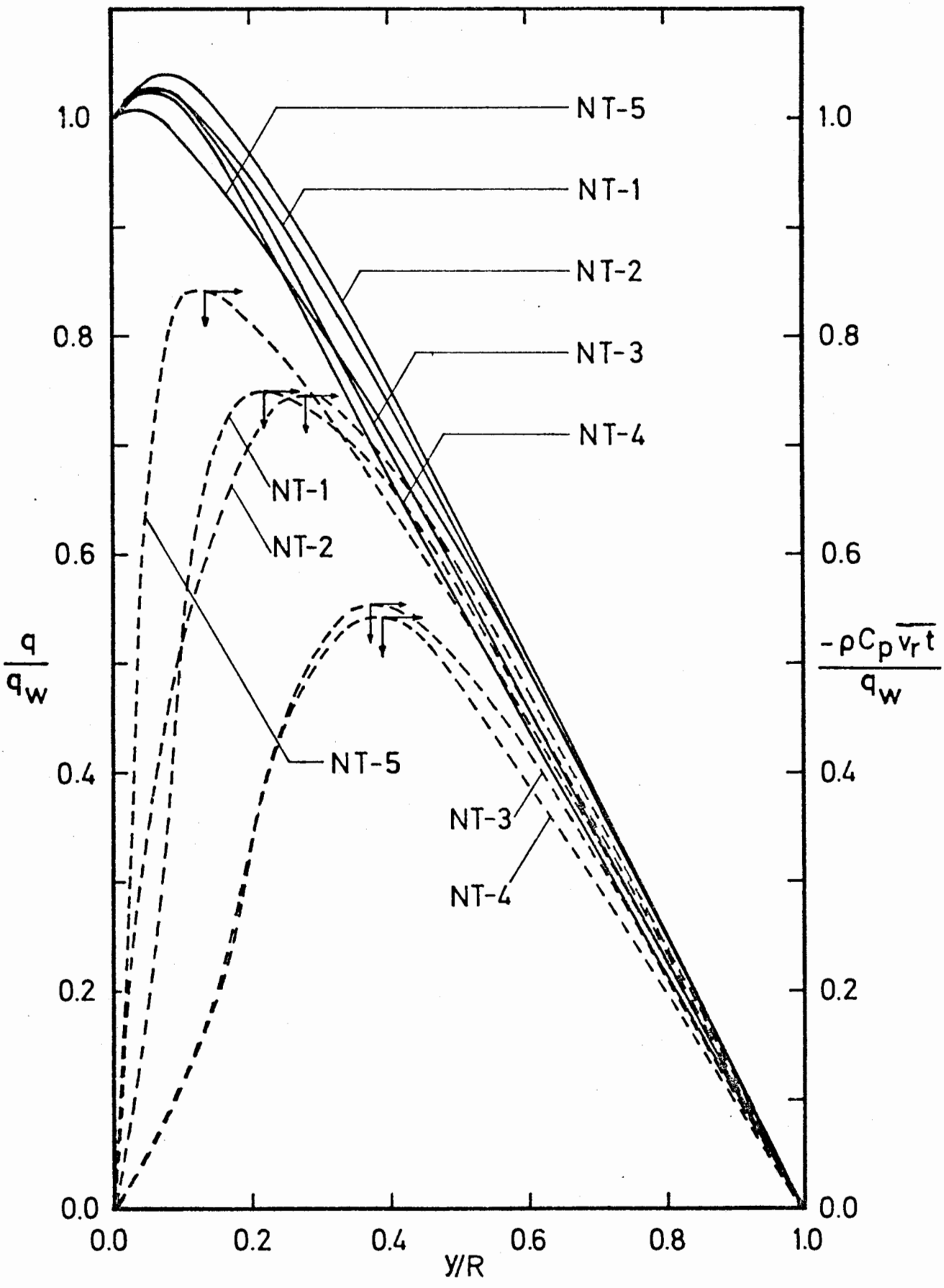

FIGURE 5.30 CALCULATED q/q_w AND $-\rho C_p \overline{v_r t}/q_w$ VALUES

particularly in the region $y/R < 0.6$, though as the velocity and temperature profiles tend towards a condition of saturation so also does the $\overline{v_r t}$ curve.

Variations are also observed to occur in the q/q_w curves and with increasing Rayleigh number the curves are observed to increase initially and then to decrease by up to 10% of their value at the lowest heat flux. Variations with Reynolds number are also noted, the peak in the total heat flux curve being observed to move closer to the wall with increasing Reynolds number.

The ratio of the radial heat flux q_r $(-\rho C_p \overline{v_r t})$ to the axial heat flux q_z $(-\rho C_p \overline{v_z t})$ is shown for runs NT-1 to NT-5 in Fig. 5.31. The curve obtained by Ibragimov et al [143] at low heat flux conditions at $Re \simeq 32500$ is included for comparison. It is apparent that run NT-5, for which the flow is barely distorted, gives a result similar to that observed by Ibragimov et al [143] but at $Re \simeq 5000$ even run NT-1 shows considerable differences from the undistorted value. At higher heat fluxes even larger variations occur, as can be seen from Fig. 5.31.

Discussion of results

At low to moderate heat inputs $\overline{v_r v_z}$ "profiles" have approximately the same shape as the isothermal "profile", though the actual $\overline{v_r v_z}$ values are lower. As the velocity maximum moves from the pipe centre a pronounced change in flow structure occurs and $\overline{v_r v_z}$ values become small over the whole pipe cross-section. At the same time v_z' and $\overline{V}_z$ values also become practically constant over most of the pipe, suggesting that a condition approaching isotropy may exist in the central regions of the pipe.

Although transport of momentum by eddy diffusion is slight Fig. 5.30 shows that the transport of heat by eddy diffusion is still important over most of the pipe. Near the pipe wall, however, a considerable reduction in the importance of eddy transport is apparent and this is reflected in corresponding decreases in t'/T^* in the wall region and in the movement of the peak in the temperature intensity profile further from the wall.

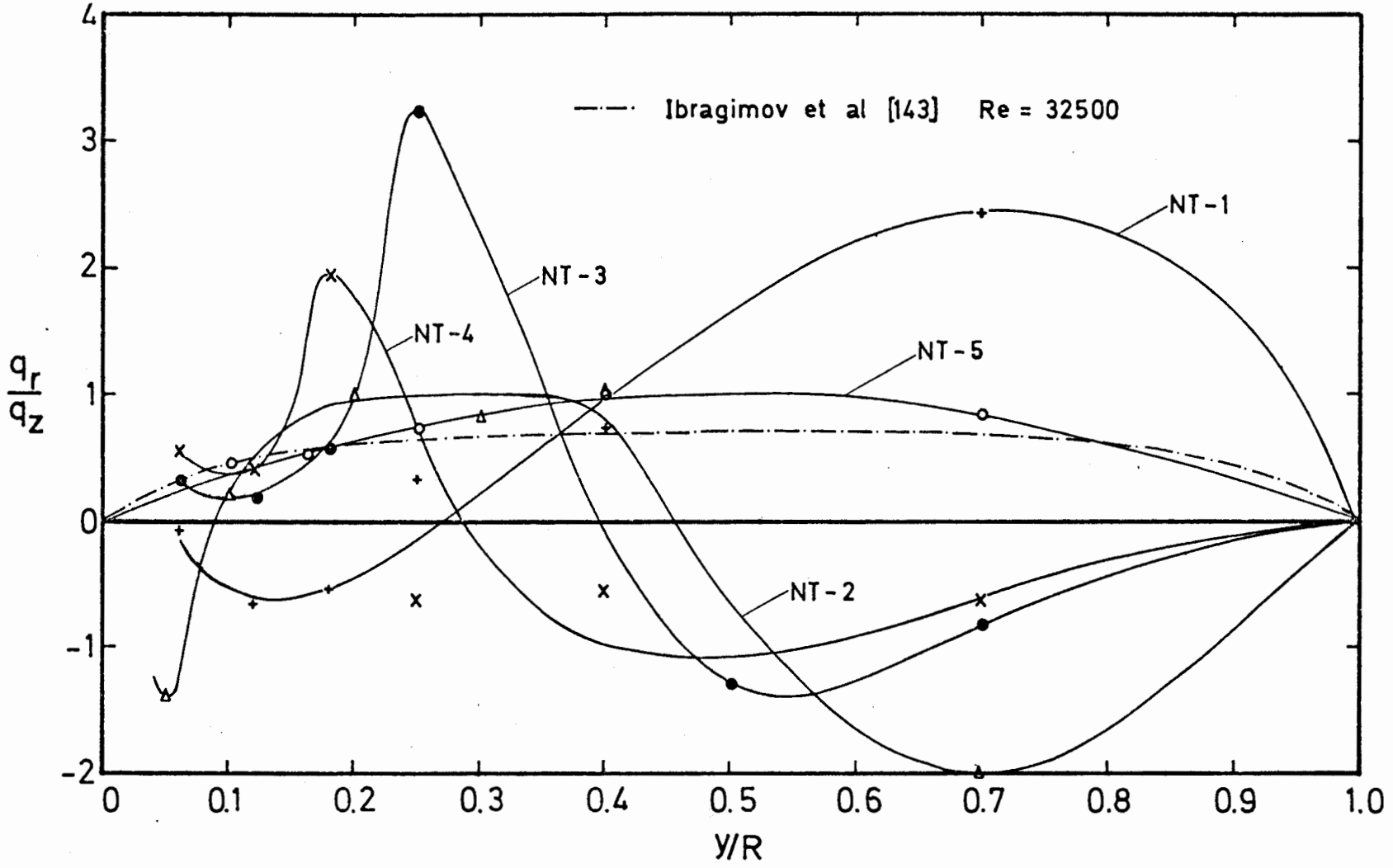

FIGURE 5.31 THE RATIO OF THE RADIAL HEAT FLUX TO THE AXIAL HEAT FLUX

CHAPTER 6

CONCLUSIONS AND RECOMMENDATIONS

The work carried out in this investigation falls into three sections, the first two of which are relatively minor:

i) Experiments to determine the temperature dependence of the hot-wire calibration parameter A

ii) Measurements in isothermal flows

iii) Measurements in heated flows

These are discussed separately below:

6.1 CALIBRATION EXPERIMENTS

Conclusions

i) The variation of the calibration parameter A in the King's Law equation is positive and of the order of 0.02 to 0.03% per ^{o}C increase in temperature. This value is opposite in sign to and smaller in magnitude than values reported by other workers.

ii) The observed variations in A are represented within the limits of experimental error by Hinze's [40] prediction, equation (2.23).

Recommendations for future work

Further experiments should be carried out to determine more precisely the nature of the temperature dependence of A. A very low speed wind tunnel in which accurate velocity and temperature measurements can be made would probably be the most suitable piece of equipment in which to carry out such a determination.

6.2 ISOTHERMAL MEASUREMENTS

A total of 22 isothermal velocity profiles at Reynolds numbers of 5000 to 32000 were measured and from these profiles eddy diffusivity of momentum values were calculated. Axial turbulence intensities were measured at Reynolds numbers of 5000 and 16000.

Conclusions

i) The measured velocity profiles could be adequately represented, except at the lowest Reynolds numbers (Re ≈ 5000 - 7000), by the relatively simple equations of the "universal velocity distribution" (equation (4.4)). The more complex predictions of Travis et al [130] and Reynolds et al [129], however, provide a much better fit to the measured data and also to the eddy diffusivity of momentum values calculated from this data.

ii) Measured axial turbulence intensities are in fair agreement with the results for low Reynolds numbers of other workers, although the present results show a tendency to increase slightly with decreasing Reynolds number whereas the results of others tend to decrease. This difference is attributed to the very low cut-off frequency of the amplifier used in the present work, which enabled the present measurements to take more of the energy in the very low frequencies into account.

Recommendations for future work

A comprehensive investigation of axial turbulence intensities at low to moderate Reynolds numbers should be made. This investigation should include a determination of the effects on axial intensities of varying such parameters as hot-wire ℓ/d, pipe L/D, mode of hot-wire operation, type of probe, etc.

At the same time accurate energy spectra for the turbulent fluctuations at low Reynolds numbers should be determined, possibly by analysis on a digital computer of recorded hot-wire output voltage signals. Such a determination would enable the importance of the contributions of the low frequency signals to the turbulence intensity to be estimated.

6.3 NON-ISOTHERMAL MEASUREMENTS

Altogether, nineteen velocity and temperature profiles were measured in flows at Re ≈ 5000, 8000 and 14000. Measurements of v_z', t' and $\overline{v_z t}$ at Re ≈ 5000 (4 heat fluxes) and Re ≈ 14000 (1 heat flux) were also obtained. From the measured results Nusselt numbers, eddy diffusivities of momentum and heat and the correlations $\overline{v_r v_z}$ and $\overline{v_r t}$ were determined.

Under combined free and forced convection conditions considerable changes in flow structure occur as the importance of the free convection effects increases. These changes are illustrated in Fig. 6.1 which shows the variations in $\bar{V}_z/\bar{V}_{z_m}$, v'_z/u^*, $\overline{v_r v_z}/u^{*2}$, $\frac{T_w - T}{T_w - T_c}$, t'/T^* and $\frac{-\rho C_p \overline{v_r t}}{q_w}$ which occur as the heat flux is increased.

For velocity measurements ($\bar{V}_z$, v'_z and $\overline{v_r v_z}$) it appears that with a considerable effect of free convection a limiting condition of practically uniform velocity, turbulent velocity intensity and $\overline{v_r v_z}$ occurs across most of the tube and in this region ($y/R > .3$) the flow tends towards a condition of isotropy. Near the wall the most noticeable change with increasing free convection effects is that the importance of eddy transport decreases considerably.

The corresponding variations in temperature $\left(\frac{T_w - T}{T_w - T_c}, \; t'/T^* \text{ and } \frac{-\rho C_p \overline{v_r t}}{q_w}\right)$ measurements appear to be closely linked to the changes in velocity measurements: the decrease in the slope of the temperature profile near the wall and the decrease near the wall of the $\frac{-\rho C_p \overline{v_r t}}{q_w}$ values are clearly due to the decreased rate of turbulent heat transfer from the wall associated with the fall in eddy diffusivity values. Also, the initial decrease and subsequent increase in t'/T^* values as the heat flux is increased can be related to the behaviour of v'_z/u^*.

Apart from the above, the following more specific conclusions are drawn

i) The fundamental change in flow structure which occurs as the velocity maximum moves from the pipe centre to a position nearer the wall takes place at a characteristic value - 8 to 10 - of the Yantovskii number (Gr/Re^{*2}). This applies for both air and water, indicating that the criterion Gr/Re^{*2} may provide a suitable basis for comparing results obtained in different fluids.

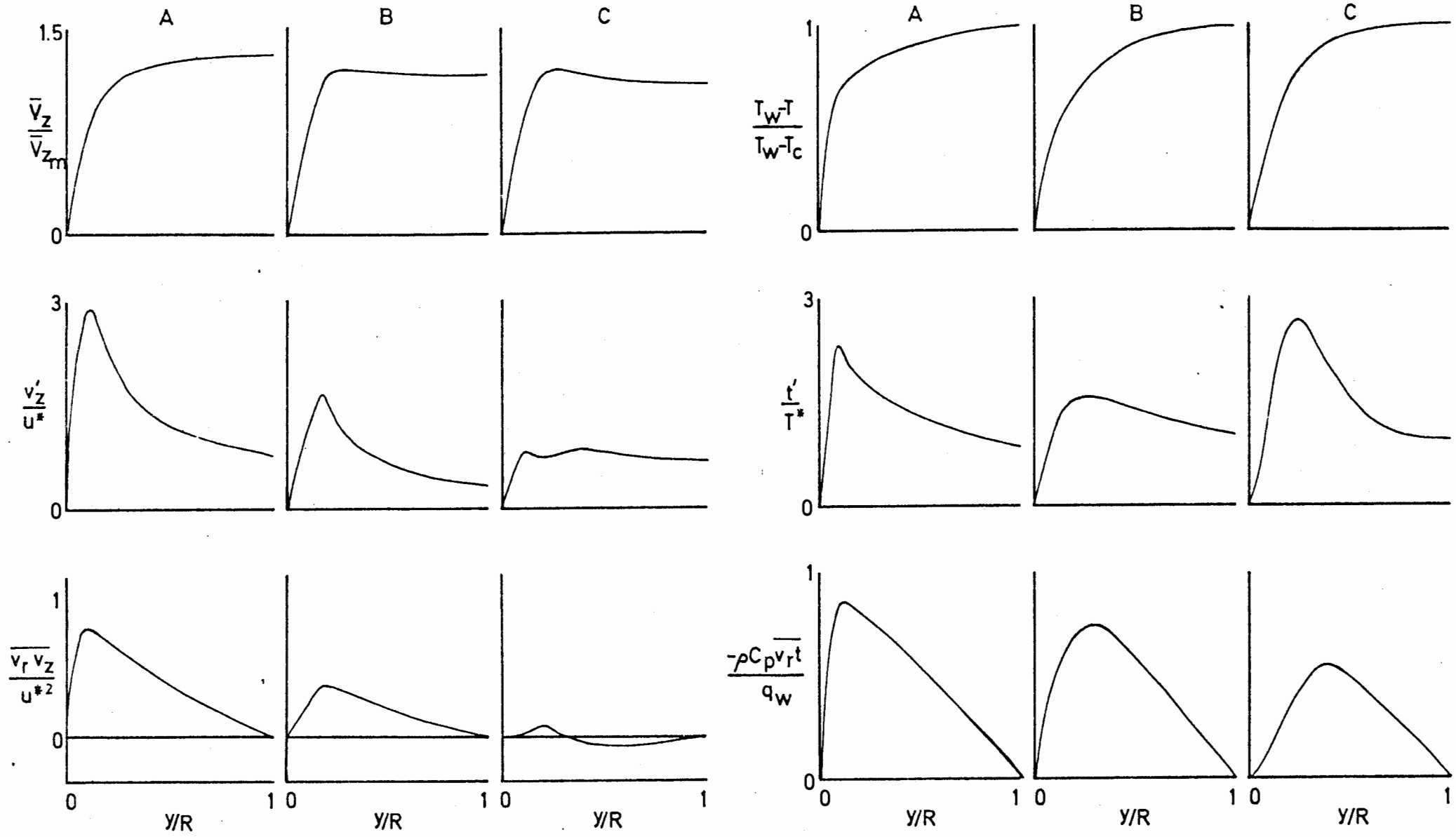

FIGURE 6.1 THE EFFECT OF INCREASING IMPORTANCE OF FREE CONVECTION ON VELOCITY, TEMPERATURE AND TURBULENCE VALUES

A : Low heat flux B : Moderate heat flux C : High heat flux

ii) At high heat fluxes a "saturation" condition is attained where, with additional increases in heat flux, very little change in the shape of the normalised fully developed profiles for $\overline{V}_z/\overline{V}_{z_m}$, $\frac{T_w-T}{T_w-T_c}$, $\frac{\overline{v_r v_z}}{u^{*2}}$ and $\frac{-\rho C_p \overline{v_r t}}{q_w}$ is observed. In air the attainment of this saturation condition occurs as $\overline{V}_z/\overline{V}_{z_m}$ at the pipe centre reaches a value of 1.07.

iii) Observations from the plot of Nu/Nu_T vs Ra/Re^2 shown in Fig. 5.21 indicate that whereas flow conditions are independent of L/D for flows where the point of maximum velocity has been displaced from the pipe centre, flows with the maximum velocity at the pipe centre are affected by inlet conditions at least as far as 100 diameters from the point where heating starts.

iv) With increasing heat flux there is a considerable decrease in the importance of turbulent heat and momentum transfer near the wall. This is particularly noticeable as the velocity profile becomes very flat just before the point of maximum velocity moves from the pipe centre; under these conditions the eddy diffusivities decrease practically to zero in the region $y/R < 0.2$.

v) Nusselt numbers are observed to be very sensitive to changes induced by buoyancy forces, particularly at low heat fluxes. At Reynolds numbers of 5000 and 8000 the same Nusselt number variations are observed, namely a rapid initial decrease with increasing heat flux followed by a gradual increase once the velocity maximum in the flow has moved from the pipe centre. The minimum Nusselt number value, as little as 0.4 to 0.5 of the pure forced convection Nusselt number, is found at the point where the velocity profile is very flat over much of the pipe and eddy diffusivities near the wall are lowest.

vi) In the calculation of hot-wire sensitivities it is shown that use of an assumption proposed by Hinze [40] yields errors of up to 30% in sensitivity values. A simple method for obviating these errors is proposed.

Recommendations for future work

For a better understanding of the mechanism of the changes occurring in flows with significant free convection effects, more measurements are needed of velocities, temperatures and turbulence quantities. These measurements should be concentrated in the Reynolds number range of the present work and also at lower Reynolds numbers, though here considerable difficulties may be experienced in developing accurate measuring techniques. At a given Reynolds number measurements should be concentrated

i) at higher heat fluxes than the highest used in the present work, in order to provide information on the permanence of the "saturation" condition observed in this work;

ii) at very low heat fluxes, in order to map out more clearly the initial changes which in many cases are significant even at very low heat fluxes. This will necessitate the development of very sensitive measuring techniques, especially for temperature measurement.

To clarify the importance of Prandtl number on these changes measurements similar to those taken in the present work should be made in other fluids.

Energy spectra and correlation coefficients should be obtained for both velocity and temperature fluctuations, in order to obtain details of eddy size and turbulent energy distribution. These results would be expected to make much clearer the changes in flow structure which occur under mixed convection conditions.

Direct measurements of the correlations $\overline{v_r t}$ and $\overline{v_r v_z}$ would confirm the results obtained by calculation in the present work. However, such measurements would be extremely difficult to make with any accuracy, particularly under conditions where $\overline{v_r v_z}$ values are small.

A full investigation of the way in which velocity and temperature profiles change with increasing L/D needs to be carried out. This should be repeated for a range of heat fluxes at different Reynolds numbers in order to determine whether the conclusions drawn from Fig. 5.21 are valid. Particularly at the lower

Reynolds numbers attention should be paid to obtaining very accurate measurements near the wall as this will enable local mixed convection friction factors to be determined and a mixed convection friction factor correlation to be developed.

NOMENCLATURE

a, a_1	Coefficients in thermal conductivity equation $k = a + a_1 T$ (T in ^{o}K)
A	Constant in King's Law equation
B	Constant in King's Law equation
c_1, c_2	Polynomial coefficients
C_p	Specific heat at constant pressure, Btu/lb ^{o}F
d	Hot-wire diameter, ft
D	Pipe diameter, ft
e	Fluctuating voltage across hot-wire, mV
f	Fanning friction factor
g	Acceleration due to gravity, ft/sec^2
g_c	Gravitational constant, 32.2 ft $lb_m/lb_f sec^2$
h	Heat transfer coefficient, Btu/hr ft^2 ^{o}F
I	Current flowing in hot-wire, mA
I_1, I_2, I_3	Integral terms from equation (A.20)
J	Mechanical equivalent of heat
k	Thermal conductivity, Btu/hr ft ^{o}F
K	Constant, R_w/R_g
ℓ	Length of hot-wire, ft
L	Distance along pipe axis from test-section inlet, ft
M	Time constant of hot-wire, μsec
n	Exponent in hot-wire calibration equations
P	Ratio defined by equation (2.27)
p	Pressure, lb/ft sec^2
p_s	Static pressure, lb_f/ft^2
q	Heat flux, Btu/hr ft^2
r	Distance measured along a radius from the pipe centre, ft
R	Radius of pipe, ft
r	(when subscripted) Fluctuating component of hot-wire resistance, ohms
R	(when subscripted) Resistance of hot-wire, ohms
s	Sensitivity of hot-wire to velocity fluctuations
s^*	Sensitivity of hot-wire to velocity fluctuations (after Hinze [40])
s_t	Sensitivity of hot-wire to temperature fluctuations
s_t^*	Sensitifity of hot-wire to temperature fluctuations (after Hinze [40])

t	Fluctuating component of temperature, ^{o}F
t^{+}	Dimensionless temperature, $(T_w-T)/T^*$
T	Temperature, ^{o}F (unless otherwise specified)
T^*	Normalising parameter, $q_w/\rho C_p u^*$ ^{o}F
U	Velocity, ft/sec
U_{ave}	Average velocity in throat of contracting cone, ft/sec
U_{max}	Velocity in central region of throat of contracting cone, ft/sec
u^{+}	Dimensionless velocity, $\bar{V}_z/u^*$
u^*	Friction velocity, $\bar{V}_{z_m}\sqrt{\frac{f}{2}}$ ft/sec
V	Velocity, ft/sec
v	Fluctuating velocity component, ft/sec
v'	Intensity of turbulent velocity fluctuations, $\sqrt{\overline{v^2}}$ ft/sec
w	Mass flow rate, lb/hr
x	Amplifier attenuation, db
X	Parameter in equation (2.31), s/s_t
y	Radial distance measured from wall, ft
y^{+}	Dimensionless distance, yu^*/ν
Y	Yantovskii number, Gr/Re^{*2}
	Parameter in equation (2.31)
z	Axial distance, ft
Z	Free convection criterion, $(16Ra/Re).(D/L)$
	Parameter in equation (2.32)

(An overscored symbol indicates that the quantity is averaged with respect to time)

α	Thermal diffusivity, $k/\rho C_p$, ft^2/hr
β	Temperature coefficient of resistance, $^{o}K^{-1}$
	Coefficient of thermal expansion at T_M, $^{o}F^{-1}$
γ	Second order coefficient in equation (C.16)
Δh	Pressure differential, in. of fluid
ε_H	Eddy diffusivity of heat, ft^2/hr
ε_M	Eddy diffusivity of momentum, ft^2/hr
η	Dimensionless radius, r/R
θ	Angular co-ordinate, radians

μ	Fluid viscosity, centipoise
ν	Kinematic viscosity, ft^2/hr
ρ	Density, lb/ft^3
τ	Shear stress, $lb_m/ft\ sec^2$
ϕ	Dimensionless temperature difference, $2k(T-T_b)/\rho_b \bar{V}_{z_m} C_p D^2 (dT/dz)$
ω	Frequency, Hz

Subscripts

av, b	Evaluated at bulk mean temperature, T_b
c	Evaluated at conditions at pipe centre
f	Evaluated at film temperature, $T_f = \frac{T_w + T_c}{2}$
g	Evaluated at local fluid temperature
M	Evaluated at radial average temperature, T_M
m	Value averaged over entire flow
O	Reference value
r	Value in radial direction
w	Evaluated at wire operating temperature
	Evaluated at pipe wall temperature
z	Value in axial direction
θ	Value in circumferential direction.

Dimensionless Groups

Gr	=	Grashof number, $D^3\rho^2 g\beta(T_w - T_c)/\mu^2$
Gz	=	Graetz number, WC_p/kL
Nu	=	Nusselt number, hD/k
Nu_v	=	Pure forced convection Nusselt number - laminar flow
Nu_T	=	Pure forced convection Nusselt number - turbulent flow
Pe	=	Peclet number, $D\bar{V}_{z_m} \rho C_p \mu/k$
Ra	=	Rayleigh number, $\rho^2 \beta g C_p D^4 (dT/dz)/16\mu k$
Re	=	Reynolds number, $D\bar{V}_{z_m} \rho/\mu$
Re*	=	Friction Reynolds number, $Re \sqrt{f/2}$

LIST OF REFERENCES.

1. Bhattacharyya, A., "Effect of buoyancy on forced convection heat transfer in vertical channels - a literature survey", Aktiebolaget Atomenergi, Sweden, Rept. AE-176 (1965).

2. Metais, B., "Criteria for mixed convection", Univ. of Minnesota Heat Transfer Lab. Rept. HTL TR No. 51 (1963).

3. Brown, C.K., and W. H. Gauvin, "Combined free-and-forced convection. Part I: Heat transfer in aiding flow", Can. J. chem. Engng, 43, 306-312 (1965).

4. Brown, C.K., and W.H. Gauvin, "Combined free-and-forced convection. Part II: Heat transfer in opposing flow", Can. J. chem. Engng, 43, 313-318 (1965).

5. Clark, J.A., and W.M. Rohsenow, "Local boiling heat transfer to water at low Reynolds numbers and high pressures", Trans. Am. Soc. mech. Engrs, 76, 553-562 (1954).

6. Eckert, E.R.G, A.J.Diaguila and A.N. Curren, "Experiments on mixed-free-and-forced-convective heat transfer connected with turbulent flow through a short tube", NACA Tech. Note 2974 (1953).

7. Kemeny, G.A., and E.V. Somers, "Combined free and forced convective flow in vertical circular tubes - experiments with water and oil", J. Heat Transfer, 84, 339-346 (1962).

8. Hallman, T.M., "Experimental study of combined forced and free laminar convection in a vertical tube", NASA Tech. Note D-1104 (1961).

9. Brown, W.G., "Die Überlagerung von erzwungener und natürlicher Konvektion bei niedrigen Durchsätzen in einem lotrechten Rohr", VDI ForschHft 480 (1960).

10. Hanratty, T.J., E.M. Rosen and R.L. Kabel, "Effect of heat transfer on flow field at low Reynolds numbers in vertical tubes", Ind. Engng Chem., 50, 815-820 (1958).

11. Scheele, G.F., and T.J. Hanratty, "Effect of natural convection on stability of flow in a vertical pipe", J. Fluid Mech., 14, 244-256 (1962).

12. Scheele, G.F., and H.L. Greene, "Laminar-turbulent transition for nonisothermal pipe flow", A.I.Ch.E.Jl, 12, 737-740 (1966).

13. Scheele, G.F., E.M. Rosen and T.J. Hanratty, "Effect of natural convection on transition to turbulence in vertical pipes", Can. J. chem. Engng, 38, 67-73 (1960).

14. Lawrence, W.T., and J.C. Chato, "Heat-transfer effects on the developing laminar flow inside vertical tubes", J. Heat Transfer, 88, 214-222 (1966).

15. Ostroumov, G.A. "Free convection under the conditions of the internal problem", NACA Tech. Translation TM 1407 (1958).

16. Hallman, T.M., "Combined forced and free-laminar heat transfer in vertical tubes with uniform internal heat generation", Trans. Am. Soc. mech. Engrs, 78, 1831-1841 (1956).

17. Greene, H.L., and G.F. Scheele, "Effect of fluid viscosity on combined free forced convection flow phenomena in vertical pipes", A.I.Ch.E.Jl, 16, 1039-1047 (1970).

18. Greene, H.L., "Effects of heat transfer on the flow of Newtonian and non-Newtonian fluids in a vertical pipe", Ph.D. Thesis, Cornell Univ. (1966).

19. Steiner, A., "On the reverse transition of a turbulent flow under the action of buoyancy forces", J. Fluid Mech., 47, 503-512 (1971).

20. Ber, L.E., "Towards a theory of thermogravitational convection under conditions of turbulent flow (in Russian)", Isvest. Akad. Nauk. SSSR, Otd. Tech. Nauk., 11, 75-83 (1957).

21. Ojalvo, M.S., and R.J. Grosh, "Combined forced and free turbulent convection in a vertical tube", Argonne National Laboratory Rept. ANL-6528 (1962).

22. Horsten, E.A., H.O. Buhr and A.D. Carr, "The prediction of non-isothermal turbulent velocity and temperature profiles in a vertical circular pipe", S. Afr. Chem. Process., 6, CP159-CP164 (1971).

23. Buhr, H.O., "Heat transfer to liquid metals, with observations on the effect of superimposed free convection in turbulent flow", Ph.D. Thesis, Univ. of Cape Town (1967).

24. Horsten, E.A., "Combined free and forced convection in turbulent flow of mercury", Ph.D. Thesis, Univ. of Cape Town (1971).

25. Colburn, A.P., "A method of correlating forced convection heat transfer data and a comparison with fluid friction", Trans. Am. Inst. chem. Engrs, 29, 174-210 (1933).

26. Martinelli, R.C., C.J. Southwell, G. Alves, H.L. Craig, E.B. Weinberg, N.F. Lansing and L.M.K. Boelter, "Heat transfer and pressure drop for a fluid flowing in the viscous region through a vertical pipe", Trans. Am. Inst. chem. Engrs, 38, 493-530 (1942).

27. Pigford, R.L., "Nonisothermal flow and heat transfer inside vertical tubes", Chem. Eng. Prog. Symp. Ser., 51, No. 17, 79-92 (1955).

28. Iqbal, M., B.D. Aggarwala and M.S. Rokerya, "Viscous dissipation effects on combined free and forced convection through vertical circular tubes", J. appl. Mech., 37, 931-935 (1970).

29. Mitsuishi, N., O. Miyatake and M. Yanagida, "Heat transfer of laminar flow in vertical tubes with constant wall heat flux", J. chem. Engng Japan, 1, 121-124 (1968).

30. Jackson, T.W., W. B. Harrison and W.C. Boteler, "Combined free and forced convection in a constant-temperature vertical tube", Trans. Am. Soc. mech. Engrs, 80, 739-743 (1958).

31. Petukhov, B.S., A.F. Polyakov and B.K. Strigin, "Heat transfer in tubes with viscous-gravity flow", Heat Transfer - Soviet Research, 1, 24-31 (1969).

32. Sherwin, K., "Combined convection of single phase turbulent flow within a vertical tube", Br. chem. Engng, 16, 367-368 (1971).

33. Eckert, E.R.G., and A.J. Diaguila, "Convective heat transfer for mixed, free and forced flow through tubes", Trans. Am. Soc. mech. Engrs, 76, 497-504 (1954).

34. Eckert, E.R.G., A.J. Diaguila and J.N. Livingood, "Free convection effects on heat transfer for turbulent flow through a vertical tube", NACA TN 3584 (1955).

35. Petukhov, B.S., and L.D. Nolde, "Gegenseitige Beeinflussung von freier und erzwungener Konvektion bei Rohrströmung", Teploenergetika, 6, 72-80 (1959); BWK 11, No. 12.5, 569-570 (1959).

36. Petukhov, B.S., and B.K. Strigin, "Experimental investigation of heat transfer with viscous-inertial-gravitational flow of a liquid in vertical tubes", High Temp., 6, 896-899 (1968).

37. Metais, B., and E.R.G. Eckert, "Forced, mixed and free convection regimes", J. Heat Transfer, 86, 295-296 (1964).

38. Sandborn, V.A., "Experimental evaluation of momentum terms in turbulent pipe flow", NACA TN 3266 (1955).

39. Patterson, G.K., W.J. Ewbank and V.A. Sandborn, "Radial pressure gradient in turbulent pipe flow", Physics Fluids, 10, 2082-2084 (1967).

40. Hinze, J.O., "Turbulence", McGraw-Hill, New York (1959).

41. Brodkey, R.S., "The Phenomena of Fluid Motions", Addison-Wesley, Reading, Mass. (1967).

42. Schneider, P.J., "Effect of axial fluid conduction on heat transfer in the entrance region of parallel plates and tubes", Trans. Am. Soc. mech. Engrs, 79, 765-773 (1957).

43. Bird, R.B., W. E. Stewart and E.N. Lightfoot, "Transport Phenomena", John Wiley, New York (1960).

59. Wasan, D.T., R. M. Davis and C.R. Wilke, "Measurements of the velocity of gases with variable fluid properties", A. I. Ch. E. Jl, 14, 227-234 (1968).

60. Champagne, F.H., C.A. Sleicher and O.H. Wehrmann, "Turbulence measurements with inclined hot-wires. Part 1. Heat transfer experiments with inclined hot wire", J. Fluid Mech., 28, 153-175 (1967).

61. Frenkiel, F.N., "Etude Statistique de la Turbulence", O.N.E.R.A., Paris, Rapport Technique No. 37 (1948).

62. Schubauer, G.B. and P.S. Klebanoff, "Theory and application of hot-wire instruments in the investigation of turbulent boundary layers", NACA ACR No. 5K27 (1946).

63. Laufer, J., "Investigation of turbulent flow in a two-dimensional channel", NACA Rept. No. 1053 (1951).

64. Betchov, R., "Theorie non-lineaire de l'anemometre à fil chaud", Proc. K. ned. Akad. Wet., 52, 195-207 (1949).

65. Lawn, C.J., "Turbulence measurements at B.N.L.", Central Electricity Generating Board Report RD/B/M 1277 (1969).

66. Verollet, E., "Contribution aux methodes de mesures de turbulence de vitesse et de temperature par l'anemometre a fil chaud", Doctoral Thesis, Univ. d'Aix-Marseille (1962).

67. Arya, S.P.S., and E.J. Plate, "Hot-wire measurements of turbulence in a thermally stratified flow", Colorado State Univ., Tech. Rept. CEM67-68SPSA-EJP11 (1968).

68. Morkovin, M.V., "Fluctuations and hot-wire anemometry in compressible flows", AGARDograph 24 (1956).

69. Kovasznay, L.S.G., "Turbulence in supersonic flow", J. Aeronaut. Sci., 20, 657 (1953).

70. Champagne, F.H., and C.A. Sleicher, "Turbulence measurements with inclined hot-wires. Part 2. Hot-wire response equations", J. Fluid Mech., 28, 177-182 (1967).

71. Guitton, D.E., "Correction of hot-wire data for high-intensity turbulence, longitudinal cooling and probe interference", McGill Univ., Mech. Engng. Res. Lab. Rept. No. 68-6 (1968).

72. Van der Hegge Zijnen, B.G., "On the construction of hot-wire anemometers for investigation of turbulence", Appl. scient. Res., 2A, 351-363 (1951).

73. Weinberg, B.C., and S. Lederman, "Constant current anemometer diagnostics of flow fields", Polytechnic Institute of Brooklyn, PIBAL Rept. No. 69-13 (1969).

74. Van Thinh, N., "Sur la mesure de la vitesse dans un écoulement turbulent par anemometrie à fil chaud, au voisinage d'une paroi lisse", C.r.hebd. Seanc. Acad. Sci., Paris, 264A, 1150-1152 (1967).

75. Bradshaw, P., "Thermal methods of flow measurement", J. of Phys. E : Sci. Instr., 1, 504-509 (1968).

76. Florent, P., and G. Thiolet, "Importance de l'orientation du support de sonde a fil chaud par rapport a une paroi sur la determination des vitesses moyennes dans une couche limite turbulente", C.r.hebd. Seanc. Acad. Sci., Paris, 269A, 405-408 (1969).

77. Gilmore, D.C., "The probe interference effect of hot-wire anemometers", McGill Univ., Mech. Eng. Research Labs. Report TN 67-3 (1967).

78. Hoole, B.J., and J.R. Calvert, "The use of a hot-wire anemometer in turbulent flow", Jl R. aeronaut. Soc., 71, 511-513 (1967).

79. Tritton, D.J., "Note on the effect of a nearby obstacle on turbulence intensity in a boundary layer", J. Fluid Mech., 28, 433-437 (1967).

80. Dahm, M., and C.G. Rasmussen, "Effect of wire mounting system on hot-wire probe characteristics", DISA Information, No. 7, 19-24 (1969).

81. Eyre, D., "End conduction and angle of incidence effects in single hot-wire anemometer probes", U.K. Atomic Energy Authority TRG Rept. 1521 (W) (1967).

82. Maye, J.P., "Sur les mesures par thermometrie a resistance au voisinage d'une paroi en ecoulement turbulent", C.r.hebd. Seanc. Acad. Sci., Paris, 272A, 441-444 (1971).

83. Wills, J.A.B., "The correlation of hot-wire readings for proximity to a solid boundary", J. Fluid Mech., 12, 388-396 (1962).

84. Piercy, N.A.V., E.G. Richardson and H.F. Winny, "On the convection of heat from a wire moving through air close to a cooling surface", Proc. phys. Soc., 69, 731-742 (1956).

85. Hoagland, L.C., Doctoral Thesis, M.I.T. (1960).

86. Coantic, M., "Contribution a l'etude theorique et experimentale de l'ecoulement turbulent dans une tube circulaire", Doctoral Thesis, Univ. d'Aix-Marseille (1959).

87. Almquist, P., and E. Legath, "The hot-wire anemometer at low air velocities", DISA Information, No. 2, 3-4 (1965).

88. Cooper, R.D., and M.P. Tulin, "Turbulence measurements with the hot-wire anemometer", AGARDograph 12 (1955).

89. Coantic, M., "Evolution, en fonction du nombre de Reynolds, de la distribution des vitesses moyennes et turbulentes dans une conduite", C.r.hebd. Seanc. Acad. Sci., Paris, 264A, 849-852 (1967).

90. Rasmussen, C.G., "Measurement of turbulence characteristics", DISA Information, No. 3, 9-20 (1966).

91. Brown, P.M.M., "Temperature, velocity and turbulence measurements in air with a hot-wire anemometer", M.Sc. Thesis, Univ. of Cape Town (1968).

92. Sleicher, C.A., "Heat transfer in a pipe with turbulent flow and arbitrary wall-temperature distribution", Ph.D. Thesis, Univ. of Michigan (1956).

93. British Standard 1042 : "Flow measurement. Part 3" (1965).

94. Wichner, R.P., "Determination of the Reynolds stresses for air and water pipe flows by the constant current, linearised response hot-wire anemometer", Ph.D. Thesis, Univ. of Tennessee (1965).

95. British Standard 1828 : "Reference tables for thermocouples (iron v. constantan)" (1962).

96. Jones, T.P., "Reference tables for thermocouples", C.S.I.R.O., Australia, Natl. Standards Lab. Tech. Paper No. 26 (1969).

97. Ross, D., "A new analysis of Nikuradse's experiments on turbulent flow in smooth pipes", Proc. of Third Midwest Conf. on Fluid Mech., 651-667 (1953).

98. Davies, P.O.A.L., and M. J. Fisher, "Heat transfer from electrically heated cylinders", Proc. R. Roc., 280A, 486-527 (1964).

99. Kung, R.J., and G.J. Binder, "Ultra low speed anemometry", Colorado State Univ. Rept. CER66-67 RJK 49 (1967).

100. Tanney, J.W., "An anemometer for very low velocities", Natl. Research Council of Canada, Aeronautical Report LR-472 (1967).

101. DISA Information, No. 7, 32-35 (1969).

102. Smith, R.H., and C. Wang, "Contracting cones giving uniform throat speeds", J. Aeronaut. Sci., 11, 356-360 (1944).

103 Christiansen, S.E., "The development of air velocity profiles in a vertical tube with a diverging conical inlet", M.Sc. Thesis, Univ. of Alberta (1965).

104. Abbrecht, P.H., and S.W. Churchill, "The thermal entrance region in fully developed turbulent flow", A.I.Ch. E. Jl, 6, 268-273 (1960).

105. Kestin, J., and P.D. Richardson, "Heat transfer across turbulent incompressible boundary layers", Int. J. Heat Mass Transfer, 6, 147-189 (1963).

106. Rein, P.W., "The turbulent velocity distribution, with particular reference to measurements in mercury", M.Sc. Thesis, Univ. of Cape Town (1967).

107. Prandtl, L, "Eine Beziehung zwischen Wärmeaustauch und Strömungswiderstand der Flüssigkeiten", Phys. Z., 11, 1072-1078 (1910).

108. Taylor, G.I., "Eddy motion in the atmosphere", Phil. Trans. R. Soc., 215A, 1-26 (1915).

109. Von Karman, T., "The analogy between fluid friction and heat transfer", Trans. Am. Soc. mech. Engrs, 61, 705-710 (1939).

110. Von Karman, T., "Turbulence and skin friction", J. Aeronaut. Sci., 1, 1-20 (1934).

111. Ruth, B.F., and H.H. Yang, "An empirical correlation for velocity distribution of turbulent fluid flow", A.I.Ch. E. Jl, 3, 117-120 (1957).

112. Laufer, J., "The structure of turbulence in fully developed pipe flow", NACA Rept. 1174 (1954).

113. Millikan, C.B., "A critical discussion of turbulent flow in channels and circular tubes", Proc. Fifth Intern. Congress for Applied Mechanics, Cambridge, Mass. 386-392 (1938).

114. Bogue, D.C., and A.B. Metzner, "Velocity profiles in turbulent pipe flow", Ind. Engng Chem. Fundamentals, 2, 143-149 (1963).

115. Nikuradse, J., "Gesetzmässigkeiten der turbulenten Strömung in glatten Rohren, Ver. dt. Ing. Forschungsheft 356 (1932). Translated as "Laws of turbulent flow in smooth pipes", NASA TT F-10, 359 (1966).

116. Deissler, R.G., "Analytical and experimental investigation of adiabatic turbulent flow in smooth tubes", NACA TN 2138 (1950).

117. Senecal, V.E., "Characteristics of transition flow in smooth tubes", Doctoral Thesis, Carnegie Inst. of Technology (1951).

118. Beckwith, W.F., and R. Fahien, "Determination of turbulent thermal diffusivities for flow of liquids in pipes", Iowa State Univ.,Ames Laboratory, R & D Report IS-734 (1963).

119. Lindgren, E.R., "Experimental study on turbulence pipe flows of distilled water", Oklahoma State Univ., School of Civil Engineering Tech. Rept. No. 2 (1965).

120. Bakewell, H.P., "An experimental investigation of the viscous sublayer in turbulent pipe flow", Defence Documentation Centre Report AD 639804 (1966).

121. Genin, L.G., V.G. Zhilin and B.S. Petukhov, "Experimental investigation of turbulent flow of mercury in a circular tube in a longitudinal magnetic field", High Temp., 5, 266-271 (1967).

122. Gardner, R.A., "Magnetic-fluid-mechanic pipe flow in a transverse magnetic field with heat transfer", Ph.D. Thesis, Purdue Univ. (1969).

123. Kudva, A.K., "Structure of turbulent velocity and temperature fields in ethylene glycol flowing in a pipe at low Reynolds number", Ph.D. Thesis, Purdue Univ. (1970).

124. Van Driest, E.R., "On turbulent flow near a wall", J. Aeronaut. Sci., 23, 1007-1036 (1956).

125. Spalding, D.B., "A single formula for the law of the wall", J. appl. Mech., 28, 455-457 (1961).

126. Gill, W.N. and M. Scher, "A modification of the momentum transport hypothesis", A.I.Ch. E. Jl, 7, 61-63 (1961).

127. Wasan, D.T., T.K.Subramaniam and S.S. Randhava, "Estimation of eddy diffusion coefficients", Chem. Engng, Albany, 73, 165-168 (1966).

128. Reichardt, H., "Die Grundlagen des Turbulenten Wärmeüberganges", Arch. ges. Wärmetechnik, 2, 129-142 (1951). Translated as "The principles of turbulent heat transfer", NACA TM 1408 (1957).

129. Reynolds, H.C., D.M. McEligot and M.E. Davenport, "Velocity profiles and eddy diffusivities for fully developed turbulent, low Reynolds number pipe flow", Paper presented at A.S.M.E. Winter Annual Meeting and Energy Systems Exposition, New York, N.Y. Dec 1 - 5 1968. Paper 68-WA/FE-34.

130. Travis, J.R., H.O. Buhr and A. Sesonske, "A model for velocity and eddy diffusivity distributions in fully turbulent pipe flow", Can. J. chem Engng, 49, 14-18 (1971).

131. McCabe, W.L., and J.C. Smith, "Unit operations of chemical engineering", McGraw-Hill, New York (1956).

132. Johnk, R.E., "Development of temperature profile for turbulent heat exchange in a pipe", Ph.D. Thesis, Univ. of Illinois (1961).

133. Boelter, L.M.K., R.C. Martinelli and F. Jonassen, "Remarks on the analogy between heat transfer and momentum transfer", Trans. Am. Soc. mech. Engrs, 63, 447-455 (1941).

134. Brookshire, W.A., "The structure of turbulent shear flow in pipes", Ph.D. Thesis, Louisiana State Univ. (1961).

135. Koo, J.K., "The measurement of diffusivity and turbulence in fully developed pipe flow", M. Eng. Thesis, McMaster Univ. (1967).

136. Sherwood, T.K., K.A. Smith and P.E. Fowles, "The velocity and eddy viscosity distribution in the wall region of turbulent pipe flow", Chem. Engng Sci., 23, 1225-1236 (1968).

137. Corcoran, W.H., and B.H. Sage, "Role of eddy conductivity in thermal transport", A.I.Ch. E. Jl, 2, 251-258 (1956).

138. Patel, V.C., and M.R. Head, "Some observations on skin friction and velocity profiles in fully developed pipe and channel flows", J. Fluid Mech., 38, 181-201 (1969).

139. Robertson, J.M., "The turbulent velocity distribution in rough pipe", Proc. of Fifth Midwest Conf. on Fluid Mech., 67-84 (1957).

140. Hall, A.A., "Measurement of intensity and scale of turbulence", A.R.C. Tech. Rep., R & M 1842 (1938).

141. Gessner, F.B., "A method of measuring Reynolds stresses with a constant-current, hot-wire anemometer", A.S.M.E. Rept. 64-WA/FE-34 (1964).

142. Bremhorst, K., and K.J. Bullock, "Spectral measurements of temperature and longitudinal velocity fluctuations in fully developed pipe flow", Int. J. Heat Mass Transfer, 13, 1313-1329 (1970).

143. Ibragimov, M., V.I. Subbotin and G.S. Taranov, "Velocity and temperature fluctuations and their correlation for the case of turbulent air flow in a tube" (In Russian), Inzhenerno-Fizicheskii Zhurnal, 19, 1060-1069 (1970).

144. Tanimoto, S., and T.J. Hanratty, "Fluid temperature fluctuations accompanying turbulent heat transfer in a pipe", Chem. Engng Sci., 18, 307-311 (1963).

145. Hochreiter, L.E., "Turbulent structure of isothermal and non-isothermal liquid metal pipe flow", Ph.D. Thesis, Purdue Univ. (1971).

146. Page, F., W. H. Schlinger, D.K. Breaux and B.H. Sage, "Point values of eddy conductivity and viscosity in uniform flow between parallel plates", Ind. Engng Chem., 44, 424-430 (1952).

147. Sesonske, A., S.L. Schrock and E.H. Buyco, "Eddy diffusivity ratios for mercury flowing in a tube", A.I.Ch. E. Preprint No. 25, Sixth National Heat Transfer Conf., Boston (1963).

148. Taylor, M.F., "A method of correlating local and average friction coefficients for both laminar and turbulent flow of gases through a smooth tube with surface to fluid bulk temperature ratios from 0.35 to 7.35", Int. J. Heat Mass Transfer, 10, 1123-1128 (1967).

149. Deissler, R.G., and C.S. Eian, "Analytical and experimental investigation of fully developed turbulent flow of air in smooth tubes with heat transfer, with variable fluid properties", NACA TN 2629 (1952).

150. Stanton, T.E., "The mechanical viscosity of fluids", Proc. R. Soc., A85, 366-376 (1911).

151. Louw, R.A., Unpublished data, Univ. of Cape Town (1971).

152. Bankston, C.A., "The transition from turbulent to laminar gas flows in a heated pipe", Paper presented at ASME-AIChE Heat Transfer Conference, Minneapolis, Minn. Aug. 3-6 (1969).

153. Yantovskii, E.I., "An estimate of the influence of free convection upon turbulent flow", Societ Phys. - Tech. Phys., 4, 1280-1282 (1960).

154. Nunner, W., "Wärmeübergang und Druckabfall in rauhen Rohren", VDI ForschHft. 455 (1956).

155. Corino, E.R., and R.S. Brodkey, "A visual investigation of the wall region in turbulent flow", J. Fluid Mech., 37, 1-30 (1969).

156. Barnes, J.F., "An experimental investigation of heat transfer from the inside surface of a hot smooth tube to air, helium and carbon dioxide", A.R.C. Reports and Memoranda No. 3246 (1960).

157. Depew, C.A., "Heat transfer to air in a circular tube having uniform heat flux", J. Heat Transfer, 84, 186-187 (1962).

158. Mills, A.F., "Experimental investigation of turbulent heat transfer in the entrance region of a circular conduit", J. Mech. Engng Sci., 4, 63-77 (1962).

159. McEligot, D.M., L.W. Ormand and H.C. Perkins, "Internal low Reynolds-number turbulent and transitional gas flow with heat transfer", J. Heat Transfer, 88, 239-245 (1966).

160. Friend, W.L., and A.B. Metzner, "Turbulent heat transfer inside tubes and the analogy among heat, mass and momentum transfer", A.I.Ch.E.Jl, 4, 393-402 (1958).

161. Sparrow, E.M., T.M. Hallman and R. Siegel, "Turbulent heat transfer in the thermal entrance region of a pipe with uniform heat flux", Appl. scient. Res., A7, 37-52 (1957).

162. Haberstroh, R.D., and L.V. Baldwin, "Application of a simplified velocity profile to the prediction of pipe-flow heat transfer", J. Heat Transfer, 90, 191-200 (1968).

163. Lafay, J., "Mesure du coefficient de frottement avec transfert de chaleur en convection forcee dans un canal circulaire", Commissariat a L'Energie Atomique, Report CEA-R-3896 (1970).

164. Costa, J., "Le coefficient de frottement dans un ecoulement turbulent en simple phase avec transfert de chaleur", Centre d'Etudes Nucleaires de Grenoble, Service des Transferts Thermiques, Bibliographie CEA-BIB-170 (1969).

165. Hinze, J.O., "Turbulent flow regions with shear stress and mean velocity gradient of opposite sign", Appl. scient. Res., 22, 163-175 (1970).

166. Eskinazi, S., and F.F. Erian, "Energy reversal in turbulent flows", Physics Fluids, 12, 1988-1998 (1969).

167. Truchasson, C., "Mesures de temperatures dans la "sous-couche laminaire" d'un ecoulement d'eau", Chem. Engng Sci., 19, 305-317 (1964).

APPENDICES

APPENDIX A

DERIVATION OF THE EQUATIONS OF CONTINUITY, MOTION AND ENERGY FOR TURBULENT UPFLOW OF AIR IN A VERTICAL PIPE.

A.1 ASSUMPTIONS AND SPECIFICATIONS.

The derivations of the equations of continuity, motion and energy are based on the following assumptions and specifications:-

i) The positive z direction is vertically upwards, i.e. in the mean flow direction.

ii) Heat flux at the wall is uniform.

iii) Static pressure is constant over any given horizontal cross-section. (Sandborn [38] and Patterson et al [39] have shown that a slight variation of pressure does in fact occur, but the changes are small enough to be neglected.)

iv) The flow region under consideration is far enough from the pipe entrance for entrance effects to be negligible. This means that, for the condition of uniform heat flux:

a) Changes in the axial direction of the normalised velocity, temperature and turbulence profiles will be very slight provided the axial temperature gradient is small. (For laminar flow it is known [10] that, under conditions where all physical properties except density are constant and where density varies linearly with temperature, normalised profiles can be obtained which are independent of axial position: for turbulent flow under the same conditions normalised profiles invariant in the axial direction should also be obtainable, provided that the $\overline{v_r v_z}$ distribution also reaches a steady value. In practice physical properties, and in particular viscosity, are not independent of temperature, but their effect on the normalised profiles is slight, however, provided the axial temperature gradient is small - this requirement was satisfied in the present experiments where the dT/dz values were generally less than $2^{\circ}F/ft$.)

b) dT/dz is constant and independent of both axial and radial position.

v) Physical properties are not constant but vary with temperature according to the relationships given in Appendix B. The effect of varying temperature on density is allowed for by employing the expansion

$$\rho = \rho_M[1-\beta(T-T_M)]$$

$$\text{(where } T_M = \int_0^{\eta} \overline{T}\eta d\eta\text{).}$$

which is accurate to $\pm\frac{1}{2}\%$ over the temperature range of interest.

vi) The variables V_r, V_θ, V_z, T, p and ρ can be expressed as the sum of a mean and a fluctuating quantity, e.g.

$$V_r = \overline{V}_r + v_r$$

The laws relating to the time-averaging of products of mean and fluctuating quantities are described in standard texts [40, 41].

vii) As a consequence of iv) $\overline{V}_r$ and $\overline{V}_\theta$ are zero. Further, because of axial symmetry there is no variation of time-averaged values in the circumferential direction, i.e. all $\frac{\partial}{\partial\theta}$ terms are zero.

viii) Turbulent interaction terms involving the fluctuating components of physical properties other than density are small enough to be neglected.

ix) Air behaves as an ideal gas over the temperature range concerned.

x) Viscous dissipation and axial heat conduction can be neglected. (The latter has been shown by Schneider [42] to be significant only for much lower Peclet numbers than are found in turbulent air flows.)

A.2 THE EQUATION OF CONTINUITY.

The general form of the continuity equation [43]

$$\frac{\partial\rho}{\partial t} + \underline{\nabla}\cdot\rho\underline{V} = 0 \qquad (A.1)$$

becomes, in cylindrical co-ordinates,

$$\frac{\partial\rho}{\partial t} + \frac{1}{r}\frac{\partial}{\partial r}(\rho r V_r) + \frac{1}{r}\frac{\partial}{\partial\theta}(\rho V_\theta) + \frac{\partial}{\partial z}(\rho V_z) = 0 \qquad (A.2)$$

Substitution of the expanded forms of the density and velocities as given in assumptions v) and vi) gives

$$\frac{\partial}{\partial t}(\rho_M[1-(\overline{T}+t-T_M)]) + \frac{1}{r}\frac{\partial}{\partial r}r(\rho_M[1-\beta(\overline{T}+t-T_M)])(\overline{V}_r+v_r)$$
$$+ \frac{1}{r}\frac{\partial}{\partial\theta}(\rho_M[1-\beta(\overline{T}+t-T_M)])(\overline{V}_\theta+v_\theta) + \frac{\partial}{\partial z}(\rho_M[1-\beta(\overline{T}+t-T_M)])(\overline{V}_z+v_z)$$
$$= 0 \qquad (A.3)$$

and on multiplying out, time-averaging and applying assumptions vi) and vii) this simplifies to

$$\frac{1}{r}\frac{\partial}{\partial r}r(-\rho_M\beta\overline{v_r t}) + \frac{\partial}{\partial z}\left\{\rho_M\overline{V}_z - \rho_M\overline{V}_z\beta(\overline{T}-T_M) - \rho_M\beta\overline{v_z t}\right\} = 0 \qquad (A.4)$$

or for convenience, the terms $\rho_M\overline{V}_z$ and $\rho_M\overline{V}_z\beta(\overline{T}-T_M)$

may be recombined to give

$$\frac{1}{r}\frac{\partial}{\partial r}r(-\rho_M\beta\overline{v_r t}) + \frac{\partial}{\partial z}\left\{\rho\bar{V}_z - \rho_M\beta\overline{v_z t}\right\} = 0 \qquad (A.5)$$

which is the continuity equation for nonisothermal turbulent flow.

This equation differs from the usual form of the continuity equation

$$\frac{\partial}{\partial z}(\rho\bar{V}_z) = 0 \qquad (A.6)$$

by including two velocity-temperature correlation terms; however, especially at low heat fluxes, equation (A.6) must be very nearly true and therefore, whatever their individual values, the sum of the two correlation terms is expected to be small.

A.3 THE EQUATION OF MOTION

A.3.1 Derivation of time-averaged equation

The standard tensor form of this equation [43],

$$\frac{\partial}{\partial t}\rho\underline{V} = -[\underline{\nabla}\cdot\rho\underline{V}\,\underline{V}] - \underline{\nabla}p - [\underline{\nabla}\cdot\tau] + \rho g \qquad (A.7)$$

where τ is the stress tensor, gives for the z direction, using cylindrical co-ordinates,

$$\frac{\partial}{\partial t}\rho V_z = -\frac{1}{r}\frac{\partial}{\partial r}r\rho V_r V_z - \frac{1}{r}\frac{\partial}{\partial\theta}\rho V_\theta V_z - \frac{\partial}{\partial z}\rho V_z V_z - \frac{dp}{dz} + \rho g_z$$
$$- \frac{1}{r}\frac{\partial}{\partial r}r\tau_{rz} - \frac{1}{r}\frac{\partial}{\partial\theta}\tau_{\theta z} - \frac{\partial}{\partial z}\tau_{zz} \qquad (A.8)$$

Substituting for the components of the stress tensor the relationships [43]:

$$\tau_{rz} = -\mu\left[\frac{\partial V_z}{\partial r} + \frac{\partial V_r}{\partial z}\right] \qquad (A.9a)$$

$$\tau_{\theta z} = -\mu\left[\frac{\partial V_\theta}{\partial z} + \frac{\partial V_z}{\partial\theta}\right] \qquad (A.9b)$$

$$\tau_{zz} = -\mu\left[2\frac{\partial V_z}{\partial z} - \frac{2}{3}(\underline{\nabla}\cdot\underline{V})\right]$$

$$= -\mu\left[2\frac{\partial V_z}{\partial z} - \frac{2}{3}\left\{\frac{1}{r}\frac{\partial}{\partial r}rV_r + \frac{1}{r}\frac{\partial V_\theta}{\partial\theta} + \frac{\partial V_z}{\partial z}\right\}\right]$$

$$= -\mu\left[\frac{4}{3}\frac{\partial V_z}{\partial z} - \frac{2}{3}\left\{\frac{1}{r}\frac{\partial}{\partial r}rV_r + \frac{1}{r}\frac{\partial V_\theta}{\partial\theta}\right\}\right] \qquad (A.9c)$$

equation (A.8) becomes

$$\frac{\partial}{\partial t}\rho V_z = -\frac{1}{r}\frac{\partial}{\partial r}r\rho V_r V_z - \frac{1}{r}\frac{\partial}{\partial \theta}\rho V_\theta V_z - \frac{\partial}{\partial z}\rho V_z V_z - \frac{dp}{dz} + \rho g_z$$
$$- \frac{1}{r}\frac{\partial}{\partial r}r\left(-\mu\left[\frac{\partial V_z}{\partial r} + \frac{\partial V_r}{\partial z}\right]\right) - \frac{1}{r}\frac{\partial}{\partial \theta}\left(-\mu\left[\frac{\partial V_\theta}{\partial z} + \frac{1}{r}\frac{\partial V_z}{\partial \theta}\right]\right)$$
$$- \frac{\partial}{\partial z}\left(-\mu\left[\frac{4}{3}\frac{\partial V_z}{\partial z} - \frac{2}{3}\left\{\frac{1}{r}\frac{\partial}{\partial r}rV_r + \frac{1}{r}\frac{\partial V_\theta}{\partial \theta}\right\}\right]\right) \qquad (A.10)$$

Then, introducing the expanded forms of the density and velocities as given in assumptions v) and vi), this becomes

$$\frac{\partial}{\partial t}\rho_M\,[1-\beta(\bar{T}+t-T_M)](\bar{V}_z+v_z) =$$
$$- \frac{1}{r}\frac{\partial}{\partial r}r\rho_M\,[1-\beta(\bar{T}+t-T_M)](\bar{V}_r+v_r)(\bar{V}_z+v_z)$$
$$- \frac{1}{r}\frac{\partial}{\partial \theta}\rho_M\,[1-\beta(\bar{T}+t-T_M)](\bar{V}_\theta+v_\theta)(\bar{V}_z+v_z)$$
$$- \frac{\partial}{\partial z}\rho_M\,[1-\beta(\bar{T}+t-T_M)]\,(\bar{V}_z+v_z)^2$$
$$- \frac{d}{dz}(\bar{p}+p) + g_z\rho_M\,[1-\beta(\bar{T}+t-T_M)]$$
$$- \frac{1}{r}\frac{\partial}{\partial r}r\left(-\mu\left[\frac{\partial}{\partial r}(\bar{V}_z+v_z) + \frac{\partial}{\partial z}(\bar{V}_r+v_r)\right]\right)$$
$$- \frac{1}{r}\frac{\partial}{\partial \theta}\left(-\mu\left[\frac{\partial}{\partial z}(\bar{V}_\theta+v_\theta) + \frac{1}{r}\frac{\partial}{\partial \theta}(\bar{V}_z+v_z)\right]\right)$$
$$- \frac{\partial}{\partial z}\left(-\mu\left[\frac{4}{3}\frac{\partial}{\partial z}(\bar{V}_z+v_z) - \frac{2}{3}\left\{\frac{1}{r}\frac{\partial}{\partial r}r(\bar{V}_r+v_r) + \frac{1}{r}\frac{\partial}{\partial \theta}(\bar{V}_\theta+v_\theta)\right\}\right]\right) \qquad (A.11)$$

Multiplying out, time-averaging, writing g_z as -g and applying assumptions vi) and vii) gives

$$- \frac{1}{r}\frac{\partial}{\partial r}r\left\{\rho\overline{v_r v_z} - \rho_M\beta\bar{V}_z\overline{v_r t} - \rho_M\beta\overline{v_r v_z t}\right\}$$
$$- \frac{\partial}{\partial z}\left\{\rho\bar{V}_z^2 + \rho\overline{v_z^2} - 2\bar{V}_z\rho_M\beta\overline{v_z t} - \rho_M\beta\overline{v_z^2 t}\right\} - \frac{d\bar{p}}{dz} - \rho_M g$$
$$+ \rho_M g\beta(\bar{T}-T_M) - \frac{1}{r}\frac{\partial}{\partial r}r\left(-\mu\frac{\partial\bar{V}_z}{\partial r}\right) - \frac{\partial}{\partial z}\left(-\frac{4}{3}\mu\frac{\partial\bar{V}_z}{\partial z}\right) = 0 \qquad (A.12)$$

A.3.2 Omission of small terms

At this point in the derivation it is desirable to introduce the following simplifications and assumptions by which certain terms can be shown to be small enough to be omitted:-

a) Far from the pipe entrance, by assumption iv), $\overline{v_z^2}/\overline{V}_z^2$ can be taken as constant, i.e.

$$\overline{v_z^2}(r,z) = C(r)\overline{V}_z^2(r,z)$$

It follows, therefore, that

$$\rho(r,z)\overline{v_z^2}(r,z) = C(r)\rho(r,z)\overline{V}_z^2(r,z)$$

$$\text{and } \frac{\partial}{\partial z}\rho(r,z)\overline{v_z^2}(r,z) = C(r)\frac{\partial}{\partial z}\rho(r,z)\overline{V}_z^2(r,z)$$

Since present measurements give C(r) a value of approximately 0.01, $\frac{\partial}{\partial z}\rho\overline{v^2}$ can therefore be neglected in comparison with $\frac{\partial}{\partial z}\rho\overline{V}_z^2$

b) Since no values are available for the two triple correlation terms in equation (A.12) these terms are therefore dropped from the equation. The reasons for believing the error thus introduced to be small are explained below:-

Since the relative turbulence intensities are generally less than 0.2, the triple correlations are an order of magnitude smaller than any double correlations present. The magnitude of these two terms is further reduced because they are both multiplied by β, the reciprocal of the absolute temperature, which is also small. It is expected therefore that, far from the pipe entrance where changes in velocity and temperature are slight and gradual, differential terms containing these triple correlations will be correspondingly small and can safely be neglected.

c) From assumption iv) $\frac{\partial \overline{V}_z}{\partial z}$ is expected to be small and practically constant

The term $-\frac{\partial}{\partial z}\left(-\frac{4}{3}\mu\frac{\partial \overline{V}_z}{\partial z}\right)$ can therefore be neglected.

A.3.3 The axial derivative terms: $-\frac{\partial}{\partial z}(\rho\overline{V}_z^2)$ and $-\frac{\partial}{\partial z}(-2\overline{V}_z\rho_M\beta\overline{v_z t})$

At this stage, apart from the term $\frac{d\overline{p}}{dz}$ which is discussed in section A.3.5, the only remaining terms containing axial derivatives are $-\frac{\partial}{\partial z}(\rho\overline{V}_z^2)$ and $-\frac{\partial}{\partial z}(-2\overline{V}_z\rho_M\beta\overline{v_z t})$. Because experimental measurements were taken at only one axial position these terms cannot be evaluated as they stand and are therefore rewritten, together with the term $-\frac{1}{r}\frac{\partial}{\partial r}r(-\rho_M\beta\overline{V}_z\overline{v_r t})$, as follows:

$$-\frac{\overline{V}_z}{r}\frac{\partial}{\partial r}r(-\rho_M\beta\overline{v_r t}) + \rho_M\beta\overline{v_r t}\frac{\partial\overline{V}_z}{\partial r} - \overline{V}_z\frac{\partial}{\partial z}(\rho\overline{V}_z)$$
$$-\rho\overline{V}_z\frac{\partial\overline{V}_z}{\partial z} + 2\overline{V}_z\frac{\partial}{\partial z}\rho_M\beta\overline{v_z t} + 2\rho_M\beta\overline{v_z t}\frac{\partial\overline{V}_z}{\partial z} \qquad (A.13)$$

or, rearranging, as

$$\overline{V}_z\left[-\frac{1}{r}\frac{\partial}{\partial r}r(-\rho_M\beta\overline{v_r t}) - \frac{\partial}{\partial z}\rho\overline{V}_z + \frac{\partial}{\partial z}\rho_M\beta\overline{v_z t}\right]$$
$$+\rho_M\beta\overline{v_r t}\frac{\partial\overline{V}_z}{\partial r} - \rho\overline{V}_z\frac{\partial\overline{V}_z}{\partial z} + \overline{V}_z\frac{\partial}{\partial z}\rho_M\beta\overline{v_z t} + 2\rho_M\beta\overline{v_z t}\frac{\partial\overline{V}_z}{\partial z} \qquad (A.14)$$

From the continuity equation the sum of the first three terms is zero. Also, present measurements have shown that $\overline{v_z t} \ll \overline{V}_z$ and therefore the term $2\rho_M\beta\overline{v_z t}\frac{\partial\overline{V}_z}{\partial z}$ can be neglected in comparison with $-\rho\overline{V}_z\frac{\partial\overline{V}_z}{\partial z}$.

Expression (A.14) then becomes

$$\rho_M\beta\overline{v_r t}\frac{\partial\overline{V}_z}{\partial r} - \rho\overline{V}_z\frac{\partial\overline{V}_z}{\partial z} + \overline{V}_z\frac{\partial}{\partial z}\rho_M\beta\overline{v_z t} \qquad (A.15)$$

which, on substituting for $\frac{\partial}{\partial z}\rho_M\beta\overline{v_z t}$ from equation (A.5) gives

$$\rho_M\beta\overline{v_r t}\frac{\partial\overline{V}_z}{\partial r} - \rho\overline{V}_z\frac{\partial\overline{V}_z}{\partial z} + \overline{V}_z\left\{-\frac{1}{r}\frac{\partial}{\partial r}r\rho_M\beta\overline{v_r t} + \frac{\partial}{\partial z}\rho\overline{V}_z\right\}$$
$$= \rho_M\beta\overline{v_r t}\frac{\partial\overline{V}_z}{\partial r} - \rho\overline{V}_z\frac{\partial\overline{V}_z}{\partial z} - \frac{\overline{V}_z}{r}\frac{\partial}{\partial r}r\rho_M\beta\overline{v_r t} + \rho\overline{V}_z\frac{\partial\overline{V}_z}{\partial z} + \overline{V}_z^2\frac{\partial\rho}{\partial z}$$
$$= \rho_M\beta\overline{v_r t}\frac{\partial\overline{V}_z}{\partial r} - \frac{\overline{V}_z}{r}\frac{\partial}{\partial r}r\rho_M\beta\overline{v_r t} + \overline{V}_z^2\frac{\partial\rho}{\partial z} \qquad (A.16)$$

and all of these terms can be evaluated from the present experimental measurements.

A.3.4 The integral form of the equation

Using the results of sections A.3.2 and A.3.3 equation (A.12) can be written

$$-\frac{1}{r}\frac{\partial}{\partial r}r\rho\overline{v_r v_z} + \rho_M\beta\overline{v_r t}\frac{\partial\bar{V}_z}{\partial r} - \frac{\bar{V}_z}{r}\frac{\partial}{\partial r}r\rho_M\beta\overline{v_r t} + \bar{V}_z^2\frac{\partial\rho}{\partial z}$$

$$-\frac{d\bar{p}}{dz} - \rho_M g + \rho_M\beta g(\bar{T}-T_M) + \frac{1}{r}\frac{\partial}{\partial r}r\mu\frac{\partial\bar{V}_z}{\partial r} = 0 \qquad (A.17)$$

Multiplying through by $\frac{D^2}{4}$ and introducing the dimensionless variable $\eta = \frac{r}{R} = \frac{2r}{D}$ gives

$$-\frac{D}{2}\frac{1}{\eta}\frac{\partial}{\partial\eta}\eta\rho\overline{v_r v_z} + \frac{D}{2}\rho_M\beta\overline{v_r t}\frac{\partial\bar{V}_z}{\partial\eta} - \frac{D}{2}\frac{\bar{V}_z}{\eta}\frac{\partial}{\partial\eta}\eta\rho_M\beta\overline{v_r t}$$

$$+\frac{D^2}{4}\bar{V}_z^2\frac{\partial\rho}{\partial z} - \frac{D^2}{4}\frac{d\bar{p}}{dz} - \frac{D^2}{4}\rho_M g + \frac{D^2}{4}\rho_M\beta g(\bar{T}-T_M)$$

$$+\frac{1}{\eta}\frac{\partial}{\partial\eta}\eta\mu\frac{\partial\bar{V}_z}{\partial\eta} = 0 \qquad (A.18)$$

On integrating with respect to η this becomes

$$\left(-\frac{D}{2}\eta\rho\overline{v_r v_z}\right)\Big|_0^\eta + \frac{D}{2}\int_0^\eta\left(\rho_M\beta\overline{v_r t}\frac{\partial\bar{V}_z}{\partial\eta}\right)\eta d\eta - \frac{D}{2}\int_0^\eta\left(\frac{\bar{V}_z}{\eta}\frac{\partial}{\partial\eta}\eta\rho_M\beta\overline{v_r t}\right)\eta d\eta$$

$$+\frac{D^2}{4}\int_0^\eta\left(\bar{V}_z^2\frac{\partial\rho}{\partial z}\right)\eta d\eta - \frac{D^2}{4}\int_0^\eta\frac{d\bar{p}}{dz}\eta d\eta - \frac{D^2}{4}\int_0^\eta\rho_M g\eta d\eta$$

$$+\frac{D^2}{4}\rho_M\beta g\int_0^\eta\left(\bar{T}-T_M\right)\eta d\eta + \left(\eta\mu\frac{\partial\bar{V}_z}{\partial\eta}\right)\Big|_0^\eta = 0 \qquad (A.19)$$

This equation provides a relationship in integral form between the turbulent shear stress $\rho\overline{v_r v_z}$ and the measured velocity and temperature distributions, the pressure drop $\frac{d\bar{p}}{dz}$ and the correlation $\overline{v_r t}$, which, as shown later, can be obtained from the energy equation.

A.3.5 The pressure drop $\frac{d\bar{p}}{dz}$

Because of the difficulties involved in obtaining accurate experimental local values of the axial pressure drop in non-isothermal flows, $\frac{d\bar{p}}{dz}$ is obtained here in terms of the measured slope of the velocity profile at the wall. The procedure employed is equivalent to carrying out a force balance over a thin horizontal section of the flow and consists of evaluating equation (A.19) between limits $\eta = 0$ and $\eta = 1$.

Then, from assumption iii), the definition of T_M and the fact that $\overline{v_r v_z} = 0$ for $\eta = 0$ and $\eta = 1$, equation (A.19) becomes

$$\frac{D}{2}\int_0^1 \left(\rho_M \beta \overline{v_r t} \frac{\partial \bar{V}_z}{\partial \eta}\right) \eta d\eta - \frac{D}{2}\int_0^1 \left(\frac{\bar{V}_z}{\eta} \frac{\partial}{\partial \eta} \eta \rho_M \beta \overline{v_r t}\right) \eta d\eta + \frac{D^2}{4}\int_0^1 \left(\bar{V}_z^2 \frac{\partial \rho}{\partial z}\right) \eta d\eta$$
$$- \frac{D^2}{8}\frac{d\bar{p}}{dz} - \frac{D^2}{8}\rho_M g + \mu_w \left(\frac{\partial \bar{V}_z}{\partial \eta}\right)_w = 0 \qquad (A.20)$$

If the three integrals in (A.20) are written as I_1, I_2 and I_3, respectively, then after multiplying through by 2, equation (A.20) rearranges to

$$-\frac{D^2}{4}\frac{d\bar{p}}{dz} - \frac{D^2}{4}\rho_M g = -\frac{D}{2} \cdot 2I_1 + \frac{D}{2} \cdot 2I_2 - \frac{D^2}{4} \cdot 2I_3$$
$$- 2\mu_w \left(\frac{\partial \bar{V}_z}{\partial \eta}\right)_w \qquad (A.21)$$

which gives $\frac{d\bar{p}}{dz}$ in terms of the velocity profile slope at the wall, as required.

A.3.6 The final equation

Substitution of equation (A.21) into the integral equation (A.19) is accomplished most easily by first substituting equation (A.21) into equation (A.18) to give

$$-\frac{D}{2}\frac{1}{\eta}\frac{\partial}{\partial \eta} \eta \rho \overline{v_r v_z} + \frac{D}{2}\left(\rho_M \beta \overline{v_r t} \frac{\partial \bar{V}_z}{\partial \eta} - 2I_1\right) - \frac{D}{2}\left(\frac{\bar{V}_z}{\eta}\frac{\partial}{\partial \eta}\eta \rho_M \beta \overline{v_r t} - 2I_2\right)$$
$$+ \frac{D^2}{4}\left(\bar{V}_z^2 \frac{\partial \rho}{\partial z} - 2I_3\right) + \frac{D^2}{4}\rho_M \beta g (\bar{T} - T_M) + \frac{1}{\eta}\frac{\partial}{\partial \eta}\eta \mu \frac{\partial \bar{V}_z}{\partial \eta}$$
$$- 2\mu_w \left(\frac{\partial \bar{V}_z}{\partial \eta}\right)_w = 0 \qquad (A.22)$$

which after multiplying through by η and integrating with respect to η becomes

$$\left(-\frac{D}{2}\eta \rho \overline{v_r v_z}\right)\Big|_0^\eta + \frac{D}{2}\int_0^\eta \left(\rho_M \beta \overline{v_r t}\frac{\partial \bar{V}_z}{\partial \eta} - 2I_1\right) \eta d\eta$$
$$- \frac{D}{2}\int_0^\eta \left(\frac{\bar{V}_z}{\eta}\frac{\partial}{\partial \eta}\eta \rho_M \beta \overline{v_r t} - 2I_2\right) \eta d\eta + \frac{D^2}{4}\int_0^\eta \left(\bar{V}_z^2 \frac{\partial \rho}{\partial z} - 2I_3\right) \eta d\eta$$
$$+ \frac{D^2}{4}\rho_M g \beta \int_0^\eta (\bar{T} - T_M) \eta d\eta + \left(\eta \mu \frac{\partial \bar{V}_z}{\partial \eta}\right)\Big|_0^\eta - 2\mu_w \left(\frac{\partial \bar{V}_z}{\partial \eta}\right)_w \int_0^\eta \eta d\eta = 0 \qquad (A.23)$$

Equation (A.23) simplifies to

$$-\frac{D}{2}\eta\rho\overline{v_r v_z} + \frac{D}{2}\int_o^\eta \left(\rho_M \beta \overline{v_r t}\frac{\partial \overline{V}_z}{\partial \eta} - 2I_1\right)\eta d\eta - \frac{D}{2}\int_o^\eta \left(\frac{\overline{V}_z}{\eta}\frac{\partial}{\partial \eta}\eta\rho_M\beta\overline{v_r t} - 2I_2\right)\eta d\eta$$
$$+ \frac{D^2}{4}\int_o^\eta \left(\overline{V}_z^2\frac{\partial \rho}{\partial z} - 2I_3\right)\eta d\eta + \frac{D^2}{4}\rho_M\beta g\int_o^\eta (\overline{T}-T_M)\,\eta d\eta$$
$$+ \eta\mu\frac{\partial \overline{V}_z}{\partial \eta} - \eta^2\mu_w\left(\frac{\partial \overline{V}_z}{\partial \eta}\right)_w = 0 \qquad (A.24)$$

and finally rearranges to

$$\left(-\overline{v_r v_z}\frac{D}{2\nu} + \frac{\partial \overline{V}_z}{\partial \eta}\right) = -\frac{D}{2\eta\mu}\int_o^\eta \left(\rho_M\beta\overline{v_r t}\frac{\partial \overline{V}_z}{\partial \eta} - 2I_1\right)\eta d\eta$$
$$+ \frac{D}{2\eta\mu}\int_o^\eta \left(\frac{\overline{V}_z}{\eta}\frac{\partial}{\partial \eta}\eta\rho_M\beta\overline{v_r t} - 2I_2\right)\eta d\eta + \eta\frac{\mu_w}{\mu}\left(\frac{\partial \overline{V}_z}{\partial \eta}\right)_w$$
$$- \frac{D^2}{4\eta\mu}\int_o^\eta \left(\overline{V}_z^2\frac{\partial \rho}{\partial z} - 2I_3\right)\eta d\eta - \frac{D^2}{4\eta\mu}\rho_M\beta g\int_o^\eta (\overline{T}-T_M)\,\eta d\eta \qquad (A.25)$$

which is the form of the equation of motion employed in calculations in the present investigation.

A.4 THE ENERGY EQUATION

A.4.1 Derivation of time-averaged equation.

The general form of the energy equation on which the following development is based is [43]:

$$\frac{\partial}{\partial t}\rho C_p T = -(\underline{\nabla}\cdot\rho C_p T\underline{V}) - (\underline{\nabla}\cdot\underline{q}) - (\tau:\underline{\nabla V}) + \left(\frac{\partial \ln V}{\partial \ln T}\right)_p\frac{Dp}{Dt} + \rho T\frac{DC_p}{Dt} \qquad (A.26)$$

Applying assumptions ix) and x) and assuming further

a) that the variation of the specific heat C_p over the temperature range of interest is small enough for $\rho T\frac{DC_p}{Dt}$ to be neglected in comparison with $-(\underline{\nabla}\cdot\rho C_p T\underline{V})$, and

b) that the heat flux vector $\underline{q}$ can be expressed as [43]:

$$\underline{q} = \left\{-k\frac{\partial T}{\partial r} - k\frac{1}{r}\frac{\partial T}{\partial \theta} - k\frac{\partial T}{\partial z}\right\},$$

the energy equation, in cylindrical co-ordinates, is

$$\frac{\partial}{\partial t}\rho C_p T = -\left\{\frac{1}{r}\frac{\partial}{\partial r}r\rho C_p T V_r + \frac{1}{r}\frac{\partial}{\partial \theta}\rho C_p T V_\theta + \frac{\partial}{\partial z}\rho C_p T V_z\right\}$$
$$+ \frac{1}{r}\left\{\frac{\partial}{\partial r}rk\frac{\partial T}{\partial r} + \frac{1}{r}\frac{\partial}{\partial \theta}k\frac{1}{r}\frac{\partial T}{\partial \theta} + \frac{\partial}{\partial z}k\frac{\partial T}{\partial z}\right\}$$
$$+ \frac{\partial p}{\partial t} + \frac{V_r}{r}\frac{\partial}{\partial r}(rp) + \frac{V_\theta}{r}\frac{\partial p}{\partial \theta} + V_z\frac{\partial p}{\partial z} \qquad (A.27)$$

On substitution of the expanded forms of the density, temperature, pressure and velocities as given in assumptions v) and vi) this becomes

$$\frac{\partial}{\partial t}(\rho_M[1-\beta(\bar{T}+t-T_M)])C_p(\bar{T}+t)$$
$$= -\left\{\frac{1}{r}\frac{\partial}{\partial r}r(\rho_M[1-\beta(\bar{T}+t-T_M)])C_p(\bar{T}+t)(\bar{V}_r+v_r)\right.$$
$$+ \frac{1}{r}\frac{\partial}{\partial \theta}(\rho_M[1-\beta(\bar{T}+t-T_M)])C_p(\bar{T}+t)(\bar{V}_\theta+v_\theta)$$
$$\left.+ \frac{\partial}{\partial z}(\rho_M[1-\beta(\bar{T}+t-T_M)])C_p(\bar{T}+t)(\bar{V}_z+v_z)\right\}$$
$$+\left\{\frac{1}{r}\frac{\partial}{\partial r}rk\frac{\partial}{\partial r}(\bar{T}+t) + \frac{1}{r}\frac{\partial}{\partial \theta}k\frac{1}{r}\frac{\partial}{\partial \theta}(\bar{T}+t) + \frac{\partial}{\partial z}k\frac{\partial}{\partial z}(\bar{T}+t)\right\}$$
$$+ \frac{\partial}{\partial t}(\bar{p}+p) + \frac{1}{r}(\bar{V}_r+v_r)\frac{\partial}{\partial r}r(\bar{p}+p) + \frac{1}{r}(\bar{V}_\theta+v_\theta)\frac{\partial}{\partial \theta}(\bar{p}+p)$$
$$+ (\bar{V}_z+v_z)\frac{\partial}{\partial z}(\bar{p}+p) \qquad (A.28)$$

Multiplying out, time-averaging and applying assumptions vi) and vii) gives

$$-\left\{\frac{1}{r}\frac{\partial}{\partial r}r[\rho C_p\overline{v_r t} - \rho_M\beta C_p\bar{T}\,\overline{v_r t} - \rho_M\beta C_p\overline{t^2 v_r}]\right.$$
$$\left.+ \frac{\partial}{\partial z}[\rho C_p\bar{T}\,\bar{V}_z + \rho C_p\overline{v_z t} - \rho_M\beta C_p\bar{T}\,\overline{v_z t} - \rho_M\beta C_p\bar{V}_z\overline{t^2} - \rho_M\beta C_p\overline{t^2 v_z}]\right\}$$
$$+ \frac{1}{r}\frac{\partial}{\partial r}rk\frac{\partial\bar{T}}{\partial r} + \frac{\partial}{\partial z}k\frac{\partial\bar{T}}{\partial z} + \frac{1}{r}\overline{v_r\frac{\partial}{\partial r}rp} + \bar{V}_z\frac{\partial\bar{p}}{\partial z} + \overline{v_z\frac{\partial p}{\partial z}} = 0 \qquad (A.29)$$

A.4.2 Further simplifications and assumptions.

It is desirable at this stage to introduce the following additional simplifications and assumptions which show that certain terms are small enough to be neglected.

a) By assumption iv) $\overline{v_z t}/\overline{V}_z\overline{T}$ is assumed to be approximately constant at a given radial position

$$\therefore \quad \overline{v_z t}(r,z) = C(r)\overline{V}_z(r,z)\overline{T}(r,z)$$

$$\therefore \quad \rho C_p\overline{v_z t}(r,z) = C(r)\rho C_p\overline{V}_z(r,z)\overline{T}(r,z)$$

$$\therefore \quad \frac{\partial}{\partial z}\rho C_p\overline{v_z t}(r,z) = C(r)\frac{\partial}{\partial z}\rho C_p\overline{V}_z(r,z)\overline{T}(r,z)$$

But, from the experimental results, $C(r) << 1$.

Therefore $\frac{\partial}{\partial z}\rho C_p\overline{v_z t}$ can be neglected in comparison with $\frac{\partial}{\partial z}\rho C_p\overline{V}_z\overline{T}$.

b) By assumption iv), any changes in the axial direction of the time-averaged turbulence quantities will be slight, and hence $\frac{\partial \overline{t^2}}{\partial z}$ will be small. Because β, too, is small it follows that the terms obtained when the differentiation of $\rho_M\beta C_p\overline{V}_z\overline{t^2}$ is carried out will also be small and can be neglected in comparison with $\frac{\partial}{\partial z}\rho C_p\overline{T}\,\overline{V}_z$.

c) As was the case also for the triple correlation terms in the equation of motion, no values are available for the terms

$$\frac{1}{r}\frac{\partial}{\partial r}r\rho_M\beta C_p\overline{t^2 v_r} \quad \text{and} \quad -\frac{\partial}{\partial z}\rho_M\beta C_p\overline{t^2 v_z}$$

On the basis of a similar argument to that given in section A.3.2 these terms are neglected in comparison with terms such as

$$-\frac{1}{r}\frac{\partial}{\partial r}r\rho C_p\overline{v_r t} \quad \text{and} \quad \frac{\partial}{\partial z}\rho C_p\overline{T}\,\overline{V}_z \quad \text{in equation (A.29).}$$

d) By assumption x) the term $\frac{\partial}{\partial z}k\frac{\partial\overline{T}}{\partial z}$ can be neglected.

e) Because relative intensities of turbulence are assumed to be low the pressure-velocity correlation terms $\overline{\frac{1}{r}v_r\frac{\partial}{\partial r}rp}$ and $\overline{V_z\frac{dp}{dz}}$ are neglected in comparison with $\overline{V}_z\frac{d\overline{p}}{dz}$. Any errors which may result from this assumption will be slight as the contribution of the $\overline{V}\frac{d\overline{p}}{dz}$ term itself to the final form of the energy equation is small.

A.4.3 The axial derivative terms : $-\frac{\partial}{\partial z}\rho C_p \overline{T}\,\overline{V}_z$ and $\frac{\partial}{\partial z}\rho_M \beta C_p \overline{T}\,\overline{v_z t}$

For the reasons given in section A.3.3 these two terms cannot be evaluated directly. However they can be expanded, together with $\frac{1}{r}\frac{\partial}{\partial r} r\rho_M \beta C_p \overline{T}\,\overline{v_r t}$, to give, since C_p is effectively constant,

$$-C_p\overline{T}\frac{\partial}{\partial z}\rho\overline{V}_z - \rho C_p\overline{V}_z\frac{\partial\overline{T}}{\partial z} + C_p\overline{T}\frac{\partial}{\partial z}\rho_M\beta\overline{v_z t} + \rho_M\beta C_p\overline{v_z t}\frac{\partial\overline{T}}{\partial z}$$

$$+ C_p\overline{T}\frac{1}{r}\frac{\partial}{\partial r}r\rho_M\beta\overline{v_r t} + \rho_M\beta C_p\overline{v_r t}\frac{\partial\overline{T}}{\partial r} \qquad (A.30)$$

This, on rearranging, becomes

$$C_p\overline{T}\left\{-\frac{\partial}{\partial z}\rho\overline{V}_z + \frac{\partial}{\partial z}\rho_M\beta\overline{v_z t} + \frac{1}{r}\frac{\partial}{\partial r}r\rho_M\beta\overline{v_r t}\right\}$$

$$- \rho C_p\overline{V}_z\frac{\partial\overline{T}}{\partial z} + \rho_M\beta C_p\overline{v_z t}\frac{\partial\overline{T}}{\partial z} + \rho_M\beta C_p\overline{v_r t}\frac{\partial\overline{T}}{\partial r} \qquad (A.31)$$

From equation (A.5) the first three terms are zero and, since $\rho_M\beta C_p\overline{v_z t} \ll \rho C_p\overline{V}_z$, the term $\rho_M\beta C_p\overline{v_z t}\frac{\partial\overline{T}}{\partial z}$ can be neglected in comparison with $-\rho C_p\overline{V}_z\frac{\partial\overline{T}}{\partial z}$. Expression (A.31) then becomes

$$-\rho C_p\overline{V}_z\frac{\partial\overline{T}}{\partial z} + \rho_M\beta C_p\overline{v_r t}\frac{\partial\overline{T}}{\partial r} \qquad (A.32)$$

A.4.4 The final equation

Applying the simplifications given in sections A.4.2 and A.4.3 to equation (A.29) gives

$$-\rho C_p\overline{V}_z\frac{\partial\overline{T}}{\partial z} - C_p\frac{1}{r}\frac{\partial}{\partial r}r\rho\overline{v_r t} + \rho_M\beta C_p\overline{v_r t}\frac{\partial\overline{T}}{\partial r} + \frac{1}{r}\frac{\partial}{\partial r}rk\frac{\partial\overline{T}}{\partial r}$$

$$+ \overline{V}_z\frac{d\overline{p}}{dz} = 0 \qquad (A.33)$$

Multiplying through by $\frac{D^2}{4}$ and introducing the dimensionless variable $\eta = \frac{r}{R} = \frac{2r}{D}$

$$-\frac{D^2}{4}\rho C_p\overline{V}_z\frac{\partial\overline{T}}{\partial z} - \frac{D}{2}C_p\frac{1}{\eta}\frac{\partial}{\partial\eta}\eta\rho\overline{v_r t} + \frac{D}{2}\rho_M\beta C_p\overline{v_r t}\frac{\partial\overline{T}}{\partial\eta}$$

$$+ \frac{1}{\eta}\frac{\partial}{\partial\eta}\eta k\frac{\partial\overline{T}}{\partial\eta} + \frac{D^2}{4}\overline{V}_z\frac{d\overline{p}}{dz} = 0 \qquad (A.34)$$

which on multiplying through by η and integrating with respect

to η becomes

$$-\frac{D^2}{4}C_p\frac{\partial\bar{T}}{\partial z}\int_o^\eta \rho\bar{V}_z)\eta d\eta - \left(\frac{D}{2}C_p\eta\rho\overline{v_r t}\right)\Big|_0^\eta + \frac{D}{2}\rho_M\beta C_p\int_o^\eta\left(\overline{v_r t}\frac{\partial\bar{T}}{\partial\eta}\right)\eta d\eta$$

$$+\left(\eta k\frac{\partial\bar{T}}{\partial\eta}\right)\Big|_0^\eta + \frac{D^2}{4}\int_o^\eta\left(\bar{V}_z\frac{d\bar{p}}{dz}\right)\eta d\eta = 0 \qquad \text{(A.35)}$$

Finally, dividing by ηk and rearranging gives

$$\left(\frac{\partial\bar{T}}{\partial\eta} - \frac{D}{2}\frac{\rho C_p}{k}\overline{v_r t}\right) = \frac{D^2}{4\eta k}C_p\frac{d\bar{T}}{dz}\int_o^\eta(\rho\bar{V}_z)\,\eta d\eta$$

$$-\frac{D^2}{4\eta k}\int_o^\eta\left(\bar{V}_z\frac{d\bar{p}}{dz}\right)\eta d\eta$$

$$-\frac{D}{2\eta k}\rho_M\beta C_p\int_o^\eta\left(\overline{v_r t}\frac{\partial\bar{T}}{\partial\eta}\right)\eta d\eta \qquad \text{(A.36)}$$

which is the form of the energy equation used in calculations.

APPENDIX B

PHYSICAL PROPERTIES OF AIR.

In the present investigation the variation with temperature of the physical properties of air was represented by the following expressions, where T is always in ^{o}Kelvin.

i) Density, ρ.

Since air was assumed to behave as an ideal gas over the range of temperatures encountered, the temperature dependence of density was calculated using the equation

$$\rho = \frac{28.97 \times 273}{359T} \text{ lb/ft}^3 \qquad \text{(B.1)}$$

ii) Viscosity, μ.

To represent the temperature dependence of viscosity the equation

$$\mu = \left(\frac{145.8\ T^{3/2}}{T + 110.4}\right) \times 10^{-5} \text{ centipoise} \qquad \text{(B.2)}$$

Hilsenrath and Touloukian [44], was used.

iii) Thermal conductivity, k.

Values of the thermal conductivity given by Chapman [45], which agree very well with those of Hilsenrath and Touloukian [44], were used to modify the latter's general equation to give a more accurate fit over the range 40^{o}F to 240^{o}F. The equation obtained,

$$k = \frac{0.00155135\sqrt{T}}{1 + \frac{254.4 \times 10^{-(12/T)}}{T}} \text{ Btu/hr ft}^2\ ^{o}\text{F} \qquad \text{(B.3)}$$

was the one used in the present work to describe the variation of thermal conductivity with temperature.

iv) Specific heat, C_p.

In this work the equation used to describe the temperature dependence of specific heat was

$$C_p = 0.2461476 - 0.000047187 + 0.0000000945T^2 \text{ Btu/lb } ^{o}\text{F} \qquad \text{(B.4)}$$

which was obtained from a least squares fit to the data of Chapman [45]

APPENDIX C

PRACTICAL CONSIDERATIONS IN HOT-WIRE MEASUREMENTS.

C.1 INTRODUCTION.

When making measurements in turbulent flows numerous practical points have to be considered. Of these some relate to the instrumentation but most are concerned with conditions under which the experimental equipment fails to meet the exact requirements of an ideal turbulence measuring instrument. These requirements, which are also discussed by Hinze [40], are:

i) The sensing element must be smaller than the microscale of turbulence. (It must also be small in order not to disturb the flow pattern.)

ii) The thermal inertia of the sensing element must be low so that response to even the most rapid fluctuations is practically instantaneous.

iii) The sensitivity of the sensing element must be high enough to enable very small differences in the fluctuations to be detected.

iv) The stability of the sensing element must be good so that calibration parameters remain constant.

v) The sensing element must be strong enough to remain rigid in highly turbulent flows.

Although the hot-wire anemometer meets most of these requirements, it remains far from ideal and the effects of departures from the ideal situation are discussed, together with other practical aspects of hot-wire anemometry, in the following sections. This discussion is restricted to normal single wire probes held perpendicular to the mean flow direction and for information on inclined wires and cross-wires reference should be made to recent publications by Champagne et al [60,70] and Guitton [71]. Since the constant current mode of operation was used in the present work, the discussion is further restricted by excluding information on constant temperature operation except where this is also relevant to constant current operation.

C.2 PRACTICAL CONSIDERATIONS.

C.2.1 Determination of optimum value of ℓ/d ratio

In deciding on the best value of the ratio of wire length, ℓ, to wire diameter, d, for a particular hot-wire probe, the conflicting requirements of several different effects must be considered. The four effects listed are all important for turbulence measurements but if only the mean velocity is of interest a minimum value of the ℓ/d ratio can be set using the criterion of section b); the maximum value of the ℓ/d ratio permitted is then dependent only on the velocity gradients in the flow.

a) The sensitivity, s, of the hot-wire to velocity fluctuations depends [40] partly on the magnitude of the ℓ/d ratio, a large value of which is desirable as it increases the sensitivity and hence the signal to noise ratio.

b) Ideally the hot-wire should lose heat only to the ambient fluid but in practice a significant proportion of the heat generated in the wire is lost by direct conduction to the wire supports. This decreases the effective length of the wire and creates a non-uniform temperature distribution along the wire. To minimise the errors thus introduced a large value of the ℓ/d ratio is required, recommended [40] values being "preferably greater than 200 but definitely greater than 100 for platinum wires" and higher still for tungsten wires, the thermal conductivity of the tungsten being $2\frac{1}{2}$ times that of platinum.

c) In turbulent flows the velocity distribution along the wire will be non-uniform if the length of the wire is greater than the microscale of turbulence. This, according to van der Hegge Zijnen [72], is about 0.5 mm in flows of moderate to low velocity. To obtain accurate point measurements of turbulence quantities hot-wire lengths of 0.5 mm or less are therefore desirable. To satisfy both this requirement and that of section b) platinum wires would have to be 2.5μ or less in diameter and tungsten wires even smaller. 2.5μ is, however, the minimum wire diameter consistent with other requirements based on considerations of wire strength.

d) With large ℓ/d ratios flow interference is reduced [73] and hence orientation effects (i.e. effects dependent on the angle of the probe to the direction of flow) are lessened. The magnitude of the change is shown by van Thinh [56,74] who presents values of the axial turbulent intensity, v_z', and the local mean velocity, $\bar{V}_z$, measured at different orientations by probes with different ℓ/d ratios; the differences decrease significantly as the ℓ/d ratio is increased from 90 to 240 and from 240 to 360.

Since the conflicting requirements listed above cannot be met simultaneously, a compromise must be made. However, recommendations differ. Van der Hegge Zijnen [72] recommends values of $\ell < 0.5$ mm and of $d < 0.005$ mm ($\ell/d=100$), but Hinze [40] suggests that wires where $0.5 \text{ mm} < \ell < 1$ mm and $2.5\mu < d < 5\mu$ ($\ell/d=200$) represent an acceptable compromise. Different conditions may, however, require different values of ℓ/d: Weinberg and Lederman [73] for example, mention that wires in normal use have ℓ/d ratios between 200 and 300 but that where large temperature fluctuations occur the value of ℓ/d should be as high as 500.

C.2.2 Determination of optimum support diameter.

The factors affecting the choice of support diameter are well discussed by van der Hegge Zijnen [72]. The main points of importance are :-

a) That supports should be of small diameter to minimise interference with the flow.

b) That supports must be rigid. If the supports are not rigid enough slight inaccuracies in positioning may occur and, more important, the vibration of the supports may contribute significantly to the measured value of the turbulent fluctuations.

c) That the ratio of support diameter to wire diameter should be at least 10. The ratio of the cross-sectional area of the support to that of the wire will then be at least 100, which will provide a large enough area for the heat gained by the

support from the wire to be conducted away without the support temperature being raised significantly above ambient. Strength and rigidity considerations will ensure that this condition is fulfilled in all cases where wires are attached directly to supports. Where, however, hot-wires have been plated along part of their length, the plated section can be considered an extension of the support to which it is attached and the diameter of the plated section should, by the same argument, also be greater than 10 times that of the wire. However, since the plating used is normally of copper, its high thermal conductivity makes much lower values of the ratio of plated diameter to wire diameter acceptable, a ratio of about 3 being permissible.

d) That the ratio of wire length to support diameter be greater than 10. This requirement is less easy to achieve for short wires, e.g. for a 0.5 mm wire the support diameter should be less than 0.05 mm, which may well be impossible in the face of strength and rigidity requirements.

Note that the requirements of sections c) and d) together confirm that an ℓ/d ratio greater than 100 should be used.

C.2.3 Choice of wire material

The two most important materials are platinum and tungsten, whose advantages and disadvantages are well discussed by van der Hegge Zijnen [72].

The advantages of using platinum are that wires of very small diameter can be obtained and, also, that it can be used at temperatures up to 500°C, enabling relatively large values of the sensitivity, s, to be achieved. Unfortunately, it possesses low mechanical strength, cannot be kept straight under tension and is easily deformed by collisions. This limits its use to clean flows and low velocities, with, typically, upper limits of 12m/sec and 25m/sec for wires 2.5μ and 6.25μ in diameter, respectively [72].

Alloys of platinum with iridium, rhodium and similar metals are used occasionally. Though similar in most respects to platinum they do have better mechanical strength; however, their temperature coefficient of electrical resistance is lower.

Wires of tungsten can be obtained with diameters as low as 3μ. Tungsten has excellent mechanical strength and is by far the best material to use in high velocity and other flows where ruggedness is a necessity. Also, it has a high temperature coefficient of electrical resistance, which is useful when simultaneous measurements of velocity and temperature are to be made. Its main disadvantage is its relatively low maximum operating temperature of 300°C, which limits the sensitivity obtainable. Until recently pure tungsten wires were the most widely used for hot-wire probes but they are rapidly being replaced by the platinum plated tungsten wires referred to by, for example, Bradshaw [75]. Such wires combine the advantages of both tungsten and platinum to give sensors with good mechanical strength and a high maximum operating temperature.

C.2.4 Orientation and interference effects

These effects are particularly important near solid boundaries or in flows where changes in flow direction relative to the direction of the wire supports occur. Investigations by several workers of the importance of these effects are reviewed below.

a) Van Thinh [56,74] measured v_z' and $\overline{V}_z$ profiles near a wall, using probes at angles of 1°, 45° and 90° to the direction of flow. He showed, first, that the correct values were those measured when the probe supports were parallel, or almost parallel, to the flow, and, second, that the differences in measured values increased both with increase in the angle between supports and flow direction and with decrease in the distance of the probe from the wall.

b) Florent and Thiolet [76] confirmed van Thinh's results and also measured the relative contributions of probe body and probe supports to the total interference. They also observed that, for probes with supports parallel to the flow direction, interference effects were only significant at distances less than 1 mm from a boundary.

c) Gilmore [77] carried out an even more comprehensive investigation of the same problem and formulated equations to describe the corrections to be applied to mean velocities

to allow for probe interference effects. An extension of his equations to include longitudinal cooling and high intensity turbulence effects has also been reported [71].

d) The effect of probe orientation in the wake of a two-dimensional flat plate was investigated by Hoole and Calvert [78]. They showed that quantities proportional to v'_z and $\overline{V}_z$ measured with the probe parallel to the flow, differed from those measured with the probe at 90° to the flow by up to 20%. From their results they were able to propose a correction applicable to their own and similar measurements.

e) The presence of additional probes or similar obstructions near a hot-wire has been studied by Tritton [79], who showed that turbulence intensity measurements were strongly affected by such obstructions even when the effect on the mean velocity measurements was relatively slight.

f) Dahm and Rasmussen [80] have attempted to determine theoretically the shape of probe body minimising orientation effects in flows where the mean flow direction fluctuates. They state that use of the body shape they recommend, together with widely spaced supports and a partially plated hot-wire with only a central sensitive region, can reduce the errors introduced by this effect to as little as 1%.

g) A theoretical analysis by Eyre [81] showed that orientation effects in conventional probes are at least partially caused by varying end losses by conduction when different sections of the supports lie within the wake of the hot-wire. His findings support the recommendations of Dahm and Rasmussen.

h) Maye [82] investigated the importance of probe interference effects near a solid boundary when a hot-wire is used as a resistance thermometer. He showed that temperature variations occur which are similar to the velocity variations reported by van Thinh [56,74] under similar conditions; he also showed, however, that these could be made practically insignificant if wires of the type recommended by Dahm and Rasmussen [80] were used.

It can be concluded from these papers that interference effects will be small in most flows provided that probe supports are kept parallel or nearly parallel to the flow direction, both during use and during calibration. If changes in flow direction relative to the probe supports are unpredictable use of designs such as that suggested by Dahm and Rasmussen [80] should keep errors to a minimum.

C.2.5 Heat loss to wall

This effect is relatively small. Very close to a solid boundary the rate of loss of heat from a hot-wire is increased by an additional loss to the boundary which can cause an apparent upswing in the velocity profile. This effect has been investigated by, among others, Wills [83] and Piercy [84]. For a 0.004 mm diameter wire Wills' results predict that the correction to be applied decreases with increasing distance from the boundary, becoming negligible at a distance of 0.5 mm in laminar flows. For turbulent flow the correction is negligible at 0.25 mm from the boundary. Piercy's results are similar but Lawn [65] refers to Hoagland [85] as reporting a negligible effect only 20 diameters (0.1 mm) from the wall for a 0.005 mm diameter wire. Should anomalous hot-wire readings be obtained close to a wall it is recommended that the work of either Wills or Piercy be referred to for details of the corrections to be applied.

C.2.6 Changes in calibration constants

The changes in hot-wire calibration constants caused by accumulation of dirt, by deformation, and even, in the case of tungsten operated at high temperature, by oxidation, have been observed and commented on by many workers, e.g. Weinberg and Lederman [73] and Coantic [86] who point out that for accurate work good filters must be used and frequent recalibrations undertaken. The effect of humidity changes appears from an observation by Almquist and Legath [87] to be negligible but changes in ambient temperature have a considerable effect and are discussed more fully in Chapter 2.

C.2.7 Problems associated with the measurement of turbulence quantities

A number of difficulties encountered in making accurate measurements of axial turbulent intensities are discussed briefly below:-

a) The accurate experimental determination of the time constant of a hot-wire is often less easy than expected and claims that hot-wire anemometer instruments can measure time constants to an accuracy of two to three per cent should be treated with caution.

b) For constant current operation of a hot-wire the value of the time constant depends partly on the magnitude of the flow velocity, changing as the velocity changes. The value set on the measuring instrument for compensation purposes is therefore a mean value and, should large slow velocity fluctuations occur, it may at times differ considerably from the true value. The significance of the distortions of the high velocity fluctuations which result from these differences depends on the characteristics of the flow and the properties of the hot-wire.

c) Cooper and Tulin [88] mention the difficulty of correctly amplifying low frequency fluctuations. Coantic [89] has shown that this can lead to considerable error; for example, the application of a correction for low frequency fluctuations to profiles of v_z'/u^* at Reynolds numbers of 40 000 and 140 000 increased them by roughly 9% and 3% respectively.

d) Noise has been shown to be more of a problem with constant temperature than with constant current anemometers, and the latter are therefore usually used for measurements in flows of low turbulence intensity where the signal to noise ratio is low. The contribution of mechanical noise to turbulence measurements is often ignored but, as is shown by Rasmussen [90], strange peaks on the energy spectrum can often be traced to vibrations or acoustic noise emitted by components of the experimental apparatus. It is recommended that in order to obtain accurate measurements a check similar to that performed by Rasmussen should be carried out.

C.3 DETAILED DERIVATION OF HOT-WIRE EQUATIONS.

C.3.1 Mean velocity correction equation.

It was shown in Chapter 2, section 2.3, that the effective cooling velocity over a hot-wire can be written

$$V_{eff} = [(\overline{V}_z + v_z)^2 + v_r^2]^{0.5} \qquad (C.1)$$

Substitution of this equation into the general hot-wire equation (2.19)

$$\frac{I^2R_w}{R_w-R_g} = A + B\,V_{eff}^{0.5} \qquad (C.2)$$

gives

$$\frac{I^2R_w}{R_w-R_g} = A + B[(\overline{V}_z + v_z)^2 + v_r^2]^{0.25} \qquad (C.3)$$

which can be written

$$\frac{I^2R_w}{R_w-R_g} = A + B\overline{V}_z^{0.5}\left(1 + \frac{2v_z}{\overline{V}_z} + \frac{v_z^2}{\overline{V}_z^2} + \frac{v_r^2}{\overline{V}_z^2}\right)^{0.25} \qquad (C.4)$$

This equation can be expanded as follows,

$$\begin{aligned}\frac{I^2R_w}{R_w-R_g} = A + B\overline{V}_z^{0.5}\Bigg\{1 &+ \frac{1}{4}\left(\frac{2v_z}{\overline{V}_z} + \frac{v_z^2}{\overline{V}_z^2} + \frac{v_r^2}{\overline{V}_z^2}\right)\\ &+ \frac{1}{2!}\left(\frac{1}{4}\right)\left(-\frac{3}{4}\right)\left(\frac{2v_z}{\overline{V}_z} + \frac{v_z^2}{\overline{V}_z^2} + \frac{v_r^2}{\overline{V}_z^2}\right)^2\\ &+ \frac{1}{3!}\left(\frac{1}{4}\right)\left(-\frac{3}{4}\right)\left(-\frac{7}{4}\right)\left(\frac{2v_z}{\overline{V}_z} + \frac{v_z^2}{\overline{V}_z^2} + \frac{v_r^2}{\overline{V}_z^2}\right)^3 + \cdots\Bigg\}\end{aligned} \qquad (C.5)$$

After multiplying out and collecting like terms this becomes

$$\frac{I^2R_w}{R_w-R_g} = A + B\overline{V}_z^{0.5}\left\{1 + \frac{v_z}{2\overline{V}_z} - \frac{1}{8}\frac{v_z^2}{\overline{V}_z^2} + \frac{1}{4}\frac{v_r^2}{\overline{V}_z^2} + \frac{1}{16}\frac{v_z^3}{\overline{V}_z^3} - -\right\} \qquad (C.6)$$

which after time-averaging and discarding third and higher order

terms, gives

$$\frac{I^2R_w}{R_w-R_g} \simeq A + B\bar{V}_z^{0.5}\left\{1 - \frac{1}{8}\frac{\overline{v_z^2}}{\bar{V}_z^2} + \frac{1}{4}\frac{\overline{v_r^2}}{\bar{V}_z^2}\right\} \qquad (C.7)$$

From equation (C.7) it can be seen that the measured velocity, V_{meas}, and the actual mean velocity $\bar{V}_z$ are related by

$$V_{meas}^{0.5} \simeq \bar{V}_z^{0.5}\left\{1 - \frac{1}{8}\frac{\overline{v_z^2}}{\bar{V}_z^2} + \frac{1}{4}\frac{\overline{v_r^2}}{\bar{V}_z^2}\right\} \qquad (C.8)$$

and therefore

$$V_{meas} \simeq \bar{V}_z\left\{1 - \frac{1}{4}\frac{\overline{v_z^2}}{\bar{V}_z^2} + \frac{1}{2}\frac{\overline{v_r^2}}{\bar{V}_z^2}\right\} \qquad (C.9)$$

which enables the correction which should be applied to measured velocities under conditions where high relative intensities of turbulence occur to be calculated.

C.3.2 Hinze's [40] equation describing the temperature dependence of A.

Using the values for A and B proposed by Kramers [50], viz:

$$A = 0.42\frac{J\pi k_f \ell}{\beta R_0}(Pr)_f^{0.2} \qquad (C.10)$$

$$B = 0.57\frac{J\pi k_f \ell}{\beta R_0}(Pr)_f^{0.33}\left(\frac{\rho_f d}{\mu_f}\right)^{0.5} \qquad (C.11)$$

where J = conversion constant

ℓ = wire length

β = temperature coefficient of resistance

R_0 = hot-wire resistance at reference temperature

and other symbols have their usual meanings,

it can be shown that for air the value of B is practically independent of temperature and the value of A is proportional to the thermal conductivity of the air, k_f, evaluated at the film temperature. If the temperature dependence of k_f is approximated by the relation

$$k_f = a + a_1 T_f$$

where a and a_1 are constants for air and T_f is the film

temperature in ^{o}K, then equation (C.10) can be written

$$A_f = 0.42 \frac{J\pi\ell}{\beta R_0} Pr^{0.2} (a + a_1 T_f) \qquad (C.12)$$

$$= A_g \left[1 + \frac{a_1}{2(a + a_1 T_g)} (T_w - T_g) \right] \qquad (C.13)$$

where A_f is equivalent to A in equation (2.6) and

$$A_g = 0.42 \frac{J\pi\ell}{\beta R_0} Pr^{0.2} (A + a_1 T_g) \qquad (C.14)$$

and T_g = ambient temperature in ^{o}K.

Substitution of equation (C.13) into equation (2.6) gives

$$\frac{I^2 R_w}{R_w - R_g} = A_g \left[1 + \frac{a_1}{2(a + a_1 T_g)} (T_w - T_g) \right] + B\bar{V}_z^{0.5} \qquad (C.15)$$

The variation of the wire resistance with temperature can be represented by the expansion

$$R_w = R_0 \left[1 + \beta(T_w - T_0) + \gamma(T_w - T_0)^2 + \cdots \right] \qquad (C.16)$$

where R_0 is the resistance of the wire at a reference temperature T_0 and β is the temperature coefficient of electrical resistance.

For tungsten, γ and higher order coefficients are very small so that equation (C.16) becomes

$$R_w = R_0 \left[1 + \beta(T_w - T_0) \right] \qquad (C.17)$$

Substituting for $(T_w - T_g)$ by making use of equation (C.17), equation (C.15) becomes

$$\frac{I^2 R_w}{R_w - R_g} = A_g \left[1 + \frac{a_1}{2(a + a_1 T_g)\beta R_0} (R_w - R_g) \right] + B\bar{V}_z^{0.5} \qquad (C.18)$$

which is the equation employed in the present work to describe the temperature dependency of A.

C.3.3 The sensitivity equation for non-isothermal turbulence measurements.

When a hot-wire is used under non-isothermal conditions in turbulent flows both T_w, the "wire" or operating temperature and T_g, the local "gas" temperature, are varying quantities. Because of this A_f cannot be used as given in equation (C.12) but must be redefined in terms of a reference temperature T_0.

By analogy with equation (C.12) A_0, the value of A at T_0, can be written as

$$A_0 = 0.42 \frac{J\pi\ell}{\beta R_0} Pr^{0.2} (a + a_1 T_0) \qquad (C.19)$$

which, on being combined with equation (C.12) gives

$$\begin{aligned} A_f &= \frac{A_0}{a + a_1 T_0} (a + a_1 T_f) \\ &= \frac{A_0}{a + a_1 T_0} \left[a + \frac{a_1}{2} (T_w + T_g)\right] \\ &= \frac{A_0}{a + a_1 T_0} \left[a + \frac{a_1}{2} (T_w - T_g)\right] + \frac{a_1 A_0 T_g}{a + a_1 T_0} \end{aligned} \qquad (C.20)$$

Substitution of equation (C.20) into equation (2.6) gives

$$\frac{I^2 R_w}{R_w - R_g} = \frac{A_0}{a + a_1 T_0} \left[a + \frac{a_1}{2}(T_w - T_g)\right] + \frac{a_1 A_0 T_g}{a + a_1 T_0} + B V_z^{0.5} \qquad (C.21)$$

Assuming that R_w, R_g, T_g, T_w, and V_z can all be written in terms of the sum of a mean and a varying quantity, e.g. $R_w = \overline{R}_w + r_w$, equation (C.21) becomes

$$\begin{aligned} \frac{I^2(\overline{R}_w + r_w)}{\overline{R}_w + r_w - \overline{R}_g - r_g} &= \frac{A_0}{a + a_1 T_0} \left[a + \frac{a_1}{2}(\overline{T}_w + t_w - \overline{T}_g - t_g)\right] \\ &\quad + \frac{a_1 A_0 (\overline{T}_g + t_g)}{a + a_1 T_0} + B(\overline{V}_z + v_z)^{0.5} \end{aligned} \qquad (C.22)$$

Expanding the left hand side of equation (C.22)

$$\begin{aligned} \frac{I^2(\overline{R}_w + r_w)}{\overline{R}_w + r_w - \overline{R}_g - r_g} &= \frac{I^2(\overline{R}_w + r_w)}{(\overline{R}_w - \overline{R}_g)\left(1 + \frac{r_w - r_g}{\overline{R}_w - \overline{R}_g}\right)} \\ &= \frac{I^2(\overline{R}_w + r_w)}{\overline{R}_w - \overline{R}_g} \left(1 + \frac{r_w - r_g}{\overline{R}_w - \overline{R}_g}\right)^{-1} \end{aligned} \qquad (C.23)$$

Expanding equation (C.23) and neglecting terms in r_w^2, $r_w r_g$ and higher order terms

$$\therefore \quad \frac{I^2(\bar{R}_w+r_w)}{\bar{R}_w+r_w-\bar{R}_g-r_g} = \frac{I^2\bar{R}_w}{\bar{R}_w-\bar{R}_g}\left(1-\left[\frac{r_w-r_g}{\bar{R}_w-\bar{R}_g}\right]\right)+\frac{I^2 r_w}{\bar{R}_w-\bar{R}_g} \qquad (C.24)$$

Expanding the right hand side of equation (C.22)

$$\frac{A_0}{a+a_1T_0}\left[a+\frac{a_1}{2}(\bar{T}_w+t_w-\bar{T}_g-t_g)\right]+\frac{a_1A_0}{a+a_1T_0}(\bar{T}_g+t_g)+B(\bar{V}_z+v_z)^{0.5}$$

$$= \frac{A_0}{a+a_1T_0}\left[a+\frac{a_1}{2}(\bar{T}_w-\bar{T}_g)\right]+\frac{a_1A_0\bar{T}_g}{a+a_1T_0}+B\bar{V}_z^{0.5}$$

$$+\frac{A_0}{a+a_1T_0}\left[\frac{a_1}{2}(t_w-t_g)\right]+\frac{a_1A_0t_g}{a+a_1T_0}+B\bar{V}_z^{0.5}\cdot\frac{v_z}{2\bar{V}_z}$$

$$= \bar{A}_f+B\bar{V}_z^{0.5}+\frac{A_0}{a+a_1T_0}\left[\frac{a_1}{2}\left(\frac{r_w}{\beta R_0}-t_g\right)\right]+\frac{a_1A_0t_g}{a+a_1T_0}$$

$$+B\bar{V}_z^{0.5}\quad\frac{v_z}{\bar{V}_z^{0.5}} \qquad (C.25)$$

If the steady state equation

$$\frac{I^2\bar{R}_w}{\bar{R}_w-\bar{R}_g} = \bar{A}_f+B\bar{V}_z^{0.5} \qquad (C.26)$$

is subtracted from the expanded form of equation (C.22), then the equation below is obtained.

$$-\frac{I^2\bar{R}_w}{\bar{R}_w-\bar{R}_g}\left(\frac{r_w-r_g}{\bar{R}_w-\bar{R}_g}\right)+\frac{I^2r_w}{\bar{R}_w-\bar{R}_g}$$

$$= \frac{A_0}{a+a_1T_0}\left[\frac{a_1}{2}\left(\frac{r_w}{\beta R_0}-t_g\right)\right]+\frac{a_1A_0t_g}{a+a_1T_0}+B\bar{V}_z^{0.5}\frac{v_z}{2\bar{V}_z} \qquad (C.27)$$

which rearranges to

$$\frac{I^2 r_w}{\bar{R}_w - \bar{R}_g} = \frac{A_0 a_1 r_w}{2(a+a_1 T_0)\beta R_0} + \frac{I^2 \bar{R}_w}{(\bar{R}_w - \bar{R}_g)^2} r_w - \frac{I^2 \bar{R}_w r_g}{(\bar{R}_w - \bar{R}_g)^2}$$

$$+ \frac{a_1 A_0 t_g}{2(a+a_1 T_0)} + B\bar{V}_z^{0.5} \frac{v_z}{2\bar{V}_z} \qquad (C.28)$$

Since $$\frac{I^2 \bar{R}_w}{\bar{R}_w - \bar{R}_g} = \bar{A}_f + B\bar{V}_z^{0.5}$$

and $$r_g = \beta R_0 t_g$$

equation (2.47) can be written

$$\frac{I^2 r_w}{\bar{R}_w - \bar{R}_g} = \left[\frac{\bar{A}_f + B\bar{V}_z^{0.5}}{\bar{R}_w - \bar{R}_g} + \frac{A_0 a_1}{2(a+a_1 T_0)\beta R_0} \right] r_w$$

$$+ \left[\frac{A_0 a_1}{2(a+a_1 T_0)} - \frac{\bar{A}_f + B\bar{V}_z^{0.5}}{\bar{R}_w - \bar{R}_g} \beta R_0 \right] t_g + B\bar{V}_z^{0.5} \frac{v_z}{2\bar{V}_z} \qquad (C.29)$$

It has been customary [40] to neglect the term $\dfrac{A_0 a_1}{2\beta(a+a_1 T_0)R_0}$

provided that

$$\left(\frac{A_0 a_1}{2(a+a_1 T_0)\beta R_0} \right) \Big/ \left(\frac{\bar{A}_f + B\bar{V}_z^{0.5}}{\bar{R}_w - \bar{R}_g} \right) < 0.1$$

However, as is shown in section C.3, this assumption can lead to errors as large as 30% in the hot-wire sensitivities to velocity and temperature fluctuations. To overcome this the development below was used:

$$\text{Let } P = \left(\frac{A_0 a_1}{2(a+a_1 T_0)\beta R_0} \right) \Big/ \left(\frac{\bar{A}_f + B\bar{V}_z^{0.5}}{\bar{R}_w - \bar{R}_g} \right)$$

Equation (C.29) can then be written

$$\frac{I^2 r_w}{\bar{R}_w - \bar{R}_g} = (1 + P) \left(\frac{\bar{A}_f + B\bar{V}_z^{0.5}}{\bar{R}_w - \bar{R}_g} \right) r_w - (1 - P) \left(\frac{\bar{A}_f + B\bar{V}_z^{0.5}}{\bar{R}_w - \bar{R}_g} \right) \beta R_0 t_g$$

$$+ B\bar{V}_z^{0.5} \frac{v_z}{2\bar{V}_z} \qquad (C.30)$$

Since $\dfrac{I^2\bar{R}_w}{\bar{R}_w-\bar{R}_g} = \bar{A}_f + B\bar{V}_z^{0.5}$

equation (C.30) can be rearranged to give

$$r_w\left[\frac{I^2\bar{R}_w(1+P)}{(\bar{R}_w-\bar{R}_g)^2} - \frac{I^2}{\bar{R}_w-\bar{R}_g}\right] = (1-P)\frac{I^2\bar{R}_w\beta R_0 t_g}{(\bar{R}_w-\bar{R}_g)^2} - B\bar{V}_z^{0.5}\frac{v_z}{2\bar{V}_z} \qquad (C.31)$$

whence

$$\frac{I^2 r_w}{(\bar{R}_w-\bar{R}_g)^2}(\bar{R}_g + \bar{R}_w P) = \frac{(1-P)\beta I^2\bar{R}_w R_0}{(\bar{R}_w-\bar{R}_g)^2} t_g - B\bar{V}_z^{0.5}\frac{v_z}{2\bar{V}_z} \qquad (C.32)$$

This rearranges to

$$e = Ir_w = \frac{(1-P)\beta I\bar{R}_w R_0}{\bar{R}_g\left(1+P\left(\frac{\bar{R}_w}{\bar{R}_g}\right)\right)} tg - \frac{(\bar{R}_w-\bar{R}_g)^2 B\bar{V}_z^{0.5}}{2I\bar{R}_g\left(1+P\left(\frac{\bar{R}_w}{\bar{R}_g}\right)\right)\bar{V}_z} v_z \qquad (C.33)$$

By writing $\bar{R}_w = K\bar{R}_g$, where K will equal the overheating ratio plus one (e.g. for an overheating ratio of 0.5, K = 1.5), equation (C.33) becomes

$$e = Ir_w = \frac{(1-P)\beta I\bar{R}_w R_0}{(1+PK)\bar{R}_g} t_g - \frac{(\bar{R}_w-\bar{R}_g)^2 B\bar{V}_z^{0.5}}{2(1+PK)IR_g\bar{V}_z} v_z \qquad (C.34)$$

$$= s_t t_g - s v_z \qquad (C.35)$$

where

$$s_t = \frac{(1-P)}{(1+PK)}\frac{\beta I\bar{R}_w R_0}{\bar{R}_g} \qquad (C.36)$$

$$s = \frac{1}{(1+PK)}\frac{(\bar{R}_w-\bar{R}_g)^2 B\bar{V}_z^{0.5}}{2IR_g\bar{V}_z} \qquad (C.37)$$

Hence

$$\overline{e^2} = s^2\overline{v_z^2} + s_t^2\overline{t^2} - 2ss_t\overline{v_z t} \qquad (C.38)$$

where for convenience the subscript on the t has been dropped.

Equation (C.38) provides a relationship between observed fluctuations of the voltage, e, across the hot-wire, and the values of the velocity and temperature intensities. The application of this equation is discussed in section 2.5.

C.4 ERRORS INTRODUCED BY INCORRECT SENSITIVITY EQUATIONS.

In section 2.5.1 it was shown that when a hot-wire held normal to the mean flow is used under non-isothermal conditions, the following equation (equation (C.29)) applies:

$$\frac{I^2 r_w}{\bar{R}_w - \bar{R}_g} = \left[\frac{\bar{A}_f + B\bar{V}_z^{0.5}}{\bar{R}_w - \bar{R}_g} + \frac{A_0 a_1}{2(a+a_1 T_0)\beta R_0} \right] r_w + \left[\frac{A_0 a_1}{2(a+a_1 T_0)} - \frac{\bar{A}_f + B\bar{V}_z^{0.5}}{\bar{R}_w - \bar{R}_g} \beta R_0 \right] t_g + B\bar{V}_z^{0.5} \frac{v_z}{2\bar{V}_z} \quad (C.39)$$

It was also shown that from this equation the following values for the sensitivities s, and s_t, could be derived:

$$s = \frac{1}{(1 + PK)} \frac{(\bar{R}_w - \bar{R}_g)^2 B\bar{V}_z^{0.5}}{2I R_g \bar{V}_z} \quad (C.40)$$

$$s_t = \frac{(1 - P)}{(1 + PK)} \frac{\beta I \bar{R}_w R_0}{\bar{R}_g} \quad (C.41)$$

where $$P = \left(\frac{A_0 a_1}{2(a+a_1 T_0)\beta R_0} \right) \Bigg/ \left(\frac{\bar{A}_f + B\bar{V}_z^{0.5}}{\bar{R}_w - \bar{R}_g} \right)$$

and $$K = \frac{\bar{R}_w}{\bar{R}_g}$$

If, however, instead of introducing these factors P and K, the suggestion of Hinze [40] is followed (see below), significantly different forms of the sensitivities are obtained. These are referred to as s^* and s_t^* in the treatment below.

Taking Hinze's assumption that

$$\frac{A_0 a_1}{2(a+a_1 T_0)\beta R_0} \ll \frac{\bar{A}_f + B\bar{V}_z^{0.5}}{\bar{R}_w - \bar{R}_g}$$

to be correct, the former term can be neglected and equation (C.39) becomes

$$\frac{I^2 r_w}{\bar{R}_w - \bar{R}_g} = \frac{\bar{A}_f + B\bar{V}_z^{0.5}}{\bar{R}_w - \bar{R}_g} r_w - \frac{\bar{A}_f + B\bar{V}_z^{0.5}}{\bar{R}_w - \bar{R}_g} \beta R_0 t_g + B\bar{V}_z^{0.5} \frac{v_z}{2\bar{V}_z} \quad (C.42)$$

whence, since $\bar{A}_f + B\bar{V}_z^{0.5} = \dfrac{I^2\bar{R}_w}{\bar{R}_w-\bar{R}_g}$,

$$\left[\frac{I^2}{\bar{R}_w-\bar{R}_g} - \frac{I^2\bar{R}_w}{(\bar{R}_w-\bar{R}_g)^2}\right] r_w = -\frac{I^2\bar{R}_w}{(\bar{R}_w-\bar{R}_g)^2}\beta R_0 t_g + B\bar{V}_z^{0.5}\frac{v_z}{2\bar{V}_z} \quad (C.43)$$

which rearranges to

$$\frac{I^2\bar{R}_g r_w}{(\bar{R}_w-\bar{R}_g)^2} = \frac{\beta I^2\bar{R}_w R_0}{(\bar{R}_w-\bar{R}_g)^2} t_g - B\bar{V}_z^{0.5}\frac{v_z}{2\bar{V}_z} \quad (C.44)$$

From this equation, since $e = Ir_w$,

$$e = \frac{\beta I\bar{R}_w R_0}{\bar{R}_g} t_g - \frac{(\bar{R}_w - \bar{R}_g)^2}{2I\bar{R}_g} B\bar{V}_z^{0.5}\frac{v_z}{\bar{V}_z} \quad (C.45)$$

$$= s_t^* t_g - s^* v_z \quad (C.46)$$

where $$s^* = \frac{(\bar{R}_w - \bar{R}_g)^2 B\bar{V}_z^{0.5}}{2I\bar{R}_g\bar{V}_z} \quad (C.47)$$

and $$s_t^* = \frac{\beta I\bar{R}_w R_0}{\bar{R}_g} \quad (C.48)$$

By comparing equations (C.40) and (C.47) and equations (C.41) and (C.48) it can be seen that

$$s = \frac{1}{(1 + PK)} s^* \quad (C.49)$$

$$s_t = \frac{(1 - P)}{(1 + PK)} s_t^* \quad (C.50)$$

and the magnitude of the errors which would be introduced if s^* and s_t^* were to be used instead of s and s_t can be found by determining P and K. This has been done using results from run N-10 and the differences between s and s^* and between s_t and s_t^* are given in Table C.1 below.

TABLE C.1

$$\frac{A_0 a_1}{2(a+a_1 T_0)\beta R_0} = 62.14$$

$$K = 1.5$$

y/R	$\frac{I^2 \overline{R}_w}{(\overline{R}_w - \overline{R}_g)^2}$	P	s	s*	% Difference	s_t	s_t^*	% Difference
1.0	666.4	0.093	13.55	15.40	13.6	1.66	2.07	25.0
0.5	657.3	0.095	13.87	15.94	14.9	1.63	2.06	26.6
0.3	644.2	0.096	14.61	16.79	14.9	1.62	2.05	26.6
0.16	567.4	0.110	16.21	18.85	16.3	1.53	2.01	31.6
0.08	564.9	0.110	21.19	24.64	16.3	1.47	1.93	31.6

From the above Table it can be seen that use of the assumption recommended by Hinze leads to values of s and s_t that are up to 16% and 31% too high, respectively. Since, for the hot-wire used in the above run, a tenfold increase in Reynolds number would still only reduce the errors in s and s_t to of the order of 7%, it is concluded that Hinze's assumption is applicable only at high Reynolds numbers and below Reynolds numbers of about 100 000 the complete forms of the sensitivity expressions (equations (C.40) and (C.41)) should be used.

APPENDIX D

DETAILS OF EXPERIMENTAL EQUIPMENT.

D.1 MINOR PIECES OF EQUIPMENT.

i) Centrifugal blower:- Supplier: Air Steel (Pty.) Ltd.; Rating: 200 cfm; Drive: 3 phase, 0.75 H.P. induction motor.

ii) Flow straightener:- Assembled from 7 x 1 ft lengths of 32 mm nominal diam. PVC tubing, glued together to form a 1 ft long bundle of maximum diameter 3.82".

iii) Air/water heat exchanger:- Supplier: J.L. Clark Engineering (Pty.) Ltd.; water cooling coil, 12" x 12", Series 18.

iv) Filters:- Made from a bonded air filter known as Vildon Fibrous Filter, supplied by Brandt Engineering (Pty.) Ltd., Johannesburg.

v) Pitot-static tube:- Supplier: F.W. Dwyer Mfg. Co., Michigan City, Indiana; Type: No. 166-12 Pocket Pitot Tube $\frac{1}{8}$" diam.; 12" length.

vi) Micromanometer:- Supplier: Flow Corporation, Watertown, Mass.; Type: Model MM3 Micromanometer; Measuring fluid: Butyl alcohol of S.G. = 0.8176 - 0.0004 (T-50) (where T is ambient temperature in ^{o}F); Resolution: 0.0001" butyl alcohol. Accuracy: ± 0.0002" butyl alcohol.

vii) Thermocouples:- Wire supplied by Claud S. Gordon Co., Richmond, Ill.; Specifications: Iron-constantan wire; Cat. No. J30-2-305, 30 gauge, to special limits of error (± 2^{o}F).

viii) Thermocouple selector switch:- Made by W.G. Pye & Co., Cambridge, England; Two pole thermocouple switch with thermoelectric effects less than 1 μV at room temperature.

ix) Heating ribbon:- Supplier: Hoskins Mfg. Co., Detroit, Michigan; Type: 1" x 0.0126" Chromel A (80% Ni, 20% Cr) alloy tape with resistance 0.0409 ohms/ft.

x) Kilowatt-hour meter:- Made by Chamberlain & Hookham Ltd., S. Africa; Type: single phase AC meter type K, scale factor 300 rev./KWH.

xi) Power supply:- Supplier: Hewlett Packard Co., Palo Alto, California; Type: Harrison 6102A DC power supply, 0-40V, 0-0.5A.

xii) Differential Voltmeter:- Manufacturer: John Fluke Mfg. Co., Seattle, Washington; Type: AC/DC differential voltmeter Model 887AB; Accuracy: ± 0.005 mV, Resolution: 0.001 mV.

xiii) Potentiometer:- Manufacturer: W.G. Pye & Co., Cambridge, England; Type: Pye portable potentiometer.

xiv) Multipoint recorder:- Manufacturer: Honeywell Controls Ltd., Scotland; Type: 153, Universal Elektronik Multipoint Recorder.

xv) Hook gauge:- Supplier: F. W. Dwyer Mfg. Co., Michigan City, Indiana; Type: No. 1420 Hook Gauge; Accuracy: ± 0.001" water.

xvi) Centrifugal blower (calibration system):- Manufacturer: Woods of Colchester, Ltd., England; Type: Fanmanco CA8x2.

xvii) Wet-gas meter:- Manufacturer: Elster & Co., AG., Mainz-Castel, Germany; Type: Elster size 5 wet-gas meter; Accuracy: within ± 0.35% for flow rates in range 600-15000 l/hr.

D.2 THE TRANSMETRICS CONSTANT CURRENT HOT-WIRE ANEMOMETER SYSTEM MODEL 6401

Details of the components of this hot-wire anemometer system, which is described briefly in Chapter 3, are discussed below. A photograph of the system is given in Fig. D.1.

a) The current control panel.
This panel enabled the current through the hot-wire to be adjusted over the range 0.4 to 300 mA.

b) The bridge unit.
This was a precision Kelvin double bridge incorporating a very sensitive galvanometer and having an accuracy of

Current Control Panel

Bridge Unit

Potentiometer

Mean square meter

Amplifier

Square wave generator

FIGURE D.1 THE TRANSMETRICS CONSTANT CURRENT HOT-WIRE ANEMOMETER

± 0.01 ohms and a resolution of ± 0.002 ohms. Use of a four conductor cable to connect the probe to this bridge enabled all lead resistance corrections to be eliminated except for those introduced by the short lengths of wire connecting the cable and the hot-wire.

c) The potentiometer.

This was a precision instrument, with an accuracy of ± 0.1% full scale and a resolution of ± 0.005% full scale. Voltage and current measurements could be made over the full scale ranges of 10, 1.0 and 0.1 volts, and 1.0, 0.1 and 0.01 amps respectively. This unit also incorporated a very sensitive galvanometer.

d) The mean square output meter.

This meter displayed the mean square value of the voltage output from the amplifier. It was calibrated against a random signal voltmeter which had itself been calibrated against the Fluke differential voltmeter described in Section D.1. No significant differences between the readings of the first two meters were observed and it was concluded that the mean square meter was giving accurate readings.

e) The amplifier.

This amplifier was a low noise, high gain, wide-band AC amplifier equipped with an overload device. It could handle signals with frequencies in the range 0.1 Hz to 320 Hz and mean square voltage readings could be made accurately at all frequencies using a self-contained thermocouple.

The frequency response was specified as:- flat ± 1% for 1 Hz < ν < 30kHz; < 10% for 0.2 Hz < ν < 150 kHz; < 30% for 0.1 Hz < ν < 300 kHz, where ν was the frequency. A measured frequency response showed however that a deviation of -2.5% existed at 5 Hz and this deviation decreased to +0.3% at 100 Hz. At higher frequencies, up to 10 kHz the greatest deviation noted was +2.0%.

A compensation circuit (an RC network with variable capacitance), which allowed for hot-wire time constants

in the range 50 μsec to 22 msec, enabled the attenuation of high frequency signals due to the finite thermal inertia of the wire to be taken into account.

The gain of the amplifier was 50 000, with a maximum output voltage of 5 volts RMS at zero attenuation. The noise voltage was specified as less than 1.25 μV on the 80 kHz setting of the high frequency cutoff dial, but this was exceeded during some of the experimental measurements because of an intermittent fault in the power supply transformer.

f) The square wave generator.
This unit supplied the square wave used during the determination of the hot-wire time constant.

D.3 THE USE OF THE HOT-WIRE ANEMOMETER - THE MEASUREMENT OF VELOCITY, TEMPERATURE AND TURBULENCE INTENSITY.

D.3.1 Introduction.

The methods of operation described below are those employed to obtain measurements of mean velocity, temperature and turbulence intensities using a normal single-wire probe.

D.3.2 Mean velocity measurements.

The procedure followed for both heated and unheated runs is outlined below:

i) The "cold" resistance, R_g, of the hot-wire was measured on the bridge unit, a very low heating current of 0.4 mA being employed so as not to heat the wire significantly above the temperature of the surrounding fluid. It was found that in this way resistances could be measured within ± 0.002 ohms and results reproducible within these limits could be obtained, except in flows where large temperature fluctuations occurred.

ii) The true R_g value was obtained by subtracting the leads resistance, R_L, from the R_g value measured above. (The value of R_L for a given probe was found, before a hot-wire was soldered to the wire supports, by bridging the gap between the tips of the wire supports with solder and then

measuring the probe resistance as described in i)).

iii) An overheating ratio (usually 0.5) was specified and the operating resistance, R_w, was calculated from the relationship

$$\text{overheating ratio} = \frac{R_w - R_g}{R_g}$$

iv) The effective R_w value was found by adding the leads resistance, R_L, to the R_w value obtained in iii).

v) One arm of the Kelvin bridge was set to the effective R_w value and the heating current through the hot-wire was increased until the bridge was balanced.

vi) The current, I, was measured on the potentiometer unit.

vii) The heating current was decreased and the cold resistance checked to make sure no changes of R_g, and hence of the overheating ratio, occurred during the reading. Because even slight changes in overheating ratio seriously affected the accuracy of the measurements, readings during which R_g changed by more than 0.01 ohms (or by more than 0.005 ohms in some cases) were discarded and the measurements repeated.

viii) The values of I, R_w and R_g were used to obtain mean velocity ($\bar{V}_z$) values from a previously determined calibration curve of

$$\frac{I^2 R_w}{R_w - R_g} \quad \text{vs} \quad \frac{1}{\bar{V}_z^2}.$$

The greatest problem encountered during the above procedure was balancing the bridge galvanometer. Particular difficulty was experienced in regions of high relative turbulence intensities and also close to the pipe wall during heated runs, where very slow fluctuations with occasional very large surges were noted. In both these cases it was necessary to observe the galvanometer over long periods to determine when the balance point had been reached. Under these conditions measured current values were less accurate than those determined under conditions of lower relative intensity, when readings reproducible within ± 0.01 mA could be obtained. Since a change of 0.01 mA corresponds to a change of only 0.01 to 0.03 ft/sec for the range of

velocities investigated it is clear that the present hot-wire anemometer system enabled very accurate velocity measurements to be made.

For the isothermal runs I-1 to I-17 an abbreviated but equally accurate version of the above method was employed. Since R_g, and hence R_w, were constant over the pipe cross-section it was necessary to set R_w only once, at the start of the velocity traverse. It was then sufficient, at each radial position where measurements were taken, only to rebalance the bridge and measure the current, I, before moving the probe to a new position. By measuring the cold resistance before (R_{g_1}) and after (R_{g_2}) the traverse, any slight changes in overheating ratio during the run could be allowed for.

D.3.3 Mean temperature measurements.

Since the current (0.4 mA) passing through the hot-wire during the measurement of R_g is low enough (< 1 mA) to prevent the wire temperature being raised significantly above the local flow temperature, then provided a calibration curve of R_g against temperature is prepared beforehand, flow temperatures can be determined directly from measured R_g values.

D.3.4 The measurement of turbulent velocity and temperature fluctuations.

The method described below was used in measuring turbulent velocity fluctuations in unheated flows and also in measuring combined velocity and temperature fluctuations in heated flows.

i) The time constant of the hot-wire was determined using a superimposed square wave method (described in the anemometer operating manual). The value of this time constant was found to be dependent on both air velocity and overheating ratio and a typical plot of time constant against radial position at different overheating ratios is shown in Fig. D.2.

ii) The value of the time constant was used to adjust the variable capacitor in the R-C compensation circuit to its correct setting.

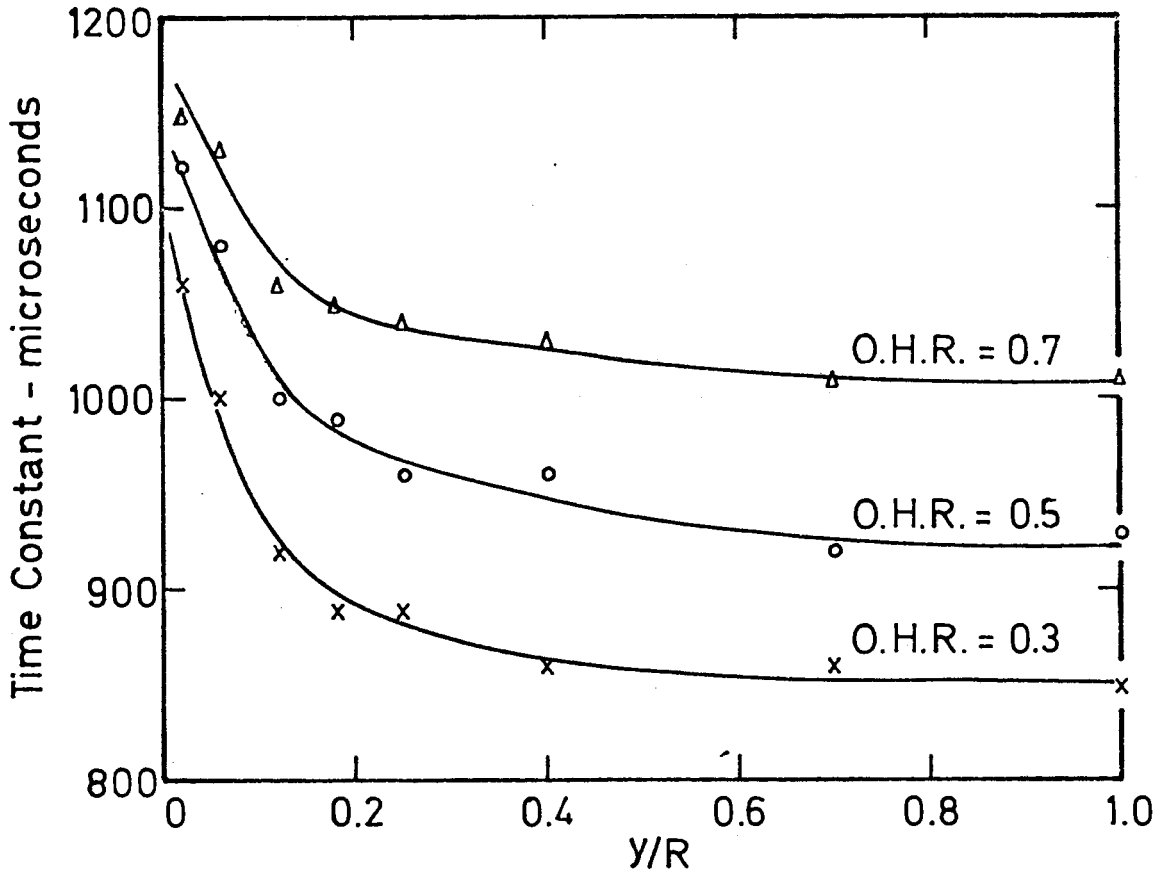

FIGURE D.2 VARIATION OF HOT-WIRE TIME CONSTANT WITH RADIAL POSITION AND OVERHEATING RATIO (O.H.R.)

iii) The hot-wire was balanced as described in section D.3.2 and the voltage signal across the hot-wire was connected to the input of the amplifier.

iv) The amplifier high and low cutoff switches were set to 20 kHz and 0.1 Hz respectively and the attenuation of the input signal reduced until a suitable reading (usually between 30% and 80% full scale, in order to avoid overloading the amplifier if sudden large fluctuations occurred) was obtained on the mean square meter. This meter reading fluctuated considerably because of the concentration of turbulent energy in the low frequency range and needed to be observed for periods of up to several minutes before an accurate mean value could be determined. Particular difficulty was experienced near the pipe wall where the pattern of slow fluctuations punctuated by occasional sudden bursts of energy made an average value very difficult to determine accurately. The meter reading was related to the root mean square value, $\sqrt{e^2}$, of the fluctuating voltage across the wire by

$$\sqrt{e^2} = \sqrt{\frac{y}{100}} \cdot 2^{x/6} \cdot 100\ \mu V \qquad (D.1)$$

where y = mean square meter reading

x = attenuation (db)

and $\sqrt{e^2}$ was in turn related to the turbulent velocity and temperature intensities by the sensitivity expressions given in Chapter 2.

The procedure followed to measure temperature intensities differed in several respects from that given above. In order to reduce the hot-wire sensitivity to velocity fluctuations the heating current employed was very low, and consequently the signal from the hot-wire was small. Under these circumstances the amount of noise introduced by the compensation circuit gave a very low signal to noise ratio and made the determination of accurate intensities very difficult. For these readings, therefore, the compensation circuit was not used. This procedure is believed to have introduced only slight errors since energy spectrum measurements showed the

frequency content of the signal to be very low above 300 Hz, the frequency at which compensation first became important for the present hot-wires.

APPENDIX E

EXPERIMENTS PERFORMED USING THE CALIBRATION DEVICE.

E.1 INTRODUCTION.

It was shown in Chapter 2 that information on the variation with temperature of the hot-wire calibration parameter A is contradictory, available experimental work suggesting that A decreases with increasing temperature while theoretical expressions predict that A increases with temperature. To resolve this contradiction the experiments described in later sections of this appendix were carried out using the calibration apparatus discussed in Chapter 3, section 3.10.3.

The essential part of this calibration apparatus was the contracting cone, designed according to the recommendations of Smith and Wang [102] to give a uniform velocity profile in the cone throat. With such a profile a knowledge of the flow temperature and of the total flow rate would be sufficient to give the throat velocity; by inserting a hot-wire into the throat and taking measurements at different temperatures and flow rates the calibration parameters of the wire could then be easily determined.

In practice it was found that the accuracy claimed by Smith and Wang for their design was unjustified and the velocity profile in the throat, though flat over most of the cross-section, showed significant departures from uniformity near the wall. To obtain the desired information on the temperature dependence of A it was therefore necessary to carry out the two sets of experiments summarised below:

i) The calibration curve at 25°C for the hot-wire was determined. Because of the non-linearity of the calibration curve at low velocities a relatively complicated method had to be employed to obtain this curve.

ii) The velocity profile in the throat was then determined at different temperatures in the range 30°C to 70°C, velocities being evaluated using the calibration curve for 25°C obtained in i) above. By integrating each of these profiles to get a mean velocity and comparing these

calculated mean values with those obtained from the known flowrate through the system, the errors introduced by using the 25°C calibration curve at higher temperatures could be evaluated. Since these errors were dependent solely on changes in the parameter A they provided a means of estimating the variations in A caused by changing temperatures.

These experiments, described in more detail in sections E.2 and E.3, showed conclusively that the variation of A with temperature was similar to that predicted by theory and that previous experimental results were incorrect. It was shown, further, that the equation (equation (2.23)) given by Hinze [40] represents the observed variations of A within the limits of experimental error.

E.2 DETERMINATION OF THE CALIBRATION CURVE FOR THE HOT-WIRE AT 25°C.

The procedure followed to obtain the above calibration curve, referred to in part i) of the previous section, is described below:

a) At a given flowrate, the hot-wire was traversed across the cone throat and values of the wire current at different radial positions were noted. This procedure was repeated at nine other flowrates and the results were used to prepare "current profile" plots such as those shown in Fig. E.1. At each flowrate the wet-gas meter reading and the air temperatures in the wet-gas meter and the cone throat were also noted. (The latter temperatures remained at 25°C ± 2°C.)

The results are reported in Tables E.1 and E.2.

b) For each flowrate the current, I_{max}, measured in the central region of the throat, was assumed to correspond to a velocity of about 1.2 $\overline{U}_{ave}$ ($\overline{U}_{ave}$ was found from the wet-gas meter reading) and from these values a plot of current I against velocity $\overline{U}$ was prepared. From this plot velocity profiles corresponding to the measured "current profiles" were evaluated. These profiles were integrated

and a mean throat velocity calculated.

c) The mean velocities obtained in b) were compared with the true $\bar{U}_{ave}$ values calculated from the wet-gas meter readings and from the observed differences a more accurate plot of current I vs velocity $\bar{U}$ was constructed. The procedure outlined in b) was then repeated until agreement between measured and calculated values of $\bar{U}_{ave}$ was within ± 1% at all flowrates. The final relationship, shown in Fig. E.2, was checked by preparing from it the plot of I^2 vs $\frac{1}{\bar{U}^2}$ shown in Fig E.3. From this figure it can be seen that the expected relationship, linear at values of $\frac{1}{\bar{U}^2}$ greater than about 1.5, and deviating from linear below that value, was in fact obtained, confirming that a satisfactory calibration curve for the hot-wire at 25°C had been developed.

The above readings together with those reported in Table E.3, also served another purpose, enabling the plot of $\frac{\bar{U}_{ave}}{\bar{U}_{max}}$ vs $\bar{U}_{ave}$ shown in Fig. E.4 to be prepared.

Having this plot made it a simple matter to calibrate other hot-wires in the calibration apparatus since the only measurements now required were the wet-gas meter reading and the air temperatures in the throat and the wet-gas meter - these readings gave $\bar{U}_{ave}$ and the velocity at the probe could then be found from Fig. E.4. As shown in Fig. 3.13 in Chapter 3 calibration points determined by this method agreed well (in the region of overlap) with those obtained in the test-section by calibrating the hot-wire against a pitot tube.

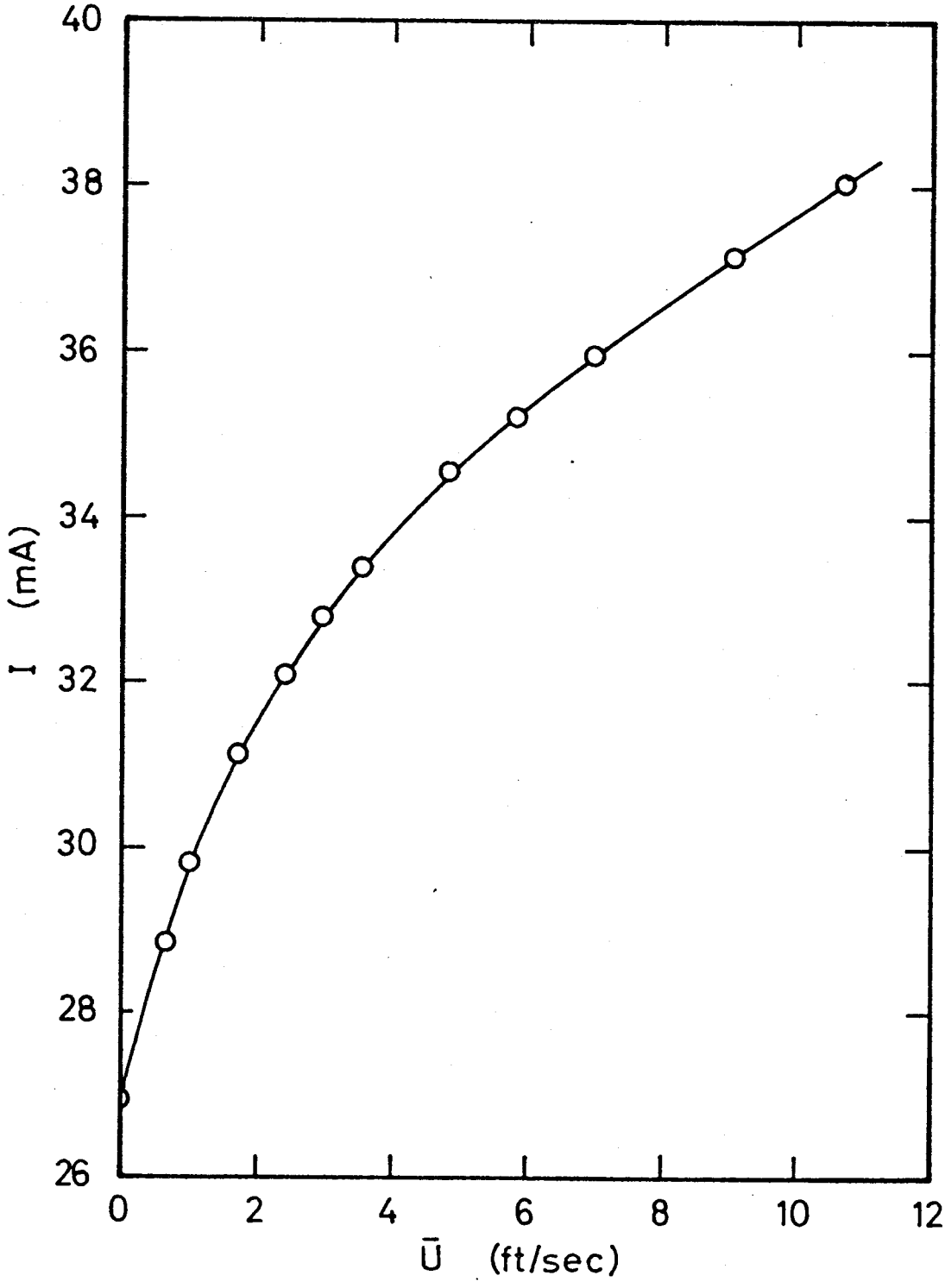

FIGURE E.2 FINAL CURRENT - VELOCITY RELATIONSHIP

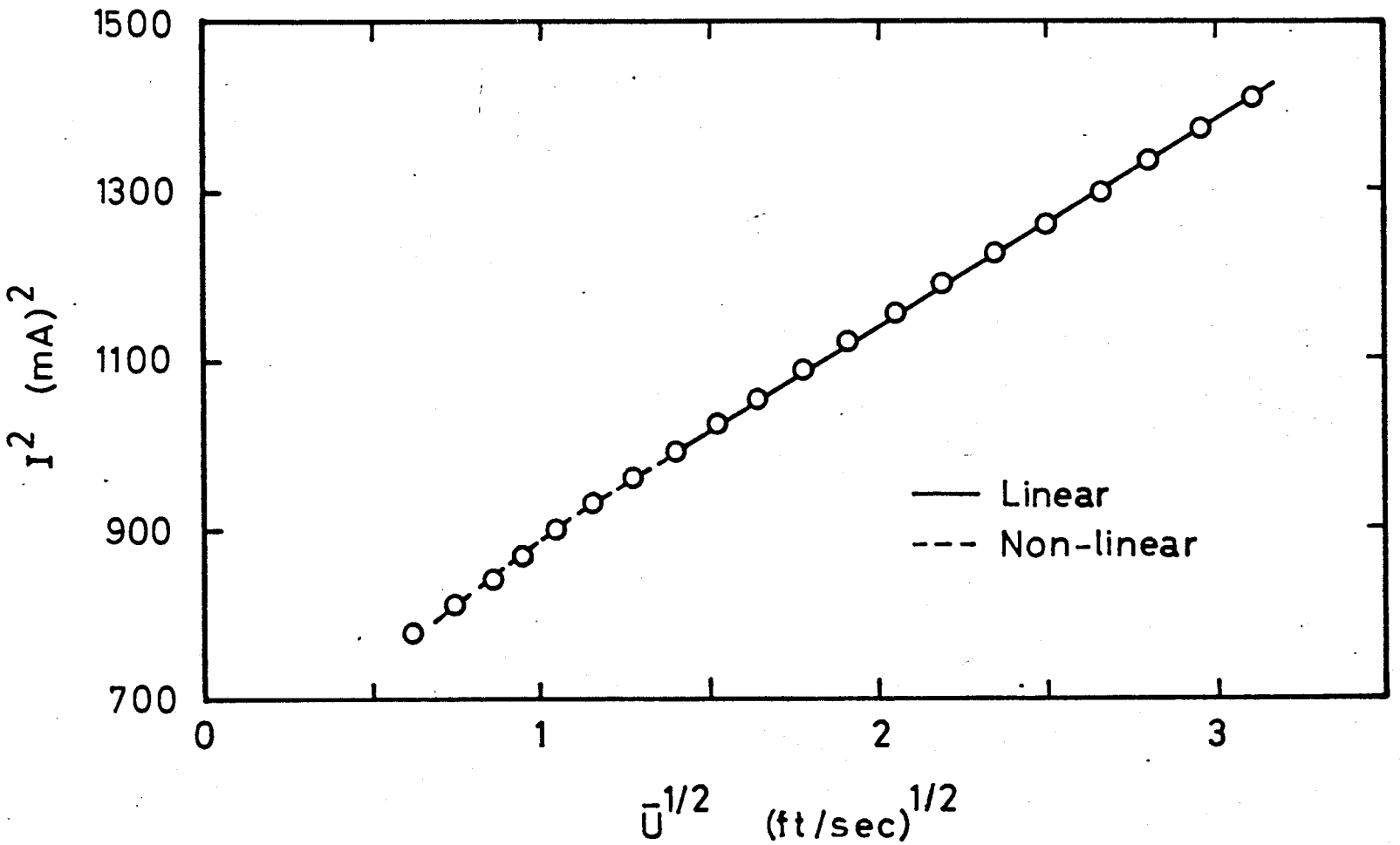

FIGURE E.3 CHECK ON FINAL CURRENT - VELOCITY RELATIONSHIP

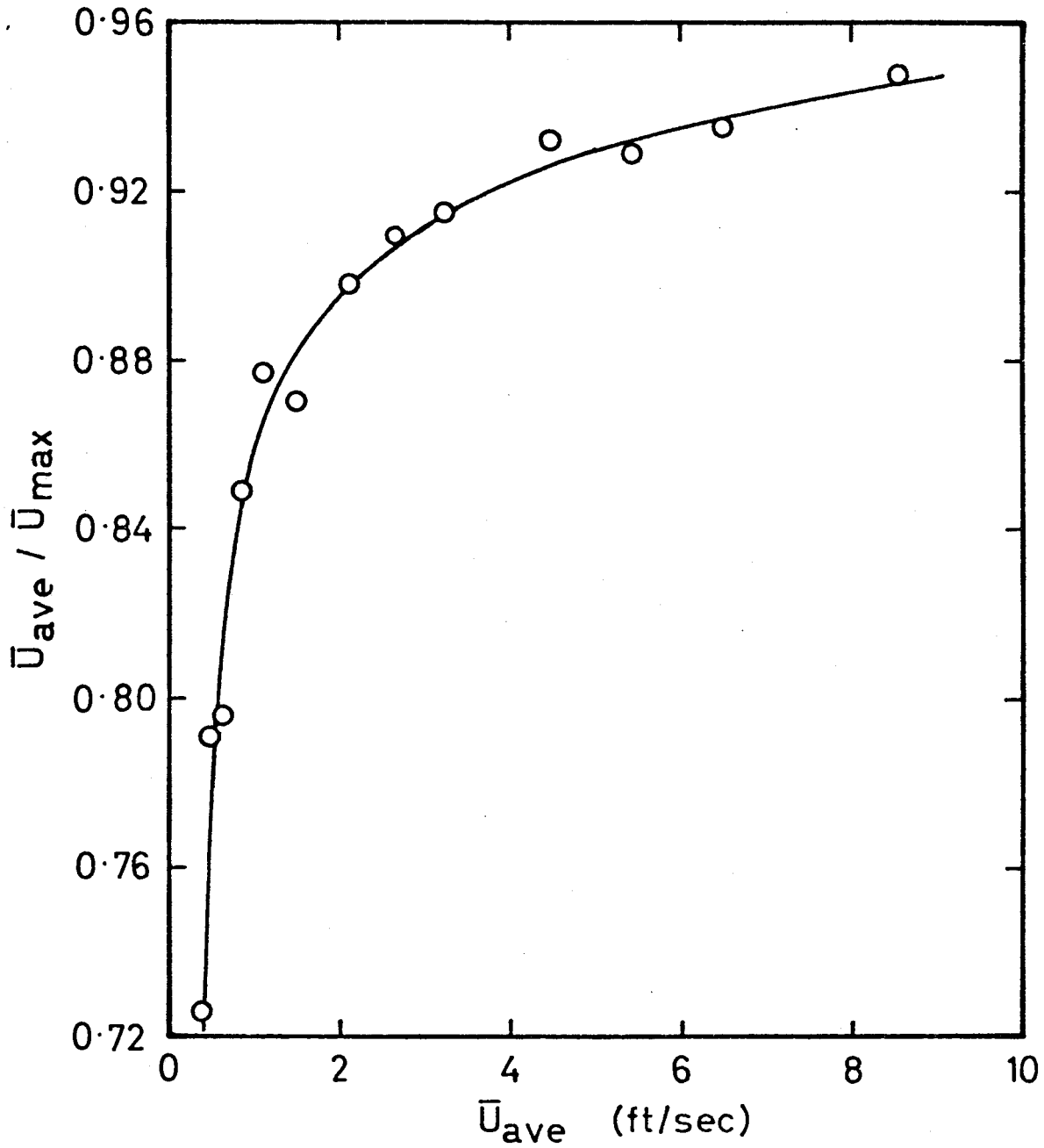

FIGURE E.4 RELATIONSHIP BETWEEN $\bar{U}_{max}$ AND $\bar{U}_{ave}$

TABLE E.1

RUN	A	B	C	D	E
Wet Gas Meter Reading - Seconds	510	308.5	180.5	126.5	99.8
Corresponding Average Velocity ft/sec	0.52	0.85	1.47	2.11	2.66
Air Temperature in Wet Gas Meter - ^{o}C	21.0	21.7	23.4	21.1	22.8
Air Temperature in Throat - ^{o}C	23.5	23.5	26.5	23.7	25.4
Corrected Average Velocity - ft/sec	0.52	0.855	1.49	2.13	2.68
U_{ave}/U_{max}	0.791	0.849	0.87	0.898	0.909

RUN	F	G	H	I	J
Wet Gas Meter Reading - Seconds	82.6	59.8	49.4	41.40	31.50
Corresponding Average Velocity ft/sec	3.23	4.43	5.39	6.47	8.44
Air Temperature in Wet Gas Meter - ^{o}C	22.4	21.4	21.8	21.8	23.1
Air Temperature in Throat - ^{o}C	26.0	24.5	25.4	24.9	27.0
Corrected Average Velocity - ft/sec	3.26	4.48	5.44	6.53	8.55
U_{ave}/U_{max}	0.915	0.926	0.929	0.935	0.948

TABLE E.2

RUN A		RUN B		RUN C		RUN D		RUN E	
y/R	I	y/R	I	y/R	I	y/R	I	y/R	I
1.0	28.82	1.0	29.775	1.0	31.095	1.0	32.015	1.0	32.815
0.5	28.835	0.35	29.80	0.2	31.095	0.1	31.615	0.2	32.80
0.05	27.38	0.2	29.66	0.05	29.22	0.2	32.02	0.1	32.485
1.0	28.835	1.0	29.84	1.0	31.14	1.0	32.03	1.0	32.805
0.2	28.51	0.1	28.955	0.1	30.48	0.02	28.81	0.02	29.405
0.02	27.60	0.02	27.80	0.02	28.25	1.0	32.08	0.05	31.255
1.0	28.835	1.0	29.815	1.0	31.12	0.05	30.32	1.0	32.835
0.1	27.88	0.05	28.00	0.15	30.81	0.15	31.99	0.15	32.815
0.35	28.81			0.2	31.08	0.2	32.09	0.12	32.66
						0.1	31.64	0.15	32.765
								1.0	32.825

RUN F		RUN G		RUN H		RUN I		RUN J	
y/R	I	y/R	I	y/R	I	y/R	I	y/R	I
1.0	33.39	1.0	34.55	1.0	35.235	1.0	35.96	1.0	37.125
0.2	33.39	0.5	34.57	0.15	35.23	0.2	35.96	0.2	37.165
0.05	31.95	0.05	33.32	0.1	35.09	0.1	35.87	0.05	36.39
1.0	33.385	0.2	34.56	0.12	35.22	0.05	34.965	1.0	37.165
0.02	29.915	1.0	34.56	0.15	35.225	1.0	35.95	0.1	37.095
0.1	33.13	0.1	34.41	0.05	34.06	0.15	35.91	0.02	33.98
1.0	33.39	0.02	31.09	0.02	31.79	0.02	32.535	1.0	37.165
0.15	33.395	0.15	34.60	1.0	35.235	0.12	35.88	0.15	37.16
0.12	33.33	1.0	34.60			1.0	35.965	0.05	36.44
		0.15	34.60					0.12	37.165
		0.12	34.545					0.1	37.14
		1.0	34.615					1.0	37.205

TABLE E.3

Probe Position y/R	1.0	1.0	1.0	1.0
Wire Current I mA	30.35	29.24	33.99	28.55
Wet Gas Meter Reading - Seconds	240.0	415.2	68.5	648.9
Corresponding Average Velocity ft/sec	1.10	0.64	3.87	0.41
Air Temperature in Wet Gas Meter ^{o}C	22.5	22.5	22.7	22.8
Air Temperature in Throat ^{o}C	24.1	24.7	24.9	25.3
Corrected Average Velocity - ft/sec	1.11	0.645	3.90	0.41
U_{max} - ft/sec	1.265	0.81	4.165	0.565
U_{ave}/U_{max}	0.877	0.796	0.935	0.726

E.3 MEASUREMENTS IN HEATED FLOWS.

The procedure summarised in part ii) of section E.1 is described in more detail below:

a) The power supply to the air heater was set to the desired value and the calibration system left for 4 to 5 hours to reach a steady temperature.

b) A "current profile" similar to those shown in Fig. E.1 was measured using the hot-wire previously calibrated at 25°C as described in section E.2. Wet-gas meter readings and air temperatures in the throat and the wet-gas meter were also recorded.

c) Using the 25°C calibration curve the measured current profile was transformed into the corresponding velocity profile and this was integrated to give a mean velocity. This calculated mean velocity was compared with the true mean velocity obtained from the wet-gas meter reading and the percentage difference between the measured and true velocities was plotted as % Error in Fig. E.5.

This procedure was repeated over a range of temperatures between 30°C and 70°C and the results are reported in Tables E.4 and E.5 and shown in Fig. E.5. The scatter of points is seen to be large but this is understandable in view of the fact that inaccuracies of as little as ± 0.5% in the measured wet-gas meter reading would greatly affect the relative positions of points on this figure. Despite the scatter in the points, however, Fig. E.5 enables several important observations to be made:

i) Errors introduced by using a calibration equation measured at one temperature for results measured in a flow at a different temperature are small - as little as 2% after a 40°C temperature change.

ii) It is shown conclusively that the variations of calibration parameters with temperature are positive and increase with increasing temperature, a trend opposite to that reported for previous experimental results and in agreement with theoretical predictions.

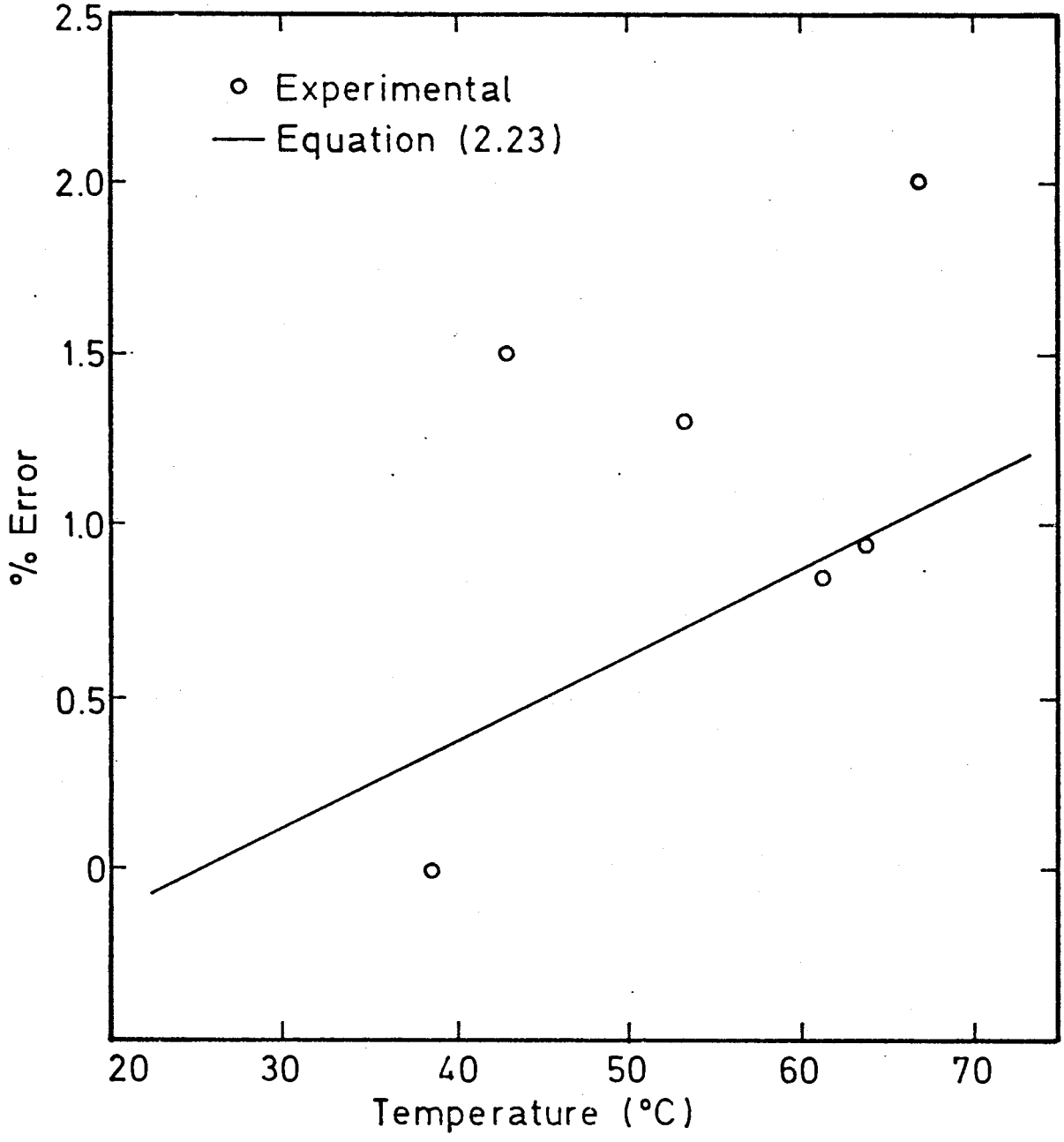

FIGURE E.5 ERRORS INTRODUCED WHEN A CALIBRATION CURVE OBTAINED AT 25°C IS USED AT OTHER TEMPERATURES

iii) The variations with temperature predicted by Hinze's [40] equation, equation (2.23), and shown on Fig. E.5, lie close to, if somewhat below, the mean line through the measured points and can be assumed to represent them adequately within the limits of experimental error.

Since the values of A and B (1945 and 731 respectively, at 25°C) are known, it is possible to estimate the temperature dependence of A from the above results. Assuming a mean velocity of about 9 ft/sec, comparable to those used in the above experiment (see Tables E.4 and E.5) and taking the "% Error" at 65°C to be 2%, a simple calculation shows that the increase in A is of the order of 0.02 - 0.03% per °C. This is very different from the figure of -0.15% per °C obtained, according to Lawn [65], by Cooper and Collis.

TABLE E.4

RUN	H1	H2	H3	H4	H5	H6
Wet Gas Meter Reading Seconds	30.75	30.45	31.29	30.95	33.25	30.98
Corresponding Average Velocity ft/sec	8.66	8.74	8.49	8.59	8.02	8.58
Air Temperature in Wet Gas Meter °C	22.7	22.3	22.8	22.5	18.7	19.5
Air Temperature in Throat °C	38.7	67.0	53.5	61.7	40.3	64.0
Corrected Average Velocity	9.13	10.06	9.44	9.73	8.62	9.88
Integrated Velocity from Profile	9.13	10.26	9.57	9.82	8.75	9.97
% Difference (% Error)	0.0	2.0	1.3	0.85	1.5	0.94

TABLE E.5

H 1		H 2		H 3	
y/R	I	y/R	I	y/R	I
1.0	37.515	0.2	38.025	1.0	37.715
0.2	37.47	0.1	37.95	0.15	37.70
0.1	37.39	1.0	38.025	0.1	37.64
0.05	36.69	0.02	35.075	1.0	37.72
1.0	37.505	0.05	37.275	0.12	37.685
0.15	37.48	1.0	38.05	0.02	34.80
0.02	34.32	0.15	38.05	1.0	37.715
0.35	37.485	0.1	38.005	0.05	36.985
1.0	37.46				
0.12	37.42				

H 4		H 5		H 6	
y/R	I	y/R	I	y/R	I
1.0	37.85	1.0	37.22	1.0	37.92
0.2	37.835	0.2	37.23	0.15	37.89
0.05	37.09	0.05	36.515	0.2	37.90
1.0	37.83	1.0	37.28	0.1	37.83
0.1	37.74	0.15	37.26	1.0	37.905
0.02	34.985	0.1	37.195	0.02	35.06
0.15	37.83	0.02	34.55	0.05	37.205
0.05	37.095			1.0	37.94
0.12	37.775				

APPENDIX F

ISOTHERMAL VELOCITY AND TURBULENCE MEASUREMENTS

F.1 RESULTS

Isothermal velocity and turbulence measurements are summarised in Tables F.1, F.2 and F.3 which follow. Table F.1 gives the isothermal velocity measurements for runs I-1 to I-17 and IT-1 to IT-5; Table F.2 gives the smoothed velocity profiles obtained from the results in Table F.1, together with the values of the eddy diffusivity of momentum computed from these smoothed profiles; Table F.3 gives the isothermal turbulence measurements for runs IT-1, IT-3, IT-4 and IT-5.

Sample calculation procedures for the above results are given in Appendix G.

TABLE F.1

ISOTHERMAL VELOCITY MEASUREMENTS

ISOTHERMAL VELOCITY PROFILE I- 1

REYNOLDS NUMBER 6966.

HOT-WIRE MEASUREMENTS

INITIAL COLD RESISTANCE RG(1)	14.945	OHMS
FINAL COLD RESISTANCE RG(2)	14.915	OHMS
HOT (OPERATING) RESISTANCE Rh	22.585	OHMS
CALIBRATION CURVE INTERCEPT A	2059.2	
CALIBRATION CURVE SLOPE B	648.0	
AIR TEMPERATURE	68.0	DEG.F.

CALCULATED RESULTS

AVERAGE VELOCITY	3.48	FT/SEC
FRICTION FACTOR	0.00852	
FRICTION VELOCITY	0.227	FT/SEC

Y/R	CURRENT MILLIAMPS	VELOCITY FT/SEC	CORRECTED VELOCITY FT/SEC	Y+	U+	U/UM	U/UC	UC-U / U+
1.301	33.965	4.35	4.35	158.94	19.12	1.248	0.956	0.87
1.201	34.070	4.48	4.48	181.68	19.69	1.285	0.984	0.30
1.101	34.105	4.53	4.53	204.42	19.91	1.299	0.995	0.08
1.001	34.125	4.55	4.55	227.61	19.99	1.305	1.000	0.00
0.901	34.110	4.53	4.53	204.87	19.91	1.299	0.995	0.08
0.801	34.075	4.48	4.48	182.13	19.69	1.285	0.984	0.30
0.701	34.000	4.38	4.38	159.39	19.25	1.256	0.962	0.74
0.601	33.920	4.28	4.28	136.65	18.81	1.228	0.940	1.18
0.501	33.810	4.14	4.14	113.92	18.20	1.188	0.910	1.79
0.401	33.650	3.94	3.94	91.18	17.32	1.130	0.866	2.67
0.301	33.470	3.72	3.72	68.44	16.36	1.068	0.818	3.63
0.201	33.250	3.46	3.46	45.70	15.22	0.993	0.761	4.77
0.181	33.185	3.39	3.39	41.15	14.91	0.973	0.745	5.07
0.161	33.130	3.33	3.33	36.60	14.65	0.956	0.732	5.34
0.141	33.080	3.27	3.28	32.06	14.39	0.939	0.719	5.60
0.121	32.920	3.10	3.11	27.51	13.65	0.891	0.682	6.34
0.101	32.850	3.02	3.03	22.96	13.31	0.869	0.665	6.68
0.081	32.540	2.71	2.72	18.41	11.96	0.781	0.598	8.02
0.061	32.220	2.41	2.43	13.87	10.67	0.697	0.534	9.31
0.041	31.720	1.97	1.98	9.32	8.70	0.568	0.435	11.29
0.031	31.200	1.58	1.59	7.04	6.98	0.456	0.349	13.00
0.021	30.490	1.11	1.11	4.77	4.87	0.318	0.243	15.11
0.016	30.020	0.86	0.86	3.63	3.77	0.246	0.189	16.21
0.011	29.490	0.61	0.61	2.50	2.68	0.175	0.134	17.31
0.006	28.890	0.39	0.39	1.36	1.71	0.111	0.085	18.28

TABLE F.1 (Contd)

ISOTHERMAL VELOCITY PROFILE I- 2

REYNOLDS NUMBER 6985.

HOT-WIRE MEASUREMENTS

INITIAL COLD RESISTANCE RG(1)	14.945	OHMS
FINAL COLD RESISTANCE RG(2)	14.915	OHMS
HOT (OPERATING) RESISTANCE Rw	22.585	OHMS
CALIBRATION CURVE INTERCEPT A	2059.2	
CALIBRATION CURVE SLOPE B	648.0	
AIR TEMPERATURE	68.0	DEG.F.

CALCULATED RESULTS

AVERAGE VELOCITY	3.49	FT/SEC
FRICTION FACTOR	0.00851	
FRICTION VELOCITY	0.228	FT/SEC

Y/R	CURRENT MILLIAMPS	VELOCITY FT/SEC	CORRECTED VELOCITY FT/SEC	Y+	U+	U/UM	U/UC	UC-U / U+
1.001	34.145	4.54	4.54	228.14	19.90	1.299	1.000	0.00
0.901	34.135	4.52	4.52	205.34	19.82	1.293	0.995	0.08
0.801	34.090	4.46	4.46	182.55	19.55	1.276	0.982	0.35
0.701	34.025	4.37	4.37	159.76	19.16	1.250	0.962	0.74
0.601	33.950	4.27	4.27	136.97	18.72	1.222	0.940	1.17
0.501	33.815	4.10	4.10	114.18	17.98	1.173	0.903	1.92
0.401	33.700	3.96	3.96	91.39	17.37	1.133	0.872	2.53
0.301	33.520	3.74	3.74	68.60	16.41	1.070	0.824	3.49
0.201	33.290	3.47	3.47	45.81	15.23	0.993	0.765	4.67
0.181	33.215	3.39	3.39	41.25	14.88	0.971	0.747	5.02
0.161	33.210	3.38	3.38	36.69	14.84	0.968	0.745	5.06
0.141	33.110	3.27	3.28	32.13	14.36	0.937	0.721	5.54
0.121	33.000	3.15	3.16	27.57	13.84	0.903	0.695	6.06
0.101	32.865	3.01	3.02	23.01	13.23	0.863	0.664	6.66
0.081	32.650	2.79	2.80	18.46	12.29	0.802	0.617	7.61
0.061	32.320	2.47	2.49	13.90	10.91	0.712	0.548	8.98
0.041	31.720	1.95	1.96	9.34	8.59	0.560	0.431	11.31
0.031	31.290	1.62	1.63	7.06	7.14	0.466	0.359	12.75
0.021	30.590	1.16	1.16	4.78	5.08	0.331	0.255	14.82
0.016	30.110	0.89	0.89	3.64	3.90	0.254	0.196	16.00
0.011	29.610	0.65	0.65	2.50	2.85	0.185	0.143	17.05
0.006	29.030	0.42	0.42	1.36	1.84	0.120	0.092	18.06

ISOTHERMAL VELOCITY PROFILE I- 3

REYNOLDS NUMBER 6777.

HOT-WIRE MEASUREMENTS

INITIAL COLD RESISTANCE RG(1)	14.675	OHMS
FINAL COLD RESISTANCE RG(2)	14.645	OHMS
HOT (OPERATING) RESISTANCE Rw	22.475	OHMS
CALIBRATION CURVE INTERCEPT A	2039.6	
CALIBRATION CURVE SLOPE B	656.6	
AIR TEMPERATURE	69.8	DEG.F.

CALCULATED RESULTS

AVERAGE VELOCITY	3.41	FT/SEC
FRICTION FACTOR	0.00858	
FRICTION VELOCITY	0.223	FT/SEC

Y/R	CURRENT MILLIAMPS	VELOCITY FT/SEC	CORRECTED VELOCITY FT/SEC	Y+	U+	U/UM	U/UC	UC-U / U+
1.002	34.010	4.42	4.42	222.49	19.77	1.295	1.000	0.00
0.902	34.000	4.41	4.41	200.29	19.72	1.292	0.997	0.04
0.802	33.970	4.36	4.36	178.08	19.50	1.278	0.986	0.26
0.702	33.920	4.30	4.30	155.88	19.23	1.260	0.973	0.53
0.602	33.830	4.18	4.18	133.67	18.70	1.225	0.945	1.06
0.502	33.710	4.03	4.03	111.47	18.03	1.181	0.912	1.73
0.402	33.600	3.89	3.89	89.26	17.41	1.140	0.880	2.36
0.302	33.410	3.67	3.67	67.05	16.42	1.076	0.830	3.34
0.202	33.175	3.40	3.40	44.85	15.22	0.997	0.770	4.54
0.182	33.140	3.36	3.36	40.41	15.04	0.986	0.761	4.72
0.162	33.060	3.27	3.27	35.97	14.64	0.959	0.740	5.12
0.142	32.970	3.17	3.18	31.53	14.20	0.930	0.718	5.56
0.122	32.880	3.07	3.08	27.09	13.76	0.901	0.696	6.00
0.102	32.730	2.91	2.92	22.64	13.05	0.855	0.660	6.71
0.082	32.520	2.70	2.71	18.20	12.13	0.795	0.613	7.63
0.062	32.165	2.37	2.39	13.76	10.69	0.700	0.540	9.06
0.042	31.580	1.88	1.89	9.32	8.45	0.554	0.427	11.31
0.032	31.075	1.51	1.52	7.10	6.79	0.445	0.343	12.97
0.022	30.410	1.09	1.09	4.88	4.87	0.319	0.246	14.89
0.017	29.940	0.84	0.84	3.77	3.75	0.246	0.190	16.01
0.012	29.450	0.62	0.62	2.66	2.77	0.181	0.140	16.99
0.007	28.860	0.40	0.40	1.55	1.78	0.117	0.090	17.98

TABLE F.1 (Contd)

ISOTHERMAL VELOCITY PROFILE I- 4

REYNOLDS NUMBER 7325.

HOT-WIRE MEASUREMENTS

INITIAL COLD RESISTANCE RG(1)	15.762	OHMS
FINAL COLD RESISTANCE RG(2)	15.766	OHMS
HOT (OPERATING) RESISTANCE RW	23.640	OHMS
CALIBRATION CURVE INTERCEPT A	1880.0	
CALIBRATION CURVE SLOPE B	718.2	
AIR TEMPERATURE	64.4	DEG.F.

CALCULATED RESULTS

AVERAGE VELOCITY	3.62	FT/SEC
FRICTION FACTOR	0.00840	
FRICTION VELOCITY	0.234	FT/SEC

Y/R	CURRENT MILLIAMPS	VELOCITY FT/SEC	CORRECTED VELOCITY FT/SEC	Y+	U+	U/UM	U/UC	UC-U / U+
1.097	33.780	4.62	4.62	214.41	19.68	1.276	0.993	0.12
0.997	33.805	4.65	4.65	236.73	19.81	1.284	1.000	0.00
0.897	33.795	4.64	4.64	212.98	19.76	1.281	0.997	0.04
0.797	33.750	4.59	4.59	189.24	19.55	1.267	0.987	0.25
0.697	33.685	4.51	4.51	165.49	19.21	1.245	0.970	0.59
0.597	33.580	4.39	4.39	141.75	18.70	1.212	0.944	1.10
0.497	33.460	4.25	4.25	118.00	18.11	1.174	0.914	1.69
0.397	33.340	4.11	4.11	94.26	17.51	1.135	0.884	2.29
0.297	33.150	3.90	3.90	70.52	16.62	1.077	0.839	3.18
0.197	32.935	3.67	3.67	46.77	15.65	1.014	0.790	4.15
0.177	32.855	3.59	3.59	42.02	15.31	0.992	0.772	4.49
0.157	32.755	3.49	3.49	37.27	14.88	0.965	0.751	4.92
0.137	32.690	3.42	3.43	32.52	14.59	0.946	0.736	5.21
0.117	32.515	3.24	3.25	27.78	13.83	0.896	0.698	5.97
0.097	32.385	3.12	3.13	23.03	13.33	0.864	0.672	6.47
0.077	32.025	2.79	2.80	18.28	11.94	0.774	0.602	7.86
0.057	31.660	2.47	2.49	13.53	10.60	0.687	0.535	9.20
0.037	30.790	1.81	1.82	8.78	7.75	0.502	0.391	12.05
0.027	30.210	1.43	1.44	6.41	6.13	0.397	0.309	13.67
0.017	29.255	0.92	0.92	4.03	3.91	0.254	0.197	15.89
0.012	28.670	0.67	0.67	2.84	2.85	0.185	0.144	16.95
0.007	28.150	0.48	0.48	1.66	2.04	0.132	0.103	17.76

ISOTHERMAL VELOCITY PROFILE I- 5

REYNOLDS NUMBER 11334.

HOT-WIRE MEASUREMENTS

INITIAL COLD RESISTANCE RG(1)	18.470	OHMS
FINAL COLD RESISTANCE RG(2)	18.440	OHMS
HOT (OPERATING) RESISTANCE RW	27.870	OHMS
CALIBRATION CURVE INTERCEPT A	1821.9	
CALIBRATION CURVE SLOPE B	668.5	
AIR TEMPERATURE	68.0	DEG.F.

CALCULATED RESULTS

AVERAGE VELOCITY	5.67	FT/SEC
FRICTION FACTOR	0.00747	
FRICTION VELOCITY	0.346	FT/SEC

Y/R	CURRENT MILLIAMPS	VELOCITY FT/SEC	CORRECTED VELOCITY FT/SEC	Y+	U+	U/UM	U/UC	UC-U / U+
1.205	34.805	7.01	7.01	275.51	20.21	1.236	0.979	0.43
1.105	34.865	7.10	7.10	310.16	20.47	1.252	0.991	0.17
1.005	34.900	7.16	7.16	348.28	20.64	1.262	1.000	0.00
0.905	34.890	7.14	7.14	313.63	20.59	1.259	0.997	0.05
0.805	34.850	7.07	7.07	278.97	20.38	1.246	0.987	0.25
0.705	34.770	6.93	6.93	244.32	19.98	1.222	0.968	0.65
0.605	34.660	6.75	6.75	209.66	19.46	1.190	0.942	1.17
0.505	34.540	6.56	6.56	175.00	18.92	1.157	0.916	1.72
0.405	34.380	6.31	6.31	140.35	18.20	1.113	0.881	2.44
0.305	34.200	6.03	6.03	105.69	17.39	1.063	0.842	3.24
0.205	33.960	5.68	5.69	71.04	16.39	1.002	0.794	4.25
0.185	33.900	5.59	5.60	64.11	16.13	0.986	0.781	4.51
0.165	33.855	5.52	5.53	57.18	15.93	0.974	0.771	4.71
0.145	33.790	5.43	5.44	50.25	15.68	0.958	0.759	4.96
0.125	33.675	5.26	5.27	43.31	15.19	0.929	0.735	5.45
0.105	33.540	5.08	5.09	36.38	14.68	0.897	0.711	5.96
0.085	33.350	4.82	4.84	29.45	13.94	0.853	0.675	6.69
0.065	33.070	4.47	4.50	22.52	12.96	0.792	0.627	7.68
0.045	32.570	3.87	3.91	15.59	11.27	0.689	0.546	9.37
0.035	32.035	3.29	3.35	12.12	9.64	0.589	0.467	10.99
0.025	31.260	2.55	2.61	8.66	7.52	0.460	0.364	13.12
0.020	30.765	2.13	2.21	6.93	6.37	0.389	0.308	14.27
0.015	30.030	1.59	1.62	5.19	4.67	0.285	0.226	15.97
0.010	29.300	1.15	1.17	3.46	3.37	0.206	0.163	17.27

TABLE F.1 (Contd)

ISOTHERMAL VELOCITY PROFILE I- 6

REYNOLDS NUMBER 11650.

HOT-WIRE MEASUREMENTS

INITIAL COLD RESISTANCE RG(1)	16.221	OHMS
FINAL COLD RESISTANCE RG(2)	16.220	OHMS
HOT (OPERATING) RESISTANCE Rw	24.495	OHMS
CALIBRATION CURVE INTERCEPT A	1868.2	
CALIBRATION CURVE SLOPE B	670.6	
AIR TEMPERATURE	62.6	DEG.F.

CALCULATED RESULTS

AVERAGE VELOCITY	5.72	FT/SEC
FRICTION FACTOR	0.00742	
FRICTION VELOCITY	0.348	FT/SEC

Y/R	CURRENT MILLIAMPS	VELOCITY FT/SEC	CORRECTED VELOCITY FT/SEC	Y+	U+	U/UM	U/UC	UC-U / U+
1.193	35.140	7.10	7.10	286.43	20.35	1.240	0.980	0.40
1.093	35.195	7.19	7.19	321.92	20.61	1.256	0.993	0.14
0.993	35.225	7.24	7.24	352.44	20.76	1.264	1.000	0.00
0.893	35.200	7.20	7.20	316.95	20.64	1.258	0.994	0.11
0.793	35.155	7.12	7.12	281.46	20.41	1.244	0.983	0.34
0.693	35.065	6.98	6.98	245.96	20.01	1.219	0.964	0.74
0.593	34.970	6.82	6.82	210.47	19.56	1.191	0.942	1.20
0.493	34.835	6.61	6.61	174.98	18.96	1.155	0.913	1.80
0.393	34.670	6.35	6.35	139.48	18.21	1.109	0.877	2.54
0.293	34.465	6.04	6.04	103.99	17.33	1.055	0.834	3.43
0.193	34.200	5.65	5.66	68.50	16.21	0.988	0.781	4.54
0.173	34.125	5.54	5.55	61.40	15.90	0.968	0.766	4.85
0.153	34.040	5.42	5.43	54.30	15.56	0.948	0.749	5.19
0.133	33.975	5.33	5.34	47.20	15.30	0.932	0.737	5.45
0.113	33.875	5.19	5.20	40.10	14.90	0.908	0.718	5.85
0.093	33.700	4.96	4.97	33.00	14.25	0.868	0.686	6.50
0.073	33.450	4.63	4.65	25.91	13.32	0.812	0.642	7.43
0.053	33.070	4.17	4.20	18.81	12.03	0.733	0.579	8.72
0.033	32.260	3.27	3.32	11.71	9.51	0.579	0.458	11.24
0.023	31.550	2.58	2.64	8.16	7.57	0.461	0.364	13.19
0.013	30.255	1.57	1.60	4.61	4.58	0.279	0.220	16.17
0.008	29.300	1.01	1.03	2.83	2.95	0.179	0.142	17.80

ISOTHERMAL VELOCITY PROFILE I- 7

REYNOLDS NUMBER 11412.

HOT-WIRE MEASUREMENTS

INITIAL COLD RESISTANCE RG(1)	16.101	OHMS
FINAL COLD RESISTANCE RG(2)	16.090	OHMS
HOT (OPERATING) RESISTANCE RW	24.315	OHMS
CALIBRATION CURVE INTERCEPT A	1911.6	
CALIBRATION CURVE SLOPE B	661.1	
AIR TEMPERATURE	60.8	DEG.F.

CALCULATED RESULTS

AVERAGE VELOCITY	5.57	FT/SEC
FRICTION FACTOR	0.00746	
FRICTION VELOCITY	0.340	FT/SEC

Y/R	CURRENT MILLIAMPS	VELOCITY FT/SEC	CORRECTED VELOCITY FT/SEC	Y+	U+	U/UM	U/UC	UC-U / U+
0.998	35.215	7.08	7.08	347.91	20.79	1.270	1.000	0.00
0.898	35.195	7.05	7.05	313.05	20.71	1.265	0.995	0.08
0.798	35.145	6.96	6.96	278.19	20.44	1.249	0.983	0.35
0.698	35.060	6.82	6.82	243.33	20.03	1.224	0.963	0.76
0.598	34.965	6.66	6.66	208.46	19.56	1.195	0.940	1.22
0.498	34.830	6.45	6.45	173.60	18.95	1.157	0.911	1.84
0.398	34.670	6.19	6.19	138.74	18.19	1.111	0.874	2.60
0.298	34.480	5.90	5.90	103.88	17.34	1.059	0.833	3.45
0.198	34.215	5.51	5.52	69.02	16.20	0.989	0.778	4.59
0.178	34.150	5.42	5.43	62.05	15.93	0.973	0.766	4.85
0.158	34.065	5.30	5.31	55.08	15.58	0.952	0.749	5.20
0.138	34.005	5.21	5.22	48.10	15.32	0.936	0.736	5.47
0.118	33.895	5.06	5.07	41.13	14.89	0.909	0.715	5.90
0.098	33.730	4.83	4.84	34.16	14.22	0.869	0.683	6.57
0.078	33.540	4.58	4.60	27.19	13.50	0.825	0.649	7.29
0.058	33.245	4.21	4.24	20.21	12.44	0.760	0.598	8.35
0.038	32.630	3.50	3.54	13.24	10.40	0.635	0.500	10.38
0.028	32.040	2.89	2.95	9.76	8.66	0.529	0.416	12.12
0.018	31.055	2.02	2.10	6.27	6.16	0.376	0.296	14.62
0.013	30.300	1.47	1.50	4.53	4.40	0.269	0.211	16.39
0.008	29.440	0.97	0.98	2.78	2.87	0.175	0.138	17.91

TABLE F.1 (Contd)

ISOTHERMAL VELOCITY PROFILE I- 8

REYNOLDS NUMBER 11172.

HOT-WIRE MEASUREMENTS

INITIAL COLD RESISTANCE RG(1)	16.179	OHMS
FINAL COLD RESISTANCE RG(2)	16.185	OHMS
HOT (OPERATING) RESISTANCE RW	24.331	OHMS
CALIBRATION CURVE INTERCEPT A	2014.7	
CALIBRATION CURVE SLOPE B	637.5	
AIR TEMPERATURE	62.6	DEG.F.

CALCULATED RESULTS

AVERAGE VELOCITY	5.48	FT/SEC
FRICTION FACTOR	0.00750	
FRICTION VELOCITY	0.336	FT/SEC

Y/R	CURRENT MILLIAMPS	VELOCITY FT/SEC	CORRECTED VELOCITY FT/SEC	Y+	U+	U/UM	U/UC	UC-U / U*
0.997	35.200	6.97	6.97	341.21	20.72	1.269	1.000	0.00
0.897	35.180	6.94	6.94	306.98	20.63	1.264	0.995	0.08
0.797	35.140	6.87	6.87	272.76	20.43	1.251	0.985	0.29
0.697	35.065	6.74	6.74	238.54	20.04	1.228	0.967	0.68
0.597	34.970	6.58	6.58	204.31	19.57	1.199	0.944	1.15
0.497	34.835	6.36	6.36	170.09	18.91	1.159	0.912	1.80
0.397	34.685	6.12	6.12	135.86	18.20	1.115	0.878	2.51
0.297	34.480	5.79	5.79	101.64	17.22	1.055	0.831	3.49
0.197	34.230	5.41	5.42	67.42	16.10	0.986	0.776	4.62
0.177	34.160	5.31	5.32	60.57	15.80	0.968	0.762	4.91
0.157	34.080	5.20	5.21	53.73	15.48	0.948	0.746	5.24
0.137	34.010	5.09	5.10	46.88	15.15	0.928	0.731	5.56
0.117	33.895	4.93	4.94	40.04	14.68	0.899	0.708	6.03
0.097	33.775	4.77	4.78	33.19	14.22	0.871	0.686	6.50
0.077	33.570	4.49	4.51	26.35	13.40	0.821	0.646	7.32
0.057	33.240	4.06	4.09	19.50	12.15	0.744	0.586	8.57
0.037	32.660	3.37	3.41	12.66	10.15	0.621	0.489	10.57
0.027	32.060	2.74	2.80	9.24	8.33	0.510	0.402	12.39
0.017	31.130	1.90	1.98	5.81	5.88	0.360	0.284	14.83
0.012	30.400	1.37	1.40	4.10	4.16	0.255	0.200	16.56
0.007	29.605	0.89	0.90	2.39	2.67	0.163	0.129	18.05

ISOTHERMAL VELOCITY PROFILE I- 9

REYNOLDS NUMBER 12357.

HOT-WIRE MEASUREMENTS

INITIAL COLD RESISTANCE RG(1)	15.885	OHMS
FINAL COLD RESISTANCE RG(2)	15.910	OHMS
HOT (OPERATING) RESISTANCE RW	23.825	OHMS
CALIBRATION CURVE INTERCEPT A	1688.9	
CALIBRATION CURVE SLOPE B	711.1	
AIR TEMPERATURE	64.4	DEG.F.

CALCULATED RESULTS

AVERAGE VELOCITY	6.10	FT/SEC
FRICTION FACTOR	0.00731	
FRICTION VELOCITY	0.369	FT/SEC

Y/R	CURRENT MILLIAMPS	VELOCITY FT/SEC	CORRECTED VELOCITY FT/SEC	Y+	U+	U/UM	U/UC	UC-U / U*
1.105	34.840	7.55	7.55	334.36	20.44	1.236	0.994	0.10
1.005	34.865	7.59	7.59	375.46	20.55	1.242	1.000	0.00
0.905	34.845	7.56	7.56	338.10	20.47	1.237	0.996	0.08
0.805	34.800	7.49	7.49	300.74	20.28	1.226	0.986	0.27
0.705	34.720	7.37	7.37	263.38	19.95	1.206	0.971	0.59
0.605	34.605	7.19	7.19	226.02	19.47	1.177	0.947	1.07
0.505	34.475	6.99	6.99	188.66	18.93	1.144	0.921	1.61
0.405	34.325	6.77	6.77	151.30	18.33	1.108	0.892	2.21
0.305	34.130	6.48	6.48	113.94	17.55	1.061	0.854	2.99
0.205	33.890	6.14	6.15	76.58	16.64	1.006	0.809	3.91
0.185	33.835	6.06	6.07	69.11	16.42	0.993	0.799	4.12
0.165	33.765	5.97	5.98	61.64	16.18	0.978	0.787	4.36
0.145	33.675	5.85	5.86	54.17	15.86	0.959	0.771	4.69
0.125	33.570	5.70	5.71	46.69	15.45	0.934	0.752	5.09
0.105	33.460	5.56	5.57	39.22	15.08	0.912	0.734	5.46
0.085	33.235	5.27	5.29	31.75	14.31	0.865	0.696	6.23
0.065	32.960	4.92	4.95	24.28	13.39	0.809	0.651	7.15
0.045	32.425	4.29	4.33	16.81	11.72	0.709	0.570	8.82
0.035	31.920	3.74	3.80	13.07	10.27	0.621	0.500	10.27
0.025	31.100	2.95	3.01	9.33	8.15	0.492	0.396	12.40
0.020	30.540	2.47	2.54	7.47	6.87	0.415	0.334	13.67
0.015	29.800	1.91	1.99	5.60	5.38	0.325	0.262	15.16
0.010	28.960	1.38	1.40	3.73	3.79	0.229	0.184	16.76

TABLE F.1 (Contd)

ISOTHERMAL VELOCITY PROFILE I-10

REYNOLDS NUMBER 21969.

HOT-WIRE MEASUREMENTS

INITIAL COLD RESISTANCE RG(1)	16.200	OHMS
FINAL COLD RESISTANCE RG(2)	16.210	OHMS
HOT (OPERATING) RESISTANCE RH	24.465	OHMS
CALIBRATION CURVE INTERCEPT A	1780.1	
CALIBRATION CURVE SLOPE B	701.9	
AIR TEMPERATURE	60.8	DEG.F.

CALCULATED RESULTS

AVERAGE VELOCITY	10.72	FT/SEC
FRICTION FACTOR	0.00633	
FRICTION VELOCITY	0.603	FT/SEC

Y/R	CURRENT MILLIAMPS	VELOCITY FT/SEC	CORRECTED VELOCITY FT/SEC	Y+	U+	U/UM	U/UC	UC-U / U*
0.996	38.220	13.14	13.14	615.55	21.77	1.224	1.000	0.00
0.896	38.200	13.09	13.09	553.75	21.69	1.220	0.996	0.08
0.796	38.160	13.00	13.00	491.94	21.54	1.211	0.989	0.23
0.696	38.060	12.77	12.77	430.14	21.16	1.190	0.972	0.60
0.596	37.935	12.49	12.49	368.34	20.69	1.164	0.950	1.07
0.496	37.780	12.15	12.15	306.54	20.13	1.132	0.924	1.63
0.396	37.590	11.73	11.73	244.73	19.44	1.093	0.893	2.32
0.296	37.325	11.17	11.18	182.93	18.51	1.041	0.850	3.25
0.196	37.000	10.50	10.51	121.13	17.41	0.979	0.799	4.36
0.176	36.935	10.37	10.38	108.77	17.19	0.967	0.789	4.57
0.156	36.825	10.15	10.16	96.41	16.83	0.947	0.773	4.93
0.136	36.725	9.96	9.97	84.05	16.52	0.929	0.758	5.24
0.116	36.615	9.74	9.76	71.69	16.16	0.909	0.742	5.60
0.096	36.465	9.46	9.48	59.33	15.70	0.883	0.721	6.06
0.076	36.290	9.13	9.16	46.96	15.17	0.853	0.696	6.59
0.056	35.985	8.58	8.62	34.60	14.28	0.803	0.656	7.48
0.036	35.445	7.66	7.72	22.24	12.79	0.719	0.587	8.97
0.026	34.895	6.78	6.86	16.06	11.36	0.639	0.522	10.40
0.016	33.680	5.07	5.14	9.88	8.51	0.479	0.391	13.25
0.011	32.560	3.76	3.80	6.79	6.29	0.354	0.289	15.47
0.006	30.950	2.27	2.30	3.70	3.81	0.214	0.175	17.96

ISOTHERMAL VELOCITY PROFILE I-11

REYNOLDS NUMBER 21650.

HOT-WIRE MEASUREMENTS

INITIAL COLD RESISTANCE RG(1)	16.405	OHMS
FINAL COLD RESISTANCE RG(2)	16.445	OHMS
HOT (OPERATING) RESISTANCE RH	24.860	OHMS
CALIBRATION CURVE INTERCEPT A	1987.0	
CALIBRATION CURVE SLOPE B	658.1	
AIR TEMPERATURE	59.0	DEG.F.

CALCULATED RESULTS

AVERAGE VELOCITY	10.50	FT/SEC
FRICTION FACTOR	0.00635	
FRICTION VELOCITY	0.592	FT/SEC

Y/R	CURRENT MILLIAMPS	VELOCITY FT/SEC	CORRECTED VELOCITY FT/SEC	Y+	U+	U/UM	U/UC	UC-U / U*
1.189	38.310	12.84	12.84	494.80	21.68	1.222	0.983	0.35
1.089	38.370	12.99	12.99	555.82	21.93	1.236	0.995	0.10
0.989	38.395	13.05	13.05	603.41	22.03	1.242	1.000	0.00
0.889	38.388	13.02	13.02	542.39	21.98	1.239	0.997	0.04
0.789	38.335	12.89	12.89	481.38	21.76	1.226	0.987	0.26
0.689	38.240	12.65	12.65	420.37	21.36	1.204	0.969	0.67
0.589	38.110	12.33	12.33	359.36	20.82	1.173	0.944	1.21
0.489	37.970	11.99	11.99	298.34	20.25	1.141	0.919	1.78
0.389	37.760	11.49	11.49	237.33	19.41	1.094	0.880	2.62
0.289	37.515	10.93	10.94	176.32	18.46	1.040	0.838	3.57
0.189	37.170	10.18	10.19	115.31	17.20	0.969	0.780	4.83
0.169	37.085	9.99	10.00	103.11	16.88	0.951	0.766	5.15
0.149	36.995	9.80	9.81	90.90	16.56	0.933	0.751	5.47
0.129	36.890	9.58	9.59	78.70	16.19	0.913	0.735	5.83
0.109	36.780	9.35	9.37	66.50	15.81	0.891	0.717	6.22
0.089	36.625	9.04	9.06	54.30	15.30	0.862	0.694	6.73
0.069	36.425	8.64	8.67	42.09	14.63	0.825	0.664	7.39
0.049	36.080	7.99	8.03	29.89	13.56	0.764	0.615	8.47
0.029	35.370	6.75	6.82	17.69	11.51	0.648	0.522	10.52
0.019	34.565	5.50	5.58	11.59	9.42	0.531	0.427	12.61
0.009	32.690	3.16	3.20	5.49	5.40	0.304	0.245	16.63
0.004	30.910	1.61	1.63	2.44	2.75	0.155	0.124	19.28
0.014	33.835	4.49	4.56	8.54	7.70	0.434	0.349	14.33

TABLE F.1 (Contd)

ISOTHERMAL VELOCITY PROFILE I-12

REYNOLDS NUMBER 21571.

HOT-WIRE MEASUREMENTS

INITIAL COLD RESISTANCE RG(1)	16.525	OHMS
FINAL CULD RESISTANCE RG(2)	16.485	OHMS
HOT (OPERATING) RESISTANCE RW	24.950	OHMS
CALIBRATION CURVE INTERCEPT A	1955.1	
CALIBRATION CURVE SLOPE B	668.7	
AIR TEMPERATURE	60.8	DEG.F.

CALCULATED RESULTS

AVERAGE VELOCITY	10.53	FT/SEC
FRICTION FACTOR	0.00635	
FRICTION VELOCITY	0.593	FT/SEC

Y/R	CURRENT MILLIAMPS	VELOCITY FT/SEC	CORRECTED VELOCITY FT/SEC	Y+	U+	U/UM	U/UC	UC-U / U+
1.105	38.400	13.01	13.01	544.31	21.90	1.235	0.992	0.16
1.005	38.445	13.11	13.11	611.21	22.07	1.244	1.000	0.00
0.905	38.425	13.05	13.05	550.39	21.97	1.239	0.995	0.10
0.805	38.380	12.93	12.93	489.58	21.77	1.227	0.986	0.30
0.705	38.290	12.70	12.70	428.76	21.38	1.205	0.968	0.68
0.605	38.165	12.39	12.39	367.94	20.86	1.176	0.945	1.20
0.505	38.010	12.02	12.02	307.12	20.24	1.141	0.917	1.82
0.405	37.820	11.57	11.57	246.31	19.48	1.098	0.882	2.58
0.305	37.590	11.05	11.06	185.49	18.61	1.049	0.843	3.45
0.205	37.260	10.32	10.33	124.67	17.39	0.980	0.787	4.68
0.185	37.190	10.17	10.18	112.51	17.14	0.966	0.776	4.93
0.165	37.105	9.98	9.99	100.34	16.82	0.948	0.762	5.25
0.145	37.010	9.78	9.79	88.18	16.48	0.929	0.746	5.58
0.125	36.910	9.57	9.58	76.02	16.13	0.910	0.731	5.93
0.105	36.795	9.33	9.35	63.85	15.74	0.887	0.713	6.33
0.085	36.630	9.00	9.03	51.69	15.20	0.857	0.688	6.87
0.065	36.420	8.59	8.63	39.53	14.52	0.819	0.658	7.54
0.045	36.045	7.90	7.96	27.36	13.39	0.755	0.607	8.67
0.035	35.760	7.39	7.46	21.28	12.56	0.708	0.569	9.50
0.025	35.210	6.48	6.56	15.20	11.04	0.622	0.500	11.02
0.020	34.715	5.72	5.80	12.16	9.76	0.550	0.442	12.30
0.015	34.090	4.84	4.91	9.12	8.26	0.466	0.374	13.80
0.010	33.110	3.55	3.69	6.08	6.21	0.350	0.281	15.86
0.005	31.535	2.13	2.15	3.04	3.62	0.204	0.163	18.45

ISOTHERMAL VELOCITY PROFILE I-13

REYNOLDS NUMBER 21504.

HOT-WIRE MEASUREMENTS

INITIAL COLD RESISTANCE RG(1)	16.563	OHMS
FINAL COLD RESISTANCE RG(2)	16.565	OHMS
HOT (OPERATING) RESISTANCE RW	25.005	OHMS
CALIBRATION CURVE INTERCEPT A	1955.1	
CALIBRATION CURVE SLOPE B	668.7	
AIR TEMPERATURE	62.6	DEG.F.

CALCULATED RESULTS

AVERAGE VELOCITY	10.56	FT/SEC
FRICTION FACTOR	0.00636	
FRICTION VELOCITY	0.595	FT/SEC

Y/R	CURRENT MILLIAMPS	VELOCITY FT/SEC	CORRECTED VELOCITY FT/SEC	Y+	U+	U/UM	U/UC	UC-U / U+
1.105	38.410	13.04	13.04	542.81	21.88	1.234	0.994	0.11
1.005	38.440	13.11	13.11	609.53	22.00	1.240	1.000	0.00
0.905	38.430	13.09	13.09	548.88	21.96	1.239	0.998	0.03
0.805	38.380	12.97	12.97	488.23	21.76	1.227	0.989	0.23
0.705	38.290	12.75	12.75	427.58	21.39	1.207	0.972	0.60
0.605	38.160	12.44	12.44	366.93	20.87	1.177	0.949	1.12
0.505	38.020	12.11	12.11	306.28	20.32	1.146	0.923	1.67
0.405	37.820	11.64	11.64	245.63	19.54	1.102	0.888	2.45
0.303	37.565	11.07	11.08	184.98	18.58	1.048	0.844	3.41
0.205	37.230	10.34	10.35	124.33	17.36	0.979	0.789	4.63
0.185	37.170	10.22	10.23	112.20	17.16	0.968	0.780	4.83
0.165	37.070	10.01	10.02	100.07	16.81	0.948	0.764	5.18
0.145	36.985	9.83	9.84	87.94	16.51	0.931	0.750	5.48
0.125	36.875	9.61	9.62	75.81	16.15	0.911	0.734	5.84
0.105	36.750	9.36	9.38	63.68	15.74	0.887	0.715	6.25
0.085	36.580	9.03	9.06	51.55	15.19	0.857	0.690	6.80
0.065	36.350	8.58	8.62	39.42	14.46	0.815	0.657	7.53
0.045	35.990	7.92	7.98	27.29	13.38	0.755	0.608	8.61
0.035	35.670	7.36	7.43	21.22	12.47	0.703	0.566	9.52
0.025	35.035	6.32	6.40	15.16	10.73	0.605	0.488	11.26
0.020	34.545	5.58	5.66	12.12	9.49	0.535	0.431	12.50
0.015	33.825	4.60	4.67	9.09	7.83	0.442	0.356	14.16
0.010	32.745	3.34	3.38	6.06	5.67	0.319	0.257	16.32
0.005	31.075	1.83	1.85	3.03	3.10	0.175	0.141	18.89
1.005	38.450	13.15	13.15	609.53	22.06	1.244	1.000	0.00

TABLE F.1 (Contd)

ISOTHERMAL VELOCITY PROFILE I-14

REYNOLDS NUMBER 31975.

HOT-WIRE MEASUREMENTS

INITIAL COLD RESISTANCE RG(1)	16.643	OHMS
FINAL COLD RESISTANCE RG(2)	16.625	OHMS
HOT (OPERATING) RESISTANCE RW	25.125	OHMS
CALIBRATION CURVE INTERCEPT A	2093.9	
CALIBRATION CURVE SLOPE B	631.3	
AIR TEMPERATURE	66.2	DEG.F.

CALCULATED RESULTS

AVERAGE VELOCITY	15.90	FT/SEC
FRICTION FACTOR	0.00578	
FRICTION VELOCITY	0.855	FT/SEC

Y/R	CURRENT MILLIAMPS	VELOCITY FT/SEC	CORRECTED VELOCITY FT/SEC	Y+	U+	U/UM	U/UC	UC-U / U+
1.005	40.615	19.57	19.57	864.48	22.87	1.230	1.000	0.00
0.905	40.605	19.53	19.53	778.46	22.82	1.228	0.997	0.04
0.805	40.550	19.33	19.33	692.44	22.59	1.215	0.987	0.27
0.705	40.460	19.03	19.03	606.42	22.24	1.196	0.972	0.62
0.605	40.345	18.64	18.64	520.41	21.79	1.172	0.952	1.08
0.505	40.170	18.07	18.07	434.39	21.12	1.136	0.923	1.74
0.405	39.965	17.42	17.43	348.37	20.36	1.095	0.890	2.50
0.305	39.715	16.64	16.65	262.35	19.45	1.046	0.850	3.41
0.205	39.350	15.58	15.59	176.33	18.22	0.980	0.796	4.65
0.185	39.265	15.30	15.31	159.13	17.89	0.963	0.782	4.97
0.165	39.165	15.01	15.02	141.93	17.56	0.944	0.767	5.31
0.145	39.070	14.73	14.75	124.72	17.23	0.927	0.753	5.63
0.125	38.960	14.42	14.44	107.52	16.87	0.908	0.737	5.99
0.105	38.805	13.99	14.02	90.31	16.38	0.881	0.716	6.49
0.085	38.660	13.59	13.63	73.11	15.92	0.857	0.696	6.94
0.065	38.420	12.96	13.01	55.91	15.21	0.818	0.664	7.66
0.045	38.090	12.12	12.20	38.70	14.25	0.767	0.623	8.61
0.035	37.840	11.50	11.60	30.10	13.55	0.729	0.592	9.32
0.025	37.330	10.31	10.40	21.50	12.15	0.654	0.531	10.71
0.020	36.935	9.44	9.51	17.20	11.11	0.598	0.485	11.75
0.015	36.300	8.15	8.22	12.90	9.60	0.516	0.420	13.26
0.010	35.280	6.31	6.36	8.60	7.43	0.399	0.324	15.44
0.005	33.350	3.58	3.62	4.30	4.23	0.227	0.184	18.64
1.005	40.655	19.55	19.55	864.48	22.85	1.229	1.000	0.00

ISOTHERMAL VELOCITY PROFILE I-15

REYNOLDS NUMBER 33078.

HOT-WIRE MEASUREMENTS

INITIAL COLD RESISTANCE RG(1)	15.735	OHMS
FINAL COLD RESISTANCE RG(2)	15.730	OHMS
HOT (OPERATING) RESISTANCE RW	23.600	OHMS
CALIBRATION CURVE INTERCEPT A	1824.0	
CALIBRATION CURVE SLOPE B	682.8	
AIR TEMPERATURE	59.0	DEG.F.

CALCULATED RESULTS

AVERAGE VELOCITY	16.05	FT/SEC
FRICTION FACTOR	0.00574	
FRICTION VELOCITY	0.860	FT/SEC

Y/R	CURRENT MILLIAMPS	VELOCITY FT/SEC	CORRECTED VELOCITY FT/SEC	Y+	U+	U/UM	U/UC	UC-U / U+
1.105	40.125	19.40	19.40	793.28	22.55	1.208	0.996	0.08
1.005	40.150	19.47	19.47	890.78	22.63	1.212	1.000	0.00
0.905	40.130	19.41	19.41	802.15	22.56	1.209	0.996	0.06
0.805	40.085	19.27	19.27	713.51	22.40	1.200	0.989	0.23
0.705	40.000	19.00	19.00	624.88	22.09	1.183	0.976	0.54
0.605	39.885	18.65	18.65	536.24	21.68	1.162	0.958	0.94
0.505	39.720	18.15	18.15	447.60	21.10	1.130	0.932	1.52
0.405	39.500	17.51	17.52	358.97	20.36	1.091	0.899	2.27
0.305	39.230	16.73	16.74	270.33	19.45	1.042	0.859	3.17
0.205	38.885	15.78	15.79	181.70	18.35	0.983	0.811	4.27
0.185	38.800	15.54	15.55	163.97	18.07	0.968	0.798	4.55
0.165	38.705	15.29	15.30	146.24	17.79	0.953	0.786	4.84
0.145	38.580	14.96	14.98	128.52	17.41	0.933	0.769	5.22
0.125	38.460	14.64	14.66	110.79	17.04	0.913	0.752	5.59
0.105	38.335	14.32	14.35	93.06	16.67	0.893	0.736	5.95
0.085	38.145	13.84	13.88	75.34	16.13	0.864	0.712	6.50
0.065	37.935	13.32	13.37	57.61	15.54	0.833	0.686	7.08
0.045	37.615	12.56	12.64	39.88	14.68	0.787	0.649	7.94
0.035	37.310	11.86	11.95	31.02	13.89	0.744	0.613	8.73
0.025	36.850	10.85	10.94	22.15	12.71	0.681	0.561	9.91
0.020	36.415	9.94	10.01	17.72	11.63	0.623	0.514	10.99
0.015	35.790	8.73	8.90	13.29	10.34	0.554	0.457	12.28
0.010	34.690	6.83	6.88	8.86	7.99	0.428	0.353	14.63
0.005	32.610	4.00	4.04	4.43	4.09	0.251	0.207	17.95
1.005	40.160	19.46	19.46	890.78	22.62	1.212	1.000	0.00

TABLE F.1 (Contd)

ISOTHERMAL VELOCITY PROFILE I-16

REYNOLDS NUMBER 32456.

HOT-WIRE MEASUREMENTS

INITIAL COLD RESISTANCE RG(1)	15.812	OHMS
FINAL COLD RESISTANCE RG(2)	15.771	OHMS
HOT (OPERATING) RESISTANCE RW	23.715	OHMS
CALIBRATION CURVE INTERCEPT A	1985.0	
CALIBRATION CURVE SLOPE B	700.0	
AIR TEMPERATURE	66.2	DEG.F.

CALCULATED RESULTS

AVERAGE VELOCITY	16.14	FT/SEC
FRICTION FACTOR	0.00576	
FRICTION VELOCITY	0.866	FT/SEC

Y/R	CURRENT I MILLIAMPS	VELOCITY FT/SEC	CORRECTED VELOCITY FT/SEC	Y+	U+	U/UM	U/UC	UC-U / U+
1.104	41.150	19.56	19.56	780.96	22.56	1.211	0.997	0.05
1.004	41.170	19.61	19.61	875.10	22.62	1.214	1.000	0.00
0.904	41.160	19.57	19.57	787.94	22.57	1.212	0.997	0.04
0.804	41.115	19.41	19.41	700.77	22.39	1.202	0.989	0.23
0.704	41.015	19.09	19.09	613.61	22.02	1.182	0.973	0.59
0.604	40.895	18.71	18.71	526.45	21.58	1.159	0.954	1.03
0.504	40.740	18.23	18.23	439.29	21.03	1.129	0.929	1.58
0.404	40.535	17.61	17.62	352.13	20.32	1.091	0.898	2.29
0.304	40.280	16.87	16.88	264.97	19.46	1.045	0.860	3.15
0.204	39.910	15.83	15.84	177.80	18.27	0.981	0.807	4.34
0.184	39.825	15.59	15.60	160.37	17.99	0.966	0.795	4.62
0.164	39.740	15.35	15.36	142.94	17.72	0.951	0.783	4.89
0.144	39.645	15.08	15.10	125.51	17.41	0.935	0.769	5.20
0.124	39.500	14.69	14.71	108.08	16.96	0.911	0.750	5.65
0.104	39.375	14.36	14.39	90.64	16.59	0.891	0.733	6.02
0.084	39.195	13.90	13.94	73.21	16.07	0.863	0.710	6.54
0.064	38.970	13.33	13.38	55.78	15.43	0.829	0.682	7.18
0.044	38.645	12.54	12.62	38.35	14.55	0.781	0.643	8.06
0.034	38.335	11.82	11.92	29.63	13.74	0.738	0.607	8.87
0.024	37.810	10.67	10.76	20.91	12.41	0.666	0.548	10.20
0.019	37.340	9.70	9.77	16.56	11.27	0.605	0.498	11.35
0.014	36.620	8.33	8.40	12.20	9.68	0.520	0.428	12.93
0.009	35.290	6.13	6.18	7.84	7.12	0.382	0.315	15.49
0.004	33.315	3.60	3.64	3.48	4.19	0.225	0.185	18.42

ISOTHERMAL VELOCITY PROFILE I-17

REYNOLDS NUMBER 31877.

HOT-WIRE MEASUREMENTS

INITIAL COLD RESISTANCE RG(1)	15.273	OHMS
FINAL COLD RESISTANCE RG(2)	15.252	OHMS
HOT (OPERATING) RESISTANCE RW	22.905	OHMS
CALIBRATION CURVE INTERCEPT A	2201.8	
CALIBRATION CURVE SLOPE B	714.7	
AIR TEMPERATURE	69.8	DEG.F.

CALCULATED RESULTS

AVERAGE VELOCITY	16.04	FT/SEC
FRICTION FACTOR	0.00579	
FRICTION VELOCITY	0.863	FT/SEC

Y/R	CURRENT I MILLIAMPS	VELOCITY FT/SEC	CORRECTED VELOCITY FT/SEC	Y+	U+	U/UM	U/UC	UC-U / U+
1.005	42.305	19.67	19.67	862.15	22.77	1.225	1.000	0.00
0.905	42.300	19.64	19.64	776.37	22.74	1.224	0.998	0.03
0.805	42.255	19.49	19.49	690.58	22.56	1.214	0.990	0.20
0.705	42.155	19.17	19.17	604.79	22.20	1.194	0.974	0.57
0.605	42.025	18.76	18.76	519.01	21.72	1.169	0.953	1.05
0.505	41.860	18.26	18.26	433.22	21.14	1.138	0.928	1.62
0.405	41.640	17.60	17.61	347.43	20.38	1.097	0.895	2.38
0.305	41.375	16.82	16.83	261.64	19.48	1.048	0.855	3.29
0.205	40.975	15.70	15.71	175.86	18.19	0.979	0.798	4.58
0.185	40.905	15.50	15.51	158.70	17.96	0.966	0.788	4.81
0.165	40.785	15.18	15.19	141.54	17.59	0.946	0.772	5.18
0.145	40.690	14.92	14.94	124.39	17.29	0.930	0.759	5.48
0.125	40.565	14.58	14.60	107.23	16.90	0.909	0.742	5.86
0.105	40.395	14.14	14.17	90.07	16.40	0.882	0.720	6.37
0.085	40.215	13.68	13.72	72.91	15.88	0.854	0.697	6.89
0.065	39.975	13.08	13.13	55.76	15.20	0.818	0.667	7.56
0.045	39.620	12.23	12.31	38.60	14.25	0.767	0.625	8.52
0.035	39.330	11.57	11.67	30.02	13.50	0.727	0.593	9.26
0.025	38.835	10.49	10.58	21.44	12.25	0.659	0.537	10.52
0.020	38.320	9.43	9.50	17.15	11.00	0.592	0.482	11.77
0.015	37.670	8.20	8.27	12.86	9.57	0.515	0.420	13.20
0.010	36.505	6.25	6.30	8.57	7.29	0.392	0.320	15.48
0.005	34.385	3.50	3.54	4.28	4.09	0.220	0.179	18.67

TABLE F.1 (Contd)

ISOTHERMAL VELOCITY PROFILE IT-1

REYNOLDS NUMBER 5590.

HOT-WIRE MEASUREMENTS

CALIBRATION CURVE INTERCEPT A	836.8	
CALIBRATION CURVE SLOPE B	2218.0	
AIR TEMPERATURE	73.4	DEG.F.

CALCULATED RESULTS

AVERAGE VELOCITY	2.84	FT/SEC
FRICTION FACTOR	0.00906	
FRICTION VELOCITY	0.191	FT/SEC

Y/R	COLD RESISTANCE RG	OPERATING RESISTANCE RW	CURRENT MILLIAMPS	VELOCITY FT/SEC	CORRECTED VELOCITY FT/SEC	Y+	U+	U/UM	U/UC	UC-U / U+
1.00	9.055	13.583	35.810	3.75	3.75	188.19	19.55	1.316	1.000	0.00
0.10	9.040	13.560	34.185	2.33	2.34	18.81	12.20	0.821	0.625	7.30
0.04	9.030	13.545	32.345	1.21	1.23	7.52	6.41	0.431	0.328	13.09
0.20	9.040	13.560	34.860	2.87	2.87	37.63	14.96	1.007	0.767	4.53
0.90	9.045	13.568	35.770	3.72	3.72	169.37	19.40	1.306	0.994	0.10
1.00	9.047	13.575	35.790	3.73	3.73	188.19	19.45	1.309	1.000	0.00
0.14	9.040	13.555	34.575	2.64	2.65	26.34	13.82	0.930	0.708	5.68
0.50	9.045	13.568	35.460	3.40	3.40	94.09	17.73	1.193	0.909	1.77
0.02	9.025	13.543	30.660	0.58	0.59	5.76	3.07	0.207	0.157	16.42
0.70	9.045	13.568	35.675	3.63	3.63	131.73	18.93	1.274	0.970	0.57
1.00	9.045	13.568	35.800	3.74	3.74	188.19	19.50	1.313	1.000	0.00
0.08	9.032	13.550	33.805	2.06	2.08	15.05	10.84	0.730	0.556	8.65
0.16	9.035	13.553	34.710	2.75	2.76	30.11	14.39	0.969	0.737	5.11
0.03	9.025	13.542	31.600	0.89	0.90	5.64	4.69	0.315	0.240	14.81
0.30	9.040	13.560	35.165	3.14	3.14	56.45	16.37	1.102	0.839	3.12
1.00	9.040	13.560	35.800	3.74	3.74	188.19	19.50	1.313	1.000	0.00
0.60	9.038	13.557	35.590	3.54	3.54	112.91	18.46	1.242	0.946	1.04
0.06	9.025	13.538	33.235	1.68	1.70	11.29	8.86	0.596	0.454	10.63
0.18	9.035	13.553	34.805	2.83	2.84	33.87	14.81	0.997	0.759	4.69

ISOTHERMAL VELOCITY PROFILE IT-2

REYNOLDS NUMBER 5401.

HOT-WIRE MEASUREMENTS

CALIBRATION CURVE INTERCEPT A	842.4	
CALIBRATION CURVE SLOPE B	2033.0	
AIR TEMPERATURE	74.8	DEG.F.

CALCULATED RESULTS

AVERAGE VELOCITY	2.76	FT/SEC
FRICTION FACTOR	0.00915	
FRICTION VELOCITY	0.187	FT/SEC

Y/R	COLD RESISTANCE RG	OPERATING RESISTANCE RW	CURRENT MILLIAMPS	VELOCITY FT/SEC	CORRECTED VELOCITY FT/SEC	Y+	U+	U/UM	U/UC	UC-U / U+
1.00	10.670	15.998	34.880	3.70	3.64	182.72	19.45	1.316	1.000	0.00
0.16	10.658	15.987	33.790	2.73	2.69	29.23	14.37	0.972	0.739	5.07
0.04	10.648	15.972	31.140	1.08	1.10	7.30	5.88	0.397	0.302	13.57
0.50	10.672	16.008	34.500	3.34	3.34	91.36	17.85	1.207	0.917	1.60
0.02	10.637	15.956	29.450	0.55	0.56	3.65	2.99	0.202	0.153	16.46
1.00	10.675	16.013	34.830	3.64	3.64	182.72	19.45	1.316	1.000	0.00
0.90	10.675	16.013	34.825	3.63	3.63	164.45	19.40	1.312	0.997	0.05
0.30	10.665	15.998	34.175	3.03	3.03	34.81	16.19	1.095	0.832	3.26
0.12	10.655	15.990	33.420	2.42	2.43	21.92	12.99	0.878	0.667	6.46
1.00	10.670	16.008	34.830	3.63	3.64	182.72	19.45	1.316	1.000	0.00
0.70	10.670	16.005	34.700	3.52	3.52	127.90	18.81	1.273	0.967	0.64
0.08	10.645	15.968	32.790	1.99	2.01	14.61	10.74	0.726	0.552	8.71
0.20	10.660	15.990	33.910	2.82	2.82	36.54	15.07	1.019	0.774	4.38
1.00	10.667	16.000	34.825	3.64	3.64	182.72	19.45	1.316	1.000	0.00

TABLE F.1 (Contd)

ISOTHERMAL VELOCITY PROFILE IT-3

REYNOLDS NUMBER 5219.

HOT-WIRE MEASUREMENTS

CALIBRATION CURVE INTERCEPT A	700.1	
CALIBRATION CURVE SLOPE B	1987.8	
AIR TEMPERATURE	75.2	DEG.F.

CALCULATED RESULTS

AVERAGE VELOCITY	2.67	FT/SEC
FRICTION FACTOR	0.00924	
FRICTION VELOCITY	0.181	FT/SEC

Y/R	COLD RESISTANCE RG	OPERATING RESISTANCE RW	CURRENT MILLIAMPS	VELOCITY FT/SEC	CORRECTED VELOCITY FT/SEC	Y+	U+	U/UM	U/UC	UC-U / U+
1.00	11.230	16.845	33.155	3.49	3.49	177.41	19.19	1.304	1.000	0.00
0.20	11.233	16.850	32.330	2.69	2.69	35.48	14.79	1.005	0.764	4.56
0.04	11.245	16.868	30.010	1.10	1.11	7.09	6.10	0.414	0.315	13.25
0.12	11.245	16.868	31.910	2.32	2.33	21.29	12.81	0.871	0.661	6.54
0.60	11.245	16.868	33.000	3.34	3.34	106.45	18.36	1.248	0.948	0.98
0.30	11.245	16.868	32.620	2.95	2.95	53.22	16.22	1.102	0.838	3.13
1.00	11.245	16.868	33.200	3.55	3.55	177.41	19.52	1.327	1.000	0.00
0.16	11.245	16.868	32.255	2.61	2.62	28.38	14.40	0.979	0.744	4.94
0.02	11.230	16.845	28.580	0.63	0.63	3.54	3.46	0.235	0.178	15.89
0.80	11.235	16.853	33.150	3.49	3.49	141.93	19.19	1.304	0.991	0.16
0.08	11.220	16.830	31.425	1.94	1.95	14.19	10.72	0.729	0.553	8.63
0.40	11.225	16.838	32.775	3.10	3.10	70.96	17.04	1.158	0.880	2.30
1.00	11.228	16.842	33.180	3.52	3.52	177.41	19.35	1.315	1.000	0.00

ISOTHERMAL VELOCITY PROFILE IT-4

REYNOLDS NUMBER 16117.

HOT-WIRE MEASUREMENTS

CALIBRATION CURVE INTERCEPT A	696.8	
CALIBRATION CURVE SLOPE B	2013.0	
AIR TEMPERATURE	68.0	DEG.F.

CALCULATED RESULTS

AVERAGE VELOCITY	8.06	FT/SEC
FRICTION FACTOR	0.00683	
FRICTION VELOCITY	0.471	FT/SEC

Y/R	COLD RESISTANCE RG	OPERATING RESISTANCE RW	CURRENT MILLIAMPS	VELOCITY FT/SEC	CORRECTED VELOCITY FT/SEC	Y+	U+	U/UM	U/UC	UC-U / U+
1.00	10.050	15.075	37.545	10.11	10.11	471.06	21.44	1.253	1.000	0.00
0.20	10.050	15.075	36.415	7.95	7.96	94.21	16.88	0.987	0.787	4.56
0.10	10.050	15.075	35.920	7.11	7.13	47.10	15.12	0.884	0.705	6.32
0.02	10.045	15.075	33.200	3.45	3.54	9.42	7.51	0.438	0.350	13.33
1.00	10.050	15.075	37.540	10.10	10.11	471.06	21.44	1.253	1.000	0.00
0.80	10.050	15.075	37.475	9.97	9.98	376.84	21.17	1.237	0.987	0.27
0.18	10.050	15.075	36.335	7.81	7.82	84.79	16.59	0.969	0.773	4.85
0.08	10.045	15.075	35.735	6.78	6.79	37.68	14.40	0.842	0.671	7.04
0.90	10.045	15.070	37.525	10.10	10.09	423.95	21.40	1.251	0.998	0.04
1.00	10.050	15.070	37.540	10.13	10.11	471.06	21.44	1.253	1.000	0.00
0.60	10.050	15.075	37.290	9.66	9.66	282.63	20.36	1.190	0.949	1.08
0.16	10.045	15.075	36.250	7.63	7.65	75.36	16.22	0.948	0.756	5.21
0.06	10.045	15.070	35.400	6.27	6.33	28.26	13.42	0.784	0.626	8.01
0.30	10.045	15.070	36.700	8.46	8.50	141.31	18.03	1.054	0.840	3.41
1.00	10.045	15.070	37.520	10.05	10.11	471.06	21.44	1.253	1.000	0.00
0.40	10.045	15.070	36.920	8.87	8.92	188.42	18.92	1.106	0.882	2.52
0.14	10.045	15.070	36.140	7.47	7.52	65.94	15.95	0.932	0.743	5.49
0.04	10.040	15.060	34.790	5.39	5.49	18.84	11.64	0.680	0.543	9.80
0.03	10.040	15.060	34.240	4.66	4.77	14.13	10.11	0.591	0.471	11.32
1.00	10.043	15.065	37.510	10.04	10.11	471.06	21.44	1.253	1.000	0.00
0.01	10.035	15.060	30.990	1.71	1.77	4.71	3.75	0.219	0.175	17.69
0.12	10.040	15.060	36.060	7.24	7.32	56.52	15.52	0.907	0.724	5.91
0.50	10.040	15.060	37.080	9.19	9.28	235.53	19.68	1.150	0.917	1.76
1.00	10.038	15.055	37.490	10.00	10.11	471.06	21.44	1.253	1.000	0.00

TABLE F.1 (Contd)

ISOTHERMAL VELOCITY PROFILE IT-5

REYNOLDS NUMBER 16280.

HOT-WIRE MEASUREMENTS

CALIBRATION CURVE INTERCEPT A	715.2	
CALIBRATION CURVE SLOPE B	1953.3	
AIR TEMPERATURE	64.4	DEG.F.

CALCULATED RESULTS

AVERAGE VELOCITY	8.04	FT/SEC
FRICTION FACTOR	0.00681	
FRICTION VELOCITY	0.469	FT/SEC

Y/R	COLD RESISTANCE RG	OPERATING RESISTANCE Rw	CURRENT MILLIAMPS	VELOCITY FT/SEC	CORRECTED VELOCITY FT/SEC	Y+	U+	U/UM	U/UC	UC-U / U+
1.00	9.975	14.963	37.515	10.06	10.06	475.23	21.41	1.250	1.000	0.00
0.20	9.970	14.955	36.370	7.94	7.95	95.04	16.92	0.987	0.793	4.40
0.10	9.970	14.955	35.865	7.10	7.11	47.52	15.13	0.883	0.709	6.19
0.01	9.962	14.943	30.996	1.77	1.82	4.75	3.87	0.226	0.181	17.45
1.10	9.973	14.960	37.480	9.99	9.99	427.71	21.26	1.241	0.997	0.06
1.00	9.972	14.960	37.500	10.02	10.02	475.23	21.32	1.245	1.000	0.00
0.90	9.970	14.955	37.480	9.99	9.99	427.71	21.26	1.241	0.997	0.06
0.12	9.970	14.955	36.000	7.52	7.53	57.02	15.60	0.910	0.731	5.72
0.50	9.973	14.960	37.085	9.23	9.23	237.61	19.64	1.146	0.921	1.68
0.03	9.967	14.950	34.245	4.79	4.86	14.25	10.34	0.603	0.485	10.98
1.00	9.973	14.960	37.500	10.03	10.03	475.23	21.34	1.246	1.000	0.00
0.30	9.970	14.955	36.675	8.47	8.47	142.57	18.02	1.052	0.845	3.29
0.06	9.970	14.955	35.400	6.38	6.41	28.51	13.64	0.795	0.639	7.68
0.70	9.973	14.960	37.355	9.75	9.75	332.66	20.75	1.211	0.973	0.57
0.16	9.970	14.955	36.210	7.67	7.68	76.03	16.34	0.954	0.766	4.98
1.00	9.973	14.960	37.505	10.04	10.04	475.23	21.37	1.247	1.000	0.00
0.02	9.965	14.945	33.170	3.56	3.64	9.50	7.74	0.452	0.363	13.58
0.60	9.973	14.960	37.230	9.50	9.50	285.14	20.22	1.180	0.948	1.10
0.04	9.967	14.950	34.830	5.56	5.61	19.00	11.94	0.697	0.559	9.38
0.18	9.970	14.955	36.230	7.80	7.81	85.54	16.62	0.970	0.779	4.70

TABLE F.2

SMOOTHED VELOCITY PROFILES AND CALCULATED EDDY DIFFUSIVITIES OF MOMENTUM

Isothermal Velocity Profile I-1

Reynolds Number 6966

y/R	$\overline{V}_z$	$\frac{\epsilon_M}{\nu}$	$\frac{\epsilon_M}{Ru^*}$
1.00	4.550		
0.95	4.540	15.16	0.0659
0.90	4.530	14.21	0.0618
0.85	4.510	14.52	0.0631
0.80	4.480	12.98	0.0564
0.75	4.440	13.69	0.0595
0.70	4.380	14.52	0.0631
0.65	4.340	14.61	0.0635
0.60	4.280	15.16	0.0659
0.55	4.200	14.52	0.0631
0.50	4.130	14.39	0.0626
0.45	4.040	14.98	0.0651
0.40	3.940	14.36	0.0624
0.35	3.850	14.28	0.0621
0.30	3.720	13.96	0.0607
0.25	3.600	13.24	0.0575
0.20	3.460	11.99	0.0521
0.18	3.390	11.22	0.0488
0.16	3.320	10.01	0.0435
0.14	3.240	7.55	0.0328
0.12	3.140	5.26	0.0228
0.10	2.960	3.47	0.0151
0.08	2.730	2.23	0.0097
0.06	2.400	1.15	0.0050
0.04	1.940	0.65	0.0028
0.02	1.080	0.13	0.0005

TABLE F.2 (Contd.)

Isothermal Velocity Profile I-2

Reynolds Number 6985

y/R	$\overline{V}_z$	$\frac{\varepsilon_M}{\nu}$	$\frac{\varepsilon_M}{Ru^*}$
1.00	4.540		
0.95	4.530	9.82	0.0426
0.90	4.520	11.37	0.0493
0.85	4.480	12.92	0.0560
0.80	4.460	13.43	0.0583
0.75	4.420	14.84	0.0644
0.70	4.370	15.24	0.0661
0.65	4.320	15.24	0.0661
0.60	4.270	15.50	0.0672
0.55	4.190	15.47	0.0671
0.45	4.040	16.01	0.0695
0.40	3.960	15.41	0.0668
0.35	3.850	14.64	0.0635
0.30	3.740	13.91	0.0603
0.25	3.610	14.19	0.0615
0.20	3.470	14.16	0.0614
0.18	3.430	12.05	0.0523
0.16	3.360	9.71	0.0421
0.14	3.270	7.28	0.0316
0.12	3.140	5.41	0.0235
0.10	3.000	3.69	0.0160
0.08	2.780	2.21	0.0096
0.06	2.450	1.12	0.0048
0.04	1.920	0.61	0.0026
0.02	1.110	0.12	0.0005

TABLE F.2 (Contd.)

Isothermal Velocity Profile I-3

Reynolds Number 6777

y/R	$\overline{V}_z$	$\frac{\varepsilon_M}{\nu}$	$\frac{\varepsilon_M}{Ru^*}$
1.00	4.420		
0.95	4.410	14.51	0.0646
0.90	4.400	15.54	0.0692
0.85	4.380	17.61	0.0784
0.80	4.360	18.85	0.0839
0.75	4.330	17.25	0.0768
0.70	4.300	15.54	0.0692
0.65	4.240	14.51	0.0646
0.60	4.180	14.27	0.0635
0.55	4.110	14.95	0.0666
0.50	4.040	15.54	0.0692
0.45	3.960	16.06	0.0715
0.40	3.880	15.36	0.0684
0.35	3.790	14.66	0.0653
0.30	3.670	13.72	0.0611
0.25	3.550	13.09	0.0583
0.20	3.410	11.09	0.0494
0.18	3.350	9.31	0.0414
0.16	3.260	7.99	0.0355
0.14	3.160	6.49	0.0289
0.12	3.040	5.12	0.0228
0.10	2.890	3.53	0.0157
0.08	2.680	2.04	0.0091
0.06	2.350	1.02	0.0045
0.04	1.800	0.55	0.0024
0.02	1.000	0.13	0.0005

TABLE F.2 (Contd.)

Isothermal Velocity Profile I-4

Reynolds Number 7325

y/R	$\overline{V}_z$	$\frac{\epsilon_M}{\nu}$	$\frac{\epsilon_M}{Ru^*}$
1.00	4.650		
0.95	4.650	18.90	0.0787
0.90	4.640	17.57	0.0732
0.85	4.620	15.72	0.0654
0.80	4.590	14.92	0.0621
0.75	4.550	15.20	0.0633
0.70	4.500	16.41	0.0683
0.65	4.450	16.41	0.0683
0.60	4.400	16.69	0.0695
0.55	4.320	16.66	0.0694
0.50	4.250	17.09	0.0712
0.45	4.170	18.16	0.0756
0.40	4.090	18.67	0.0777
0.35	4.000	18.27	0.0761
0.30	3.910	17.57	0.0732
0.25	3.790	15.66	0.0652
0.20	3.670	12.70	0.0529
0.18	3.590	10.52	0.0438
0.16	3.510	8.59	0.0357
0.14	3.410	7.25	0.0302
0.12	3.270	5.47	0.0227
0.10	3.130	3.58	0.0149
0.08	2.890	2.11	0.0088
0.06	2.500	1.08	0.0045
0.04	1.930	0.61	0.0025
0.02	1.070	0.18	0.0007

TABLE F.2 (Contd.)

Isothermal Velocity Profile I-5

Reynolds Number 11334

y/R	$\overline{V}_z$	$\frac{\epsilon_M}{\nu}$	$\frac{\epsilon_M}{Ru^*}$
1.00	7.160		
0.95	7.150	36.56	0.1043
0.90	7.140	25.12	0.0717
0.85	7.120	21.53	0.0614
0.80	7.060	20.08	0.0573
0.75	6.990	19.86	0.0566
0.70	6.920	21.53	0.0614
0.65	6.830	22.89	0.0653
0.60	6.740	23.78	0.0678
0.55	6.640	25.25	0.0720
0.50	6.530	25.82	0.0737
0.45	6.420	26.54	0.0757
0.40	6.290	27.16	0.0775
0.35	6.160	27.10	0.0773
0.30	6.020	26.67	0.0761
0.25	5.860	24.54	0.0700
0.20	5.680	21.69	0.0619
0.18	5.580	20.14	0.0575
0.16	5.490	17.39	0.0496
0.14	5.380	13.72	0.0391
0.12	5.230	10.47	0.0298
0.10	5.010	7.55	0.0215
0.08	4.750	4.70	0.0134
0.06	4.350	2.27	0.0064
0.04	3.610	1.34	0.0038
0.02	2.080	0.46	0.0013

TABLE F.2 (Contd.)

Isothermal Velocity Profile I-6

Reynolds Number 11650

y/R	$\overline{V}_z$	$\frac{\varepsilon_M}{\nu}$	$\frac{\varepsilon_M}{Ru^*}$
1.00	7.240		
0.95	7.230	18.34	0.0511
0.90	7.200	21.10	0.0588
0.85	7.170	21.64	0.0603
0.80	7.130	22.35	0.0622
0.75	7.060	22.44	0.0625
0.70	6.990	23.11	0.0644
0.65	6.910	24.48	0.0682
0.60	6.820	25.62	0.0713
0.55	6.720	26.30	0.0733
0.50	6.620	26.63	0.0742
0.45	6.500	26.23	0.0731
0.40	6.370	25.90	0.0722
0.35	6.220	25.46	0.0709
0.30	6.070	24.33	0.0678
0.25	5.890	22.54	0.0628
0.20	5.680	20.32	0.0566
0.18	5.580	19.51	0.0543
0.16	5.480	18.09	0.0504
0.14	5.370	15.41	0.0429
0.12	5.240	11.17	0.0311
0.10	5.050	7.88	0.0219
0.08	4.740	4.98	0.0138
0.06	4.360	2.57	0.0071
0.04	3.670	1.60	0.0044
0.02	2.290	0.51	0.0014

TABLE F.2 (Contd.)

Isothermal Velocity Profile I-7

Reynolds Number 11412

y/R	$\bar{V}_z$	$\frac{\varepsilon_M}{\nu}$	$\frac{\varepsilon_M}{Ru^*}$
1.00	7.080		
0.95	7.070	18.78	0.0532
0.90	7.050	18.78	0.0532
0.85	7.010	18.77	0.0532
0.80	6.960	19.46	0.0552
0.75	6.890	21.47	0.0609
0.70	6.820	23.05	0.0654
0.65	6.750	24.32	0.0690
0.60	6.660	24.52	0.0695
0.55	6.560	24.43	0.0693
0.50	6.450	24.35	0.0691
0.45	6.330	24.49	0.0695
0.40	6.190	25.18	0.0714
0.35	6.050	24.71	0.0701
0.30	5.910	23.87	0.0677
0.25	5.720	22.18	0.0629
0.20	5.520	20.61	0.0584
0.18	5.430	19.30	0.0547
0.16	5.330	16.99	0.0482
0.14	5.220	13.76	0.0390
0.12	5.070	10.69	0.0303
0.10	4.870	8.00	0.0227
0.08	4.610	5.22	0.0148
0.06	4.260	2.56	0.0072
0.04	3.610	1.55	0.0044
0.02	2.200	0.48	0.0013

TABLE F.2 (Contd.)

Isothermal Velocity Profile I-8

Reynolds Number 11172

y/R	$\bar{V}_z$	$\frac{\varepsilon_M}{\nu}$	$\frac{\varepsilon_M}{Ru^*}$
1.00	6.970		
0.95	6.960	25.15	0.0727
0.90	6.940	22.97	0.0664
0.85	6.920	23.66	0.0683
0.80	6.870	22.97	0.0664
0.75	6.820	21.47	0.0620
0.70	6.750	22.32	0.0645
0.65	6.660	23.26	0.0672
0.60	6.580	24.29	0.0702
0.55	6.490	25.42	0.0734
0.50	6.380	24.68	0.0713
0.45	6.270	23.92	0.0691
0.40	6.130	23.14	0.0668
0.35	5.980	22.08	0.0638
0.30	5.810	21.62	0.0625
0.25	6.620	20.72	0.0598
0.20	5.420	19.28	0.0557
0.18	5.320	18.16	0.0524
0.16	5.220	16.76	0.0484
0.14	5.110	14.46	0.0418
0.12	4.980	11.16	0.0322
0.10	4.800	7.67	0.0221
0.08	4.540	4.89	0.0141
0.06	4.130	2.47	0.0071
0.04	3.510	1.51	0.0043
0.02	2.160	0.47	0.0013

TABLE F.2 (Contd.)

Isothermal Velocity Profile I-9

Reynolds Number 12357

y/R	$\overline{V}_z$	$\frac{\varepsilon_M}{\nu}$	$\frac{\varepsilon_M}{Ru^*}$
1.00	7.590		
0.95	7.580	21.99	0.0582
0.90	7.560	23.63	0.0625
0.85	7.520	26.23	0.0694
0.80	7.480	27.16	0.0719
0.75	7.430	26.81	0.0710
0.70	7.360	26.23	0.0694
0.65	7.270	26.43	0.0699
0.60	7.180	28.04	0.0742
0.55	7.080	30.04	0.0795
0.50	6.980	31.23	0.0827
0.45	6.870	31.99	0.0847
0.40	6.750	31.59	0.0836
0.35	6.620	31.03	0.0821
0.30	6.470	29.76	0.0787
0.25	6.310	28.35	0.0750
0.20	6.120	25.49	0.0674
0.18	6.040	22.67	0.0600
0.16	5.940	19.75	0.0522
0.14	5.820	16.58	0.0439
0.12	5.670	12.39	0.0328
0.10	5.500	8.82	0.0233
0.08	5.190	5.43	0.0143
0.06	4.790	2.63	0.0069
0.04	4.040	1.61	0.0042
0.02	2.460	0.53	0.0014

TABLE F.2 (Contd.)

Isothermal Velocity Profile I-10

Reynolds Number 21969

y/R	$\overline{V}_z$	$\frac{\varepsilon_M}{\nu}$	$\frac{\varepsilon_M}{Ru^*}$
1.00	13.140		
0.95	13.130	50.80	0.0813
0.90	13.100	52.28	0.0836
0.85	13.060	50.80	0.0813
0.80	13.000	47.44	0.0759
0.75	12.910	44.26	0.0708
0.70	12.790	43.40	0.0694
0.65	12.650	45.29	0.0724
0.60	12.500	46.82	0.0749
0.55	12.350	48.95	0.0783
0.50	12.160	48.86	0.0782
0.45	11.980	46.71	0.0747
0.40	11.750	45.24	0.0724
0.35	11.480	44.06	0.0705
0.30	11.200	43.25	0.0692
0.25	10.910	41.36	0.0661
0.20	10.560	35.94	0.0575
0.18	10.390	34.10	0.0545
0.16	10.200	31.33	0.0501
0.14	10.010	28.82	0.0461
0.12	9.780	25.24	0.0403
0.10	9.520	20.25	0.0324
0.08	9.190	14.07	0.0225
0.06	8.720	7.30	0.0116
0.04	7.890	4.88	0.0078
0.02	5.890	1.58	0.0025

TABLE F.2 (Contd.)

Isothermal Velocity Profile I-11

Reynolds Number 21650

y/R	$\overline{V}_z$	$\frac{\varepsilon_M}{\nu}$	$\frac{\varepsilon_M}{Ru^*}$
1.00	13.050		
0.95	13.040	49.17	0.0797
0.90	13.030	49.17	0.0797
0.85	12.960	44.16	0.0715
0.80	12.910	40.05	0.0649
0.75	12.800	40.05	0.0649
0.70	12.670	39.14	0.0634
0.65	12.530	40.05	0.0649
0.60	12.370	40.76	0.0660
0.55	12.180	42.01	0.0681
0.50	11.980	43.27	0.0701
0.45	11.780	43.55	0.0706
0.40	11.550	42.70	0.0692
0.35	11.280	41.23	0.0668
0.30	10.990	39.65	0.0642
0.25	10.670	36.79	0.0596
0.20	10.300	32.24	0.0522
0.18	10.100	30.39	0.0492
0.16	9.910	28.46	0.0461
0.14	9.700	27.52	0.0446
0.12	9.470	23.99	0.0388
0.10	9.230	19.27	0.0312
0.08	8.870	13.10	0.0212
0.06	8.390	7.08	0.0114
0.04	7.520	4.81	0.0078
0.02	5.650	1.58	0.0025

TABLE F.2 (Contd.)

Isothermal Velocity Profile I-12

Reynolds Number 21571

y/R	$\overline{V}_z$	$\frac{\varepsilon_M}{\nu}$	$\frac{\varepsilon_M}{Ru^*}$
1.00	13.110		
0.95	13.090	33.73	0.0548
0.90	13.050	36.62	0.0595
0.85	12.990	39.43	0.0641
0.80	12.920	38.69	0.0629
0.75	12.820	38.60	0.0627
0.70	12.680	38.26	0.0622
0.65	12.540	38.75	0.0630
0.60	12.370	40.51	0.0658
0.55	12.180	41.32	0.0672
0.50	11.990	42.62	0.0693
0.45	11.770	43.54	0.0708
0.40	11.540	44.15	0.0718
0.35	11.290	42.96	0.0698
0.30	11.030	39.51	0.0642
0.25	10.690	35.63	0.0579
0.20	10.280	33.40	0.0543
0.18	10.110	32.80	0.0533
0.16	9.940	30.80	0.0501
0.14	9.740	27.73	0.0451
0.12	9.510	23.91	0.0388
0.10	9.240	19.50	0.0317
0.08	8.910	14.02	0.0228
0.06	8.450	7.40	0.0120
0.04	7.680	4.98	0.0081
0.02	5.760	1.60	0.0026

TABLE F.2 (Contd.)

Isothermal Velocity Profile I-13

Reynolds Number 21504

y/R	$\overline{V}_z$	$\frac{\epsilon_M}{\nu}$	$\frac{\epsilon_M}{Ru^*}$
1.00	13.110		
0.95	13.100	52.15	0.0850
0.90	13.080	47.84	0.0780
0.85	13.030	42.72	0.0696
0.80	12.960	40.07	0.0653
0.75	12.850	39.70	0.0647
0.70	12.730	40.70	0.0663
0.65	12.590	42.62	0.0695
0.60	12.440	44.18	0.0720
0.55	12.270	44.43	0.0724
0.50	12.090	42.86	0.0698
0.45	11.870	41.47	0.0676
0.40	11.610	40.22	0.0656
0.35	11.340	39.64	0.0646
0.30	11.040	38.40	0.0626
0.25	10.710	36.33	0.0592
0.20	10.320	34.23	0.0558
0.18	10.150	33.08	0.0539
0.16	9.980	30.83	0.0502
0.14	9.780	27.70	0.0451
0.12	9.550	23.32	0.0380
0.10	9.280	18.61	0.0303
0.08	8.920	13.49	0.0220
0.06	8.430	6.98	0.0113
0.04	7.670	4.66	0.0076
0.02	5.590	1.54	0.0025

TABLE F.2 (Contd.)

Isothermal Velocity Profile I-14

Reynolds Number 31975

y/R	$\bar{V}_z$	$\frac{\varepsilon_M}{\nu}$	$\frac{\varepsilon_M}{Ru^*}$
1.00	19.570		
0.95	19.560	62.44	0.0718
0.90	19.520	56.49	0.0649
0.85	19.440	54.75	0.0629
0.80	19.310	55.18	0.0634
0.75	19.170	59.12	0.0679
0.70	19.000	62.44	0.0718
0.65	18.830	61.82	0.0710
0.60	18.610	59.57	0.0684
0.55	18.340	58.13	0.0668
0.50	18.030	58.35	0.0670
0.45	17.720	59.59	0.0685
0.40	17.370	60.33	0.0693
0.35	17.000	59.40	0.0683
0.30	16.590	55.11	0.0633
0.25	16.130	49.14	0.0565
0.20	15.510	43.11	0.0495
0.18	15.230	42.66	0.0490
0.16	14.950	41.06	0.0472
0.14	14.650	38.47	0.0442
0.12	14.330	33.56	0.0385
0.10	13.930	27.51	0.0316
0.08	13.430	21.28	0.0244
0.06	12.770	12.28	0.0141
0.04	11.860	8.81	0.0101
0.02	9.440	2.87	0.0033

TABLE F.2 (Contd.)

Isothermal Velocity Profile I-15

Reynolds Number 33078

y/R	$\overline{V}_z$	$\frac{\varepsilon_M}{\nu}$	$\frac{\varepsilon_M}{Ru^*}$
1.00	19.470		
0.95	19.440	75.25	0.0839
0.90	19.400	73.75	0.0823
0.85	19.350	76.28	0.0851
0.80	19.260	71.62	0.0799
0.75	19.140	70.12	0.0782
0.70	18.980	71.39	0.0796
0.65	18.820	71.12	0.0793
0.60	18.630	69.27	0.0773
0.55	18.390	66.54	0.0742
0.50	18.110	64.28	0.0717
0.45	17.810	63.52	0.0708
0.40	17.460	63.25	0.0705
0.35	17.090	62.70	0.0699
0.30	16.690	61.06	0.0681
0.25	16.250	56.92	0.0635
0.20	15.730	49.51	0.0552
0.18	15.470	45.07	0.0502
0.16	15.190	42.58	0.0475
0.14	14.870	40.34	0.0450
0.12	14.560	36.41	0.0406
0.10	14.190	30.80	0.0343
0.08	13.730	23.59	0.0263
0.06	13.120	13.51	0.0150
0.04	12.230	9.73	0.0108
0.02	9.940	3.10	0.0034

TABLE F.2 (Contd.)

Isothermal Velocity Profile I-16

Reynolds Number 32456

y/R	$\overline{V}_z$	$\frac{\varepsilon_M}{\nu}$	$\frac{\varepsilon_M}{Ru^*}$
1.00	19.610		
0.95	19.600	84.87	0.0963
0.90	19.570	70.28	0.0797
0.85	19.510	63.40	0.0719
0.80	19.390	58.97	0.0669
0.75	19.250	59.54	0.0675
0.70	19.070	61.97	0.0703
0.65	18.890	65.78	0.0746
0.60	18.670	68.64	0.0778
0.55	18.460	68.96	0.0782
0.50	18.200	67.69	0.0768
0.45	17.910	65.39	0.0742
0.40	17.570	65.28	0.0740
0.35	17.210	62.46	0.0708
0.30	16.840	58.16	0.0660
0.25	16.340	53.26	0.0604
0.20	15.770	50.51	0.0573
0.18	15.540	50.83	0.0576
0.16	15.290	46.85	0.0531
0.14	15.040	40.30	0.0457
0.12	14.690	34.53	0.0391
0.10	14.270	28.70	0.0325
0.08	13.800	22.57	0.0256
0.06	13.190	13.04	0.0147
0.04	12.270	9.33	0.0105
0.02	9.910	2.98	0.0033

TABLE F.2 (Contd.)

Isothermal Velocity Profile I-17

Reynolds Number 31877

y/R	$\bar{V}_z$	$\frac{\varepsilon_M}{\nu}$	$\frac{\varepsilon_M}{Ru^*}$
1.00	19.670		
0.95	19.660	96.49	0.1112
0.90	19.640	79.53	0.0916
0.85	19.580	68.45	0.0789
0.80	19.480	59.73	0.0688
0.75	19.340	57.24	0.0660
0.70	19.150	57.80	0.0666
0.65	18.950	59.58	0.0687
0.60	18.730	62.59	0.0721
0.55	18.480	63.86	0.0736
0.50	18.220	62.43	0.0719
0.45	17.920	61.31	0.0706
0.40	17.550	59.73	0.0688
0.35	17.180	57.02	0.0657
0.30	16.760	53.70	0.0619
0.25	16.240	49.82	0.0574
0.20	15.650	47.15	0.0543
0.18	15.410	45.02	0.0519
0.16	15.140	41.97	0.0483
0.14	14.830	37.24	0.0429
0.12	14.490	31.99	0.0368
0.10	14.060	26.69	0.0307
0.08	13.540	20.68	0.0238
0.06	12.890	12.12	0.0139
0.04	11.920	8.72	0.0100
0.02	9.500	2.85	0.0032

TABLE F.2 (Contd.)

Isothermal Velocity Profile IT-1

Reynolds Number 5590

y/R	$\overline{V}_z$	$\frac{\varepsilon_M}{\nu}$	$\frac{\varepsilon_M}{Ru^*}$
1.00	3.740		
0.95	3.730	14.03	0.0737
0.90	3.720	11.88	0.0624
0.85	3.710	14.03	0.0737
0.80	3.680	14.69	0.0772
0.75	3.660	14.55	0.0764
0.70	3.630	14.46	0.0760
0.65	3.590	13.68	0.0719
0.60	3.540	13.43	0.0706
0.55	3.490	13.76	0.0723
0.50	3.430	13.55	0.0712
0.45	3.370	14.03	0.0737
0.40	3.290	14.03	0.0737
0.35	3.230	13.13	0.0690
0.30	3.140	11.38	0.0598
0.25	3.030	9.95	0.0523
0.20	2.880	8.70	0.0457
0.18	2.840	6.93	0.0364
0.16	2.760	5.55	0.0292
0.14	2.650	3.96	0.0208
0.12	2.510	2.81	0.0148
0.10	2.340	1.80	0.0094
0.08	2.080	1.08	0.0056
0.06	1.700	0.56	0.0029
0.04	1.230	0.34	0.0018
0.02	0.590	0.18	0.0009

TABLE F.2 (Contd.)

Isothermal Velocity Profile IT-2

Reynolds Number 5401

y/R	$\overline{V}_z$	$\frac{\varepsilon_M}{\nu}$	$\frac{\varepsilon_M}{Ru^*}$
1.00	3.640		
0.95	3.630	9.68	0.0524
0.90	3.620	10.39	0.0562
0.85	3.600	11.81	0.0639
0.80	3.580	12.67	0.0686
0.75	3.550	13.24	0.0716
0.70	3.520	12.85	0.0696
0.65	3.480	13.59	0.0735
0.60	3.430	14.19	0.0768
0.55	3.390	14.69	0.0795
0.50	3.340	15.12	0.0818
0.45	3.280	14.16	0.0766
0.40	3.220	14.08	0.0762
0.35	3.140	13.06	0.0707
0.30	3.070	11.46	0.0620
0.25	2.960	9.85	0.0533
0.20	2.830	7.57	0.0409
0.18	2.770	5.90	0.0319
0.16	2.680	4.76	0.0258
0.14	2.570	3.62	0.0196
0.12	2.430	2.65	0.0143
0.10	2.260	1.62	0.0087
0.08	2.010	0.90	0.0048
0.06	1.600	0.49	0.0026
0.04	1.100	0.30	0.0016
0.02	0.560	0.22	0.0011

TABLE F.2 (Contd.)

Isothermal Velocity Profile IT-3

Reynolds Number 5219

y/R	$\overline{V}_z$	$\frac{\varepsilon_M}{\nu}$	$\frac{\varepsilon_M}{Ru^*}$
1.00	3.520		
0.95	3.520	10.52	0.0586
0.90	3.510	12.44	0.0693
0.85	3.490	12.82	0.0715
0.80	3.475	13.66	0.0761
0.75	3.450	13.66	0.0761
0.70	3.420	13.23	0.0737
0.65	3.380	13.85	0.0772
0.60	3.340	13.66	0.0761
0.55	3.300	12.96	0.0722
0.50	3.240	12.22	0.0681
0.45	3.170	12.04	0.0671
0.40	3.100	12.08	0.0673
0.35	3.030	11.78	0.0657
0.30	2.940	10.88	0.0606
0.25	2.840	9.69	0.0540
0.20	2.720	8.44	0.0471
0.18	2.660	6.48	0.0361
0.16	2.600	5.11	0.0285
0.14	2.490	3.54	0.0197
0.12	2.360	2.51	0.0140
0.10	2.170	1.57	0.0087
0.08	1.950	0.91	0.0051
0.06	1.560	0.49	0.0027
0.04	1.110	0.28	0.0015
0.02	0.550	0.16	0.0009

TABLE F.2 (Contd.)

Isothermal Velocity Profile IT-4

Reynolds Number 16117

y/R	$\overline{V}_z$	$\frac{\varepsilon_M}{\nu}$	$\frac{\varepsilon_M}{Ru^*}$
1.00	10.110		
0.95	10.100	38.65	0.0811
0.90	10.090	33.69	0.0707
0.85	10.040	34.43	0.0722
0.80	9.980	32.64	0.0685
0.75	9.920	32.84	0.0689
0.70	9.820	32.64	0.0685
0.65	9.710	32.21	0.0676
0.60	9.580	32.14	0.0674
0.55	9.450	32.08	0.0673
0.50	9.280	32.04	0.0672
0.45	9.110	31.83	0.0668
0.40	8.920	32.47	0.0681
0.35	8.700	32.25	0.0677
0.30	8.490	31.38	0.0658
0.25	8.240	29.75	0.0624
0.20	7.950	25.58	0.0537
0.18	7.820	25.22	0.0529
0.16	7.650	22.94	0.0481
0.14	7.520	21.33	0.0447
0.12	7.320	17.58	0.0369
0.10	7.130	12.79	0.0268
0.08	6.790	8.22	0.0172
0.06	6.330	3.99	0.0083
0.04	5.490	2.53	0.0053
0.02	3.540	0.90	0.0018

TABLE F.2 (Contd.)

Isothermal Velocity Profile IT-5

Reynolds Number 16280

y/R	$\overline{V}_z$	$\frac{\epsilon_M}{\nu}$	$\frac{\epsilon_M}{Ru^*}$
1.00	10.020		
0.95	10.010	36.21	0.0753
0.90	9.990	36.21	0.0753
0.85	9.950	37.94	0.0789
0.80	9.900	36.84	0.0766
0.75	9.840	35.24	0.0733
0.70	9.750	32.49	0.0676
0.65	9.640	32.39	0.0674
0.60	9.500	33.35	0.0694
0.55	9.380	34.62	0.0720
0.50	9.230	34.55	0.0719
0.45	9.070	33.88	0.0705
0.40	8.870	34.07	0.0709
0.35	8.680	33.55	0.0698
0.30	8.470	32.97	0.0686
0.25	8.220	30.59	0.0636
0.20	7.950	28.07	0.0584
0.18	7.810	25.54	0.0531
0.16	7.680	23.39	0.0486
0.14	7.510	20.98	0.0436
0.12	7.330	17.41	0.0362
0.10	7.110	13.83	0.0287
0.08	6.810	8.99	0.0187
0.06	6.410	4.23	0.0088
0.04	5.610	2.63	0.0054
0.02	3.640	0.90	0.0018

TABLE F.3

TURBULENCE MEASUREMENTS

Run No. IT-1

Reynolds Number 5590

y/R	x	y	$\sqrt{\overline{V}_z}$	B	$\sqrt{\overline{e^2}}$	s	v'_z	$\overline{V}_z$	$\frac{v'_z}{\overline{V}_z}$	$\frac{v'_z}{u^*}$
1.00	30	48	1.937	810	2.22	13.22	0.168	3.75	0.0447	0.877
0.10	42	42	1.527	837	8.295	18.12	0.458	2.33	0.1965	2.39
0.04	45	26	1.101	909	9.23	28.81	0.320	1.21	0.2648	1.67
0.20	39	41	1.693	825	5.795	15.80	0.367	2.87	0.1278	1.915
0.90	33	31	1.928	811	2.52	13.30	0.189	3.72	0.0509	0.986
1.00	33	27	1.932	810	2.35	13.27	0.177	3.73	0.0475	0.924
0.14	42	30	1.626	829	7.01	16.63	0.422	2.64	0.1597	2.202
0.50	36	30	1.845	815	3.51	14.09	0.249	3.40	0.0732	1.300
0.02	42	25	0.761	990	6.40	47.98	0.133	0.58	0.2300	0.694
0.70	33	37	1.904	812	2.75	13.52	0.204	3.63	0.0561	1.065
1.00	33	29	1.934	810	2.44	13.23	0.184	3.74	0.0493	0.960
0.08	45	24	1.436	848	8.87	19.75	0.449	2.06	0.2181	2.343
0.16	42	26	1.657	827	6.53	16.25	0.402	2.75	0.1461	2.098
0.03	45	22	0.946	942	8.49	35.62	0.238	0.89	0.2678	1.242
0.30	39	26	1.772	820	4.62	14.87	0.310	3.14	0.0988	1.618
1.00	-	-	1.935	810	-	-	-	3.74	-	-
0.60	36	25	1.881	814	3.20	13.74	0.233	3.54	0.0658	1.216
0.06	45	26	1.296	871	9.23	22.82	0.405	1.68	0.2408	2.114
0.18	42	23	1.682	826	6.14	15.94	0.385	2.83	0.1361	2.009

TABLE F.3 (Contd.)

Run No. IT-3

Reynolds Number 5219

y/R	$\sqrt{\overline{V}_z}$	B	$\sqrt{\overline{e^2}}$ *	s	v'_z	$\overline{V}_z$	$\frac{v'_z}{\overline{V}_z}$	$\frac{v'_z}{u^*}$
1.00	1.868	700.13	2.34	15.87	0.147	3.49	0.042	0.81
0.20	1.639	700.13	6.22	18.56	0.335	2.69	0.1246	1.84
0.04	1.048	821.9	9.28	36.74	0.253	1.10	0.2296	1.39
0.12	1.522	700.13	7.97	20.27	0.393	2.32	0.1695	2.16
0.60	1.827	700.13	3.24	16.33	0.198	3.34	0.0594	1.09
0.30	1.719	700.13	4.96	17.55	0.283	2.95	0.0957	1.56
1.00	1.883	700.13	2.32	15.74	0.147	3.55	0.0415	0.81
0.16	1.617	700.13	7.25	18.87	0.384	2.61	0.147	2.11
0.02	0.793	1305	7.20	80.83	0.089	0.63	0.141	0.49
0.80	1.867	700.13	2.64	15.89	0.166	3.49	0.0476	0.91
0.08	1.393	700.13	9.23	22.43	0.411	1.94	0.2121	2.26
0.40	1.762	700.13	4.32	17.01	0.254	3.10	0.0819	1.40
1.00	1.875	700.13	2.34	15.79	0.148	3.52	0.0421	0.81

* In this run values of $\sqrt{\overline{e^2}}$ were determined using a chart recorder and the R.M.S. meter on the anemometer was not used.

TABLE F.3 (Contd.)

Run No. IT-4

Reynolds Number 16117

Calibration Curve Slope B 696.8

y/R	x	y	$\sqrt{\overline{V}_z}$	$\sqrt{\overline{e^2}}$	s	v'_z	$\overline{V}_z$	$\frac{v'_z}{\overline{V}_z}$	$\frac{v'_z}{u^*}$
1.00	33	38	3.180	2.79	7.33	0.38	10.11	0.0376	0.81
0.20	39	50	2.820	6.03	8.53	0.71	7.95	0.0893	1.50
0.10	42	43.5	2.666	8.44	9.14	0.92	7.11	0.1294	1.96
0.02	48	40.5	1.857	16.29	14.23	1.14	3.45	0.3304	2.43
1.00	33	39.5	3.178	2.84	7.33	0.39	10.10	0.0386	0.82
0.80	33	49	3.159	3.17	7.39	0.43	9.98	0.0431	0.91
0.18	39	54	2.795	6.65	8.62	0.77	7.81	0.0986	1.64
0.08	42	54	2.602	9.41	9.44	1.00	6.77	0.1477	2.12
0.90	33	41	3.176	2.90	7.34	0.39	10.09	0.0386	0.84
0.60	36	42	3.098	4.15	7.58	0.55	9.60	0.0573	1.16
0.16	39	56	2.764	6.77	8.76	0.77	7.64	0.1008	1.64
0.06	45	35	2.508	10.71	9.86	1.09	6.29	0.1733	2.30
0.30	39	39	2.915	5.65	8.19	0.69	8.50	0.0812	1.46
0.40	36	60	2.987	4.96	7.94	0.62	8.92	0.0695	1.32
0.14	39	62	2.740	7.13	8.84	0.81	7.51	0.1079	1.71
0.04	45	53	2.330	13.18	10.79	1.22	5.43	0.2247	2.59
0.03	48	34	2.166	14.93	11.79	1.27	4.69	0.2708	2.69
0.01	45	53	1.311	13.18	21.52	0.61	1.72	0.3547	1.29
0.12	42	35.5	2.704	7.63	8.98	0.85	7.31	0.1163	1.80
0.50	36	48	3.046	4.43	7.74	0.57	9.28	0.0614	1.22

TABLE F.3 (Contd.)

Run No. IT-5

Reynolds Number 16280

Calibration Curve Slope B 715.2

y/R	x	y	$\sqrt{\overline{V}_z}$	$\sqrt{\overline{e^2}}$	s	v'_z	$\overline{V}_z$	$\frac{v'_z}{\overline{V}_z}$	$\frac{v'_z}{u^*}$
1.00	33	35	3.172	2.68	7.50	0.36	10.06	0.0355	0.77
0.20	39	45	2.818	6.07	8.70	0.70	7.94	0.0879	1.49
0.10	42	39	2.665	7.99	9.33	0.86	7.10	0.1207	1.83
0.01	45	53	1.330	13.18	21.60	0.61	1.77	0.3447	1.30
1.10	33	41	3.161	2.90	7.53	0.385	9.99	0.0385	0.83
1.00	33	34	3.165	2.64	7.52	0.35	10.02	0.0350	0.76
0.90	33	37	3.161	2.75	7.52	0.37	9.99	0.0366	0.79
0.12	42	32.5	2.706	7.30	9.15	0.80	7.32	0.1089	1.70
0.50	36	44	3.038	4.25	7.91	0.54	9.23	0.0581	1.15
0.03	48	31	2.189	14.25	11.89	1.20	4.79	0.2504	2.56
1.00	33	36	3.167	2.72	7.51	0.36	10.03	0.0361	0.78
0.30	39	35	2.910	5.35	8.35	0.64	8.47	0.0757	1.36
0.06	45	33	2.526	10.40	9.97	1.04	6.38	0.1635	2.22
0.70	33	58	3.122	3.45	7.64	0.45	9.75	0.0462	0.96
0.16	39	52	2.769	6.53	8.89	0.73	7.67	0.0957	1.55
1.00	33	36	3.169	2.72	7.50	0.36	10.04	0.0360	0.78
0.02	48	37	1.887	15.57	14.23	1.09	3.56	0.3062	2.32
0.60	36	37.5	3.082	3.92	7.77	0.50	9.50	0.0531	1.06
0.04	45	50	2.358	12.80	10.86	1.18	5.56	0.2120	2.51
0.18	39	50	0.854	6.40	8.79	0.73	7.80	0.0933	1.55

APPENDIX G

SAMPLE CALCULATION PROCEDURES - ISOTHERMAL RUNS

G.1 INTRODUCTION

The sample calculation procedures by which the following results

(a) Isothermal velocity profiles

(b) Eddy diffusivities

(c) Isothermal axial turbulence intensities

were obtained from measured data are presented separately in sections G.2 to G.4, respectively. These procedures are illustrated using results from runs IT-3 and IT-5.

G.2 ISOTHERMAL VELOCITY PROFILES

G.2.1 Hot-wire calibration against pitot tube

The hot-wire was calibrated against a pitot tube as described in Chapter 3, pressure differences being measured either on a Hook Gauge containing water or on a micromanometer containing butyl alcohol. Velocities were evaluated from the pitot tube reading using the standard pitot tube equation [131]

$$\bar{V}_z = \sqrt{\frac{2g_c(p_s-p)}{\rho}}$$

where p_s = static pressure lb_f/ft^2

p = impact pressure lb_f/ft^2

The pressure difference across the taps of the pitot tube is related to the manometer reading Δh (inches) by

$$p_s - p = \frac{1}{12} \Delta h \, \rho_{water} \, (S.G.)_f \qquad (G.2)$$

where $(S.G.)_f$ is the specific gravity of the manometer fluid, 1.0 for water, and given by

$$S.G. = 0.8176 - 0.0004 \, (T-50) \qquad (G.3)$$

(where T is the manometer fluid temperature in ^{o}F)

for butyl alcohol.

Substituting equation (G.2) into equation (G.1) and

rearranging,

$$\therefore \quad \overline{v}_z^2 = \frac{2 \times 32.17 \times \Delta h \times 62.43 \times (S.G.)_f \times 359 \times T'_{av}}{28.97 \times 273 \times 12}$$

$$= 15.16\ T'_{av}\ \Delta h\ (S.G.)_f \qquad (G.4)$$

where T'_{av} is the flow temperature in ^{o}K.

During a typical calibration reading for run IT-5 the following measurements were obtained:

manometer fluid temperature = $60^{o}F$

$\Delta h = 0.0135"$ $\qquad T'_{av} = 291.4\ ^{o}K$

From equation (G.3)

$\therefore (S.G.)_f = 0.8176 - 0.0004\ (60-50) = 0.8136$

From equation (G.4)

$\therefore \overline{v}_z^2 = 15.16 \times 291.4 \times 0.0135 \times 0.8136 = 48.49$

$\therefore \overline{v}_z^{\frac{1}{2}} = 2.639\ (ft/sec)^{\frac{1}{2}}$

During the same reading the following values of the hot-wire current, I, and the cold resistance, R_g, were obtained:

$I = 35.78$ mA $\qquad R_{g_{meas}} = 10.24$ ohms

The leads resistance R_L was 0.25 ohms.

$\therefore$ True R_g value $= R_{g_{meas}} - R_L = 10.24 - 0.25 = 9.99$ ohms

For an overheating ratio, $(R_w - R_g)/R_g$, of 0.5

$\therefore$ True R_w value $= 0.5\ R_g + R_g = 1.5 \times 9.99$

$= 14.985$ ohms

$$\therefore \quad \frac{I^2 R_w}{R_w - R_g} = \frac{35.78^2 \times 14.985}{14.985 - 9.99} = 3840.6$$

From these readings a point (3840.6, 2.639) on the hot-wire calibration curve of $\frac{I^2 R_w}{R_w - R_g}$ vs $\overline{v}_z^{\frac{1}{2}}$ was obtained. Further readings enabled a plot such as that in Fig. 3.13 to be prepared.

G.2.2 Hot-wire calibration in calibration device.

This method of hot-wire calibration, described in Chapter 3, was used for low Reynolds number runs such as IT-3 (Re = 5219), from

which measured results used below were taken.

A relationship between the wet-gas meter reading and the average velocity through the throat of the contracting cone in the calibration device was obtained as follows:

When the time taken for the wet-gas meter to turn through 360° is 60 seconds, the flow rate through the meter is 10 000 l/hr, or 0.0981 ft^3/sec. Since the throat diameter is 2.016", the corresponding average throat velocity

$$\bar{U}_{ave} = \frac{0.0981 \times 4 \times 144}{\pi \times 2.016^2} = 4.43 \text{ ft/sec.}$$

Velocities corresponding to other "times of revolution" were calculated by proportion, e.g. for a "time" of 45 sec the average throat velocity

$$\bar{U}_{ave} = 4.43 \times \frac{60}{45} = 5.91 \text{ ft/sec.}$$

During a typical calibration reading the following results were obtained:

Time for one revolution on wet-gas meter = 65.65 secs

Temperature in cone throat = 26.0 $^{\circ}$C

Temperature in wet-gas meter = 21.4 $^{\circ}$C

Allowing for the temperature difference between the throat and the meter, the average throat velocity is therefore

$$\bar{U}_{ave} = \frac{60}{65.65} \times 4.43 \times \frac{(273 + 26.0)}{(273 + 21.4)} = 4.09 \text{ ft/sec}$$

To find the velocity $\bar{U}_{max}$ in the centre of the cone throat where the hot-wire is situated, use is made of Fig. E.4. From this figure, for $\bar{U}_{ave} = 4.09$, $\bar{U}_{ave}/\bar{U}_{max} = 0.921$ and hence

$$\bar{U}_{max} = \frac{4.09}{0.921} = 4.44 \text{ ft/sec}$$

and $\overline{U^2_{max}} = 2.108 \text{ (ft/sec)}^{\frac{1}{2}}$

Measurement of I and R_g during the above reading enabled a point on the calibration curve to be established (see G.2.1) and repetition of the procedure at different flow rates enabled a calibration curve of $\frac{I^2 R_w}{R_w - R_g}$ vs $\overline{V^2_z}$ to be prepared.

G.2.3 Point velocity measurements

From the calibration curve prepared as described in either G.2.1 or G.2.2 the values of the calibration parameters A and B in the equation

$$\frac{I^2 R_w}{R_w - R_g} = A + B\overline{V}_z^{\frac{1}{2}} \qquad (G.5)$$

could be determined. From a knowledge of these two parameters equation (G.5) could be used to obtain point velocity measurements from measured I, R_g and R_w values, as illustrated below:

for run IT-5 A = 1953.3; B = 715.2

At y/R = 0.1 the following measurements were obtained:

I = 35.865 mA; R_g = 9.97 ohms; R_w = 14.955 ohms

∴ From equation (G.5) the velocity at y/R = 0.1 is given by

$$\frac{35.865^2 \times 14.955}{14.955 - 9.97} = 1953.3 + 715.2\,\overline{V}_z^{\frac{1}{2}}$$

whence $\overline{V}_z$ = 7.10 ft/sec.

These point velocity readings were corrected for the effects of turbulence intensity as described in section G.2.4 below. Corrections were also applied if a slight change in measured centre velocity readings was observed during the run. For example, in run IT-4 the centre velocity altered by 1%, not enough to warrant discarding the measured profile but enough to make it necessary to correct measurements during the run to allow for this change.

G.2.4 Correction of mean velocity readings under conditions of high relative turbulence intensity

It was shown in Chapter 2 that point velocity readings should be corrected using the equation

$$\overline{V}_{z_{meas}} = \overline{V}_z \left\{ 1 - \frac{1}{4}\frac{\overline{v_z^2}}{\overline{V}_z^2} + \frac{1}{2}\frac{\overline{v_r^2}}{\overline{V}_z^2} \right\} \qquad (G.6)$$

In order to use this equation measurements of $\frac{v'_z}{\overline{V}_z}$ and either $\frac{v'_r}{\overline{V}_z}$ or $\frac{v'_z}{v'_r}$ are needed. In the present work $\frac{v'_z}{\overline{V}_z}$ values were obtained

from measurements at Re ≈ 16000 and 5000. $\frac{v'_z}{v'_r}$ values, shown in Fig. G.1, were taken from the work of Brown [91] which gave results in fair agreement with the less extensive measurements of Gessner [141].

The method of calculation is as follows:

For y/R = 0.1 (Run IT-5)

$\overline{V}_{z_{meas}} = 7.10$ $\qquad \frac{v'_z}{\overline{V}_z} = 0.1207$

$\frac{v'_z}{v'_r} = 2.13$ (From Fig. G.1)

∴ rewriting equation (G.6) as

$$\overline{V}_z = \frac{\overline{V}_{z_{meas}}}{\left\{1 - \frac{1}{4}\frac{\overline{v_z^2}}{\overline{V}_z^2} + \frac{1}{2}\left(\frac{v'_z}{\overline{V}_z}\Big/\frac{v'_z}{v'_r}\right)^2\right\}} \qquad (G.7)$$

and substituting the values above

$$\therefore \quad \overline{V}_z = \frac{7.10}{\left\{1 - \frac{1}{4}(0.1207)^2 + \frac{1}{2}(\frac{0.1207}{2.13})^2\right\}}$$

$$= 7.11 \text{ ft/sec}$$

This procedure was repeated for other point velocities, and the original and corrected velocities for each isothermal run are given in Appendix F, Table F.1.

G.2.5 Mean velocity

The mean velocity was obtained by integrating the velocity profile according to

$$\overline{V}_{z_m} = 2\int_0^1 \overline{V}_z \, \eta d\eta \qquad (G.8)$$

This was done by plotting and smoothing by hand the corrected velocities obtained as described above. (The corrected velocity values for run IT-5, together with the smoothed velocity profile are shown in Fig. G.2, from which it is clear that the amount of smoothing required is very small indeed.) Values from

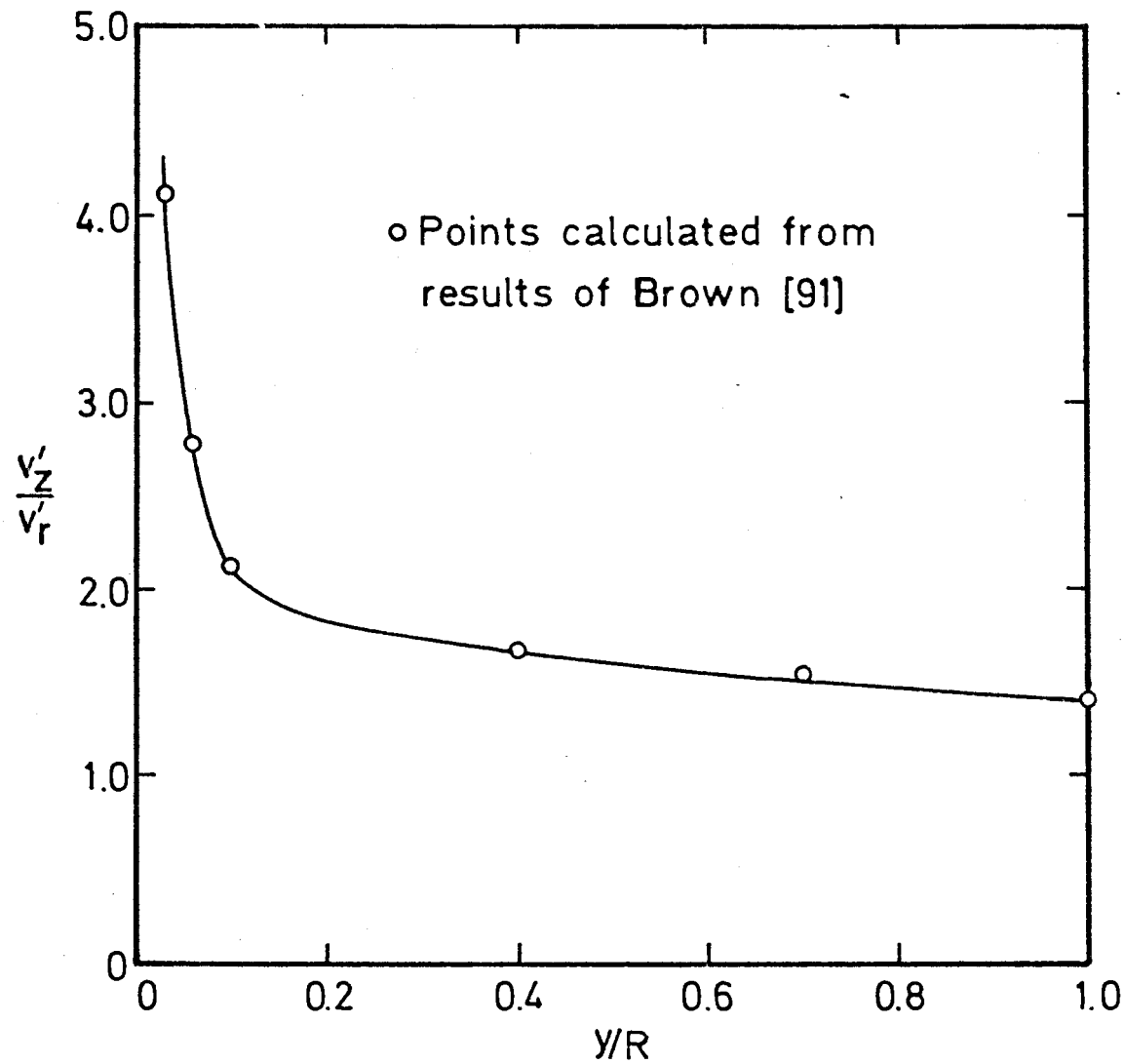

FIGURE G.1 v'_z / v'_r VALUES USED IN EQUATION (G.7)

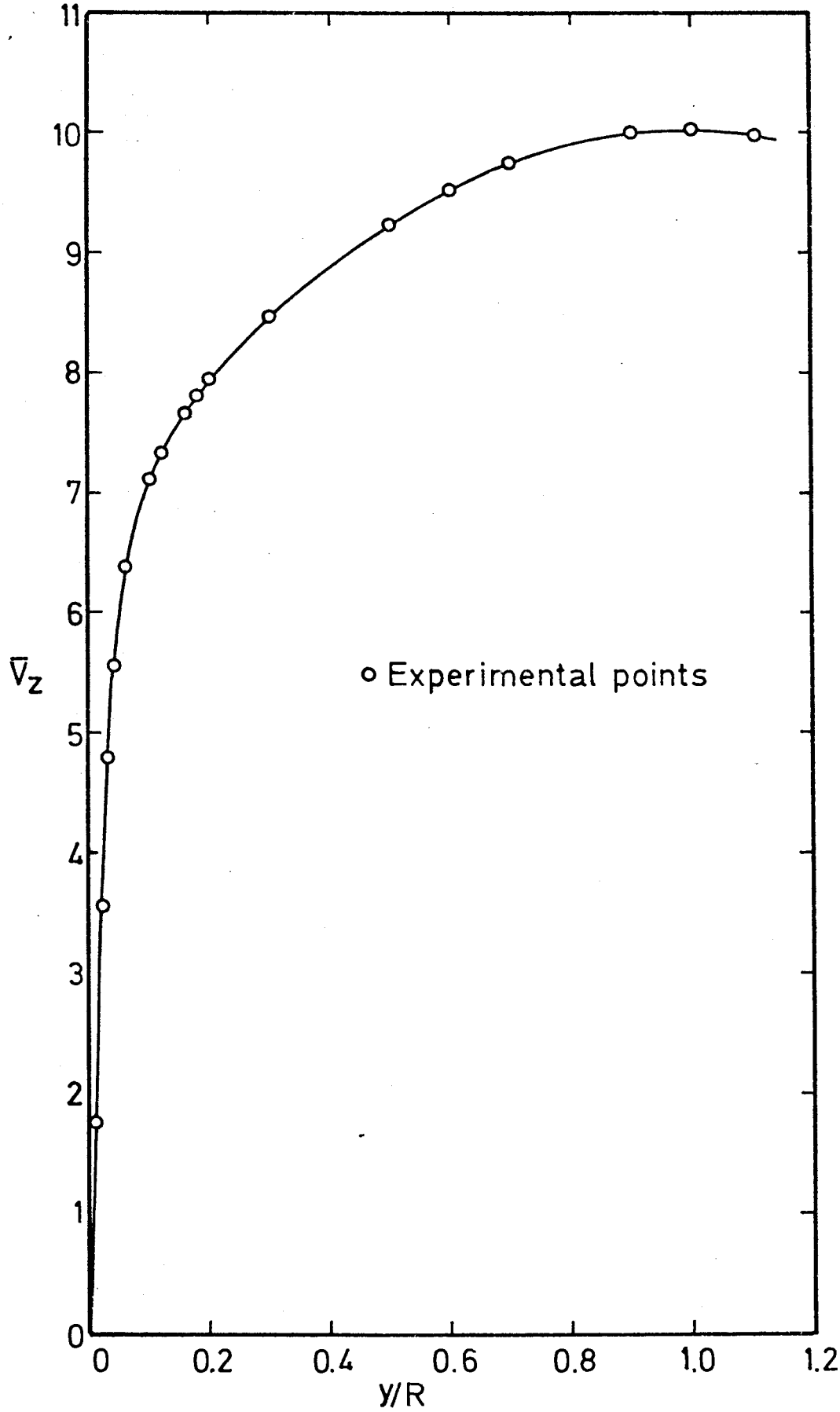

FIGURE G.2 EXPERIMENTAL POINTS AND SMOOTHED VELOCITY PROFILE FOR RUN IT-5

the smoothed profile were then integrated, using a Simpson's rule procedure, on an IBM 1130 computer.

G.2.6 System parameters

The Reynolds number was calculated from a knowledge of the mean velocity and of the physical properties at the flow temperature. The mean velocity was obtained as described in G.2.5 and the physical properties were obtained from the relationships given in Appendix B.

For run IT-5: $\bar{V}_{z_m}$ = 8.04 ft/sec; flow temperature = 64.4°F

$$\therefore \quad Re = \frac{D\bar{V}_{z_m}\rho}{\mu} = \frac{3.886 \times 8.04 \times 0.0757 \times 1488}{12 \times 0.018}$$

$$= 16280$$

Friction factors were calculated according to the equation [131]

$$\frac{1}{\sqrt{f}} = 4.0 \log_{10}(Re\sqrt{f}) - 0.4 \qquad (G.9)$$

For run IT-5, therefore,

$$\frac{1}{\sqrt{f}} = 4.0 \log_{10}(16280\sqrt{f}) - 0.4$$

whence f = 0.00681

The friction velocity $u^* = \bar{V}_{z_m}\sqrt{\frac{f}{2}}$ could then be calculated, e.g. for run IT-5

$$u^* = 8.04\sqrt{\frac{0.00681}{2}} = 0.469 \text{ ft/sec.}$$

From a knowledge of u^* the values of u^+, y^+ and $(u_c^+ - u^+)$ were easily determined.

G.3 EDDY DIFFUSIVITIES OF MOMENTUM

To determine the isothermal value of $\frac{\varepsilon_M}{\nu}$ the smoothed velocity values obtained as explained in section G.2.5 were used. The smoothed data, in η increments of 0.02 between the wall and η = 0.8 and increments of 0.05 between η = 0.8 and the pipe centre were differentiated on an IBM 1130 digital computer.

$$\sqrt{\overline{e^2}} = s^* v'_z$$

whence, for y/R = 0.1

$$v'_z = \frac{7.99}{9.33} = 0.86$$

Values of u^* and $\overline{V}_z$ are known and hence the ratios $\frac{v'_z}{\overline{V}_z}$ and $\frac{v'_z}{u^*}$ can be easily found. These turbulence quantities are reported in Appendix F, Table F.2.

APPENDIX H

EXPERIMENTAL MEASUREMENTS AND CALCULATED RESULTS FOR NON-ISOTHERMAL RUNS.

In this appendix are reported the experimental velocity, temperature and turbulence measurements for runs N-1 to N-14 and NT-1 to NT-5. Also given are calculated values of the eddy diffusivities of heat and momentum together with $\overline{v_r v_z}$ and $\overline{v_r t}$ values.

TABLE H.1

EXPERIMENTAL VELOCITY AND TEMPERATURE MEASUREMENTS FOR RUNS N-1 TO N-14

Non-isothermal velocity profile N-1
Reynolds number 25360
Bulk mean temperature 167°F
Mean velocity 16.56 ft/sec.

y/R	Velocity $\overline{V}_z$ ft/sec	$\frac{\overline{V}_z}{\overline{V}_{z_m}}$	$\frac{\overline{V}_z}{\overline{V}_{z_c}}$	Temperature °F
1.0	20.03	1.209	1.000	133.5
0.9	20.01	1.208	0.999	134.1
0.8	19.91	1.202	0.994	135.1
0.7	19.78	1.194	0.988	137.5
0.6	19.35	1.168	0.966	140.5
0.5	18.71	1.130	0.934	144.1
0.4	18.43	1.113	0.920	148.5
0.3	17.27	1.043	0.862	154.4
0.2	16.17	0.976	0.807	162.7
0.15	15.41	0.931	0.769	163.2
0.1	14.62	0.883	0.730	169.3
0.05	12.94	0.781	0.646	178.7
0.02	9.86	0.595	0.492	192.9

TABLE H.1 (Contd)

NON-ISOTHERMAL VELOCITY PROFILE N-2

REYNOLDS NUMBER	8031.
RAYLEIGH NUMBER	1462.7
WALL HEAT FLUX (BTU/HR.SQ.FT.)	64.9

HOT-WIRE MEASUREMENTS

CALIBRATION CURVE INTERCEPT A	1792.6	
CALIBRATION CURVE SLOPE B	845.7	
CALIBRATION TEMPERATURE	66.0	DEG.F.
TEMPERATURE COEFFICIENT OF RESISTANCE	-0.01236	OHMS/DEG.R.
RESISTANCE AT 0 DEG.R. R0	-2.7508	OHMS

TEMPERATURES

WALL TEMPERATURE TW	245.3	DEG.F.
BULK MEAN TEMPERATURE TB	160.6	DEG.F.
RADIAL MEAN TEMPERATURE TM	167.0	DEG.F.
AXIAL TEMPERATURE GRADIENT DT/DZ	2.71	DEG.F./FT.

CALCULATED RESULTS

MEAN VELOCITY	5.37	FT/SEC
PRANDTL NUMBER	0.698	
GRASHOF NUMBER	4144586.	
NUSSELT NUMBER	14.4	
YANTOVSKII NUMBER	15.30	
Z CRITERION	0.0384	

Y/R	CURRENT I MILLIAMPS	COLD RESISTANCE RG	OPERATING RESISTANCE RW	VELOCITY FT/SEC	CORRECTED VELOCITY FT/SEC	U/UM	U/UC	TEMPERATURE T DEG.F.	TW-T ----- TW-TC
1.00	35.735	17.580	26.370	5.80	5.73	1.065	1.000	136.8	1.000
0.90	35.750	17.590	26.430	5.80	5.73	1.065	1.000	137.1	0.996
0.80	35.755	17.605	26.420	5.81	5.74	1.067	1.001	137.5	0.993
0.70	35.735	17.660	26.480	5.83	5.76	1.070	1.005	139.1	0.978
0.60	35.800	17.755	26.660	5.94	5.88	1.093	1.026	142.0	0.951
0.50	35.865	17.795	26.710	5.94	5.87	1.091	1.024	143.1	0.941
0.40	35.860	17.915	26.840	6.02	5.95	1.106	1.038	146.7	0.908
0.30	36.010	18.115	27.200	6.11	6.02	1.119	1.050	152.4	0.855
0.20	35.920	18.635	27.950	6.04	5.95	1.106	1.038	167.7	0.714
0.16	35.790	18.995	28.505	5.86	5.76	1.070	1.005	178.3	0.616
0.12	35.510	19.425	29.195	5.66	5.54	0.992	0.931	190.9	0.500
0.08	34.710	20.055	30.050	4.68	4.58	0.851	0.799	209.5	0.330
0.04	33.110	20.605	30.935	3.10	3.01	0.559	0.525	225.5	0.182
0.02	31.400	20.905	31.370	1.89	1.81	0.336	0.315	234.3	0.101
0.01	30.445	21.065	31.595	1.37	1.30	0.241	0.226	239.2	0.056

NON-ISOTHERMAL VELOCITY PROFILE N-3

REYNOLDS NUMBER	8016.
RAYLEIGH NUMBER	1267.5
WALL HEAT FLUX (BTU/HR.SQ.FT.)	57.3

HOT-WIRE MEASUREMENTS

CALIBRATION CURVE INTERCEPT A	1792.6	
CALIBRATION CURVE SLOPE B	845.7	
CALIBRATION TEMPERATURE	68.0	DEG.F.
TEMPERATURE COEFFICIENT OF RESISTANCE	-0.01238	OHMS/DEG.R.
RESISTANCE AT 0 DEG.R. R0	-2.7508	OHMS

TEMPERATURES

WALL TEMPERATURE TW	250.7	DEG.F.
BULK MEAN TEMPERATURE TB	162.3	DEG.F.
RADIAL MEAN TEMPERATURE TM	169.8	DEG.F.
AXIAL TEMPERATURE GRADIENT DT/DZ	2.39	DEG.F./FT.

CALCULATED RESULTS

MEAN VELOCITY	5.40	FT/SEC
PRANDTL NUMBER	0.698	
GRASHOF NUMBER	4249829.	
NUSSELT NUMBER	12.2	
YANTOVSKII NUMBER	15.74	
Z CRITERION	0.0333	

Y/R	CURRENT I MILLIAMPS	COLD RESISTANCE RG	OPERATING RESISTANCE RW	VELOCITY FT/SEC	CORRECTED VELOCITY FT/SEC	U/UM	U/UC	TEMPERATURE T DEG.F.	TW-T ----- TW-TC
1.00	35.700	17.605	26.410	5.76	5.70	1.053	1.000	137.5	1.000
0.90	35.690	17.635	26.440	5.77	5.71	1.055	1.001	138.4	0.992
0.80	35.735	17.660	26.490	5.80	5.74	1.061	1.007	139.1	0.985
0.70	35.785	17.750	26.605	5.90	5.84	1.079	1.024	141.8	0.961
0.60	35.840	17.795	26.695	5.93	5.86	1.083	1.028	143.1	0.950
0.50	35.920	17.875	26.845	5.98	5.90	1.090	1.035	145.5	0.929
0.40	35.965	17.985	26.960	6.09	6.01	1.111	1.054	148.7	0.901
0.30	35.990	18.205	27.325	6.09	6.01	1.111	1.054	155.1	0.844
0.20	36.045	18.655	28.045	6.08	5.99	1.107	1.050	168.3	0.727
0.16	35.905	19.005	28.630	5.96	5.88	1.083	1.028	180.4	0.621
0.12	35.520	19.545	29.505	5.87	5.78	1.069	0.967	194.5	0.496
0.08	34.760	20.135	30.265	4.69	4.58	0.846	0.803	211.8	0.343
0.04	33.140	20.805	31.240	3.12	3.02	0.558	0.529	231.5	0.169
0.02	31.335	21.085	31.675	1.83	1.75	0.323	0.307	239.7	0.097

TABLE H.1 (Contd)

NON-ISOTHERMAL VELOCITY PROFILE N-4

REYNOLDS NUMBER	8638.
RAYLEIGH NUMBER	948.2
WALL HEAT FLUX (BTU/HR.SQ.FT.)	31.9

HOT-WIRE MEASUREMENTS

CALIBRATION CURVE INTERCEPT A	1792.6	
CALIBRATION CURVE SLOPE B	845.7	
CALIBRATION TEMPERATURE	68.0	DEG.F.
TEMPERATURE COEFFICIENT OF RESISTANCE	-0.01238	OHMS/DEG.R.
RESISTANCE AT 0 DEG.R. RO	-2.7508	OHMS

TEMPERATURES

WALL TEMPERATURE TW	171.5	DEG.F.
BULK MEAN TEMPERATURE TB	120.8	DEG.F.
RADIAL MEAN TEMPERATURE TM	125.0	DEG.F.
AXIAL TEMPERATURE GRADIENT DT/DZ	1.30	DEG.F./FT.

CALCULATED RESULTS

MEAN VELOCITY	5.14	FT/SEC
PRANDTL NUMBER	0.703	
GRASHOF NUMBER	3486442.	
NUSSELT NUMBER	12.6	
YANTOVSKII NUMBER	11.32	
Z CRITERION	0.0231	

Y/R	CURRENT I MILLIAMPS	COLD RESISTANCE RG	OPERATING RESISTANCE Rw	VELOCITY FT/SEC	CORRECTED VELOCITY FT/SEC	U/UM	U/UC	TEMPERATURE T DEG.F.	TW-T / TW-TC
1.00	35.430	16.440	24.670	5.42	5.39	1.047	1.000	103.3	1.000
0.90	35.440	16.460	24.685	5.46	5.43	1.055	1.007	104.0	0.992
0.80	35.470	16.480	24.720	5.49	5.46	1.060	1.012	104.5	0.984
0.70	35.490	16.530	24.775	5.54	5.52	1.072	1.024	106.0	0.962
0.60	35.545	16.575	24.865	5.57	5.54	1.076	1.027	107.2	0.944
0.50	35.635	16.625	24.955	5.66	5.61	1.090	1.040	108.9	0.920
0.40	35.750	16.729	25.095	5.80	5.76	1.119	1.068	111.6	0.880
0.30	35.810	16.935	25.360	5.98	5.93	1.152	1.100	117.9	0.788
0.20	35.810	17.265	25.930	5.84	5.78	1.123	1.072	127.6	0.645
0.16	35.580	17.465	26.200	5.62	5.56	1.080	1.031	133.3	0.560
0.12	35.280	17.725	26.635	5.19	5.12	0.994	0.949	141.1	0.447
0.08	34.430	18.025	27.055	4.32	4.26	0.827	0.790	149.9	0.317
0.04	32.650	18.355	27.535	2.75	2.70	0.524	0.500	159.4	0.177
0.02	30.790	18.520	27.765	1.55	1.51	0.293	0.280	164.3	0.105

NON-ISOTHERMAL VELOCITY PROFILE N-5

REYNOLDS NUMBER	8474.
RAYLEIGH NUMBER	878.4
WALL HEAT FLUX (BTU/HR.SQ.FT.)	28.3

HOT-WIRE MEASUREMENTS

CALIBRATION CURVE INTERCEPT A	1962.6	
CALIBRATION CURVE SLOPE B	808.3	
CALIBRATION TEMPERATURE	76.2	DEG.F.
TEMPERATURE COEFFICIENT OF RESISTANCE	-0.03575	OHMS/DEG.R.
RESISTANCE AT 0 DEG.R. RO	-0.6480	OHMS

TEMPERATURES

WALL TEMPERATURE TW	165.9	DEG.F.
BULK MEAN TEMPERATURE TB	119.3	DEG.F.
RADIAL MEAN TEMPERATURE TM	123.3	DEG.F.
AXIAL TEMPERATURE GRADIENT DT/DZ	1.19	DEG.F./FT.

CALCULATED RESULTS

MEAN VELOCITY	5.02	FT/SEC
PRANDTL NUMBER	0.703	
GRASHOF NUMBER	3219461.	
NUSSELT NUMBER	12.2	
YANTOVSKII NUMBER	10.80	
Z CRITERION	0.0218	

Y/R	CURRENT I MILLIAMPS	COLD RESISTANCE RG	OPERATING RESISTANCE Rw	VELOCITY FT/SEC	CORRECTED VELOCITY FT/SEC	U/UM	U/UC	TEMPERATURE T DEG.F.	TW-T / TW-TC
1.10	35.830	12.435	18.655	5.45	5.42	1.078	1.005	104.1	0.995
1.00	35.815	12.425	18.645	5.42	5.40	1.074	1.000	103.8	1.000
0.90	35.825	12.430	18.645	5.45	5.43	1.080	1.007	104.0	0.997
0.80	35.835	12.445	18.660	5.48	5.45	1.086	1.012	104.6	0.986
0.70	35.855	12.465	18.695	5.50	5.47	1.088	1.014	105.5	0.972
0.60	35.880	12.485	18.725	5.53	5.50	1.094	1.020	106.4	0.958
0.50	35.945	12.530	18.735	5.60	5.58	1.110	1.035	108.3	0.927
0.40	36.000	12.590	18.885	5.67	5.65	1.124	1.048	110.9	0.886
0.30	36.100	12.720	19.095	5.77	5.73	1.140	1.063	116.5	0.795
0.25	36.100	12.825	19.240	5.80	5.76	1.146	1.068	121.0	0.722
0.20	35.990	12.940	19.425	5.63	5.58	1.110	1.035	126.0	0.642
0.16	35.780	13.080	19.620	5.40	5.35	1.064	0.992	132.0	0.545
0.12	35.445	13.250	19.830	4.96	4.91	0.977	0.910	139.4	0.427
0.08	34.700	13.430	20.145	4.17	4.12	0.819	0.764	147.1	0.302
0.04	33.115	13.610	20.425	2.66	2.64	0.525	0.489	154.9	0.177
0.02	31.485	13.675	20.560	1.52	1.48	0.294	0.274	157.7	0.132

TABLE H.1 (Contd)

NON-ISOTHERMAL VELOCITY PROFILE N-6

REYNOLDS NUMBER	8567.
RAYLEIGH NUMBER	776.3
WALL HEAT FLUX (BTU/HR.SQ.FT.)	28.1

HOT-WIRE MEASUREMENTS

CALIBRATION CURVE INTERCEPT A	1597.8	
CALIBRATION CURVE SLOPE B	818.9	
CALIBRATION TEMPERATURE	78.8	DEG.F.
TEMPERATURE COEFFICIENT OF RESISTANCE	-0.01668	OHMS/DEG.R.
RESISTANCE AT 0 DEG.R. RO	-1.9611	OHMS

TEMPERATURES

WALL TEMPERATURE TW	180.3	DEG.F.
BULK MEAN TEMPERATURE TB	130.6	DEG.F.
RADIAL MEAN TEMPERATURE TM	134.7	DEG.F.
AXIAL TEMPERATURE GRADIENT DT/DZ	1.15	DEG.F./FT.

CALCULATED RESULTS

MEAN VELOCITY	5.21	FT/SEC
PRANDTL NUMBER	0.702	
GRASHOF NUMBER	3241389.	
NUSSELT NUMBER	11.1	
YANTOVSKII NUMBER	10.81	
Z CRITERION	0.0192	

Y/R	CURRENT MILLIAMPS	COLD RESISTANCE RG	OPERATING RESISTANCE Rw	VELOCITY FT/SEC	CORRECTED VELOCITY FT/SEC	U/UM	U/UC	TEMPERATURE T DEG.F.	TW-T / TW-TC
1.10	34.200	16.760	25.140	5.45	5.42	1.038	1.001	112.4	0.995
1.00	34.200	16.750	25.135	5.43	5.40	1.034	1.000	112.1	1.000
0.90	34.240	16.760	25.150	5.48	5.45	1.044	1.007	112.4	0.995
0.80	34.270	16.795	25.180	5.55	5.52	1.057	1.020	113.5	0.979
0.70	34.335	16.840	25.245	5.63	5.60	1.073	1.035	114.9	0.959
0.60	34.410	16.890	25.320	5.72	5.69	1.090	1.051	116.4	0.936
0.50	34.460	16.960	25.425	5.78	5.75	1.101	1.062	118.5	0.905
0.40	34.530	17.060	25.575	5.87	5.83	1.117	1.077	121.6	0.860
0.30	34.585	17.270	25.875	5.96	5.92	1.134	1.094	128.0	0.766
0.25	34.665	17.400	26.100	6.01	5.97	1.143	1.103	132.0	0.708
0.20	34.580	17.580	26.370	5.90	5.86	1.122	1.083	137.5	0.627
0.16	34.440	17.780	26.685	5.71	5.66	1.084	1.046	143.6	0.537
0.12	34.050	18.030	27.045	5.27	5.22	1.000	0.964	151.2	0.426
0.08	33.295	18.310	27.495	4.41	4.36	0.835	0.805	159.8	0.300
0.04	31.520	18.620	27.945	2.84	2.79	0.534	0.515	169.3	0.161
0.02	29.760	18.780	28.170	1.67	1.64	0.314	0.303	174.2	0.089

NON-ISOTHERMAL VELOCITY PROFILE N-7

REYNOLDS NUMBER	8783.
RAYLEIGH NUMBER	406.1
WALL HEAT FLUX (BTU/HR.SQ.FT.)	11.6

HOT-WIRE MEASUREMENTS

CALIBRATION CURVE INTERCEPT A	1597.8	
CALIBRATION CURVE SLOPE B	818.9	
CALIBRATION TEMPERATURE	78.8	DEG.F.
TEMPERATURE COEFFICIENT OF RESISTANCE	-0.01668	OHMS/DEG.R.
RESISTANCE AT 0 DEG.R. RO	-1.9611	OHMS

TEMPERATURES

WALL TEMPERATURE TW	117.3	DEG.F.
BULK MEAN TEMPERATURE TB	102.5	DEG.F.
RADIAL MEAN TEMPERATURE TM	103.0	DEG.F.
AXIAL TEMPERATURE GRADIENT DT/DZ	0.48	DEG.F./FT.

CALCULATED RESULTS

MEAN VELOCITY	4.92	FT/SEC
PRANDTL NUMBER	0.705	
GRASHOF NUMBER	1124671.	
NUSSELT NUMBER	16.1	
YANTOVSKII NUMBER	3.54	
Z CRITERION	0.0097	

Y/R	CURRENT MILLIAMPS	COLD RESISTANCE RG	OPERATING RESISTANCE Rw	VELOCITY FT/SEC	CORRECTED VELOCITY FT/SEC	U/UM	U/UC	TEMPERATURE T DEG.F.	TW-T / TW-TC
1.10	34.680	16.360	24.465	6.01	5.99	1.216	0.996	98.3	0.999
1.00	34.680	16.310	24.450	6.05	6.01	1.220	1.000	98.7	1.000
0.90	34.700	16.290	24.475	5.96	6.00	1.218	0.998	98.0	1.015
0.70	34.560	16.320	24.480	5.88	5.86	1.189	0.975	99.0	0.966
0.60	34.515	16.335	24.510	5.81	5.79	1.175	0.963	99.4	0.942
0.80	34.630	16.305	24.495	5.98	5.96	1.210	0.991	98.5	0.990
0.50	34.459	16.350	24.555	5.70	5.68	1.153	0.945	99.9	0.918
0.40	34.290	16.390	24.570	5.58	5.56	1.128	0.925	101.1	0.854
0.30	34.165	16.430	24.645	5.41	5.39	1.094	0.896	102.3	0.789
0.20	33.885	16.500	24.720	5.13	5.12	1.039	0.851	104.5	0.676
0.16	33.780	16.525	24.735	4.97	4.96	1.005	0.823	105.2	0.636
0.12	33.405	16.540	24.835	4.53	4.51	0.915	0.750	105.7	0.612
0.08	32.860	16.625	24.925	4.03	4.02	0.816	0.668	108.3	0.475
0.04	31.295	16.755	25.140	2.67	2.65	0.538	0.440	112.3	0.266
0.02	29.450	16.825	25.260	1.49	1.47	0.298	0.244	114.4	0.153

TABLE H.1 (Contd)

NON-ISOTHERMAL VELOCITY PROFILE N-8

REYNOLDS NUMBER	8659.	
RAYLEIGH NUMBER	659.7	
WALL HEAT FLUX (BTU/HR.SQ.FT.)	19.5	
HOT-WIRE MEASUREMENTS		
CALIBRATION CURVE INTERCEPT A	1627.0	
CALIBRATION CURVE SLOPE B	826.6	
CALIBRATION TEMPERATURE	76.8	DEG.F.
TEMPERATURE COEFFICIENT OF RESISTANCE	-0.01668	OHMS/DEG.R.
RESISTANCE AT 0 DEG.R. RO	-1.9611	OHMS
TEMPERATURES		
WALL TEMPERATURE TW	142.5	DEG.F.
BULK MEAN TEMPERATURE TB	107.1	DEG.F.
RADIAL MEAN TEMPERATURE TM	110.6	DEG.F.
AXIAL TEMPERATURE GRADIENT DT/DZ	0.81	DEG.F./FT.
CALCULATED RESULTS		
MEAN VELOCITY	4.94	FT/SEC
PRANDTL NUMBER	0.705	
GRASHOF NUMBER	2763135.	
NUSSELT NUMBER	11.2	
YANTOVSKII NUMBER	8.93	
Z CRITERION	0.0160	

Y/R	CURRENT MILLIAMPS	COLD RESISTANCE RG	OPERATING RESISTANCE RW	VELOCITY FT/SEC	CORRECTED VELOCITY FT/SEC	U/UM	U/UC	TEMPERATURE T DEG.F.	TW-T / TW-TC
1.10	34.580	16.170	24.250	5.61	5.59	1.130	1.002	94.4	0.994
1.00	34.580	16.160	24.250	5.58	5.57	1.126	1.000	94.1	1.000
0.90	34.580	16.170	24.250	5.61	5.59	1.130	1.002	94.4	0.994
0.80	34.575	16.175	24.260	5.60	5.58	1.128	1.001	94.5	0.991
0.70	34.570	16.210	24.300	5.61	5.60	1.132	1.004	95.6	0.969
0.60	34.570	16.240	24.355	5.59	5.58	1.128	1.001	96.5	0.950
0.50	34.600	16.300	24.435	5.65	5.63	1.138	1.010	98.3	0.912
0.40	34.660	16.390	24.585	5.69	5.67	1.146	1.017	101.1	0.855
0.30	34.650	16.530	24.795	5.68	5.66	1.144	1.015	105.4	0.766
0.20	34.475	16.805	25.200	5.49	5.46	1.104	0.979	113.8	0.593
0.35	34.660	16.460	24.690	5.69	5.67	1.146	1.017	103.2	0.811
0.25	34.605	16.650	24.975	5.63	5.60	1.132	1.004	109.1	0.691
0.16	34.200	16.960	25.425	5.18	5.15	1.041	0.923	118.5	0.495
0.12	33.720	17.120	25.695	4.62	4.58	0.926	0.821	123.4	0.394
0.08	32.890	17.310	25.980	3.80	3.76	0.760	0.674	129.2	0.274
0.04	31.130	17.500	26.250	2.39	2.36	0.477	0.423	135.1	0.154
0.02	29.350	17.580	26.385	1.33	1.30	0.262	0.233	137.5	0.103

NON-ISOTHERMAL VELOCITY PROFILE N-9

REYNOLDS NUMBER	6794.	
RAYLEIGH NUMBER	1203.3	
WALL HEAT FLUX (BTU/HR.SQ.FT.)	41.6	
HOT-WIRE MEASUREMENTS		
CALIBRATION CURVE INTERCEPT A	1727.8	
CALIBRATION CURVE SLOPE B	779.1	
CALIBRATION TEMPERATURE	69.8	DEG.F.
TEMPERATURE COEFFICIENT OF RESISTANCE	-0.03284	OHMS/DEG.R.
RESISTANCE AT 0 DEG.R. RO	-0.7316	OHMS
TEMPERATURES		
WALL TEMPERATURE TW	226.9	DEG.F.
BULK MEAN TEMPERATURE TB	150.7	DEG.F.
RADIAL MEAN TEMPERATURE TM	157.7	DEG.F.
AXIAL TEMPERATURE GRADIENT DT/DZ	2.08	DEG.F./FT.
CALCULATED RESULTS		
MEAN VELOCITY	4.43	FT/SEC
PRANDTL NUMBER	0.699	
GRASHOF NUMBER	4067439.	
NUSSELT NUMBER	10.4	
YANTOVSKII NUMBER	20.04	
Z CRITERION	0.0373	

Y/R	CURRENT MILLIAMPS	COLD RESISTANCE RG	OPERATING RESISTANCE RW	VELOCITY FT/SEC	CORRECTED VELOCITY FT/SEC	U/UM	U/UC	TEMPERATURE T DEG.F.	TW-T / TW-TC
1.00	33.750	13.385	20.070	4.72	4.68	1.055	1.000	127.5	1.000
0.90	33.750	13.405	20.095	4.73	4.69	1.057	1.002	128.3	0.990
0.80	33.790	13.430	20.130	4.78	4.74	1.068	1.012	129.4	0.980
0.70	33.820	13.465	20.175	4.82	4.79	1.080	1.023	130.8	0.965
0.60	33.870	13.500	20.245	4.85	4.81	1.084	1.027	132.3	0.950
0.50	33.940	13.555	20.325	4.93	4.89	1.102	1.044	134.6	0.927
0.40	33.990	13.630	20.445	4.98	4.93	1.111	1.053	137.7	0.896
0.30	34.065	13.780	20.670	5.07	5.01	1.129	1.070	144.0	0.833
0.25	34.070	13.915	20.865	5.09	5.03	1.134	1.074	149.6	0.777
0.20	34.005	14.120	21.165	5.02	4.97	1.120	1.061	158.1	0.691
0.16	33.930	14.370	21.555	4.91	4.84	1.091	1.034	168.5	0.586
0.12	33.590	14.670	22.020	4.50	4.43	0.999	0.946	181.0	0.461
0.08	32.830	15.060	22.590	3.79	3.72	0.838	0.794	197.2	0.298
0.04	31.165	15.430	23.145	2.32	2.26	0.509	0.482	212.6	0.143
0.02	29.460	15.615	23.425	1.23	1.19	0.268	0.254	220.3	0.066
0.25	34.020	13.310	20.025	4.90	4.85	1.102	1.044	149.4	0.779

TABLE H.1 (Contd)

NON-ISOTHERMAL VELOCITY PROFILE N-10

REYNOLDS NUMBER	5354.
RAYLEIGH NUMBER	489.5
WALL HEAT FLUX (BTU/HR.SQ.FT.)	8.3

HOT-WIRE MEASUREMENTS

CALIBRATION CURVE INTERCEPT A		
Y/R = 0.02	1755.5	
Y/R = 0.04	1884.2	
Y/R > 0.04	2123.4	
CALIBRATION CURVE SLOPE B		
Y/R = 0.02	1111.1	
Y/R = 0.04	969.7	
Y/R > 0.04	774.2	
CALIBRATION TEMPERATURE	80.6	DEG.F.
TEMPERATURE COEFFICIENT OF RESISTANCE	-0.03086	OHMS/DEG.R.
RESISTANCE AT 0 DEG.R. RU	-1.2842	OHMS

TEMPERATURES

WALL TEMPERATURE TW	111.5	DEG.F.
BULK MEAN TEMPERATURE TB	99.8	DEG.F.
RADIAL MEAN TEMPERATURE TM	101.1	DEG.F.
AXIAL TEMPERATURE GRADIENT DT/DZ	0.56	DEG.F./FT.

CALCULATED RESULTS

MEAN VELOCITY	2.97	FT/SEC
FRICTION FACTOR	0.00797	
FRICTION VELOCITY	0.188	FT/SEC
PRANDTL NUMBER	0.706	
GRASHOF NUMBER	914834.	
NUSSELT NUMBER	14.8	
YANTOVSKII NUMBER	8.00	
Z CRITERION	0.0145	

Y/R	CURRENT I MA	RG	RW	VELOCITY FT/SEC	CORR. VELOCITY FT/SEC	Y+	U+	U/UM	U/UC	T DEG.F.	T+	TW-T / TW-TC
1.00	34.900	10.955	16.440	3.89	3.89	168.9	20.69	1.306	1.000	96.4	20.85	1.000
0.30	34.420	11.030	16.538	3.41	3.41	50.6	18.13	1.144	0.881	99.9	16.14	0.773
0.04	31.000	11.215	16.830	1.05	1.05	6.7	5.58	0.352	0.271	108.1	4.71	0.226
0.90	34.865	10.960	16.440	3.86	3.86	152.0	20.53	1.296	1.000	96.4	20.85	1.000
1.00	34.865	10.955	16.433	3.86	3.86	168.9	20.53	1.296	1.000	96.4	20.85	1.000
0.08	32.510	11.165	16.740	1.82	1.82	13.5	9.68	0.611	0.470	106.0	7.69	0.369
0.50	34.710	10.985	16.478	3.69	3.69	84.4	19.62	1.239	0.953	97.9	18.87	0.904
0.02	29.530	11.250	16.875	0.60	0.60	3.3	3.19	0.201	0.155	109.8	2.48	0.119
0.16	33.815	11.080	16.620	2.83	2.83	27.0	15.05	0.950	0.731	102.2	12.91	0.619
1.00	34.850	10.955	16.425	3.86	3.86	168.9	20.53	1.296	1.000	96.4	20.85	1.000
0.70	34.795	10.965	16.448	3.78	3.78	118.2	20.10	1.269	0.976	97.0	20.11	0.964
0.12	33.380	11.120	16.680	2.46	2.46	20.2	13.08	0.826	0.635	104.0	10.42	0.500
0.20	34.070	11.070	16.598	3.08	3.08	33.7	16.38	1.034	0.795	101.7	13.65	0.654
1.00	34.865	10.955	16.425	3.87	3.87	168.9	20.58	1.299	1.000	96.4	20.85	1.000

NON-ISOTHERMAL VELOCITY PROFILE N-11

REYNOLDS NUMBER	5258.
RAYLEIGH NUMBER	724.7
WALL HEAT FLUX (BTU/HR.SQ.FT.)	13.3

HOT-WIRE MEASUREMENTS

CALIBRATION CURVE INTERCEPT A		
Y/R = 0.02	1732.7	
Y/R = 0.04	1920.6	
Y/R > 0.04	2054.1	
CALIBRATION CURVE SLOPE B		
Y/R = 0.02	1090.5	
Y/R = 0.04	878.7	
Y/R > 0.04	770.7	
CALIBRATION TEMPERATURE	82.2	DEG.F.
TEMPERATURE COEFFICIENT OF RESISTANCE	-0.05121	OHMS/DEG.R.
RESISTANCE AT 0 DEG.R. RU	-0.6832	OHMS

TEMPERATURES

WALL TEMPERATURE TW	138.2	DEG.F.
BULK MEAN TEMPERATURE TB	109.8	DEG.F.
RADIAL MEAN TEMPERATURE TM	113.0	DEG.F.
AXIAL TEMPERATURE GRADIENT DT/DZ	0.91	DEG.F./FT.

CALCULATED RESULTS

MEAN VELOCITY	3.02	FT/SEC
FRICTION FACTOR	0.00834	
FRICTION VELOCITY	0.195	FT/SEC
PRANDTL NUMBER	0.704	
GRASHOF NUMBER	1989690.	
NUSSELT NUMBER	9.5	
YANTOVSKII NUMBER	17.25	
Z CRITERION	0.0219	

Y/R	CURRENT I MA	RG	RW	VELOCITY FT/SEC	CORR. VELOCITY FT/SEC	Y+	U+	U/UM	U/UC	T DEG.F.	T+	TW-T / TW-TC
1.00	34.230	10.245	15.368	3.58	3.50	169.7	17.90	1.156	1.000	102.7	31.45	1.000
0.20	34.080	10.470	15.705	3.42	3.36	33.9	17.19	1.110	0.959	114.4	21.07	0.666
0.04	30.890	10.825	16.235	1.13	1.11	6.7	5.70	0.368	0.318	132.6	4.94	0.156
0.90	34.190	10.240	15.360	3.56	3.50	152.8	17.93	1.157	1.001	102.6	31.61	1.000
1.00	34.185	10.240	15.365	3.52	3.50	169.7	17.90	1.156	1.000	102.6	31.61	1.000
0.30	34.240	10.358	15.533	3.59	3.58	50.9	18.31	1.182	1.022	100.7	26.18	0.828
0.12	33.310	10.610	15.907	2.72	2.72	20.3	13.91	0.898	0.777	121.6	14.68	0.464
0.02	29.420	10.875	16.305	0.62	0.62	3.3	3.17	0.204	0.177	135.1	2.71	0.085
0.25	34.210	10.405	15.615	3.54	3.55	42.4	16.16	1.172	1.014	111.0	24.10	0.762
1.00	34.150	10.238	15.365	3.48	3.50	169.7	17.90	1.156	1.000	102.4	31.76	1.000
0.08	32.490	10.695	16.058	2.04	2.05	13.5	10.48	0.677	0.585	126.0	10.85	0.343
0.50	34.210	10.270	15.405	3.56	3.57	84.8	18.26	1.179	1.019	104.2	30.17	0.954
0.16	33.555	10.525	15.780	2.94	2.95	27.1	15.09	0.974	0.842	117.1	18.67	0.590
0.70	34.170	10.250	15.372	3.52	3.52	118.8	18.03	1.164	1.007	103.1	31.13	0.984
1.00	34.155	10.235	15.353	3.50	3.50	169.7	17.90	1.156	1.000	102.4	31.76	1.000

TABLE H.1 (Contd)

NON-ISOTHERMAL VELOCITY PROFILE N-12

REYNOLDS NUMBER	5278.
RAYLEIGH NUMBER	960.0
WALL HEAT FLUX (BTU/HR.SQ.FT.)	20.7

HOT-WIRE MEASUREMENTS

* CALIBRATION CURVE INTERCEPT A	1750.9	
* CALIBRATION CURVE SLOPE B	1073.8	
CALIBRATION TEMPERATURE	77.5	DEG.F.
TEMPERATURE COEFFICIENT OF RESISTANCE	-0.03350	OHMS/DEG.R.
RESISTANCE AT 0 DEG.R. RO	-1.1038	OHMS

TEMPERATURES

WALL TEMPERATURE TW	164.8	DEG.F.
BULK MEAN TEMPERATURE TB	125.8	DEG.F.
RADIAL MEAN TEMPERATURE TM	129.7	DEG.F.
AXIAL TEMPERATURE GRADIENT DT/DZ	1.37	DEG.F./FT.

CALCULATED RESULTS

MEAN VELOCITY	3.19	FT/SEC
FRICTION FACTOR	0.00971	
FRICTION VELOCITY	0.222	FT/SEC
PRANDTL NUMBER	0.702	
GRASHOF NUMBER	2465590.	
NUSSELT NUMBER	10.5	
YANTOVSKII NUMBER	18.22	
Z CRITERION	0.0289	

Y/R	CURRENT MA	RG	RW	VELOCITY FT/SEC	CORR. VELOCITY FT/SEC	Y+	U+	U/UM	U/UC	T DEG.F.	T+	TW-T / TW-TC
1.00	34.260	10.670	15.998	3.48	3.42	183.8	15.37	1.071	1.000	115.2	31.35	1.000
0.16	34.320	11.105	16.658	3.51	3.46	29.4	15.55	1.083	1.011	136.4	17.94	0.568
0.02	30.025	11.605	17.408	0.72	0.71	3.6	3.19	0.222	0.207	160.7	2.61	0.082
0.50	34.420	10.710	16.065	3.63	3.60	91.9	16.18	1.127	1.052	117.0	30.21	0.956
0.90	34.260	10.665	15.998	3.46	3.44	165.5	15.46	1.077	1.005	114.8	31.58	1.000
1.00	34.230	10.660	15.990	3.43	3.42	183.8	15.37	1.071	1.000	114.6	31.69	1.000
0.30	34.570	10.845	16.253	3.81	3.80	55.1	17.08	1.190	1.111	123.6	26.01	0.823
0.08	33.025	11.380	17.062	2.36	2.35	14.7	10.56	0.736	0.687	149.7	9.54	0.302
0.20	34.460	11.010	16.515	3.66	3.65	36.7	16.40	1.143	1.067	131.7	20.90	0.661
0.25	34.585	10.910	16.373	3.78	3.77	45.9	16.94	1.180	1.102	126.9	23.97	0.758
1.00	34.225	10.665	15.998	3.43	3.42	183.8	15.37	1.071	1.000	114.6	31.58	1.000
0.12	33.795	11.220	16.830	3.00	2.99	22.0	13.44	0.936	0.874	142.0	14.42	0.456
0.70	34.295	10.680	16.020	3.50	3.49	128.7	15.68	1.093	1.020	115.5	31.12	0.985
0.04	31.490	11.535	17.310	1.35	1.35	7.3	6.06	0.422	0.394	157.3	4.77	0.151
1.00	34.220	10.665	15.998	3.42	3.42	183.8	15.37	1.071	1.000	114.8	31.58	1.000
0.28	34.560	10.875	16.313	3.77	3.77	50.5	16.94	1.180	1.102	125.1	25.10	0.794

* FOR THIS RUN THE EXPONENT n IN THE CALIBRATION EQUATION WAS TAKEN AS 0.4

NON-ISOTHERMAL VELOCITY PROFILE N-13

REYNOLDS NUMBER	5032.
RAYLEIGH NUMBER	1109.6
WALL HEAT FLUX (BTU/HR.SQ.FT.)	26.9

HOT-WIRE MEASUREMENTS

CALIBRATION CURVE INTERCEPT A		
Y/R = 0.02	1888.7	
Y/R = 0.04	2027.4	
Y/R > 0.04	2077.1	
CALIBRATION CURVE SLOPE B		
Y/R = 0.02	967.7	
Y/R = 0.04	832.3	
Y/R > 0.04	796.0	
CALIBRATION TEMPERATURE	81.9	DEG.F.
TEMPERATURE COEFFICIENT OF RESISTANCE	-0.02945	OHMS/DEG.R.
RESISTANCE AT 0 DEG.R. RO	-1.2697	OHMS

TEMPERATURES

WALL TEMPERATURE TW	192.5	DEG.F.
BULK MEAN TEMPERATURE TB	143.8	DEG.F.
RADIAL MEAN TEMPERATURE TM	148.3	DEG.F.
AXIAL TEMPERATURE GRADIENT DT/DZ	1.82	DEG.F./FT.

CALCULATED RESULTS

MEAN VELOCITY	3.21	FT/SEC
FRICTION FACTOR	0.01077	
FRICTION VELOCITY	0.235	FT/SEC
PRANDTL NUMBER	0.700	
GRASHOF NUMBER	2663245.	
NUSSELT NUMBER	10.6	
YANTOVSKII NUMBER	19.52	
Z CRITERION	0.0356	

Y/R	CURRENT MA	RG	RW	VELOCITY FT/SEC	CORR. VELOCITY FT/SEC	Y+	U+	U/UM	U/UC	T DEG.F.	T+	TW-T / TW-TC
0.30	34.800	11.315	16.973	3.77	3.72	55.5	15.78	1.158	1.081	146.5	23.00	0.744
0.10	34.605	11.435	17.243	3.56	3.51	23.5	14.83	1.088	1.020	155.1	18.69	0.604
0.50	34.695	11.080	16.536	3.65	3.60	92.3	15.27	1.121	1.046	134.1	29.21	0.944
0.02	30.420	12.160	18.240	0.81	0.80	3.6	3.39	0.249	0.232	187.2	2.69	0.087
0.90	34.515	10.990	16.495	3.46	3.43	166.1	14.65	1.088	0.997	130.8	30.82	0.997
1.00	34.490	10.995	16.485	3.49	3.44	184.6	14.59	1.071	1.000	131.0	30.73	1.000
0.06	31.645	12.055	18.083	1.44	1.43	7.5	6.06	0.445	0.415	182.1	5.21	0.168
0.20	34.705	11.375	17.070	3.63	3.63	36.7	15.40	1.130	1.055	149.4	21.57	0.697
0.12	34.170	11.650	17.475	3.15	3.15	22.1	13.30	0.980	0.915	162.5	15.00	0.485
1.00	34.440	10.985	16.478	3.42	3.44	184.6	14.59	1.071	1.000	130.5	31.00	1.000
0.08	33.400	11.840	17.760	2.47	2.48	14.7	10.52	0.772	0.720	171.7	10.42	0.337
0.70	34.525	11.005	16.508	3.50	3.51	129.2	14.89	1.093	1.020	131.5	30.46	0.985
0.25	34.700	11.255	16.883	3.67	3.67	46.1	15.93	1.144	1.068	143.6	24.44	0.790
1.00	34.470	10.990	16.493	3.44	3.44	184.6	14.59	1.071	1.000	130.8	30.62	1.000
0.30	34.750	11.185	16.778	3.72	3.72	55.5	15.78	1.158	1.081	140.2	26.15	0.845

TABLE H.1 (Contd)

NON-ISOTHERMAL VELOCITY PROFILE N-14

REYNOLDS NUMBER	13978.
RAYLEIGH NUMBER	1264.1
WALL HEAT FLUX (BTU/HR.SQ.FT.)	89.3

HOT-WIRE MEASUREMENTS

CALIBRATION CURVE INTERCEPT A	2337.1	
CALIBRATION CURVE SLOPE B	778.6	
CALIBRATION TEMPERATURE	73.4	DEG.F.
TEMPERATURE COEFFICIENT OF RESISTANCE	-0.04098	OHMS/DEG.R.
RESISTANCE AT 0 DEG.R. R0	-0.7894	OHMS

TEMPERATURES

WALL TEMPERATURE TW	196.7	DEG.F.
BULK MEAN TEMPERATURE TB	149.5	DEG.F.
RADIAL MEAN TEMPERATURE TM	152.1	DEG.F.
AXIAL TEMPERATURE GRADIENT DT/DZ	2.16	DEG.F./FT.

CALCULATED RESULTS

MEAN VELOCITY	9.04	FT/SEC
FRICTION FACTOR	0.00726	
FRICTION VELOCITY	0.545	FT/SEC
PRANDTL NUMBER	0.699	
GRASHOF NUMBER	2382442.	
NUSSELT NUMBER	36.3	
YANTOVSKII NUMBER	3.35	
Z CRITERION	0.0143	

Y/R	CURRENT I MA	RG	RW	VELOCITY FT/SEC	CORR. VELOCITY FT/SEC	Y+	U+	U/UM	U/UC	T DEG.F.	T+	TW-T / TW-TC
1.00	40.770	9.965	14.948	11.48	11.22	421.3	20.58	1.240	1.000	138.9	19.91	1.000
0.30	39.920	10.150	15.222	9.76	9.56	126.3	17.53	1.057	0.852	149.?	16.37	0.822
0.04	37.645	10.530	15.780	5.99	5.89	16.8	10.80	0.651	0.524	170.4	9.05	0.454
0.90	40.710	9.973	14.970	11.29	11.14	379.1	20.43	1.232	0.992	139.5	19.72	0.990
1.00	40.700	9.965	14.948	11.33	11.22	421.3	20.58	1.240	1.000	138.9	19.91	1.000
0.20	39.540	10.210	15.315	9.03	8.95	84.2	16.42	0.989	0.797	152.6	15.19	0.763
0.02	35.770	10.715	16.050	3.68	3.65	8.4	6.69	0.403	0.325	180.7	5.52	0.277
0.12	39.120	10.300	15.450	8.27	8.21	50.5	15.06	0.907	0.731	157.6	13.45	0.676
0.70	40.510	10.000	15.007	10.89	10.82	294.9	19.65	1.196	0.964	140.9	19.22	0.965
1.00	40.680	9.965	14.948	11.28	11.22	421.3	20.58	1.240	1.000	138.9	19.91	1.000
0.08	38.765	10.365	15.540	7.70	7.67	33.7	14.07	0.848	0.683	161.2	12.21	0.613
0.16	39.340	10.245	15.375	8.63	8.61	67.4	15.79	0.952	0.767	154.6	14.51	0.728
0.50	40.210	10.060	15.090	10.32	10.31	210.6	18.31	1.140	0.918	144.1	18.11	0.909
1.00	40.670	9.965	14.955	11.22	11.22	421.3	20.58	1.240	1.000	138.9	19.91	1.000

TABLE H.2

VELOCITY AND TEMPERATURE PROFILES* FOR RUNS

NT-1 to NT-5

Non-isothermal velocity profile NT-1

Reynolds number	5405
Rayleigh number	344.8
Wall heat flux	5.0 Btu/hr ft^2
Wall temperature	89.7 ^oF
Bulk mean temperature	83.0 ^oF
Radial mean temperature	83.7 ^oF
Axial temperature gradient	0.35 $^oF/ft$
Mean velocity	2.85 ft/sec
Friction factor	0.00807
Prandtl number	0.709
Grashof number	5.753×10^5
Nusselt number	16.1
Yantovskii number	4.88
Z criterion	0.0101

y/R	Velocity $\bar{V}_z$ ft/sec	$\frac{\bar{V}_z}{\bar{V}_{z_m}}$	Temperature T ^oF	$\frac{T_w - T}{T_w - T_c}$
1.00	3.66	1.286	81.39	1.000
0.90	3.62	1.272	81.46	0.991
0.80	3.58	1.258	81.55	0.980
0.70	3.54	1.244	81.69	0.963
0.60	3.48	1.223	81.87	0.941
0.50	3.43	1.205	82.11	0.913
0.40	3.35	1.177	82.41	0.876
0.30	3.23	1.135	82.88	0.819
0.20	2.98	1.047	83.73	0.717
0.16	2.80	0.984	84.20	0.660
0.12	2.53	0.889	84.88	0.578
0.08	1.99	0.699	85.92	0.452
0.04	1.03	0.361	87.67	0.241
0.02	0.50	0.175	88.66	0.121

* Because a very large number of experimental readings was taken during each of these runs only the final smoothed velocity and temperature profiles are reported.

Non-isothermal velocity profile NT-2

Reynolds number	5525
Rayleigh number	699.5
Wall heat flux	10.7 Btu/hr ft^2
Wall temperature	102.6 ^oF
Bulk mean temperature	87.3 ^oF
Radial mean temperature	89.1 ^oF
Axial temperature gradient	0.73 ^oF/ft
Mean velocity	2.95 ft/sec
Friction factor	0.00811
Prandtl number	0.708
Grashof number	1.267×10^6
Nusselt number	14.8
Yantovskii number	10.23
Z criterion	0.0201

y/R	Velocity $\bar{V}_z$ ft/sec	$\frac{\bar{V}_z}{\bar{V}_{z_m}}$	Temperature T ^oF	$\frac{T_w - T}{T_w - T_c}$
1.00	3.76	1.272	83.7	1.000
0.90	3.755	1.270	83.8	0.995
0.80	3.75	1.269	83.8	0.990
0.70	3.73	1.262	84.2	0.971
0.60	3.71	1.255	84.6	0.952
0.50	3.67	1.241	85.1	0.923
0.40	3.60	1.218	85.8	0.885
0.30	3.46	1.170	87.0	0.823
0.20	3.11	1.052	89.2	0.709
0.16	2.85	0.964	90.7	0.628
0.12	2.43	0.822	92.9	0.509
0.08	1.78	0.602	95.5	0.376
0.04	0.85	0.287	98.4	0.219
0.02	0.40	0.135	100.2	0.123

Non-isothermal velocity profile NT-3

Reynolds number	5419
Rayleigh number	774.4
Wall heat flux	13.4 Btu/hr ft^2
Wall temperature	128.5 ^oF
Bulk mean temperature	100.1 ^oF
Radial mean temperature	103.1 ^oF
Axial temperature gradient	0.90 $^oF/ft$
Mean velocity	3.02 ft/sec
Friction factor	0.00835
Prandtl number	0.706
Grashof number	2.196×10^6
Nusselt number	9.8
Yantovskii number	19.10
Z criterion	0.0227

y/R	Velocity $\bar{V}_z$ ft/sec	$\frac{\bar{V}_z}{\bar{V}_{z_m}}$	Temperature T ^oF	$\frac{T_w - T}{T_w - T_c}$
1.00	3.40	1.124	92.1	1.000
0.90	3.41	1.127	92.2	0.997
0.80	3.42	1.130	92.3	0.995
0.70	3.44	1.137	92.5	0.990
0.60	3.46	1.144	92.8	0.980
0.50	3.50	1.157	93.7	0.957
0.40	3.55	1.173	95.2	0.915
0.37	3.555	1.175	95.8	0.899
0.30	3.53	1.167	98.1	0.836
0.20	3.35	1.107	104.4	0.663
0.16	3.15	1.041	108.2	0.556
0.12	2.79	0.922	112.9	0.428
0.08	2.23	0.737	117.8	0.294
0.04	1.13	0.373	123.3	0.143
0.02	0.57	0.188	126.0	0.069

Non-isothermal velocity profile NT-4

Reynolds number	5154
Rayleigh number	1054.8
Wall heat flux	21.1 Btu/hr ft^2
Wall temperature	161.6 ^oF
Bulk mean temperature	119.9 ^oF
Radial mean temperature	123.9 ^oF
Axial temperature gradient	1.44 $^oF/ft$
Mean velocity	3.06 ft/sec
Friction factor	0.00970
Prandtl number	0.703
Grashof number	2.795×10^6
Nusselt number	10.1
Yantovskii number	21.65
Z criterion	0.0325

y/R	Velocity $\bar{V}_z$ ft/sec	$\frac{\bar{V}_z}{\bar{V}_{z_m}}$	Temperature T ^oF	$\frac{T_w - T}{T_w - T_c}$
1.00	3.22	1.051	107.4	1.000
0.90	3.23	1.054	107.6	0.996
0.80	3.25	1.061	108.0	0.990
0.70	3.28	1.071	108.3	0.983
0.60	3.33	1.087	109.0	0.970
0.50	3.42	1.116	110.3	0.946
0.40	3.52	1.149	112.3	0.910
0.34	3.57	1.165	114.3	0.873
0.30	3.58	1.169	116.6	0.830
0.26	3.575	1.167	119.5	0.777
0.20	3.48	1.136	125.4	0.667
0.16	3.36	1.097	131.2	0.561
0.12	3.04	0.992	138.6	0.425
0.08	2.38	0.777	145.6	0.295
0.04	1.32	0.431	153.7	0.146
0.02	0.67	0.218	157.6	0.073

Non-isothermal velocity profile NT-5

Reynolds number	14701
Rayleigh number	1345.6
Wall heat flux	103.9 Btu/hr ft^2
Wall temperature	199.4 ^oF
Bulk mean temperature	146.9 ^oF
Radial mean temperature	149.8 ^oF
Axial temperature gradient	2.26 $^oF/ft$
Mean velocity	9.44 ft/sec
Friction factor	0.00716
Prandtl number	0.700
Grashof number	2.640×10^6
Nusselt number	38.2
Yantovskii number	3.4
Z criterion	0.0145

y/R	Velocity $\bar{V}_z$ ft/sec	$\frac{\bar{V}_z}{\bar{V}_{z_m}}$	Temperature T ^oF	$\frac{T_w - T}{T_w - T_c}$
1.00	11.79	1.248	136.6	1.000
0.90	11.70	1.239	136.9	0.994
0.80	11.56	1.224	137.6	0.984
0.70	11.36	1.203	138.6	0.968
0.60	11.12	1.177	139.8	0.948
0.50	10.84	1.148	141.4	0.922
0.40	10.48	1.109	143.6	0.888
0.30	10.05	1.064	146.5	0.842
0.20	9.42	0.997	150.1	0.785
0.16	9.04	0.957	152.2	0.750
0.12	8.53	0.903	154.9	0.707
0.08	7.83	0.829	158.9	0.644
0.04	5.85	0.619	168.1	0.498
0.02	4.00	0.423	178.7	0.329

TABLE H.3

EXPERIMENTAL TURBULENCE MEASUREMENTS

RUN NUMBER NT-1

Reynolds number 5405

Prandtl number	0.709
Mean velocity	2.845 ft/sec
Mean temperature	82.97 ^{o}F
Friction factor	0.00806
Friction velocity u*	0.181 ft/sec
Fraction factor (Taylor's equation)	0.00938
Wall heat flux	5.0 Btu/hr ft^2
Wall temperature	89.67 ^{o}F
T*	0.437 ^{o}F

y/R	v_z' ft/sec	t' ^{o}F	$\overline{v_z t}$ ft - ^{o}F/sec	$\frac{v_z'}{\overline{V}_z}$	$\frac{v_z'}{u^*}$	$\frac{t'}{T^*}$	$\frac{t'}{T^* Pr}$	$\frac{\overline{v_z t}}{u^* T^*}$
1.00	0.135	0.387	-0.00666	0.038	0.745	0.886	1.250	-0.085
.70	0.176	0.491	-0.01134	0.051	0.972	1.125	1.586	-0.143
.40	0.251	0.644	-0.0736	0.078	1.387	1.475	2.081	-0.932
.25	0.343	0.801	-0.1791	0.115	1.895	1.834	2.587	-2.266
.18	0.448	0.848	0.1073	0.165	2.475	1.940	2.738	1.358
.12	0.505	1.004	0.0724	0.218	2.790	2.299	3.244	0.916
.10	-	0.848	-	-	-	1.940	2.738	-
.08	-	0.778	-	-	-	1.779	2.511	-
.06	0.444	0.686	0.2509	0.306	2.453	1.569	2.215	3.174
.02	0.109	0.263	-0.0083	0.227	0.602	0.601	0.848	-0.105

TABLE H.3 (Contd.)

RUN NUMBER NT-2

Reynolds number 5525

Prandtl number	0.708
Mean velocity	2.95 ft/sec
Mean temperature	87.2 ^{o}F
Friction factor	0.00811
Friction velocity u*	0.188 ft/sec
Friction factor (Taylor's equation)	0.00932
Wall heat flux	10.7 Btu/hr ft^2
Wall temperature	102.6 ^{o}F
T*	0.908 ^{o}F

y/R	v_z' ft/sec	t' ^{o}F	$\overline{v_z t}$ ft - ^{o}F/sec	$\frac{v_z'}{\overline{V}_z}$	$\frac{v_z'}{u^*}$	$\frac{t'}{T^*}$	$\frac{t'}{T^* Pr}$	$\frac{\overline{v_z t}}{u^* T^*}$
1.00	0.061	0.929	0.00666	0.016	0.324	1.023	1.445	0.038
.70	0.086	1.103	0.03042	0.024	0.457	1.215	1.716	0.178
.40	0.157	1.373	-0.1125	0.044	0.835	1.512	2.136	-0.659
.30	0.182	1.390	-0.1548	0.052	0.968	1.531	2.163	-0.906
.20	0.300	1.431	-0.1204	0.096	1.595	1.576	2.226	-0.705
.10	0.171	1.055	-0.3829	0.079	0.909	1.162	1.641	-2.242
.05	0.145	0.551	0.04176	0.131	0.771	0.607	0.857	0.245
.02	0.052	0.214	-0.00468	0.131	0.276	0.236	0.333	-0.027

TABLE H.3 (Contd.)

RUN NUMBER NT-3

Reynolds number 5419

Prandtl number	0.706
Mean velocity	3.02 ft/sec
Mean temperature	99.8 ^{o}F
Friction factor	0.00835
Friction velocity u*	0.196 ft/sec
Friction factor (Taylor's equation)	0.00937
Wall heat flux	13.4 Btu/hr ft^2
Wall temperature	128.5 ^{o}F
T*	1.116 ^{o}F

y/R	v_z' ft/sec	t' ^{o}F	$\overline{v_z t}$ ft - ^{o}F/sec	$\frac{v_z'}{\overline{V}_z}$	$\frac{v_z'}{u^*}$	$\frac{t'}{T^*}$	$\frac{t'}{T^* Pr}$	$\frac{\overline{v_z t}}{u^* T^*}$
1.00	0.109	1.156	0.0619	0.032	0.552	1.035	1.465	0.283
.70	0.116	1.328	0.0839	0.033	0.587	1.190	1.685	0.384
.40	0.118	2.120	0.0932	0.033	0.596	1.899	2.689	0.426
.25	0.145	2.547	-0.0284	0.041	0.731	2.282	3.230	-0.130
.18	0.166	2.435	-0.1107	0.050	0.837	2.182	3.089	-0.506
.12	0.174	1.728	-0.1759	0.062	0.878	1.547	2.191	-0.805
.06	0.101	0.851	-0.0322	0.059	0.510	0.762	1.080	-0.147
.02	0.023	0.212	-0.0045	0.040	0.116	0.190	0.269	-0.021

TABLE H.3 (Contd.)

RUN NUMBER NT-4

Reynolds number	5154
Prandtl number	0.704
Mean velocity	3.061 ft/sec
Mean temperature	119.5 ^{o}F
Friction factor	0.0097
Friction velocity u*	0.213 ft/sec
Friction factor (Taylor's equation)	0.00949
Wall heat flux	21.1 Btu/hr ft^2
Wall temperature	161.6 ^{o}F
T*	1.663 ^{o}F

y/R	v_z' ft/sec	t' ^{o}F	$\overline{v_z t}$ ft - ^{o}F/sec	$\frac{v_z'}{\overline{V}_z}$	$\frac{v_z'}{u^*}$	$\frac{t'}{T^*}$	$\frac{t'}{T^* Pr}$	$\frac{\overline{v_z t}}{u^* T^*}$
1.00	0.144	1.633	0.1244	0.044	0.679	0.981	1.395	0.350
.70	0.155	1.969	0.1660	0.047	0.728	1.184	1.683	0.468
.40	0.176	3.355	0.3407	0.050	0.828	2.018	2.868	0.960
.30	-	4.108	-	-	-	2.470	3.511	-
.25	0.165	4.399	0.2554	0.046	0.774	2.645	3.761	0.720
.18	0.151	2.330	-0.0461	0.044	0.710	2.405	3.419	-0.130
.12	0.180	2.898	-0.1247	0.059	0.844	1.742	2.477	-0.351
.06	0.110	1.316	-0.0439	0.058	0.516	0.791	1.124	-0.123
.02	0.022	0.313	-0.0058	0.033	0.105	0.188	0.267	-0.016

TABLE H.3 (Contd.)

RUN NUMBER NT-5

Reynolds number 14701

Prandtl number	0.7
Mean velocity	9.44 ft/sec
Mean temperature	146.3 ^{o}F
Friction factor (Taylor's equation)	0.00708
Friction velocity u*	0.562 ft/sec
Wall heat flux	103.9 Btu/hr ft^2
Wall temperature	199.4 ^{o}F
T*	3.253 ^{o}F

y/R	v_z' ft/sec	t' ^{o}F	$\overline{v_z t}$ ft - ^{o}F/sec	$\frac{v_z'}{\overline{V}_z}$	$\frac{v_z'}{u^*}$	$\frac{t'}{T^*}$	$\frac{t'}{T^* Pr}$	$\frac{\overline{v_z t}}{u^* T^*}$
1.00	0.462	1.985	-0.4534	0.039	0.822	0.610	0.871	-0.247
.70	0.587	2.443	-1.0363	0.051	1.043	0.750	1.072	-0.566
.40	0.807	3.253	-1.6852	0.077	1.435	0.999	1.428	-0.921
.25	0.943	3.697	-2.8478	0.096	1.677	1.136	1.623	-1.557
.16	1.281	4.277	-4.1920	0.141	2.278	1.314	1.878	-2.292
.12	-	4.849	-	-	-	1.490	2.129	-
.10	1.373	5.166	-4.8677	0.166	2.442	1.587	2.268	-2.661
.08	-	5.150	-	-	-	1.583	2.260	-
.06	1.660	5.744	-7.3292	0.231	2.953	1.765	2.522	-4.007
.04	-	5.918	-	-	-	1.819	2.598	-
.03	-	5.479	-	-	-	1.684	2.406	-
.02	1.201	0.425	-0.8815	0.300	2.136	0.130	0.187	-0.482

TABLE H.4

EVALUATION OF TERMS IN EQUATION OF MOTION (EQUATION 1.11)

Non-isothermal velocity profile N-10

Reynolds number 5354

Slope of measured velocity profile at the wall -31.773

y/R	Friction term (VI*)	Buoyancy term (VII)	Integral term (III)	Integral term (IV)	Integral term (V)	Resultant	$d\bar{V}_z/d\eta$ (II)	$\overline{v_r v_z}$ term (I)
1.00	0	0	0	0	0	0	0	0
0.90	-3.242	1.930	0.028	-0.048	0.039	-1.293	-0.200	-1.093
0.80	-6.482	3.751	0.056	-0.141	0.077	-2.740	-0.290	-2.449
0.70	-9.721	5.464	0.083	-0.213	0.112	-4.275	-0.410	-3.865
0.60	-12.954	6.982	0.108	-0.276	0.143	-5.998	-0.590	-5.408
0.50	-16.182	8.214	0.130	-0.329	0.169	-7.998	-0.910	-7.088
0.40	-19.396	9.013	0.147	-0.365	0.187	-10.415	-1.330	-9.085
0.30	-22.594	9.182	0.153	-0.376	0.193	-13.442	-2.420	-11.022
0.20	-25.759	8.377	0.135	-0.331	0.179	-17.399	-4.979	-12.420
0.16	-27.014	7.661	0.115	-0.279	0.164	-19.353	-7.472	-11.881
0.12	-28.245	6.610	0.082	-0.203	0.141	-21.616	-12.504	-9.113
0.08	-29.450	5.068	0.037	-0.127	0.105	-24.367	-17.924	-6.443
0.04	-30.642	2.933	0.000	-0.049	0.056	-27.701	-22.046	-5.655
0.02	-31.212	1.581	-0.006	-0.018	0.028	-29.628	-26.247	-3.381

* Roman numerals refer to terms designated in this way in equation (1.11).

TABLE H.4 (Contd.)

Non-isothermal velocity profile N-11

Reynolds number 5259

Slope of measured velocity profile at the wall -31.690

y/R	Friction term (VI*)	Buoyancy term (VII)	Integral term (III)	Integral term (IV)	Integral term (V)	Resultant	$d\bar{V}_z/dn$ (II)	$\overline{v_r v_z}$ term (I)
1.00	0	0	0	0	0	0	0	0
0.90	-3.319	4.160	0.007	-0.090	0.030	0.787	0.050	0.737
0.80	-6.638	8.264	0.015	-0.236	0.060	1.465	0.120	1.345
0.70	-9.952	12.227	0.023	-0.361	0.091	2.028	0.150	1.878
0.60	-13.262	15.972	0.032	-0.476	0.124	2.390	0.204	2.186
0.50	-16.562	19.376	0.042	-0.563	0.159	2.451	0.206	2.245
0.40	-19.832	22.024	0.050	-0.613	0.195	1.824	0.112	1.712
0.38	-20.481	22.400	0.052	-0.616	0.202	1.557	0.082	1.475
0.36	-21.127	22.710	0.053	-0.616	0.209	1.229	0.040	1.189
0.34	-21.772	22.947	0.054	-0.611	0.216	0.835	-0.041	0.876
0.32	-22.409	23.093	0.055	-0.603	0.223	0.359	-0.128	0.487
0.30	-23.046	23.141	0.056	-0.593	0.230	-0.212	-0.263	0.050
0.28	-23.677	23.075	0.056	-0.580	0.236	-0.891	-0.653	-0.239
0.24	-24.927	22.566	0.047	-0.538	0.246	-2.606	-2.679	0.079
0.20	-26.152	21.449	0.025	-0.459	0.249	-4.888	-5.670	0.782
0.16	-27.349	19.574	-0.008	-0.324	0.238	-7.869	-9.135	1.266
0.12	-28.490	16.715	-0.035	-0.153	0.208	-11.755	-12.876	1.121
0.08	-29.585	12.568	-0.038	-0.040	0.157	-16.937	-18.620	1.683
0.04	-30.645	6.983	-0.020	-0.004	0.085	-23.601	-25.275	1.674
0.02	-31.176	3.662	-0.009	-0.001	0.043	-27.481	-28.212	0.731

* Roman numerals refer to terms designated in this way in equation (1.11)

TABLE H.4 (Contd.)

Non-isothermal velocity profile N-12

Reynolds number 5278

Slope of measured velocity profile at the wall -39.098

y/R	Friction term (VI*)	Buoyancy term (VII)	Integral term (III)	Integral term (IV)	Integral term (V)	Resultant	$d\bar{V}_z/d\eta$ (II)	$\overline{v_r v_z}$ term (I)
1.00	0	0	0	0	0	0	0	0
0.90	-4.161	5.512	0.018	-0.115	0.020	1.274	0.188	1.086
0.80	-8.321	10.924	0.038	-0.309	0.044	2.375	0.268	2.107
0.70	-12.477	16.215	0.059	-0.472	0.071	3.397	0.378	3.019
0.60	-16.622	21.242	0.083	-0.623	0.104	4.185	0.548	3.636
0.50	-20.751	25.797	0.112	-0.744	0.146	4.561	0.776	3.785
0.40	-24.830	29.348	0.148	-0.807	0.200	4.059	1.147	2.912
0.36	-26.435	30.265	0.164	-0.812	0.226	3.408	1.128	2.279
0.32	-28.019	30.745	0.177	-0.811	0.254	2.346	0.602	1.744
0.30	-28.803	30.790	0.181	-0.802	0.268	1.634	0.178	1.455
0.28	-29.579	30.689	0.183	-0.780	0.282	0.794	-0.353	1.147
0.26	-30.350	30.426	0.181	-0.743	0.295	-0.191	-0.930	0.739
0.24	-31.106	29.973	0.177	-0.692	0.306	-1.341	-1.650	0.309
0.20	-32.578	28.371	0.160	-0.567	0.322	-4.292	-3.587	-0.705
0.16	-34.005	25.679	0.125	-0.414	0.322	-8.293	-8.292	-0.001
0.12	-35.360	21.672	0.075	-0.246	0.294	-13.565	-13.918	0.353
0.08	-36.657	16.112	0.029	-0.118	0.229	-20.405	-20.269	-0.136
0.04	-37.900	8.905	-0.001	-0.135	0.127	-28.905	-28.859	-0.047
0.02	-38.506	4.668	-0.005	-0.011	0.065	-33.789	-33.398	-0.392

*Roman numerals refer to terms designated in this way in equation (1.11)

TABLE H.4 (Contd.)

Non-isothermal velocity profile N-13

Reynolds number 5033

Slope of measured velocity profile at the wall -42.825

y/R	Friction term (VI*)	Buoyancy term (VII)	Integral term (III)	Integral term (IV)	Integral term (V)	Resultant	$d\bar{V}_z/dn$ (II)	$\overline{v_r v_z}$ term (I)
1.00	0	0	0	0	0	0	0	0
0.90	-4.611	6.029	0.011	-0.142	0.028	1.315	0.186	1.129
0.80	-9.219	11.950	0.024	-0.377	0.059	2.436	0.280	2.156
0.70	-13.818	17.652	0.038	-0.576	0.095	3.391	0.362	3.029
0.60	-18.405	22.981	0.056	-0.764	0.138	4.005	0.458	3.547
0.50	-22.960	27.628	0.077	-0.942	0.188	3.991	0.582	3.409
0.40	-27.470	31.173	0.103	-1.105	0.248	2.949	0.716	2.233
0.36	-29.255	32.170	0.114	-1.152	0.275	2.152	0.602	1.549
0.32	-31.023	32.845	0.122	-1.160	0.303	1.087	0.274	0.813
0.30	-31.897	33.031	0.124	-1.134	0.317	0.440	-0.053	0.493
0.28	-32.764	33.092	0.123	-1.081	0.330	-0.300	-0.447	0.146
0.26	-33.614	32.991	0.119	-1.001	0.342	-1.163	-0.762	-0.401
0.24	-34.442	32.679	0.115	-0.908	0.359	-2.205	-1.044	-1.161
0.20	-36.042	31.252	0.101	-0.726	0.366	-5.049	-2.105	-2.944
0.16	-37.572	28.546	0.072	-0.529	0.367	-9.115	-5.807	-3.308
0.12	-39.022	24.335	0.020	-0.276	0.344	-14.597	-12.887	-1.710
0.08	-40.355	18.275	-0.025	-0.043	0.275	-21.872	-21.562	-0.310
0.04	-41.603	10.168	-0.026	0.016	0.154	-31.290	-30.028	-1.262
0.02	-42.225	5.345	-0.013	0.007	0.079	-36.807	-35.579	-1.228

* Roman numerals refer to terms designated in this way in equation (1.11)

TABLE H.4 (Contd.)

Non-isothermal velocity profile N-14

Reynolds number 13983
Friction factor (Taylor's equation) 0.00726

y/R	Friction term (VI*)	Buoyancy term (VII)	Integral term (III)	Integral term (IV)	Integral term (V)	Resultant	$\frac{d\bar{V}_z}{d\eta}$ (II)	$\overline{v_r v_z}$ term (I)
1.00	0	0	0	0	0	0	0	0
0.90	-23.265	4.334	1.201	-1.567	0.983	-18.314	-1.060	-17.255
0.80	-46.493	8.395	2.362	-4.693	1.876	-38.553	-1.560	-36.994
0.70	-69.662	12.080	3.454	-7.055	2.645	-58.538	-2.120	-56.417
0.60	-92.716	15.183	4.458	-9.150	3.240	-78.985	-2.500	-76.484
0.50	-115.636	17.457	5.357	-10.995	3.636	-100.181	-3.020	-97.162
0.40	-138.378	18.707	6.107	-12.542	3.798	-122.308	-3.740	-118.570
0.30	-160.924	18.726	6.627	-13.672	3.687	-145.556	-5.020	-140.535
0.20	-183.106	17.186	6.680	-14.052	3.227	-170.065	-7.706	-162.358
0.16	-191.799	15.967	6.491	-13.813	2.911	-180.243	-9.083	-171.160
0.12	-200.234	14.227	6.165	-13.077	2.500	-190.419	-11.220	-179.198
0.08	-208.387	11.774	5.213	-10.569	1.982	-199.987	-25.836	-174.152
0.04	-215.094	7.939	2.064	-4.664	1.221	-208.534	-73.861	-134.672
0.02	-216.971	4.670	0.550	-1.724	0.675	-212.800	-130.984	-81.816

*Roman numerals refer to terms designated in this way in equation (1.11)

TABLE H.5

EDDY DIFFUSIVITIES OF HEAT AND MOMENTUM

Non-isothermal run N-10.

Reynolds number 5354
Friction factor 0.00797
Friction velocity u* 0.188 ft/sec
Wall heat flux q_w 8.4 Btu/hr ft^2

y/R	$\overline{v_r v_z}$	$\frac{\overline{v_r v_z}}{u^{*2}}$	$\frac{\varepsilon_M}{\nu}$	$\frac{\varepsilon_M}{Ru^*}$	$\overline{v_r t}$	$\frac{\varepsilon_H}{\alpha}$	$\frac{-\rho C_p \overline{v_r t}}{q_w}$	$\frac{q}{q_w}$	t^+
1.00	0.0000	0.0000	-	-	0.0000	-	0.000	0.000	20.85
0.90	0.0012	0.0339	5.46	0.0315	-0.0149	5.32	0.110	0.131	20.61
0.80	0.0026	0.0761	8.44	0.0488	-0.0322	10.66	0.238	0.261	20.36
0.70	0.0042	0.1202	9.42	0.0545	-0.0479	10.06	0.354	0.389	20.06
0.60	0.0059	0.1685	9.16	0.0531	-0.0629	9.11	0.464	0.515	19.51
0.50	0.0078	0.2212	7.78	0.0452	-0.0763	7.37	0.562	0.638	18.84
0.40	0.0100	0.2842	6.83	0.0397	-0.0878	5.81	0.646	0.756	17.68
0.30	0.0122	0.3461	4.55	0.0265	-0.0956	4.21	0.702	0.867	16.14
0.20	0.0138	0.3922	2.49	0.0146	-0.0972	2.78	0.712	0.963	13.65
0.16	0.0133	0.3762	1.59	0.0093	-0.0897	1.90	0.656	0.995	12.41
0.12	0.0102	0.2899	0.72	0.0043	-0.0733	1.08	0.535	1.020	10.42
0.08	0.0072	0.2062	0.35	0.0021	-0.0594	0.70	0.431	1.032	7.69
0.04	0.0064	0.1822	0.25	0.0015	-0.0349	0.32	0.253	1.027	4.71
0.02	0.0038	0.1094	0.12	0.0007	-0.0079	0.05	0.057	1.017	2.48

TABLE H.5 (Contd.)

Non-isothermal run N-11

Reynolds number 5259
Friction factor 0.00834
Friction velocity u^* 0.195 ft/sec
Wall heat flux q_w 13.3 Btu/hr ft^2

y/R	$\overline{v_r v_z}$	$\frac{\overline{v_r v_z}}{u^{*2}}$	$\frac{\varepsilon_M}{\nu}$	$\frac{\varepsilon_M}{Ru^*}$	$\overline{v_r t}$	$\frac{\varepsilon_H}{\alpha}$	$\frac{-\rho C_p \overline{v_r t}}{q_w}$	$\frac{q}{q_w}$	t^+
1.00	0.0000	0.0000	-	-	0.0000	-	0.000	0.000	31.61
0.90	-0.0006	-0.0169	11.55	0.0654	-0.0243	17.05	0.112	0.118	31.57
0.80	-0.0011	-0.0301	8.55	0.0484	-0.0480	13.34	0.221	0.236	31.46
0.70	-0.0015	-0.0411	9.33	0.0529	-0.0718	12.44	0.330	0.354	31.17
0.60	-0.0017	-0.0455	7.60	0.0431	-0.0950	10.77	0.436	0.473	30.78
0.50	-0.0016	-0.0427	7.05	0.0401	-0.1127	6.33	0.516	0.593	30.18
0.40	-0.0008	-0.0225	6.81	0.0389	-0.1228	3.52	0.561	0.714	28.77
0.38	-0.0005	-0.0146	6.05	0.0346	-0.1249	3.25	0.570	0.738	28.37
0.36	-0.0002	-0.0052	4.42	0.0253	-0.1244	2.81	0.568	0.762	27.93
0.34	0.0001	0.0049	4.05	0.0232	-0.1237	2.44	0.564	0.786	27.45
0.32	0.0006	0.0174	4.58	0.0264	-0.122	2.10	0.555	0.810	26.79
0.30	0.0012	0.0314	4.00	0.0231	-0.1200	1.83	0.546	0.834	26.15
0.28	0.0015	0.0410	2.10	0.0121	-0.1188	1.64	0.540	0.858	25.39
0.24	0.0012	0.0337	0.41	0.0024	-0.1118	1.23	0.506	0.904	23.63
0.20	0.0005	0.0142	0.08	0.0004	-0.0981	0.84	0.442	0.948	21.39
0.16	0.0000	0.0012	0.00	0.0000	-0.0724	0.47	0.325	0.986	18.68
0.12	0.0002	0.0075	0.01	0.0001	-0.0301	0.14	0.134	1.014	14.85
0.08	-0.0003	-0.0084	-0.01	0.0000	0.0002	0.00	-0.001	1.029	10.22
0.04	-0.0002	-0.0066	0.00	0.0000	0.0109	-0.04	-0.048	1.026	5.11
0.02	0.0009	0.0245	0.02	0.0000	0.0165	-0.06	-0.072	1.016	2.71

TABLE H.5 (Contd.)

Non-isothermal run N-12

Reynolds number 5278
Friction factor 0.00971
Friction velocity u^* 0.222 ft/sec
Wall heat flux q_w 20.7 Btu/hr ft^2

y/R	$\overline{v_r v_z}$	$\frac{\overline{v_r v_z}}{u^{*2}}$	$\frac{\varepsilon_M}{\nu}$	$\frac{\varepsilon_M}{Ru^*}$	$\overline{v_r t}$	$\frac{\varepsilon_H}{\alpha}$	$\frac{-\rho C_p \overline{v_r t}}{q_w}$	$\frac{q}{q_w}$	t^+
1.00	0.0000	0.0000	-	-	0.0000	-	0.000	0.000	31.58
0.90	-0.0010	-0.0209	4.73	0.0245	-0.0350	11.78	0.101	0.110	31.47
0.80	-0.0019	-0.0403	6.41	0.0331	-0.0726	19.37	0.210	0.221	31.36
0.70	-0.0028	-0.0573	6.44	0.0333	-0.1078	14.59	0.311	0.333	31.19
0.60	-0.0033	-0.0674	5.21	0.0270	-0.1417	10.78	0.409	0.447	30.79
0.50	-0.0032	-0.0665	3.62	0.0188	-0.1696	6.52	0.489	0.563	30.16
0.40	-0.0020	-0.0416	1.52	0.0079	-0.1860	3.54	0.534	0.683	28.80
0.36	-0.0012	-0.0249	0.92	0.0048	-0.1863	2.65	0.533	0.732	27.88
0.32	-0.0005	-0.0104	0.72	0.0038	-0.1873	2.13	0.535	0.781	26.70
0.30	-0.0001	-0.0026	0.60	0.0032	-0.1879	1.93	0.535	0.806	26.02
0.28	0.0002	0.0057	0.66	0.0035	-0.1839	1.66	0.523	0.831	25.24
0.26	0.0008	0.0165	0.73	0.0039	-0.1789	1.42	0.508	0.856	24.43
0.24	0.0013	0.0279	0.69	0.0037	-0.1668	1.13	0.472	0.880	23.40
0.20	0.0027	0.0550	0.62	0.0033	-0.1443	0.76	0.406	0.927	20.9
0.16	0.0019	0.0398	0.19	0.0010	-0.1181	0.50	0.330	0.969	17.95
0.12	0.0016	0.0331	0.09	0.0005	-0.0784	0.27	0.217	1.003	14.20
0.08	0.0023	0.0480	0.09	0.0005	-0.0493	0.14	0.135	1.003	9.88
0.04	0.0023	0.0483	0.06	0.0003	-0.0186	0.05	0.050	1.024	5.11
0.02	0.0029	0.0588	0.06	0.0003	-0.0010	0.00	0.003	1.016	2.61

TABLE H.5 (Contd.)

Non-isothermal run N-13

Reynolds number 5033
Friction factor 0.01077
Friction velocity u^* 0.236 ft/sec
Wall heat flux q_w 26.9 Btu/hr ft^2

y/R	$\overline{v_r v_z}$	$\frac{\overline{v_r v_z}}{u^{*2}}$	$\frac{\varepsilon_M}{\nu}$	$\frac{\varepsilon_M}{Ru^*}$	$\overline{v_r t}$	$\frac{\varepsilon_H}{\alpha}$	$\frac{-\rho C_p \overline{v_r t}}{q_w}$	$\frac{q}{q_w}$	t^+
1.00	0.0000	0.0000	-	-	0.0000	-	0.000	0.000	30.92
0.90	-0.0012	-0.0231	5.65	0.0289	-0.0471	12.99	0.102	0.110	30.83
0.80	-0.0024	-0.0439	7.14	0.0366	-0.0949	13.42	0.206	0.226	30.72
0.70	-0.0034	-0.0615	7.72	0.0396	-0.1419	11.71	0.307	0.334	30.43
0.60	-0.0039	-0.0714	7.07	0.0363	-0.1858	8.79	0.401	0.448	30.02
0.50	-0.0037	-0.0670	5.19	0.0268	-0.2271	6.62	0.489	0.564	29.22
0.40	-0.0021	-0.0395	2.47	0.0128	-0.2659	5.11	0.570	0.681	28.05
0.36	-0.0013	-0.0237	1.75	0.0091	-0.2791	4.48	0.597	0.729	27.42
0.32	-0.0003	-0.0066	1.07	0.0056	-0.2841	3.50	0.607	0.777	26.64
0.30	0.0000	0.0009	0.77	0.0040	-0.2803	2.88	0.597	0.801	26.16
0.28	0.0005	0.0091	0.90	0.0047	-0.2708	2.27	0.576	0.825	25.62
0.26	0.0012	0.0219	1.26	0.0067	-0.2521	1.67	0.535	0.849	24.90
0.24	0.0022	0.0397	1.66	0.0088	-0.2306	1.25	0.488	0.873	23.96
0.20	0.0045	0.0822	1.68	0.0091	-0.1945	0.78	0.408	0.918	21.57
0.16	0.0051	0.0928	0.67	0.0037	-0.1605	0.52	0.334	0.961	18.61
0.12	0.0031	0.0568	0.18	0.0010	-0.0973	0.24	0.200	0.998	15.01
0.08	0.0013	0.0243	0.04	0.0002	-0.0328	0.06	0.067	1.020	10.42
0.04	0.0027	0.0497	0.06	0.0003	0.0101	-0.01	-0.020	1.024	5.21
0.02	0.0027	0.0498	0.05	0.0003	0.0254	-0.04	-0.050	1.016	2.69

TABLE H.5 (Contd.)

Non-isothermal run N-14

Reynolds number 13983
Friction factor 0.00726
Friction velocity u^* 0.545 ft/sec
Wall heat flux q_w 89.5 Btu/hr ft^2

y/R	$\overline{v_r v_z}$	$\frac{\overline{v_r v_z}}{u^{*2}}$	$\frac{\varepsilon_M}{\nu}$	$\frac{\varepsilon_M}{Ru^*}$	$\overline{v_r t}$	$\frac{\varepsilon_H}{\alpha}$	$\frac{-\rho C_p \overline{v_r t}}{q_w}$	$\frac{q}{q_w}$	t^+
1.00	0.0000	0.0000	-	-	0.0000	-	0.000	0.000	19.91
0.90	0.0215	0.0726	16.27	0.0369	-0.2601	26.98	0.167	0.126	19.76
0.80	0.0463	0.1560	23.71	0.0539	-0.5244	37.86	0.337	0.250	19.54
0.70	0.0709	0.2385	26.61	0.0606	-0.7799	37.73	0.500	0.372	19.23
0.60	0.0965	0.3247	30.59	0.0700	-1.0265	35.16	0.657	0.489	18.73
0.50	0.1232	0.4147	32.17	0.0740	-1.2668	34.67	0.808	0.603	18.11
0.40	0.1514	0.5094	31.70	0.0734	-1.4963	33.49	0.951	0.710	17.34
0.30	0.1808	0.6083	27.99	0.0653	-1.7084	30.17	1.081	0.811	16.44
0.20	0.2110	0.7101	21.06	0.0496	-1.8841	22.57	1.185	0.902	15.20
0.16	0.2237	0.7528	18.84	0.0446	-1.9226	17.04	1.206	0.935	14.51
0.12	0.2361	0.7946	15.97	0.0381	-1.9374	12.33	1.209	0.965	13.52
0.08	0.2320	0.7805	6.74	0.0162	-1.8121	6.06	1.125	0.992	12.22
0.04	0.1840	0.6192	1.82	0.0045	-1.3282	1.90	0.813	1.010	9.05
0.02	0.1150	0.3869	0.62	0.0015	-0.6529	0.54	0.393	1.011	5.52

TABLE H.6

EDDY DIFFUSIVITIES OF HEAT

Non-isothermal run N-2

Reynolds number 8037
Wall heat flux 64.9 Btu/hr ft^2

y/R	$\frac{\varepsilon_H}{\alpha}$	$\overline{v_r t}$	$\frac{-\rho C_p \overline{v_r t}}{q_w}$	$\frac{q}{q_w}$
1.00	-	-	-	-
0.90	42.45	-0.436	0.387	0.111
0.80	47.34	-0.875	0.776	0.223
0.70	48.03	-1.315	1.165	0.335
0.60	47.55	-1.758	1.552	0.448
0.50	38.54	-2.190	1.927	0.562
0.40	34.46	-2.627	2.297	0.676
0.30	16.40	-2.948	2.555	0.792
0.20	7.45	-3.075	2.601	0.904
0.16	5.57	-3.052	2.542	0.945
0.12	4.62	-3.042	2.485	0.981
0.08	3.47	-2.900	2.318	1.008
0.04	3.01	-2.809	2.182	1.018
0.02	2.93	-2.771	2.126	1.014

Non-isothermal run N-3

Reynolds number 8023
Wall heat flux 57.3 Btu/hr ft^2

y/R	$\frac{\varepsilon_H}{\alpha}$	$\overline{v_r t}$	$\frac{-\rho C_p \overline{v_r t}}{q_w}$	$\frac{q}{q_w}$
1.00	-	-	-	-
0.90	16.58	-0.366	0.367	0.111
0.80	33.56	-0.764	0.765	0.222
0.70	40.95	-1.158	1.158	0.334
0.60	40.86	-1.550	1.545	0.447
0.50	35.07	-1.935	1.922	0.562
0.40	26.53	-2.304	2.275	0.677
0.30	14.58	-2.590	2.530	0.792
0.20	6.80	-2.686	2.571	0.904
0.16	4.02	-2.513	2.369	0.945
0.12	3.03	-2.407	2.215	0.982
0.08	2.64	-2.363	2.120	1.009
0.04	2.52	-2.346	2.047	1.019
0.02	2.58	-2.355	2.028	1.014

TABLE H.6 (Contd.)

Non-isothermal run N-4

Reynolds number 8636
Wall heat flux 31.9 Btu/hr ft^2

y/R	$\frac{\varepsilon_H}{\alpha}$	$\overline{v_r t}$	$\frac{-\rho C_p \overline{v_r t}}{q_w}$	$\frac{q}{q_w}$
1.00	-	-	-	-
0.90	17.17	-0.187	0.358	0.109
0.80	20.08	-0.388	0.740	0.218
0.70	32.22	-0.586	1.117	0.329
0.60	30.00	-0.782	1.487	0.440
0.50	27.30	-0.978	1.855	0.553
0.40	15.35	-1.140	2.150	0.668
0.30	10.26	-1.291	2.410	0.788
0.20	6.37	-1.381	2.534	0.905
0.16	4.95	-1.374	2.499	0.947
0.12	3.87	-1.344	2.415	0.983
0.08	3.35	-1.326	2.347	1.010
0.04	2.81	-1.267	2.209	1.020
0.02	2.42	-1.196	2.067	1.014

Non-isothermal run N-5

Reynolds number 8481
Wall heat flux 28.3 Btu/hr ft^2

y/R	$\frac{\varepsilon_H}{\alpha}$	$\overline{v_r t}$	$\frac{-\rho C_p \overline{v_r t}}{q_w}$	$\frac{q}{q_w}$
1.00	-	-	-	-
0.90	25.28	-0.175	0.378	0.111
0.80	30.16	-0.355	0.764	0.223
0.70	34.20	-0.537	1.153	0.335
0.60	29.94	-0.714	1.531	0.448
0.50	21.95	-0.881	1.884	0.562
0.40	14.62	-1.031	2.193	0.678
0.30	10.29	-1.165	2.457	0.794
0.20	5.29	-1.198	2.485	0.909
0.16	4.42	-1.202	2.471	0.950
0.12	3.93	-1.210	2.459	0.985
0.08	3.53	-1.206	2.419	1.011
0.04	2.84	-1.139	2.253	1.019
0.02	2.35	-1.059	2.079	1.014

TABLE H.6 (Contd.)

Non-isothermal run N-6

Reynolds number 8515
Wall heat flux 28.1 Btu/hr ft^2

y/R	$\frac{\varepsilon_H}{\alpha}$	$\overline{v_r t}$	$\frac{-\rho C_p \overline{v_r t}}{q_w}$	$\frac{q}{q_w}$
1.00	-	-	-	-
0.90	14.64	-0.165	0.353	0.108
0.80	15.21	-0.333	0.711	0.218
0.70	20.00	-0.513	1.093	0.328
0.60	22.15	-0.693	1.472	0.440
0.50	17.46	-0.859	1.817	0.554
0.40	12.54	-1.008	2.120	0.670
0.30	9.11	-1.140	2.374	0.786
0.20	5.15	-1.186	2.432	0.902
0.16	3.94	-1.165	2.366	0.944
0.12	3.22	-1.144	2.295	0.982
0.08	2.91	-1.139	2.253	1.009
0.04	2.47	-1.088	2.121	1.019
0.02	2.11	-1.020	1.973	1.014

Non-isothermal run N-7

Reynolds number 8790
Wall heat flux 11.6 Btu/hr ft^2

y/R	$\frac{\varepsilon_H}{\alpha}$	$\overline{v_r t}$	$\frac{-\rho C_p \overline{v_r t}}{q_w}$	$\frac{q}{q_w}$
1.00	-	-	-	-
0.90	34.21	-0.078	0.415	0.123
0.80	36.45	-0.156	0.828	0.245
0.70	40.92	-0.234	1.239	0.365
0.60	40.02	-0.309	1.635	0.482
0.50	29.34	-0.377	1.995	0.597
0.40	23.84	-0.442	2.338	0.708
0.30	19.56	-0.503	2.650	0.814
0.20	15.60	-0.554	2.912	0.912
0.16	13.26	-0.568	2.979	0.949
0.12	9.05	-0.562	2.945	0.981
0.08	4.54	-0.509	2.657	1.007
0.04	2.49	-0.431	2.237	1.018
0.02	1.82	-0.380	1.958	1.014

TABLE H.6 (Contd.)

Non-isothermal run N-8

Reynolds number 8661
Wall heat flux 19.5 Btu/hr ft^2

y/R	$\frac{\varepsilon_H}{\alpha}$	$\overline{v_r t}$	$\frac{-\rho C_p \overline{v_r t}}{q_w}$	$\frac{q}{q_w}$
1.00	-	-	-	-
0.90	28.37	-0.123	0.393	0.116
0.80	29.40	-0.247	0.786	0.232
0.70	23.88	-0.367	1.165	0.348
0.60	20.38	-0.485	1.535	0.464
0.50	16.18	-0.596	1.883	0.580
0.40	11.81	-0.696	2.186	0.697
0.30	7.70	-0.768	2.395	0.813
0.20	4.58	-0.790	2.428	0.923
0.16	4.10	-0.801	2.444	0.962
0.12	3.65	-0.802	2.427	0.994
0.08	3.48	-0.809	2.423	1.016
0.04	2.96	-0.774	2.297	1.021
0.02	2.38	-0.713	2.104	1.015

Non-isothermal run N-9

Reynolds number 6799
Wall heat flux 41.6 Btu/hr ft^2

y/R	$\frac{\varepsilon_H}{\alpha}$	$\overline{v_r t}$	$\frac{-\rho C_p \overline{v_r t}}{q_w}$	$\frac{q}{q_w}$
1.00	-	-	-	-
0.90	13.00	-0.255	0.359	0.111
0.80	24.80	-0.537	0.753	0.222
0.70	32.33	-0.818	1.146	0.334
0.60	31.60	-1.094	1.529	0.447
0.50	27.74	-1.367	1.902	0.561
0.40	19.48	-1.616	2.237	0.677
0.30	10.79	-1.797	2.462	0.794
0.20	4.39	-1.762	2.359	0.908
0.16	3.06	-1.669	2.201	0.951
0.12	2.41	-1.597	2.062	0.987
0.08	2.28	-1.607	2.031	1.013
0.04	2.33	-1.631	2.014	1.021
0.02	2.56	-1.679	2.050	1.015

TABLE H.6 (Contd.)

Non-isothermal run NT-1

Reynolds number 5405
Wall heat flux 5.0 Btu/hr ft^2

y/R	$\frac{\varepsilon'_H}{\alpha}$	$\overline{v_r t}$	$\frac{-\rho C_p \overline{v_r t}}{q_w}$	$\frac{q}{q_w}$
1.00	-	-	-	-
0.90	7.71	-0.0090	0.114	0.128
0.80	10.88	-0.0185	0.234	0.255
0.70	11.58	-0.0277	0.351	0.379
0.60	11.89	-0.0367	0.464	0.501
0.50	11.34	-0.0453	0.573	0.620
0.40	9.45	-0.0529	0.669	0.736
0.30	5.83	-0.0577	0.728	0.846
0.20	3.69	-0.0594	0.749	0.946
0.16	2.65	-0.0569	0.717	0.980
0.12	1.52	-0.0488	0.614	1.009
0.08	0.58	-0.0304	0.382	1.027
0.04	0.16	-0.0119	0.149	1.026
0.02	0.07	-0.0058	0.073	1.016

Non-isothermal run NT-2

Reynolds number 5525
Wall heat flux 10.7 Btu/hr ft^2

y/R	$\frac{\varepsilon_H}{\alpha}$	$\overline{v_r t}$	$\frac{-\rho C_p \overline{v_r t}}{q_w}$	$\frac{q}{q_w}$
1.00	-	-	-	-
0.90	12.78	-0.0205	0.121	0.128
0.80	12.76	-0.0410	0.242	0.256
0.70	11.35	-0.0609	0.359	0.384
0.60	12.13	-0.0814	0.480	0.510
0.50	10.66	-0.1004	0.591	0.635
0.40	8.53	-0.1173	0.690	0.756
0.30	5.08	-0.1267	0.744	0.871
0.20	2.47	-0.1213	0.709	0.972
0.16	1.43	-0.1039	0.606	1.005
0.12	1.02	-0.0920	0.535	1.029
0.08	0.71	-0.0769	0.445	1.039
0.04	0.38	-0.0509	0.293	1.030
0.02	0.15	-0.0246	0.141	1.018

TABLE H.6 (Contd.)

Non-isothermal run NT-3

Reynolds number 5419
Wall heat flux 13.4 Btu/hr ft^2

y/R	$\frac{\varepsilon_H}{\alpha}$	$\overline{v_r t}$	$\frac{-\rho C_p \overline{v_r t}}{q_w}$	$\frac{q}{q_w}$
1.00	-	-	-	-
0.90	16.24	-0.0232	0.108	0.115
0.80	23.28	-0.0475	0.220	0.230
0.70	17.01	-0.0704	0.326	0.346
0.60	10.29	-0.0910	0.422	0.463
0.50	7.04	-0.1100	0.509	0.581
0.40	3.97	-0.1216	0.561	0.701
0.30	1.69	-0.1130	0.518	0.821
0.20	0.55	-0.0740	0.336	0.934
0.16	0.26	-0.0456	0.206	0.974
0.12	0.16	-0.0314	0.141	1.006
0.08	0.08	-0.0177	0.079	1.026
0.04	0.03	-0.0078	0.034	1.026
0.02	0.04	-0.0102	0.045	1.016

Non-isothermal run NT-4

Reynolds number 5154
Wall heat flux 21.1 Btu/hr ft^2

y/R	$\frac{\varepsilon_H}{\alpha}$	$\overline{v_r t}$	$\frac{-\rho C_p \overline{v_r t}}{q_w}$	$\frac{q}{q_w}$
1.00	-	-	-	-
0.90	7.61	-0.0331	0.095	0.108
0.80	11.95	-0.0695	0.200	0.217
0.70	12.00	-0.1048	0.301	0.327
0.60	8.68	-0.1368	0.393	0.439
0.50	6.74	-0.1683	0.482	0.554
0.40	4.17	-0.1906	0.544	0.674
0.30	1.60	-0.1741	0.493	0.797
0.20	0.56	-0.1190	0.332	0.916
0.16	0.22	-0.0641	0.177	0.959
0.12	0.15	-0.0501	0.137	0.996
0.08	0.11	-0.0389	0.105	1.021
0.04	0.04	-0.0150	0.040	1.024
0.02	0.03	-0.0123	0.033	1.016

TABLE H.6 (Contd.)

Non-isothermal run NT-5

Reynolds number 14701
Wall heat flux 103.9 Btu/hr ft^2

y/R	$\frac{\varepsilon_H}{\alpha}$	$\overline{v_r t}$	$\frac{-\rho C_p \overline{v_r t}}{q_w}$	$\frac{q}{q_w}$
1.00	-	-	-	-
0.90	33.46	-0.288	0.160	0.127
0.80	40.06	-0.576	0.320	0.252
0.70	42.50	-0.859	0.475	0.374
0.60	44.61	-1.134	0.627	0.492
0.50	41.12	-1.397	0.770	0.606
0.40	36.34	-1.645	0.904	0.715
0.30	31.74	-1.877	1.026	0.816
0.20	23.62	-2.071	1.125	0.908
0.16	18.96	-2.124	1.150	0.941
0.12	13.83	-2.146	1.157	0.970
0.08	6.77	-2.022	1.084	0.996
0.04	2.12	-1.516	0.801	1.011
0.02	0.46	-0.642	0.333	1.011

TABLE H.7

THE RATIO OF THE EDDY DIFFUSIVITY OF HEAT TO THE EDDY DIFFUSIVITY OF MOMENTUM FOR RUNS N-10 TO N-14

y/R	RUN N-10			RUN N-11		
	$\frac{\varepsilon_M}{\nu}$	$\frac{\varepsilon_H}{\alpha}$	$\frac{\varepsilon_H}{\varepsilon_M}$	$\frac{\varepsilon_M}{\nu}$	$\frac{\varepsilon_H}{\alpha}$	$\frac{\varepsilon_H}{\varepsilon_M}$
0.9	5.46	5.32	1.39	-	-	-
0.8	8.44	10.5	1.78	8.55	13.8	2.31
0.7	9.42	10.2	1.55	9.13	12.75	1.99
0.6	9.10	9.1	1.43	8.5	10.77	1.81
0.5	8.05	7.55	1.34	7.35	6.33	1.23
0.4	6.5	5.81	1.28	5.73	3.52	0.88
0.3	4.55	4.15	1.30	3.58	1.83	0.73
0.2	2.49	2.55	1.46	0.08	0.75	13.4
0.1	0.46	1.10	3.4	0.00	0.04	-

y/R	RUN N-12			RUN N-13		
	$\frac{\varepsilon_M}{\nu}$	$\frac{\varepsilon_H}{\alpha}$	$\frac{\varepsilon_H}{\varepsilon_M}$	$\frac{\varepsilon_M}{\nu}$	$\frac{\varepsilon_H}{\alpha}$	$\frac{\varepsilon_H}{\varepsilon_M}$
0.9	4.73	11.78	3.56	5.65	12.99	3.28
0.8	6.41	19.37	4.32	7.14	13.42	2.69
0.7	6.44	15.25	3.38	7.72	11.71	2.17
0.6	5.21	10.45	2.87	7.07	9.50	1.92
0.5	3.50	6.35	2.59	5.19	7.10	1.95
0.4	1.64	3.54	3.08	2.55	4.95	2.77
0.3	0.80	1.93	3.45	1.18	2.80	3.39
0.2	0.36	0.76	3.02	0.50	1.00	2.86

TABLE H.7 (Contd.)

y/R	RUN N-14		
	$\frac{\varepsilon_M}{\nu}$	$\frac{\varepsilon_H}{\alpha}$	$\frac{\varepsilon_H}{\varepsilon_M}$
0.9	16.27	26.98	2.365
0.8	23.71	37.86	2.279
0.7	26.61	37.73	2.024
0.6	30.59	35.16	1.641
0.5	32.17	34.67	1.539
0.4	31.70	33.49	1.509
0.3	27.99	30.17	1.540
0.2	21.06	22.57	1.532
0.1	11.89	9.49	1.143

APPENDIX I.

SAMPLE CALCULATION PROCEDURES - NON-ISOTHERMAL RUNS

The methods followed to obtain velocity and temperature profiles from measured data, and to calculate eddy diffusivities and values of $\overline{v_r t}$ and $\overline{v_r v_z}$ from these profiles, are given below in sections I.1 and I.2 respectively. The evaluation of the turbulence quantities v'_z, t' and $\overline{v_z t}$ from hot-wire measurements is discussed in section I.3.

I.1 EVALUATION OF VELOCITIES, TEMPERATURES AND FLOW PARAMETERS

Where the procedure outlined below is illustrated with sample calculations the results used are those for run N-10.

Hot-wire calibration

The temperature calibration curve was obtained by measuring a number of (R_g, T) points in the temperature calibration system described in Chapter 3. The straight line through the results gave the values

$$\beta = -0.03086 \quad {}^{\circ}K^{-1}$$

$$R_0 = -1.28416 \quad \text{ohms}$$

for the parameters β and R_0 in the equation

$$R_g = R_0(1 + \beta T) \qquad \text{(I.1)}$$

(where T is in $^{\circ}K$)

used to describe the line.

The velocity calibration curve was obtained as explained in Appendix G. For runs N-2 to N-9 the calibration procedure followed that for runs I-1 to I-17 while for the remaining runs that for runs IT-1 to IT-5 was employed. The calibration points were fitted by the King's Law equation

$$\frac{I^2 R_w}{R_w - R_g} = A_f + B\,\overline{V}_z^{0.5} \qquad \text{(I.2)}$$

giving, for run N-10,

$$A_f = 2123.4 \qquad B = 774.2$$

The calibration temperature was $27^{\circ}C \equiv 80.6^{\circ}F$

(To allow for the deviation of the actual calibration curve from the above line at very low velocities, velocities at y/R positions of 0.02 and 0.04 were evaluated from separate calibration lines drawn to approximate the variation of the calibration curve in the vicinity of each of the points.)

Effect of temperature on A

In order to allow for the variation with temperature of the calibration parameter A when evaluating point velocities, the following procedure was employed:

Equation (2.23) can be rearranged to give

$$A_g = \frac{A_f}{1 + \frac{a_1}{2(a+a_1T_g)\beta R_0}(R_w - R_g)} \qquad (I.3)$$

For run N-10, at the calibration temperature of 27°C,

R_g = 10.605 ohms; R_w = 15.91 ohms

Also, β = -0.03086 $^{\circ}K^{-1}$; R_0 = -1.28416 ohms

A_f = 2123.4; T_g = 300 °K

and, from [40]: $a = 12 \times 10^{-6}$; $a_1 = 0.17 \times 10^{-6}$

$$\therefore A_g = \frac{2123.4}{1 + \frac{0.17 \times 10^{-6} \times (15.91 - 10.605)}{2(12\times10^{-6} + 0.17\times10^{-6} \times 300) \times -0.03086 \times -1.28416}}$$

$$= 1798.5$$

The value of A_g can then be used to give the value of A at any temperature from

$$A = A_g\left[1 + \frac{a_1}{2(a + a_1T_g)\beta R_0}(R_w - R_g)\right] \qquad (I.4)$$

as explained in the section below describing the evaluation of point velocities.

Point temperature measurements

These were obtained from measured R_g values using equation (I.1) e.g. at y/R = 1.0, R_g = 10.955

$$T = \frac{1}{\beta}\left(\frac{R_g}{R_0} - 1\right) = \frac{1}{-0.03086}\left(\frac{10.955}{-1.2842} - 1\right)$$

$$= 308.8\ ^{\circ}K \equiv 96.4\ ^{\circ}F$$

Point velocity measurements

The product $\frac{I^2R_w}{R_w-R_g}$ was calculated from measured values of the hot-wire current I, the wire cold resistance R_g and the wire operating resistance R_w:

For y/R = 1.0

$I = 34.90$ mA; $R_g = 10.955$ ohms; $R_w = 16.44$ ohms

$$\therefore \frac{I^2R_w}{R_w-R_g} = \frac{34.90^2 \times 16.44}{16.44 - 10.955} = 3654.0$$

The value of A at the local temperature (308.8 °K) was found from equation (I.4)

For y/R = 1.0, using values given or calculated previously,

$$A = 1798.5\left[1 + \frac{0.17 \times 10^{-6}\ (16.44 - 10.955)}{2(12\times10^{-6} + 0.17\times10^{-6} \times 308.8)(-0.03086)(-1.28416)}\right]$$

$$= 2126.2$$

Substituting into the King's Law equation

$$\frac{I^2R_w}{R_w-R_g} = A + B\bar{V}_z^{0.5}$$

$$\therefore 3654.0 = 2126.2 + 74.2\ \bar{V}_z^{0.5}$$

$$\therefore \bar{V}_z = 3.89 \text{ ft/sec}$$

Bulk mean temperature, T_b

This was calculated from

$$T_b = \frac{\int_0^1 T\bar{V}_z\rho\eta d\eta}{\int_0^1 \bar{V}_z\rho\eta d\eta} \qquad (I.5)$$

using the integration procedure described in section I.2.

For run N-10, $T_b = 99.8$ °F.

Radial mean temperature, T_M

This was calculated from

$$T_M = \frac{\int_0^1 T\eta d\eta}{\int_0^1 \eta d\eta} \qquad (I.6)$$

using the integration procedure from section I.2. For run N-10, T_M = 101.1 °F.

Mean velocity $\overline{V}_{z_m}$

This was calculated from

$$\overline{V}_{z_m} = \frac{\int_0^1 \overline{V}_z \rho n dn}{\rho_b} \qquad (I.7)$$

$$= 2.97 \text{ ft/sec} \quad \text{for run N-10}$$

(ρ_b, at T_b = 99.8 °F, is 0.0709 lb/ft^3)

The integration procedure described in section I.2 was used. $\overline{V}_z$ values were taken from the smoothed velocity profile through the measured data. From the mean velocity the Reynolds number was calculated:

$$Re = \frac{D\overline{V}_{z_m} \rho_b}{\mu_b} = \frac{3.886 \times 2.97 \times 0.0709 \times 1488}{12 \times 0.0189}$$

$$= 5354$$

Friction factor

i) Taylor's correlation :-

The friction factor correlation of Taylor [148]:

$$\frac{f}{2} = \left(0.0007 + \frac{0.0625}{(Re_w)^{0.32}} \right) \left(\frac{T_b}{T_w} \right)^{0.5} \qquad (I.8)$$

gives, for run N-10, where

$$T_w = 111.5 \text{ °F}; \quad T_b = 99.8 \text{ °F}; \quad Re_w = 5163,$$

$$f = 2 \left(0.0007 + \frac{0.0625}{(5163)^{0.32}} \right) \left(\frac{559.8}{571.5} \right)^{0.5}$$

$$= 0.00940$$

ii) The slope at the wall:

The slope of the velocity profile was evaluated from the smoothed velocity distribution by fitting the five points nearest the wall (y/R = 0.02, 0.04, 0.06, 0.08 and 0.10) with a rational

function of the form

$$\bar{V}_z = \frac{c_1 \eta}{1+c_2 \eta} \qquad (I.9)$$

using a matrix inversion technique. This rational function was differentiated to give the slope at the wall.

For N-10, $\left(\frac{d\bar{V}_z}{d\eta}\right)_w = -31.77$

and this was related to the friction factor since from equation (1.18)

$$\left(\frac{d\bar{V}_z}{d\eta}\right)_w = -0.25 \; f \; Re \; \bar{V}_{z_m} \qquad (I.10)$$

$$\therefore \quad f = \frac{-31.77}{0.25 \times 5354 \times 2.97}$$

$$= 0.00797$$

and this value was used in preference to that calculated by Taylor's method.

From the above value of f the friction velocity u* was calculated

$$u^* = \bar{V}_{z_m} \sqrt{f/2} = 2.97 \sqrt{0.00797/2}$$

$$= 0.188 \text{ ft/sec}$$

It was then a simple matter to calculate u^+ ($= \bar{V}_{z_m}/u^*$) and y^+ ($= yu^*/\nu$) values.

Wall heat flux

The wall heat flux was calculated in two ways

i) From the axial temperature gradient calculated from the wall thermocouples:

For run N-10, $d\bar{T}/dz = 0.54\ ^{\circ}F/ft$ (from wall thermocouple readings)

By a heat balance

$$q_w \pi D = \frac{\pi D^2}{4} \cdot \bar{V}_{z_m} \rho C_p \frac{d\bar{T}}{dz} \qquad (I.11)$$

$$D = 3.886/12; \quad \bar{V}_{z_m} = 2.97 \text{ ft/sec}$$

$$\rho = 0.0709 \text{ lb/ft}^3; \quad C_p = 0.2406 \text{ Btu/lb } ^\circ\text{F}$$

$$\therefore \quad q_w = \frac{3.886 \times 2.97 \times 0.0709 \times 0.2406 \times 0.54}{12 \times 4}$$

$$= 8.0 \text{ Btu/hr ft}^2$$

ii) From the slope of the temperature profile at the wall:

For run N-10, $T_w = 111.5\ ^\circ\text{F}$; $T_{0.02} = 109.8\ ^\circ\text{F}$

$$\therefore \quad \frac{dT}{dr} = \frac{(111.5 - 109.8) \times 24}{0.02 \times 3.886}$$

and since $q_w = k \frac{dT}{dr}$ (I.12)

and $k = 0.0158$ Btu/hr ft $^\circ$F

$$q_w = \frac{(111.5 - 109.8) \times 24 \times 0.0158}{0.02 \times 3.886}$$

$$= 8.7 \text{ Btu/hr ft}^2$$

Taking an average of the two values of q_w above gives

$$q_w = 8.3 \text{ Btu/hr ft}^2$$

for which the corresponding value of $\frac{d\bar{T}}{dz}$ is $0.56\ ^\circ\text{F/ft}$

With a knowledge of q_w, the value of T^* was then calculated

$$T^* = \frac{q_w}{\rho_b C p_b u^*}$$

$\rho = 0.0709$; $C_p = 0.2406$

$u^* = 0.188$ ft/sec; $q_w = 8.3$ Btu/hr ft^2

$$\therefore \quad T^* = \frac{8.3}{0.0709 \times 0.2406 \times 0.188 \times 3600} = 0.719\ ^\circ\text{F}$$

t^+ $((T_w - T)/T^*)$ values can then easily be calculated.

Dimensionless parameters

These were calculated using properties evaluated at the bulk mean temperature. For run N-10 the following values of the properties at $T_b = 99.8\ ^\circ$F were obtained from the relationships in Appendix B:

$\rho = 0.0709$ lb/ft^3; $C_p = 0.2406$ Btu/lb $^\circ$F

$\mu = 0.0189$ cp; $k = 0.0156$ Btu/hr ft $^\circ$F

Also $Re = 5354$; $f = 0.00797$; $D = 3.886''$

L/D (Loop II) $= 100$; $d\bar{T}/dz = 0.56\ ^{o}F/ft$

$T_w = 115.5\ ^{o}F$; $T_c = 96.4\ ^{o}F$

Then,

$Ra = \rho^2 \beta g C_p D^4 (dT/dz)/16\mu k = 489.5$

$Pr = C_p \mu/k = 0.706$

$Gr = D^3 \rho^2 g\beta(T_w - T_c)/\mu^2 = 9.148 \times 10^5$

$Re^* = Re\sqrt{f/2} = 338$

$Y = Gr/Re^{*2} = 8.00$

$Z = (16\ Ra/Re)(D/L) = 0.0145$

Nusselt number

$$Nu = \frac{hD}{k} = \frac{q_w}{T_w - T_b} \cdot \frac{D}{k} \qquad (I.13)$$

For run N-10

$$Nu = \frac{8.0}{111.5 - 99.8} \cdot \frac{3.886}{12 \times 0.0156} = 14.8$$

I.2 CALCULATION OF EDDY DIFFUSIVITIES, $\overline{v_r t}$ AND $\overline{v_r v_z}$

The calculations to obtain the above values were performed on an IBM 1130 digital computer. The following integration and differentiation techniques were employed:

The measured velocity and temperature data were smoothed and second or third order polynomials were fitted to the smoothed data using a matrix inversion technique. In the regions where profiles curved sharply data was fed to the computer at η intervals of 0.02; for the remaining sections of the profiles intervals of $\eta = 0.05$ were used. In the latter region a second order polynomial was used, while in the region of greatest curvature a third order polynomial was employed. In the wall region the rational functions

$$\bar{V}_z = \frac{c_1 \eta}{1 + c_2 \eta}$$

and

$$T = \frac{c_1 + c_2 \eta}{1 + c_3 \eta}$$

were used to approximate the velocity and temperature distributions.

For differentiation purposes the above curves were fitted to 5 points at a time and the derivative evaluated at the centre point. For integration purposes 6 data points were taken and integration was carried out over the middle interval.

Evaluation of $\overline{v_r t}$ and ε_H/α

$\overline{v_r t}$ is obtained from the equation

$$\left(\frac{\partial \bar{T}}{\partial \eta} - \frac{D}{2}\frac{\rho C_p}{k}\overline{v_r t}\right) = \frac{D^2}{4\eta k} C_p \frac{d\bar{T}}{dz}\int_o^\eta (\rho \bar{V}_z)\,\eta d\eta$$

I II III

$$- \frac{D^2}{4\eta k}\int_o^\eta \left(\bar{V}_z \frac{d\bar{p}}{dz}\right)\eta d\eta$$

IV

$$- \frac{D}{2\eta k}\rho_M \beta C_p \int_o^\eta \left(\overline{v_r t}\frac{\partial \bar{T}}{\partial \eta}\right)\eta d\eta$$

V

The term IV is extremely small and can be neglected.

Then, for $y/R = 0.3$

Term I = 14.436

Term III = 75.063

Term V = 0.219

Term II = 75.063 + 0.219 - 14.436

= 60.846

$$\therefore \overline{v_r t} = -\frac{k}{\rho C_p}\cdot\frac{2}{D} \times 60.846$$

At $T_{0.3}$ (= 99.86 °F) ρ = 0.0709 lb/ft^3; C_p = 0.2406

k = 0.0156 Btu/hr ft °F

$$\therefore \overline{v_r t} = -\frac{0.0156 \times 2 \times 60.846 \times 12}{0.0709 \times 0.2406 \times 3.886 \times 3600}$$

$$= -0.0956$$

Since term II, $\frac{\rho C_p}{k}\cdot\frac{D}{2}\overline{v_r t} = \frac{\varepsilon_H}{\alpha}\cdot\frac{dT}{d\eta}$

$$\therefore \frac{\varepsilon_H}{\alpha} = \frac{60.846}{dT/d\eta} = \frac{60.846}{14.436}$$

$$= 4.21$$

Evaluation of $\overline{v_r v_z}$ and ε_M/ν

$\overline{v_r v_z}$ is obtained from the equation (A.25)

$$-\overline{v_r v_z}\frac{D}{2\nu} + \frac{\partial \bar{V}_z}{\partial \eta} = -\frac{D}{2\eta\mu}\int_o^\eta (\rho_M \beta \overline{v_r t}\frac{\partial \bar{V}_z}{\partial \eta} - 2I_1)\eta d\eta$$

I II III

$$+\frac{D}{2\eta\mu}\int_o^\eta \left(\frac{\bar{V}_z}{\eta}\frac{\partial}{\partial \eta}\eta\rho_M\beta\overline{v_r t} - 2I_2\right)\eta d\eta$$

IV

$$+\eta\frac{\mu_w}{\mu}\left(\frac{\partial \bar{V}_z}{\partial \eta}\right)_w - \frac{D^2}{4\eta\mu}\int_o^\eta \left(\bar{V}_z^2\frac{\partial \rho}{\partial z} - 2I_3\right)\eta d\eta$$

V VI

$$-\frac{D^2}{4\eta\mu}\rho_M\beta g\int_o^\eta (\bar{T}-T_M)\eta d\eta$$

VII

For y/R = 0.3

Term II = -2.4199

Term III = 0.1533

Term IV = -0.3761

Term V = -22.5939

Term VI = 0.1929

Term VII = 9.1815

$\therefore$ Term I = 0.1533 - 0.3761 - 22.5939 + 0.1929 + 9.1815 + 2.4199

= -11.0223

$\therefore$ $\overline{v_r v_z} = -\frac{2\mu}{\rho D} \times (-11.0223)$

Since ρ = 0.0709; μ = 0.0189 cp

$\therefore$ $\overline{v_r v_z} = -\frac{2 \times 0.0189 \times 12}{1488 \times 0.0709 \times 3.886}(-11.0223)$

= 0.0122

Since Term I = $(\varepsilon_M/\nu)(d\bar{V}_z/d\eta)$

$\therefore$ $\frac{\varepsilon_M}{\nu} = \frac{-11.0223}{-2.4199} = 4.55$

Eddy diffusivity ratio

Since $\varepsilon_H/\varepsilon_M = (\varepsilon_H/\alpha)/(\varepsilon_M/\nu)Pr$

For $y/R = 0.3$, the calculated $\varepsilon_H/\varepsilon_M$ value

$$= \frac{4.21}{4.55 \times 0.706} = 1.311$$

(Because of the scatter in the ε_M/ν and ε_H/α results, the $\varepsilon_H/\varepsilon_M$ values reported in Table H.7 of Appendix H were calculated from smoothed curves through the ε_M/ν and ε_H/α values.)

I.3 TURBULENCE MEASUREMENTS.

The method by which values of v_z', t' and $\overline{v_z t}$ were calculated is illustrated using results for the measurements for run NT-2 at $y/R = 0.4$.

Velocity determination

Calibration procedures were similar to those described in Section I.1 except that they were carried out here for five overheating ratios. I, R_g and R_w measurements were taken as described previously and the values of $I^2R_w/(R_w-R_g)$ at each overheating ratio are given below in Table I.1. Values of A and B for each overheating ratio, together with the $\overline{V}_z$ values, calculated as described in section I.1, are also given.

TABLE I.1

OHR	$\frac{I^2R_w}{R_w-R_g}$	A	B	$\overline{V}_z$
0.05	3795.3	2386.0	737.0	3.655
0.1	3797.3	2117.0	884.0	3.610
0.3	3764.6	2182.0	834.0	3.593
0.5	3748.8	2222.0	805.0	3.583
0.7	3741.3	2238.0	788.0	3.621

$\overline{e^2}$

Values of $\overline{e^2}$, the mean square value of the fluctuating voltage across the hot-wire, were calculated, as described in Appendix G, from measurements of the mean square meter reading, y, and the amplifier attenuation, x. The values for run NT-2, y/R = 0.4 are given in Table I.2 below. The readings in the last row were taken using a very low current, in order to eliminate the contribution of velocity fluctuations to the hot-wire signal and thus determine $\sqrt{\overline{t^2}}$.

TABLE I.2

OHR	x	y	$\overline{e^2}$
0.05	15	38.0	0.1216
0.1	21	25.0	0.3200
0.3	30	20.0	2.048
0.5	33	33.0	6.7584
0.7	39	17.0	13.9264
0.001	0	24.0	0.0024

Sensitivity values

The sensitivity, s, of the hot-wire to voltage fluctuations was determined from equation (2.25) together with the definitions of P and K given in equations (2.27) and (2.28):

$$s = \frac{1}{(1+PK)} \quad \frac{(R_w-R_g)^2 \, B\bar{V}_z^{0.5}}{2IR_g\bar{V}_z} \tag{2.25}$$

$$P = \left(\frac{A_0 a_1}{2(a+a_1T_0)\beta R_0} \right) \Big/ \left(\frac{\bar{A}_f + B\bar{V}_z^{0.5}}{\bar{R}_w - \bar{R}_g} \right) \tag{2.27}$$

$$K = \frac{R_w}{R_g} \tag{2.28}$$

For run NT-2, y/R = 0.4, OHR = 0.5

$\therefore$ R_w = 13.455 ohms; R_g = 8.97 ohms

B = 805.0; $\bar{V}_z$ = 3.583 ft/sec

I = 35.35 mA; a = 12×10^{-6}

a_1 = 0.17×10^{-6}; βR_0 = 0.03157

A_0 was obtained from A in the same way that A_g was obtained from A_f, assuming $T_0 = 273\ ^{\circ}K$ (see section I.1).

For O.H.R. = 0.5, $A_0 = 1709.9$

$$\therefore \quad P = \left(\frac{1709.9 \times 0.17 \times 10^{-6}}{2(12 \times 10^{-6} + 0.17 \times 10^{-6} \times 0.03157)} \right) \Big/ \left(\frac{2222.0 + 805.0 \times 3.583^{0.5}}{13.455 - 8.97} \right)$$

$$= 0.0943$$

$$K = R_w/R_g = 13.455/8.970 = 1.500$$

$$\therefore \quad s = \frac{1}{(1+0.0943 \times 1.5)} \quad \frac{(13.455-8.97)^2 \times 805.0 \times 3.583^{0.5}}{2 \times 35.35 \times 8.97 \times 3.583}$$

$$= 11.815$$

The sensitivity s_t of the hot-wire to temperature fluctuations was determined using equation (2.26)

$$s_t = \frac{(1-P)}{(1 + PK)} \quad \frac{\beta R_0 I R_w}{R_g}$$

$$= \frac{(1 - 0.0943)}{(1 + 0.0943 \times 1.5)} \quad \frac{0.03157 \times 35.35 \times 13.455}{8.97}$$

$$= 1.328$$

Sensitivity values, $\overline{e^2}$, P, K and values of X ($= s/s_t$) and Y ($= \overline{e^2}/s_t^2$) are shown for y/R = 0.4 in Table I.3 below.

TABLE I.3

OHR	$\overline{e^2}$	P	K	s	s_t	X	Y
0.05	0.1216	0.0116	1.05	0.317	0.435	0.729	0.642
0.1	0.3200	0.0203	1.1	1.098	0.618	1.776	0.836
0.3	2.0480	0.0590	1.3	5.595	1.057	5.292	1.832
0.5	6.7584	0.0943	1.5	11.815	1.328	8.894	3.829
0.7	13.9264	0.1252	1.7	19.114	1.519	12.581	6.033
0.001	0.0024	-	1.001	0.003	0.064	0.050	0.581

$\sqrt{\overline{t^2}}$

From equation (2.29)

$$\overline{e^2} = s_t^2 \overline{t^2}$$

when the heating current is very low.

$\therefore$ For y/R = 0.4

$$\sqrt{\overline{t^2}} = \sqrt{\overline{e^2}/s_t^2} = \sqrt{0.0024/0.064^2}$$

$$= 0.763$$

$\sqrt{\overline{v_z^2}}$ and $\overline{v_z t}$

From equation (2.32)

$$Z = Y - \overline{t^2} = \overline{v_z^2} X - 2\overline{v_z t} X \qquad (2.32)$$

From the results shown in Table 1.3 five (Z,X) points were calculated and the equation of the form of (2.32) giving the best fit to the calculated points was determined using a least squares criterion. The resulting curve, together with the (Z,X) points is shown in Fig. I.1.

For y/R = 0.4 the equation obtained was

$$Z = 0.02489X + 0.12507X^2$$

$\therefore$ $\sqrt{\overline{v_z^2}} = \sqrt{0.02489} = 0.158$

$$-2\overline{v_z t} = 0.12507$$

$\therefore$ $\overline{v_z t} = -0.0625$

These values are discussed in Chapter 5.

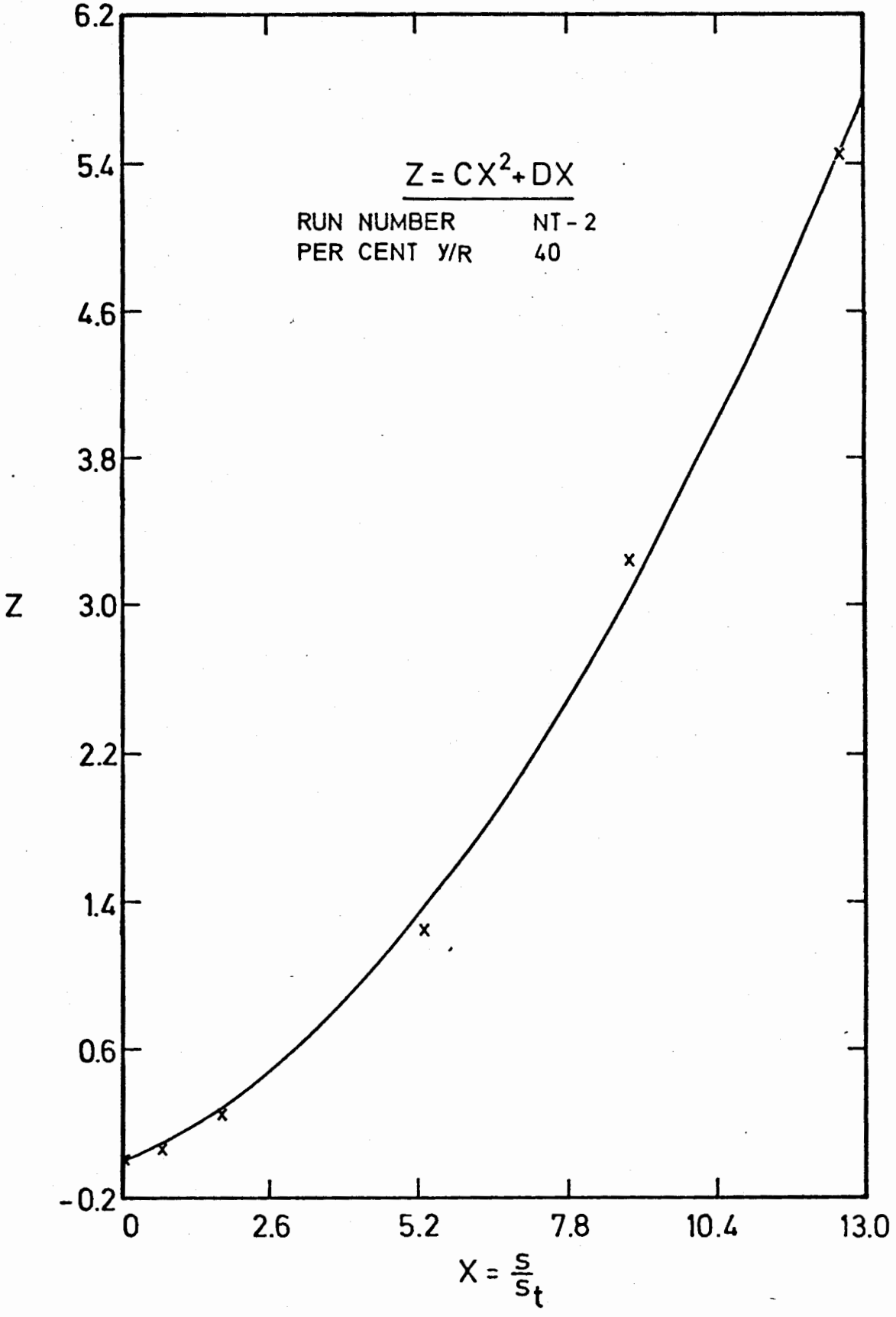

FIGURE I.1 TYPICAL LEAST SQUARES FIT TO EXPERIMENTAL MEASUREMENTS